Université de Lille

Ecole Doctorale des Sciences de la Matière, du Rayonnement et de l'Environnement

THÈSE

Pour obtenir le grade de

DOCTEUR

En Spécialité : Chimie des Matériaux

par

Noura HAIDAR

DOCTORAT DELIVRE PAR UNIVERSITE DE LILLE

Titre de la thèse :

Nano-oxyhydrides based on Ni and ceria, or doped with Zr or Al ceria, for the production of H_2 by low temperature oxidative steam reforming of ethanol

Nano-oxyhydrures à base de Ni et cérine, ou cérine dopée avec Zr ou Al, pour la production d'H_2 par vaporeformage oxydant à basse température de l'éthanol

Soutenue le 13/12/2021 devant le jury d'examen :

Rapporteur	Nadine Essayem	Directrice de Recherche CNRS	IRCELYON
Rapporteur	Florence Epron	Directrice de Recherche CNRS	IC2MP Poitiers
Président	Sébastien Paul	Professeur	Centrale Lille
Examinateur	Nicolas Bion	Chargé de Recherche CNRS, HDR	IC2MP Poitiers
Directrice de thèse	Louise Duhamel	Chargée de Recherche CNRS, HDR	Université de Lille

Thèse préparée à l'UCCS (Unité de Catalyse et Chimie du Solide)

Ecole Doctorale SMRE 104

Acknowledgements

This work is performed in Unité de Catalyse et Chimie du Solide – CNRS UMR8181.

First, I would like to thank Pr. F. Dumeignil, the director of the UCCS laboratory, for the acceptance in the lab allowing me to carry out this thesis work and giving me access to all the infrastructure necessary for my research.

I would like to sincerely acknowledge the university of Lille for funding this PhD study.

I shall express my sincere gratitude to my supervisor, Dr. Louise Duhamel, who helped me quite a lot in every aspect. I would like to thank her for the advice, supervision, and availability which encouraged the thesis progress. Our scientific discussions have given me a lot and allowed me to broaden my skills and knowledge and also to take a step back from the results obtained. We were a good team based on trust, autonomy and sincerity.

I am greatly thankful to Pr. S. Paul, the responsible of VAALBIO team. I would like to express my gratitude to all VAALBIO group members, for the fruitful discussions and meetings carried out during this doctoral research work.

My thanks also go to all the jury members for agreeing to evaluate my research work.

Last but not least, I would also like to dedicate my acknowledgements to all those who helped me during my PhD studies, our professional engineers and technicians: Ms. J. Thuriot, Mr. O. Gardoll, Ms. C. Delabre, Ms. M. Trentesaux, Ms. P. Simon, Mr. D. Romero and Mr. S. Chambrey. As well as our nice secretaries, my colleagues in the office and in the laboratory. I express all my friendly feelings for the wonderful working atmosphere, and all the good times spent together.

Finally, I would like to greatly thank and express my gratitude to my beloved family and husband who have always been beside me although being very far in distance. I owe you a lot. I love you forever!

Table of contents

General introduction

Global warming is the long-term heating of Earth's climate system observed since the pre-industrial period (between 1850 and 1900) due to unbalanced human activities, mainly because of fossil fuel burning that increased greenhouse gas levels in our Earth's atmosphere [1]. The term is often used along with climate change, even though the latter is connected to both human- and naturally produced warming and the effects it has on our planet. It is most commonly measured as the average increase in Earth's global surface temperature.

Starting from the pre-industrial period, this burning of fossil fuels is estimated to have increased Earth's global average temperature by about 1 °C (1.8 degrees Fahrenheit), a number that is currently increasing by 0.2 °C (0.36 degrees Fahrenheit) in one decade. As a reason, this left the atmosphere, ocean, and land warmed leading to the destruction of many habitats, endangering and extinction of some creatures.

Hence, after all these climatic changes, access to clean, affordable and reliable energy has been a cornerstone of the world's increasing prosperity and economic growth. Worldwide use of energy in the 21th century must also be sustainable. To counter this climatic crisis, one of the solutions is to use hydrogen gas as an energy vector instead of fossil fuels. Many techniques are possible to synthesize this hydrogen. According to the "Société Chimique de France", in 2014, 96 % of hydrogen production is of fossil origin, half of which is from natural gas. The other half comes from coal and liquid hydrocarbons. The remaining 4% corresponds to the production of hydrogen from electrolysis. It is urgently required to produce hydrogen from renewable energy sources, such as biomass-derived materials and/or biogas.

Many scientific publications have been found in literature in this direction and one of the techniques that comes up is the use of bioethanol as a renewable resource. A promising route for clean hydrogen production could be via oxidative steam reforming of bioethanol. Thanks to a catalyst, it is possible to transform bioethanol into hydrogen for direct application. However, it is necessary to find an effective catalyst, allowing excellent activity, selectivity (to H_2 and CO_2 in this case) and stability. Ni metal or noble metals are often used as catalytically active components. Nickel catalysts have been widely studied because of low cost and high activity although this metal favors coke deposition. Catalytic activities are affected by surface and structural properties as well as dispersion and reducibility of catalysts. Deactivation, related to carbonaceous compounds deposition, or sintering of the metal are considered the principal inconveniences of the catalytic system based on transition metals supported on oxides.

This study focuses on the production of hydrogen gas from bioethanol by $CeNi_xO_y$ and ternary mixed oxyhydrides ($CeNi_xAl_{0.5}O_y$ and $CeNi_xZr_{0.5}O_y$) at low temperatures of 50 °C. The goal is to obtain a high-performance and good stability catalyst, while having a maximum of

hydrogen and CO_2 in the products distribution, thus minimizing the other byproducts such as carbon monoxide, methane, acetaldehyde or solid carbon.

As a first step, a bibliographic study is carried out concerning the production of hydrogen from bioethanol, thus constituting chapter I. In this part, the processes for hydrogen production are detailed and in particular, those from steam reforming and oxidative steam reforming of ethanol (OSRE). The catalysts proposed for these hydrogen production processes are studied and divided according to the nature of material used (noble or transition-based metals) and according to the temperature of performance of the reaction (high or low). The complications followed by OSRE, our field of study, are then highlighted. Finally, a general proposed mechanism for OSRE is represented and detailed.

The catalytic test part concerning oxidative steam reforming of ethanol for production of hydrogen gas is presented in chapter II. Several binary and ternary catalysts prepared by coprecipitation based on nickel and ceria are studied in OSRE. The effect of different parameters such as O_2 / EtOH ratio, nickel content as well as the addition of a dopant, calcination, pretreatment temperature in H_2 and mass of catalyst, on OSRE are analyzed. Products distribution percentages obtained over time with these catalysts under OSRE are plotted and described. By optimizing the experimental and catalytic conditions, the best performant catalysts are identified and their stability is studied over a long time.

Chapter III is devoted to the preparation and the characterization of binary and ternary catalysts, with the analysis by different techniques such as XRF, BET, DRX, Raman, TPR and XPS before test. As well, this chapter includes the characterizations of these catalysts after OSRE process by Raman and XPS in order to study the changes of the catalyst.

Finally, a discussion part is introduced in chapter IV. In this chapter, all the summaries obtained from the previous chapters are analyzed to draw a relationship between the synthesized material, characterizations and catalytic results. A mechanism including active sites responsible for the OSRE performance is proposed based on the obtained results.

At the end, a general conclusion is drawn out. It summarizes the main points of interest and findings that emerge from this research work.

Chapter I: Bibliographic review

Energy is an indispensable element in our everyday lives. Most of the energy we use nowadays comes from burning fossil fuels. The total world fuel consumption for 2016 was 13276.3 million tons oil equivalent and the CO_2 emissions were estimated to be 33432 million tons [2]. However, fossil fuels have negative impacts, being the dominant source of local air pollution and emitter of carbon dioxide (CO_2) and other greenhouse gases. In addition, there is a big demand on fossil fuel energy which in turn cannot be enough for the future. The world must therefore balance the role of energy in social and economic development with the need to decarbonize, reduce our reliance on fossil fuels, and transition towards lower-carbon energy sources. From this point, scientists are searching for renewable resources of energy to overcome the hazardous effects and the future lack of energy produced by the conventional energy sources. In this context, hydrogen is proposed to be the green energy of the future [3-5] .

Moreover, today hydrogen is already largely used and produced. It is the gas the most used in industry. Therefore, it is an important chemical product and the demand is increasing.

I. Production of hydrogen gas

Most of hydrogen used nowadays (~95%) is produced from fossil fuels. There are four main sources for the commercial production of hydrogen: natural gas, oil, coal, and electrolysis; which account for 48 %, 30 %, 18 % and 4 % of the world's hydrogen production, respectively (Figure 1) [6, 7]. It is therefore mainly produced by methane steam reforming but also from oil/naphta reforming, coal gasification and electrolysis of water with only a small quantity by other routes such as biomass gasification.

Figure 1: Primary energy distribution through the sources for the production of hydrogen, adapted from ref. [6, 7].

Hydrogen production could be optimized with the objective of a better environment [8-10], and with this objective, "hydrogen production" field has generated numerous researches throughout the world with more than 123,816 publications (Web of Science Core collection), as shown in

Figure 2 when refined the results to only “chemistry physical” which leads to about 30,457 records.

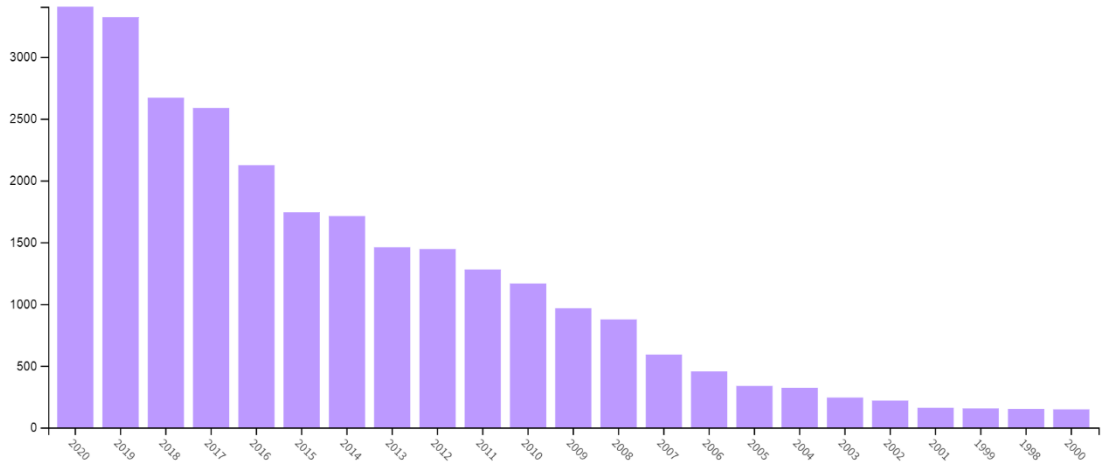

Figure 2: Number of records on “hydrogen production” refined to “chemistry physical” only (Web of Science Core collection)

I.1 Reforming of natural gas

This process consists of heating the gas to between 700-1100 °C in the presence of steam and a nickel catalyst [11, 12]. The resulting endothermic reaction breaks up the methane molecules and forms carbon monoxide CO and hydrogen H_2. The carbon monoxide gas can then be passed with steam over adequate catalysts to undergo water gas shift reactions (high and low temperature WGS) to obtain further quantities of H_2.

The first stage for production of hydrogen from methane at high temperature is reported in equation 1:

$$CH_4 + H_2O \rightarrow CO + 3\ H_2 \qquad \text{(equation 1)}$$

Some additional hydrogen is generated through the, exothermic, water gas shift reaction equation 2:

$$CO + H_2O \rightarrow CO_2 + H_2 \qquad \text{(equation 2)}$$

However, the downside to this process is that its major byproducts are CO, CO_2 and other greenhouse gases, as a high amount of energy is required to perform the process.

I.2 Coal gasification

For the production of hydrogen from coal, coal gasification is used. The process of coal gasification uses steam and a carefully controlled concentration of gases to break molecular bonds in coal and form a gaseous mix of hydrogen and carbon monoxide [13, 14]. The gas obtained from coal gasification can later be used to produce electricity more efficiently and allow a better capture of greenhouse gases than the traditional burning of coal. However, this process produces sulfur oxides and nitrous oxides that are very dangerous for the environment in addition to the high energy requirements.

I.3 Electrolysis

Electrolysis consists of using electricity to split water into hydrogen and oxygen. This source of hydrogen requires high input of energy that is furnished by electricity [6, 7.] If the electricity comes from renewable energy, the hydrogen produced is clean, and numerous studies are done to ameliorate the system [15].

II. Uses and importance of hydrogen gas

Hydrogen, is the gas the most used in the world, in many industrial applications to produce different materials. The main uses of hydrogen are for ammonia production, hydro-treating processes, and methanol synthesis.

Hydrogen is used during fuel refining to remove sulfur via a process of desulfurization or softening. Hydrogen is introduced at a high temperature (over 350 °C) and high pressure (60 bar) during the refining process. It reacts with the sulfur contained in the hydrocarbon molecules to form new compound hydrogen sulfur (H_2S) which is removed. This hydrogen sulfur can then react with oxygen to yield sulfur, forming a yellow compound that is sometimes seen in refineries. This sulfur is then used as a raw material in industry.

In electronics, hydrogen is used as a carrier gas (a gas that transports active gases) for diverse applications such as the manufacture of electronic components. It offers excellent protection against impurities and oxidation.

It is a reagent that enters into the composition of textile fibers such as nylon, polyurethane foam and a number of plastic materials. In the glass industry, it is essential to the manufacture of the flat glass used for flat screens. Most flat glass uses the float process, for which high purity hydrogen constitutes a protective atmosphere.

Hydrogen is used in metallurgy for heat treatment atmospheres that enable to produce mechanical parts (the sintering of molded parts) or to alter their properties (annealing of metallic parts).

In the future, the use of hydrogen could reduce 6 Gt of CO_2 emissions annually, and create 30 million new jobs by 2050 [4]. A recent report shows that hydrogen could power over 400 million cars, 15-20 million trucks, and around 5 million buses in 2050, which make up about 20-25 % of the transportation industry. Along with its significant economic and environmental benefits, hydrogen energy systems are expected to operate at higher efficiencies in the future. Hydrogen is seen as the key to sustainable growth and solution to global warming issues.

III. Bioethanol

Research on ethanol production is of growing interest as shown by the high number of recent reviews [16-19]. Out of various liquid hydrogen sources, ethanol is a sustainable candidate because of its renewable nature, increasing availability, biodegradable nature, low toxicity, and ease of transport. Ethanol, ethyl alcohol, is the same as that found in all alcoholic beverages and largely used. Bioethanol is also a biofuel usable in engines with gasoline. Bioethanol can easily be produced from biomass by transformation of plants containing sucrose (beet, sugar cane ...) or starch (wheat, corn ...), that can be transformed to give bioethanol, it can be obtained by fermentation of the sugar extracted from the sugar plant or by enzymatic hydrolysis of the starch contained in cereals [20]. There are many biomass conversion processes leading to ethanol production and many other important products [21]. The two main ways for fuel ethanol production are: the first and the second-generation technologies [22].

III.1 1st generation bioethanol

The first generation fuel ethanol are mainly produced from the crops rich in starch or sugars, such as corn, cassava and sugar cane [23]. These feedstocks consist of glucose polysaccharides joined by α-glycosidic linkages. These can be easily hydrolyzed into monosaccharides and utilized by microbes. In addition, there are also some trace elements in the feedstock such as fatty acids, protein, and other ingredients which have some benefits in microbial fermentation. The process is divided into several steps that are: liquefaction, saccharification, fermentation, distillation.

With several decades, the production of ethanol with the first generation technology has been mostly used in industry. However, the crops which are rich in starch and sugars are also the

main component in the food pyramid of human beings and animals. So, if the consumption of starch and sugars for fuel ethanol production increases excessively, the food supply of these organisms will decrease, leading to elevations in the prices of raw materials, and some other impacts.

III.2 2nd generation bioethanol

Second generation bioethanol production is a good route to replace the first generation and to reduce the problems caused by it [24]. This is because it employs non-edible feedstock that ends up from agriculture and forestry wastes. Second generation bioethanol is based on lignocellulosic and starchy materials that are further converted to fermentable sugars. These materials are present in the wood, the bark of trees, in, to use the example of sugar beet, all that is not cut into chips (leaves, skin ...) or more generally in what is unfit for animal or human consumption. Lignocellulosic biomass is composed of cellulose, hemicellulose and lignin. In mass, between 40 and 50 % of it is composed of cellulose, 30-35 % hemicellulose and 15-30 % of lignin. Many methodologies have been suggested for 2nd generation bioethanol namely pre-treatment, hydrolysis, fermentation and distillation.

III.3 Bioethanol applications

A high quantity of bioethanol produced in the world is used as fuel, mixed in different proportions (SP95-E10 or E85, for the most part). Nevertheless, ethanol is also a platform molecule in the chemical industry [25]. It makes it possible in particular to produce ethyl halides, ethyl esters, ethylene or acetic acid.

III.4 Bioethanol in hydrogen production

Recent researches have shown that ethanol is a promising molecule for production of hydrogen. Some researchers have written very comprehensive reviews on hydrogen production processes from ethanol [26-37]. Ethanol seems to be the main vector for hydrogen production; because it is of low toxicity and can be easily produced by fermentation from biomass. Bioethanol might contain some impurities that could reduce the yield of hydrogen production by coke deposition such as fusel alcohols, acetic acid and ethyl acetate [38]. This renewable resource offers huge benefits because it would produce very little CO_2 compared to the fossil resources currently used knowing that the CO_2 produced would be equivalent to the CO_2 absorbed by the biomass, which would generate a theoretical carbon-neutral cycle.

IV. Ethanol reforming

To obtain hydrogen directly from bioethanol, steam reforming, partial oxidation or oxidative steam reforming can be done. The absence of sulfuric impurities in bioethanol avoids the problem of catalyst poisoning due to the sulfuric impurities. However, when using raw bioethanol different kind of impurities can be present and depending on the bioethanol origin, that should be taken into account [33]. Any way when considering a modeled bioethanol as mainly a mixture of ethanol and water, the main problems for the catalyst in this process are the sintering of the active phase due to the high temperatures required and the carbon deposition [26-37]. There are many parallel possible reactions besides the desired reactions, which can lead to the increase of carbonaceous depositions over catalytic surface. The operating conditions such as water and ethanol molar ratio, presence of O_2 and temperature are very important factors that may affect easily this process. The active phase used in the catalyst, different kind of supports and precursor play an important role too by considering the interaction between the different elements. Many catalysts have been studied for ethanol reforming analysing the infuence of different parameters, like different elements and different formulations.

There has been growing attention towards hydrogen production from ethanol in the scientific fields, as it has been reported by the increase in the number of scientific publications present in the literature (Figure 3).

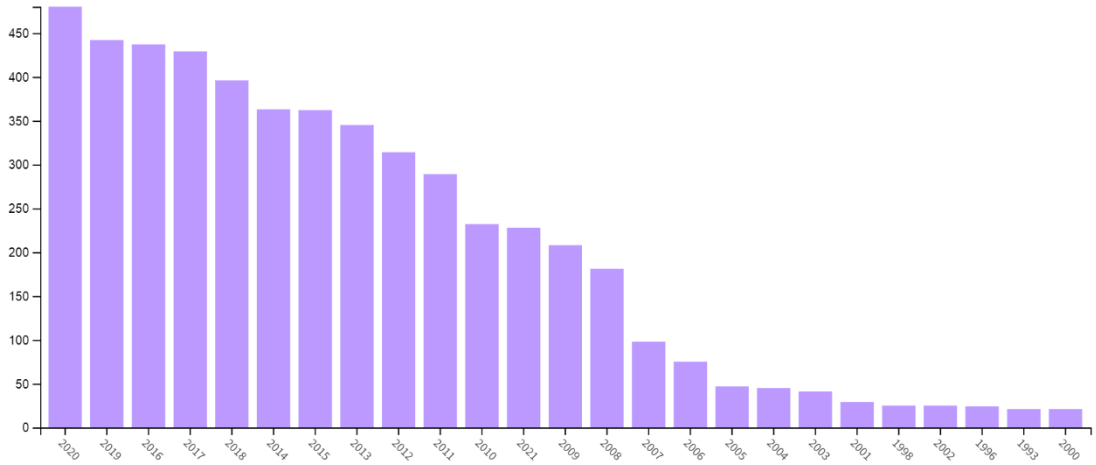

Figure 3: Number of scientific publications on "H_2 production from ethanol" per year. Web of Science Core collection.

The present study will focus on the different catalysts studied in heterogeneous catalysis in steam reforming, oxidative steam reforming and autothermal reforming of ethanol for hydrogen production. However, this field is also of great importance in electro-catalysis [39, 40] and photo-catalysis [41] with applications also in fuel cells [42] that will not be developed here.

In the present study, the catalysts for steam reforming and oxidative steam reforming of ethanol were classified according to active phase used: noble metals and transition metals and according to the operating temperature (high and low), following the classification previously reported [26]. As the objective of the present study is to focus on low temperature reaction and the use of a transition metal based catalyst (Ni) this will allow easy comparison to literature.

IV.1 Steam reforming of ethanol (SRE)

Steam reforming of ethanol to produce hydrogen is a potentially attractive process [26-32, 43-45]. Ethanol steam reforming to produce hydrogen is a promising clean process since ethanol is a green product arising from biomass through the conventional fermentation process [46-49]. The steam reforming of ethanol consists in using a water/ethanol mixture or raw bioethanol, which will produce, ideally, hydrogen and carbon dioxide using a catalyst. The development of suitable catalysts for this reaction is crucial for the viability of the process. In many publications, the reactions are reported at high temperature (600 °C - 700 °C), as expected due to the endothermic nature of the reaction. Different parameters have been studied on this process including catalytic preparation, impregnation, formulation and reaction conditions.

The maximum amount of hydrogen obtained in the ethanol steam reforming is given by the stoichiometry of equation 3, as a matter of fact 6 moles of hydrogen can be produced from ethanol and water [50, 51]:

$C_2H_5OH + 3\ H_2O \rightarrow 6\ H_2 + 2\ CO_2 \quad \Delta_rH° = 173$ kJ/mol (equation 3)

Due to the endothermic nature of the ESR reaction, high temperatures (generally > 600 °C) are needed. Low pressures and water excess also favors high hydrogen yields [52, 53].

However, this process is very competitive and challenging since many other reactions are possible such as:

$C_2H_5OH \rightarrow C + CO + 3\ H_2$ (equation 4)

$C_2H_5OH \rightarrow CO + CH_4 + H_2$ (equation 5)

$C_2H_5OH \rightarrow CH_3CHO + H_2$ (equation 6)

$C_2H_5OH \rightarrow C_2H_4 + H_2O$ (equation 7)

$CH_3CHO \rightarrow CO + CH_4$ (equation 8)

$CO + H_2O \rightarrow H_2 + CO_2$ (equation 9)

Many published papers have been considering hydrogen production from bioethanol by means of steam reforming processes using catalysts based on Co, Cu, Ni, Rh, Pd, Pt, Ir, Ru or Rh metals that have shown good performances in ethanol conversion and high selectivity regarding hydrogen production [26-37, 54-63].

IV.1.1 SRE catalysts operating at high temperature

Most of the catalysts used in literature for ethanol steam reforming work in high temperature. High temperature corresponds to the ones higher than 450 °C [26]. Most of these catalysts, showed a high performance with low carbon formation and high selectivity to hydrogen [31, 64, 65]. However, this process at high temperature favors CO formation in large amounts. The catalyst appropriated to SRE should give maximum H_2 production with minimized by products formation. Among these catalysts used, some are noble based metals and some are transition based metals.

IV.1.1.1 SRE catalysts based on noble metals

Noble metal catalysts show a high activity and selectivity for ethanol steam reforming with a low or null carbon [66-68]. However, they are not cost effective as a result they are not used in high percentage loadings in the catalyst. These catalysts can be added to transition based catalysts to get a better activity [67].

On this basis, the addition of the noble metals to the magnesium aluminate-supported cobalt catalysts was studied [69] to show a marked modification in activity of the catalysts, better stability of the reaction and a higher hydrogen yield. Promoting the catalyst with noble metals reduced the reduction temperature of the cobalt species interacting with the support, which is due to hydrogen spillover phenomenon that occurs in noble metals. It has also been seen that the addition of noble metal stabilized the Co sites in the reduced state throughout the reaction.

It should also be counted that the different noble metals nature and the amount of loadings have different activities in ethanol reforming. Rh is more active and selective to hydrogen formation in comparison to Ru, Pt and Pd in the temperature range of 600-850 °C and with a metal loading of 0-5 wt. % [61] Al_2O_3, MgO and TiO_2 supports, that for 5 % Ru/Al_2O_3 catalyst is able to obtain

100 % conversion of ethanol with selectivity towards hydrogen above 95 % and the only by-product being methane.

Other similar works done by Osorio [70, 71] on the influence of the support has been done for a supported catalyst based on rhodium but at 1 % by mass. The authors first used a simple alumina then modified it by adding lanthanum oxides and ceria with different percentages. It turns out that at 500 °C, after 50 hours of test a conversion to ethanol up to 97 % is obtained, with a percentage of 58 % of hydrogen in the products distribution, for a supported rhodium catalyst on a La_2O_3-CeO_2-Al_2O_3 mixture at 47.5, 2.5 and 50 % by weight, respectively. At the same percentage in rhodium, Hou [72] used a 100 % supported catalyst on ceria. With 3 times more catalyst than Osorio-Vargas, and at 550 °C, it gets a total conversion to ethanol and 53 % of hydrogen in the products distribution, after 60 hours.

Pt has also been used widely in SRE reactions [73-76]. Several catalysts were prepared and tested in SRE at high temperature. For example, $Pt/Ce_{0.97}Ru_{0.03}O_2$ catalysts were prepared and tested under SRE conditions at a temperature of 600 °C to get a 70 % conversion to hydrogen. However, stability tests of these compounds showed a deactivaton after 10 hours process although a good conversion to H_2 was achieved [76].

The shape and structure play an important role in the catalyst activity, as it has been investigated with RhPd catalysts on different supports (polycrystalline ceria, nanoshaped CeO_2-cubes and CeO_2-rods). It was shown that at 650–700 K the $RhPd/CeO_2$ cubes catalyst gives higher hydrogen yield than $RhPd/CeO_2$-rods and $RhPd/CeO_2$-polycrystalline which are the least selective to hydrogen. However, at temperatures higher than 800K the catalytic performance of all samples is similar and close to the thermodynamic equilibrium. This high performance of $RhPd/CeO_2$-cubes and $RhPd/CeO_2$-rods for ESR at low temperature is mainly due to higher water–gas shift activity and strong interactions between the bimetallic–oxide support interaction.

IV.1.1.2 SRE catalysts based on transition metals

Many researchers have focused on transition based metals for hydrogen production from bioethanol [29, 32, 77, 78] Ni, Co, Cu and Fe are the most studied transition metals to produce H_2 [33, 44, 79]. It has been shown that the most selective catalysts for H_2 (higher than 90 %) were: $NiCeO_2ZrO_2$, $Ni/CaCO_2ZrO_2$, Ni/MgO, Ni/ZnO, $NiF/La_2O_2CO_3$, Ni/Cs-zeolite-Y and $NiCu/SiO_2$, $NiAl_2O_3ZrO_2$, and $Ni/C_{1x}Zr_xO_2$ 36, [80].

On the basis that Ni based catalysts have a good activity in ethanol steam reforming [81- 83] $Ni/Ce_{0.9}Sm_{0.1}O_{2-\delta}$ nanowires prepared by hydrothermal method followed by impregnation [84] were prepared and tested in ethanol steam reforming under a reaction temperature of 550 °C with a water/ethanol molar ratio of 3 to achieve an ethanol conversion of 100 % with 35 % selectivity to hydrogen. The products obtained were mainly CO_2 and H_2 with the production of methane (~0.5 %) and carbon monoxide (~10 %) as by-products. These results were in agreement with studies evidencing that temperatures in the range of 450-600 °C showed the best performances in terms of both ethanol conversion and H_2 selectivity [42]. Improved Ni based hydrotalcite catalysts with 10 % wt Ni revealed good catalytic activity with high selectivity to H_2 (72 %) and only CH_4 and CO_2 as by- products (with 9 % and 20 % selectivity respectively) [85]. Moreover, when Ozkan et al. [86] investigated the selectivity of hydrogen utilizing several active metals such as Ni, and their combinations, it was found that the selectivity was affected by the increase in the amount of Ni. It was also discovered that the upper-limit of Ni was between 6 % and 10 %.

It has been proposed that the number of oxygen vacancies formed on the Ni- La doped ceria catalyst play a key role in the steam reforming process [87]. As it has been demonstrated that using $Ni/Ce_{0.9}Sm_{0.1}O_{2-\delta}$ under same conditions of preparation and catalytic test stated in the latter, a better selectivity up to 60 % was obtained with a long term stability and without formation of carbon [84]. This has been related to the increase in the number of oxygen vacancies, the high specific surface area and the small thickness of the catalyst obtained by the preparation of the Sm doped-ceria nanowires. Similar effect was proven on metal (La, Tb, Zr)-doped CeO_2 supported Ni catalysts prepared with different methods. These catalysts showed different catalytic results at a reaction temperature of 600 °C due to the variation of the number of oxygen vacancies obtained [87]. It has been shown that the oxygen vacancies help to dissociate water and form surface hydroxyl groups which will enhance catalytic activity [88, 89].

Many publications have focused on the influence of the support on the activity of the catalyst. Some studies dealt with nickel at 8.2 % by weight as the active phase and ceria, perovskites $MgAl_2O_4$ and $Ce_{0.6}Zr_{0.4}O_2$ [90, 91] where their BET analysis showed a specific surface area of 90 m^2 / g for the catalyst supported on $Ce_{0.6}Zr_{0.4}O_2$ and 113 m^2/g for the catalyst supported on ceria. XRD analysis were also carried out on these two catalysts and show an average crystallites size of 10 nm for the catalyst supported on ceria and 15 to 20 nm for the supported catalyst on ceria-zirconia. Moreover, by increasing the percentage of cerium in zirconia, the selectivity to

hydrogen also increased, from 52 % for an unmodified zirconia to 60 % for a zirconia in which 70 % of zirconium atoms were replaced by cerium. However, with 90 % of cerium in zirconia, the selectivity dropped.

The type of material used and dopants play a very important role in the catalytic activity of the catalyst. It has been found that there is a good reforming stability of catalysts with the increase in La content to prevent the formation of carbon filaments, this was achieved by the use of Ni/La-Al_2O_3 catalysts prepared by citrate method at a reaction temperature of 500 °C to obtain 100 % conversion [92].

The catalytic behavior of Ni/Al_2O_3 catalysts modified with La and Ag was investigated to also show that activity and stability against carbon deposition was strongly dependent on the presence of La and only slightly sensitive to Ag. Moreover, on the same type of catalysts it has been shown that the Ni/La–Al_2O_3 catalysts become inactive at low temperatures, and the activity could be regenerated with reduction of NiO by ethanol on raising the reaction temperature [93]. Other catalysts based on Co supported on Zn-hydrotalcite can be improved by means of ethanol conversion, high hydrogen selectivity, and high stability by the steam reforming if they are promoted with La [94].

For some reactions using nickel based catalysts comprising nanoparticles and strong metal-support interactions (SMSI) behave highly active and resistant to coking [26, 29, 31, 95-101] and among which are ex-hydrotalcite Ni–Mg–Al–O based compounds which have been tested [102-105]. Thermal treatment of hydrotalcite (HT)-like compounds is a largely studied strategy for preparation of mixed oxides with high activity and mechanical strength, such as in H_2 production. The HT-like compounds enable to incorporate various metal cations such as Ni^{2+}, Co^{2+} and Cu^{2+}, and so they have been employed and studied as catalyst precursor or as catalyst support [94]. As a matter of fact, it is known that the catalyst composition as well as preparation are of paramount importance whatever for catalyst activity, selectivity and stability.

On this basis, Cerda-Moreno et al. [94] were interested in studying Co and La supported on Zn-Hydrotalcite-derived material by testing samples of Zn-hydrotalcite containing different amounts of Co (5, 10, 20, and 30 wt. %) under a water/ethanol molar ratio of 10 and temperature ranging between 673–873 K. The best results were obtained with the sample containing 20 wt. % of Co (20CoHT), with a complete conversion of ethanol and yields to hydrogen close to the equilibrium (73 mol. %). Further incorporation of this catalyst with 1 wt. % of La improved

the stability of this catalytic material against deactivation as shown before [93, 92] in agreement with the previous study done on La compounds.

Another approach for finding a good catalyst for ethanol steam reforming is through adding some alkaline metals such as Ca in the A site of perovskites composed of $La_{1-x}Ca_xAl_{1-y}Ni_yO_3$ (x = 0, 0.1; y = 0, 0.1, 0.2, 0.3) The size of the alkaline metal matters also in the reforming process, and so replacing Ca later by Mg, another alkaline metal with a smaller radius, gives the suitable basic character and it allowed a complete insertion of Ni in the structure due to its smaller radius [106].

It should also be noted that the nature of dopant has a very effective role on catalysts. It was revealed that [107] when doped with Cs, Ni/ZrO_2 catalysts yielded higher levels of H_2 than the catalysts doped with Ce, Li, K and La.

Finally, it is important to draw out the attention on the effect of the preparation method on the catalytic performance of the catalysts [108]. Some tests were done on prepared Ni-based catalysts by using three synthesis methods involving sol-gel, impregnation, and co-precipitation (under a reaction temperature of 525 °C with a H_2O/C_2H_5OH molar ratio of 8:1) [109]. Characterizations and catalytic activity tests results revealed that sol-gel process produced the most promising catalyst with 80 % selectivity to H_2 and the favorable Ni/Al_2O_3 mesoporous structure that was responsible for its better activity in steam reforming of ethanol. The CH_4 and CO products were almost negligible, which indicateed that this catalyst prepared by sol gel was sufficient to reform the CH_4 intermediate product into H_2 and it also promoted the water-gas shift reaction. This has also been investigated on Ni/MgO catalysts supported on nanocrystalline MgO which were also prepared by sol-gel process [110]. The low CH_4 and CO selectivity directed the process towards a low tendency for coke formation. This was caused by either methane decomposition or CO disproportionation. However, when the catalysts were prepared by impregnation and co-precipitation, the selectivity for CO and CH_4 showed a slight increase at the expense of H_2 production. The two catalysts produced by the latter methods gave almost the same H_2 selectivity with only 74 %, but the CH_4/CO ratio for the impregnation method was a bit higher than that of co-precipitation.

IV.1.2 SRE catalysts operating at low temperature

According to previous classification, this corresponds to temperatures equal or below 450 °C [26].

IV.1.2.1 With noble metals

At temperatures below 400 °C, the studies are rare in the field of noble metals. Platinum has been reported as an active metal for steam reforming of ethanol at low temperatures [73, 111, 112]. K. Marios obtained a 60 % conversion of ethanol with 40 % H_2, 27 % CH_4, 23 % CO, 7 % CO_2, 5 % acetaldehyde and 3 % acetone in the products distribution using a Pt/CeO_2 catalyst at 300 °C with 100 mg catalyst at a H_2O/EtOH molar ratio of 3 [112]. But, G. Jacobs et al. postponed a very low conversion at 300 °C (5.4 %) on their Pt/CeO_2 catalyst [31]. The best result obtained on noble metals remain the commercial Pd/C catalyst of Galvita et al. who claimed to have achieved total conversion at 330 °C, H_2 production of 12.8 % by volume and very good stability after 100 hours of reaction [113]. Other studies were performed on $Pd_{0.01}Zn_{0.29}Mg_{0.7}Al_2O_4$ spinel catalyst at 450 °C with water/ethanol ratio of 3 and 100 % conversion of ethanol was obtained with 80 % selectivity but the amount of carbon (coke) deposited on 1.0 g of catalyst was of 0.336 mg [114].

Regarding supports in this process, it has been found that the Pt/Al_2O_3 catalyst very efficiently converts ethanol (94% conversion) but gives a very low H_2 selectivity (S_{H2} = 6 %) at 450 °C but with the use of a support as ZrO_2 or CeO_2, a decrease in ethanol conversion (46% and 87% respectively) and a significant increase in H_2 selectivity (42.3 % and 40 % respectively) were observed [115]. Breen also found the same effect by comparing two Pt/Al_2O_3 and Pt/CeO_2-ZrO_2 catalysts. It has been also shown that a support like CeO_2 is more suitable than the support Al_2O_3 [113]. Other studies used Pt in a dragon fruit like nanocomposite of Pt-Cu@mSiO_2, this structure allowed good term stability results over 150 hours in low temperature steam reforming with 70% selectivity to hydrogen and low by-products production [116]. Some studies were focusing on rhodium performance at low temperatures using CeO_2 or CeO_2-ZrO_2 [117]. Nevertheless, the rhodium metal remains little studied at low temperatures.

To improve the performance of the catalyst, mesoporous SiO_2 shell embedded with Pt-Cu alloy nanoparticles were used [116, 118] to have better access to the metals and to prevent leaching and aggregation of active sites as well as suppressing the carbon deposition on the active surface, thus maintaining a good catalytic activity during around 150 h stability test at 400 °C. For this same catalyst, selectivities towards H_2 and acetaldehyde do not change with the increase of temperature due to the limited ability in C-C bond cleavage. The encapsulation of the bimetallic Pt-Cu alloy nanoparticles inside the mSiO_2 shells was proved to be vital for maintaining stable

ethanol conversion and give full play to the catalytic activity of active sites to maintain a good conversion of ethanol.

In ethanol reforming tests, the molar ratio of metals in the catalyst and water/ethanol ratio should be optimized according to the other factors to get the best catalytic activity and selectivity to hydrogen. Divins used catalysts based on rhodium and palladium supported on ceria loaded with 3 % w/w total with respect to Ce support and Rh:Pd molar ratio 1:1, with a water/ethanol ratio of 3 to obtain 70 % selectivity to hydrogen.

It should also be considered that the low temperature steam reforming can produce lots of carbon. On this basis, one of studies [119] have been performed to minimize the problem of carbon buildup on Ni-based catalysts and it was found that Pt addition to Ni/CeO_2-nanocube promotes the hydrogenation of highly active carbon species adsorbed at the surface at a higher rate than carbon diffusion into bulk nickel and thus minimizing carbon buildup. Using these catalysts having 10 wt % Ni and 1 wt % Pt (prepared by co-impregnation) with a feed of H_2O/Ethanol ratio 3 (under a reaction mixture of 2.5 mol % ethanol, 7.5 mol % H_2O and 90 mol % N_2) 69 % conversion of ethanol and 42 % of H_2 in products distribution were obtained; unlike the catalyst without Pt that showed lower conversion of ethanol (54 %) and higher H_2 formation (50 % in products distribution).

The concentrations of water play important role in H_2 performance [120] as on Rh/Al_2O_3 catalyst it has been concluded that the slight increase in the amount of water in the system helps to balance the reaction towards the steam-reforming and water-gas-shift and thus increase the yield of H_2.

IV.1.2.2 With transition metals

Ni-based catalysts are the most studied due to their high activity and lower cost with respect to noble metals catalysts [121] but carbon deposition and sintering effects are always present and may lead to deactivation problems [122-128].

In this sense, the catalytic support plays an important role in the inhibition of secondary reactions such as dehydration and polymerization, which lead to the formation of carbonaceous residues [129-133]. It is also considered to allow the gasification of carbonaceous residues by action of adsorbed species (CO_2, H_2O) or interaction with O^{2-} ions of the support itself; The type of support used can enhance metal-support interactions that can prevent sintering effects on the catalyst. In general, different metal oxides (Al_2O_3, MgO, SiO_2, ZrO_2, TiO_2, La_2O_3) are used as

catalytic supports since they provide suitable acid-base properties for the different stages in the reaction mechanism, high specific area and high mechanical and thermal resistance [134, 122]. However, in ethanol steam reforming reaction [135], the acidic sites of γ-Al_2O_3 favored ethanol dehydration to undesirable reaction byproducts, such as ethylene. The presence of ethylene led to a decrease in the selectivity for H_2 and to deactivation of the catalysts, since this reactant is involved in polymerization reactions that favor coke formation. The presence of suitable promoters such as K can neutralize the acidic sites of γ-Al_2O_3, thereby reducing coke formation [136]. The impregnation of Al_2O_3 with La_2O_3 reduced also carbon deposition [137] .

Promotion of the active phase by addition of a second metal can also improve or worsen the catalyst performance[138]. For example, using nickel in the active phase [32], a transition metal at 5 % by mass (from cobalt or iron) was added, using ceria-zirconia as a support ($Ce_{0.5}Zr_{0.5}O_2$) to show that this catalyst without a promotor allows at 350 °C to have a total conversion to ethanol and 4.5 moles of hydrogen formed per mole of ethanol. However, the addition of these elements makes it possible to maintain these results (with iron) or to reduce the conversion as well as the number of moles of hydrogen formed (with cobalt). Binary catalysts based on nickel and alumina have shown better results at 400 °C than that of the same catalyst promoted by addition of magnesium as the conversion of ethanol dropped drastically from 67 % and same for hydrogen selectivity that became lower than the value of the binary catalyst 42 %. Although structured manganese oxides (birnessite and todorokite) containing Co have shown a noticeable activity in steam reforming of ethanol for hydrogen production, exhibiting high values of conversion of ethanol and selectivities to hydrogen (100 % and 70 %, respectively) [139] when these experiments were performed at 673 K, 773 K and 873 K, lasting for 5h each. However, the use of zinc, molybdenum or cobalt allowed a total conversion of ethanol and a hydrogen selectivity of up to 59 %, using cobalt.

The presence of a second metal can affect the number/type of active sites, preserve the active phase integrity playing a sacrificial role or induce metal-metal interactions, all of which leads to an improvement of the catalytic activity and higher resistance to deactivation or even the opposite. In the influence of studying the addition of boron in a Ni catalyst supported on ceria [140], some tests were performed at a temperature of 350 °C with a H_2O/EtOH ratio of 13. It was found that the addition of boron allows a total conversion to ethanol as well as between 2 and 5 times more moles of hydrogen formed per mole of ethanol than those with the catalysts without boron. Another study done on doping catalysts with boron with a coprecipitation

method allowed to see the effects of boron in promoting the activity of the catalyst $Ni/Ce_{0.5}Zr_{0.5}O_2$. Well dispersed active species and formation of a Ni-B alloy coming from B-doped catalyst can promote catalyst performance and reaction pathway. Further, it could improve the selectivity of hydrogen for a SRE reaction. In addition, the B-doped ceria catalysts possess a high oxygen storage capacity through the formation of $CeBO_3$ under SRE conditions, which plays a key role in removal of the carbonaceous species [141].

Preparation steps used for the synthesis of the catalyst (Impregnation humid - IH or co-precipitation - CP) have a clear effect also on the results and each preparation could give a different structure for the catalyst and thus different catalytic results. TPR analysis carried out on nickel based catalysts prepared by co-precipitation method [140] revealed the presence of two main peaks, one which was attributed to the reduction of nickel cations in a mixed oxide phase, and the other to the reduction of NiO particles into metallic nickel Ni^0. This was explained by the presence of a solid solution which would have formed by the incorporation of Ni^{2+} cations in ceria replacing some Ce^{4+} ions. The solid solution allows the interaction between the metallic species by redox processes and as a result the conversion of ethanol and selectivity to hydrogen increased. Other studies were done using redox precipitation method of preparation on cobalt modified manganese oxide catalysts at 390 °C using a water/ethanol ratio of 12:1 and it has been shown that only 50 % conversion of ethanol was achieved with a high selectivity to undesired products (54 % CH_3CHO and 5 % CO) [142]. In addition, that this process led to the deactivation of the catalyst by carbon formation, it was shown that synthesis of cobalt manganese oxide by this method led to the formation of strongly dispersed cobalt ionic species within cryptomelane-based manganese oxide structure. In another study, the sol-gel strategy was used for preparation. Different amounts of Pr were doped into ceria and compared with the traditional impregnation methods. This method showed more highly dispersed Ni nanoparticles, abundant oxygen vacancies and enhanced metal-support interactions [143].

In this sense, the literature reports several hydrocarbon reforming reactions with Ni-based catalysts promoted with Sn as part of intermetallic compounds [144, 145]. Due to the similarity of the electronic structure of Sn and C (along with other tetra and pentavalent p metals) and since deactivation in this type of catalysts is mainly due to carbide formation, the interaction between the two metals can inhibit carbide formation increasing the catalytic lifespan [122]. On the other hand, a decrease in the catalytic activity of the Ni_xSn_y system with the increase in the proportion of Sn in the intermetallic compound has been reported [146].

The process of ethanol steam reforming is mainly affected by the thermal conditions, as expected, due to the endothermicity of the reaction. In fact, results demonstrated that the conversion increased with the increase in temperature [141] on Ce, Ni and Zr based catalysts. It has been investigated that with a temperature range rising between 200 °C and 500 °C, the conversion can exceed 90 % depending on catalyst used (T90, the temperature of 90 % EtOH conversion) around 310-340 °C for all Ni-based catalysts, and the order of T90 decreased in the order of BNiCeZr(C) < NiCeZr(C) < NiCeZr(I) < BNiCeZr(I) with a water/ethanol molar ratio of 13 and over 100 mg catalyst).

Water-to-ethanol ratio can enhance the process too. As the water-ethanol molar ratio increased in the feed, the concentration of hydrogen and carbon dioxide increased and the formation of carbon monoxide, acetone, aldehyde and ethylene decreased [147].

Finally, there are some processes used recently to promote the steam reforming process of ethanol. It is the phenomenon of electrochemical promotion of catalysis (EPOC), also known as non-faradaic electrochemical modification of catalytic activity (NEMCA), that was discovered by Stoukides and Vayenas in 1981 [148]. It was shown to be an alternative way to promote and enhance catalytic reaction rates. This process is based on activating the catalyst by an electrochemical supply of promoter ions from an electro-active catalyst support (solid electrolyte). The electrochemical promotion phenomenon allowed to control in a continuous and reversible manner the addition or removal of promoters to the catalyst [149]. Additionally, in the last years this phenomenon has been used for modifying the reversible oxidation state of a catalyst [39, 150], preventing poisoning effects [151] or even regenerating the catalyst from carbon deposition during the catalytic reaction [152]. The application of the EPOC phenomenon in hydrogen production reactions has been already studied in different catalytic systems [40]. For example, it has been studied on the water-gas shift reaction using Pt as catalyst and yttria-stabilized zirconia (YSZ, O^{2-} conductor) as solid electrolyte, and Ni supported on K-β”Al_2O_3 (K+ conductor) [153]. The steam reforming reaction has also been studied on Ni and Pt, both supported over YSZ solid electrolyte [154, 155]. On the other hand the EPOC effect has also been studied using Ni and Cu supported over K-β”Al_2O_3 [153]. All these studies have been reviewed in a recent work [156].

In the UCCS laboratory different catalysts based on cerium and nickel [157] and based on magnesium, aluminum and nickel [105, 158] were studied in SRE and have shown high performances at low temperature.

IV.2. Oxidative steam reforming of ethanol

Many simultaneous and/or consecutive competitive reactions may occur in ethanol steam reforming that may end up in different undesirable products such as carbon deposition which can be generated by different reactions such as the decomposition of ethylene and acetaldehyde. So even if the ethanol steam reforming process provides a high yield of hydrogen (according to the stoichiometry of the reaction, Eq. 5) however it is not always favored to the oxidative steam reforming reaction (OSRE, Equation 10) [31, 159]. Coke deposition is one of the important problem regarding reforming which will lead to the loss of catalytic activity. The catalysts could be generated back but it is unfavorable by the industrial processes due to its high cost. Hence, to inhibit the catalysts deactivation, the removal of carbonaceous by-products can be promoted by adding oxygen to the process or in another words by oxidative steam reforming knowing that the selectivity to hydrogen decreases in this process compared to the non-oxidative one. Many researches have been done on oxidative steam reforming in addition to the different catalysts that were synthesized during this process and the different conditions used in each study [129, 160-169].

Oxidative steam reforming (OSRE) process, with the particular case of the so-called autothermal reforming (ATRE) process, that will be presented later on, can be seen as a mixture of SRE and partial oxidation reaction POE (Eq. 11). The needed heating may be brought by simultaneous burning a portion of ethanol when oxygen or air is added to the feedstock. POE could be performed at relatively lower temperature, but it is relatively less studied because of the high exothermicity of the reaction which could lead to hot-spots and usually related to deactivation of the catalyst.

$C_2H_5OH + a\ H_2O + b\ O_2 \rightarrow c\ CO_2 + d\ H_2$ (equation 10)

$C_2H_5OH + 1.5\ O_2 \rightarrow 2\ CO_2 + 3\ H_2 \quad \Delta H^0_{298K} = -545\ KJ\ mol^{-1}$ (equation 11)

IV.2.1 OSRE catalysts operating at high temperature

IV.2.1.1 With noble metals

Among the noble metals used in oxidative steam reforming, Pt is able to enhance ethanol adsorption and water gas shift reaction as well as the hydrogenation of coke precursors [170]. Bimetallic catalysts (Pt-Co) [171] supported on a CeO_2-SiO_2 mixed oxide and prepared by wet impregnation were tested in oxidative steam reforming and conversion of ethanol of 80 % was reached after 70 h of time-on-stream at 500 °C. However, the activation energy for this reaction

was higher than that obtained on Ni-Co based catalysts low. Same results were obtained at 500 °C on platinum-cobalt bimetallic catalysts supported on CeO_2-SiO_2 mixed oxides with a 3 % wt. for Pt with respect to ceria mass and using 10 % volume of ethanol in the gaseous mixture which allowed obtaining 80 % conversion of ethanol after 70 hours of time on stream.

In particular, the Rh/Al_2O_3 catalyst that V. Fierro prepare [70, 172] allowed getting better performance at 650 °C with total conversions and the highest selectivity in H_2 on this catalyst (85 %), compared to the Pt/Al_2O_3 (20 %), Pd/Al_2O_3 (23 %) and Ru/Al_2O_3 (75 %) catalysts. In addition, the Rh/Al_2O_3 catalyst showed a very good stability after 140 h reaction at 650 °C. The good activity of rhodium was also ameliorated in Rh-Ni/CeO_2-ZrO_2 catalysts that enhanced the selectivity from 59 % to 73 % for Rh-Ni/CeO_2-ZrO_2 in comparison with Ni catalysts [173] in addition that these catalysts were reported to have a lower reducibility [174,] .

In addition to the different parameters studied, Gac 142 investigated different types of reactors in the oxidative steam reforming process. Pt-Ni/CeO_2-SiO_2 catalyst obtained by impregnation of high-surface area SiO_2 (400 m^2g^{-1}) with cerium nitrate hexahydrate and double activated by nickel and platinum was used in this process in a packed (PBR) and fluidized bed reactors (FBR) for comparison (under these reaction conditions: H_2O/C_2H_5OH = 4, O_2/C_2H_5OH = 0.5, T = 500 °C) to show that in the fixed bed reactor, a faster deactivation and lower hydrogen yields were observed and that fluidized bed operation reduced carbon formation rate of almost 4 times. Moreover, coke selectivity decreases with time-on-stream and the carbon formation rate remained unchanged at steady conditions.

IV.2.1.2 With transition metals

Among the transition metal based catalysts, Ni and Co are the most studied ones for oxidative steam reforming of hydrocarbons due to their high cleavage capability of C-C and C-H bonds [28, 30, 31, 175-179] .

Ni catalysts are largely studied because of its high activity and low cost [170, 171, 180]. However, Ni can be deactivated by formation of carbon deposits and oxidation of metallic sites and/or sintering [181, 182]. It has been reported that higher amount of carbon deposition can be related to larger Ni particles during SR [183]. Also, lower H_2O/EtOH ratios favor the deposition of filamentous carbon [184].

Many researches have been conducted recently for the improvement of the catalytic performance of Ni-based catalysts. One of the strategies was by the addition of a promoter to

get better Ni dispersion and thus preventing sintering [185] or by using bimetallic catalysts to minimize deactivation.

Other factors such as oxygen mobility favors catalytic performance, in addition to low particles size, defined crystallographic planes and specific concentrations of oxygen vacancies [186]. In fact, it has also been shown that there is a relation between reducibility of metals, H_2 production and carbon deposition where copper in the NiCu bimetallic catalyst enhanced nickel reducibility, promoted higher H_2 production and mitigated the deposition of graphitic carbon [179].

The nature of the support can also enhance the activity of the catalysts as this has been shown on nickel catalysts on Al_2O_3 supports that were either unpromoted or promoted with CeO_2, ZrO_2 and CeO_2–ZrO_2 [187]. The unpromoted catalyst showed lower activity and a lower hydrogen yield than the promoted catalyst. The characterization of the Ni-based catalysts promoted with CeO_2 and/or ZrO_2 showed that the catalysts properties ware altered by enhancing Ni dispersion and reducing Ni particles size. The promoters, especially CeO_2–ZrO_2, increased the H_2 yield and the CO_2/CO and the H_2/CO values while decreasing coke formation. This is due to the addition of ZrO_2 to CeO_2. This is in conformation that oxygen storage capacity and of mobile oxygen vacancies increase the number of surface oxygen species. The addition of oxygen facilitates the reaction by regenerating the surface oxygenation of the promoters and by oxidizing surface carbon species and carbon-containing products. In fact, the dispersion of the metal on the support was shown to strictly affect the diffusion of oxygenated species along the ceria surface [163], the surface basicity, and the concentration of coupled sites formed at the metal/support interface. All of these factors were found to be critical for ethanol conversion, selectivity toward hydrogen production, and resistance to aging upon long-term testing. Many publications have focused on the influence of the support on the activity of the catalyst. cobalt was used as the active phase at 20 % by weight, alumina and ceria, or a mixture of both as a carrier. With a temperature of 500 °C, with a low ratio of oxygen (O_2/EtOH = 0.2, a total conversion to ethanol and up to 5.6 moles of hydrogen per mole of ethanol were obtained for a catalyst supported on alumina only [188]. However, with a ceria-alumina mixture, 5.3 moles of H_2 per mole of ethanol were still obtained.

Another factor influencing activity is the element used in the active phase. For this reason some studies were performed on various catalysts with MgO-Al_2O_3 as support [189, 190]. The catalysts used were based on nickel and/or cobalt, at approximately 30 % by weight, supported and then

two promoters were added: cerium and praseodymium, at 1 % by mass. With 50 mg of catalyst, reaction carried out at 550 °C and an $EtOH/H_2O/O_2$ ratio equal to 1: 3: 0.4, all the catalysts make possible to obtain a total conversion of ethanol. Moreover, the catalysts doped with cerium or praseodymium allowed increasing from 3 to 3.4 moles of hydrogen per mole of ethanol (for catalysts based on cobalt alone). No difference was observed between cerium and praseodymium doping under these conditions. However, by the use of cobalt alone instead of nickel and cobalt together and by adding more cerium and/or praseodymium (about 3 % by weight) and with almost the same conditions (here $EtOH/H_2O/O_2$ = 1:3:0.5), substantially identical results are obtained, whether or not promoters were used (from 66 % without promoter to 68 % with 2.5 % cerium and 2 % praseodymium).

Other researchers have analyzed various aspects influencing the activity of the catalyst. Da Silva [191] et al. used a cobalt-based catalyst (16 %) supported on carbon nanofibers. He analyzed the influence of the reduction by reporting 2 catalysts, one not reduced and the other one reduced under hydrogen flow at 350 °C for one hour. They found that the reduction allows a total conversion to ethanol, against 90 % without reduction and that the percentage of hydrogen increases by 13 % with the reduction.

In another register, Da Silva analyzed the influence of the calcination temperature of the catalyst. A mixed oxide catalyst was used ($LaCoO_3$) and reduced at 600 °C and then 800 °C. With a reaction temperature of 500 °C, identical hydrogen percentage is obtained (58 %) but the increase in the calcination temperature caused a decrease in the conversion of ethanol, from a total conversion to 95 % conversion.

The influence of catalyst preparation should also be investigated in the oxidative steam reforming process of ethanol and some studies were done using two different methods: ultrasound and microwaves. At 550 °C and with an $EtOH/O_2/H_2O$ ratio equal to 1:0.5:3 total conversion of ethanol with approximately 3.1 moles of hydrogen per mole of ethanol were obtained after 100 hours in the case of a conventional preparation. However, using the other two methods mentioned above and under same other conditions, around 3.3 moles of hydrogen per mole of ethanol were obtained. The pH of the impregnation solution used in the preparation of the catalyst has a great influence as it has been shown that by varying the pH from 7 to 12 (using ammoniac solution) for a nickel catalyst (3.6 %) supported on Y_2O_3, the percentage of hydrogen obtained increased from 42 % to 47 % for a reaction at 500 °C [192] .

The catalyst formulation is also a key factors to be focused on in the oxidative steam reforming reaction [193], for this purpose a catalyst in the form of $La_2Ce_{2-x}Ni_xO_{7-\delta}$ mixed oxide was tested with different values of x (0.05-0.45) at a constant H_2O/EtOH ratio of 3 and constant temperature of 500 °C. At x equal to 0.05, between 65 and 70 % conversion of ethanol and 37 % of selectivity in hydrogen were found while at x = 0.45, the conversion of ethanol became total and the selectivity to hydrogen increased to more than 80 %. Moreover, the CO selectivity also increased with the value of x, from 47 % for x = 0.05 to about 70 % for x = 0.45. In fact, doping the catalysts with other metals could enhance the catalytic performance or can lead to a decrease of the performance. K-addition to the Ni-based sample worsens the catalytic performance as quite high carbon formation was observed during stability tests. Moreover, the K containing catalyst displayed a not negligible by-products selectivity (i.e. acetaldehyde) [194].

The effect of the percentage of oxygen in the reaction mixture on the conversion to ethanol was also investigated and it was observed that there is a very sharp decrease in these conversions at the highest oxygen ratios [195]. Indeed, at a ratio of 0.4, all the formulations made possible to have a total conversion whereas for a ratio 0.7, none of the formulations allowed total conversion. In fact, at low carbon to oxygen ratio, the conversion is higher. This is because the C/O composition affected the contribution of the total and partial oxidations of the oxidative steam reforming reactions and the optimized value varied with the catalyst used. The total and the partial oxidation of the ethanol reactions were favored under a low C/O value (C/O = 0.4). The total oxidation reaction dominated under a high concentration of oxygen (low C/O) and reduced the yield of hydrogen formation. When the C/O ratio was higher than 0.6, the low concentration of oxygen was not enough to support the partial oxidation reaction of ethanol and the conversion of ethanol dropped rapidly. The selectivities of hydrogen and other products as a function of the C/O ratio showed the optimal condition of hydrogen production at C/O = 0.6 for the $La_2Ce_{2-x}Ni_xO_{7-y}$ catalyst [195].

In summary, many parameters seem to be very important and a single change can lead to a big difference in the catalytic activity and selectivity. Hence, it is hard to choose the perfect optimal parameters for each catalyst.

IV.2.2 OSRE catalysts operating at low temperature

IV.2.2.1 With noble metals

The catalysts used in low temperature oxidative steam reforming are mostly based on transition metals. However, some researches have shown results performed on noble metal catalysts and more of which have a low loading of noble metals in addition to the transition ones. Several factors affect the activity of the catalyst, the conversions of ethanol and hydrogen selectivity in this process.

Some studies were carried out on the influence of the support (with iridium as reference active phase) [196] and on the influence of the active phase (with lanthanum oxide as support). It was observed that at a temperature ranging between 410 and 440 °C, the most suitable support with 1% iridium is lanthanum oxide, with a conversion up to 89 % and a hydrogen selectivity of 36 %. Increasing the percentage of iridium in this last catalyst dropped the conversion to 74 % under the same conditions. Another study showed that with an equal weight content, palladium converted ethanol more easily (99 % conversion), but the selectivity to hydrogen was only of 22 %, whereas ruthenium led to 92 % conversion of ethanol but with a selectivity to H_2 of 35 %. Mattos et al. [31] included the variation of the support and with 4.8 wt % iridium supported on lanthanum, 100 % conversion of ethanol was obtained whereas with Al_2O_3 support, only 82 % of ethanol was converted. Palma [197] also investigated the influence of the support by varying the CeO_2/SiO_2 ratio in a catalyst composed of a CeO_2-SiO_2 support with nickel (10 wt %) and platinum (3 wt %) as the active phase. At 300 °C and with an $EtOH/H_2O/O_2$ ratio of 1:4:0.5, the best result was obtained for a support composed of 30 % ceria and 70 % silica where the conversion of ethanol was of 90 % and the hydrogen yield was only of about 15 %. Han [198] changed the concentrations of ceria and lanthanum oxide in the support, using 1 % rhodium as the active phase. It was then revealed that for a support composed of 30 % of lanthanum oxide and 70 % of ceria, at a reaction temperature of 300 °C and using 100 mg of catalyst, as well as an $EtOH/H_2O/O_2$ ratio equal to 1:3:0.5, an almost total conversion of ethanol (99 %) and 2.3 moles of hydrogen per mole of ethanol were obtained. Some scientists prepared ceria with different specific surface areas (74, 92 and 154 m^2/g) and then impregnated it with 5 % nickel and doped with 1 % rhodium. It was reported that the ceria having 92 m^2/g as a specific surface has a lower activity than that with 74 m^2/g [199]. However, going from 92 to 154 m^2/g made possible to increase the conversion, from 40 to 58 %. The percentage of hydrogen, meanwhile, increased from 35 to 52 % in product distribution.

Later, other studies were conducted using iridium as a promoter, using similar formulation of catalysts [200]. At 300 °C and with 5 % of iridium supported on the same support as above, better results were obtained with about 55 % conversion of ethanol and a little less selectivity to hydrogen (35 %).

By taking alumina as a reference and varying the active phase [201], it turns out that at 400 °C, with an EtOH/H_2O/O_2 ratio of 1:3:0.3, rhodium, ruthenium and gold played a substantially equivalent role in terms of conversion of ethanol (between 82 and 84 %) but that Rh and Ru allowed selectivity of 45 to 47 % to hydrogen while gold did not exceed 4 %. Ru was used to optimize metal oxides of $Y_2Ce_{2-x}Ru_xO_{7-\delta}$ giving 84 % selectivity to hydrogen for a long term under C/O ratio of 0.5, O_2/C_2H_5OH ratio of 1.5 and at a temperature of 300 °C [202]. On the same catalyst, when the Ru dopant amount increased from 0.1 to 0.4, the conversion of ethanol shifted from 70 % to maximum percentages.

Similar tests were done on Pt catalysts supported on alumina and modified by La or Co (the active phase) [172]. The catalysts modified with Ce were better than those modified with La. This better activity observed was correlated with the interaction between Pt and cerium. Pt-Ce interaction affected the adsorption–decomposition of ethanol to CH_4 and CO and the reforming of these products with water. However, when both cerium and lanthanum were together in the support, a low catalytic activity was observed as a consequence of the lower Pt–Ce interaction caused by the decrease in surface ceria dispersion with respect to that achieved on the lanthanum free ceria-alumina support.

In the same means, the variation of H_2O/EtOH and O_2/EtOH ratios were studied. Increasing the percentage of water gave better results as it has been shown that by raising it from 3 to 10 (at a reaction temperature of 400 °C) the conversion of ethanol also raised from 84 to 96 %, in addition that the hydrogen yield increased from 47 to 87 %. A decrease in CO selectivity as well as an increase in methane were also noted. As for O_2/EtOH ratio, the variation from 0.03 to 0.3 made possible to increase the conversion of ethanol from 62 to 84 % and the hydrogen yield from 15 to 47 % [201].

The effect of C/O ratio has been investigated on $Y_2Ce_{2-x}Ru_xO_{7-\delta}$ catalysts by Hsieh et al who found a gradual decrease in ethanol conversion at 300 °C when increasing the ratio of C/O from 0.1 to 0.4. Following the same trend, higher selectivities to CO, CH_4 and C_2H_4 were obtained while decreasing selectivities to H_2 and CO_2 [202].

Analysis on the addition of promoters were carried out in the presence of noble metals. For example, a catalyst having 1 % by weight of platinum as the active phase with 1 % by weight of ruthenium supported on zirconia was used on the same support to obtain 96 % conversion of ethanol and 69 % selectivity to hydrogen at 300 °C [203]. Adding magnesium appeared to significantly decrease the activity of the catalyst (less than 75 % conversion) while in case of sodium as a promoter, it allowed a total conversion of ethanol with 72 % of hydrogen formed.

Another factor seems to be important in this oxidative steam reforming reaction of ethanol is the catalyst reduction temperature. Indeed, the interactions will not be the same depending on it. Casanovas [204] investigated this issue using a zinc oxide-supported palladium catalyst with a reduction temperature of 225 °C, 90 % conversion was achieved while with a higher temperature (450 °C), only 84 % of ethanol was converted. This trend was confirmed by the drop of hydrogen selectivity from 56 % to 48 %.

Moreover, the effect of H_2O on oxidative steam reforming of ethanol is similar to that of O_2, but is less obvious. The most significant impact is on the ethanol conversion. When the ethanol/water ratio increases, the ethanol conversion increases too (this is true for low O/C values or smaller O_2 content). It has a limited effect on the yield of H_2 and all other product selectivities. It was found that when increasing H_2O/ethanol molar ratio from 3.0 to 5.0 led to a decrease in acetaldehyde and ethene formation [205]. These results were in agreement with the studies of Dömök et al. [206], who investigated that increasing the H_2O/ethanol molar ratio from 3.0 to 9.0 led to a decrease in ethene production during OSRE over alumina-supported Pt catalysts. water inhibits the dehydration of ethanol, and thus limits the amount of ethene produced. Kugai et al. [207] also noticed that the addition of water and oxygen over Ni/CeO_2 catalyst increased the ethanol conversion for ED, SR, POX, and OSR.

The reaction temperature has to be taken into account, in particular too, since for reaction temperatures lower than 450 °C, hydrogen yield profiles recorded over the Pt-Ni and Ni-Co samples exceeded equilibrium predictions [171]. It has been reported that the reaction mechanism being very complex, at intermediate temperatures, the hydrogen yield deviated from thermodynamics because the system was not capable to reach equilibrium values kinetically. Previous studies [194] demonstrated that, in this temperature range, the reaction rate of water gas shift was higher than methanation, which also resulted in a methane concentration lower than that predicted by thermodynamics.

Overall, many factors have been studied and each of them can either promote or be unacceptable for the reaction.

IV.2.2.2 With transition metals

Good catalytic performances (in terms of hydrogen yield and stability over time) could be assured by the optimization of the catalyst formulation and optimal operating conditions [208, 209, 210]. Using transition metals as an active phase in comparison with noble metals under same conditions (and both having alumina as a support) gave a lower conversion of ethanol than that using noble ones [211].

It was revealed [200, 212] that the choice of the chemical support strongly affects the deactivation due to the carbon formation in addition to the conversion of ethanol and selectivity to hydrogen. For example, it was found that $Ni_xCu_yCs/LiAlO_2$ catalyst allowed higher hydrogen percentage than Ni_xCu_yCs catalyst due to the effect of support material. In addition, $Ni_xCu_yCs/LiAlO_2$ led to the highest hydrogen production at 600 °C with low and high H_2O/EtOH molar ratios (1.85 and 9) [213]. In general, acidic supports such as Al_2O_3, stimulated the dehydration of ethanol to ethylene which is the common precursor of coke [137], while basic supports such as MgO were resistant to coke deposition [214]. Redox supports such as ZrO_2 and CeO_2, possess a high oxygen storage capability, high oxygen mobility and were reported as active in the WGS reaction [187]. In fact, ceria, too, has a considerable role in catalysts used for reforming because it possess an oxygen storage capacity (OSC), a redox ability [215], and $Ce^{3+} \leftrightarrow Ce^{4+}$ transformation [216]. In fact, some rare earth oxides (such as CeO_2 or ZrO_2) possess a redox ability and an oxygen storage capacity (OSC) which can promote the oxidation of the deposited carbon on the surface of the catalyst and thus increasing the activity in the reforming processes [217].

The oxidative steam reforming results indicated that O_2 plays an important role in altering the catalytic behavior [218]. O_2 effectively promoted the ethanol conversion, which in turn led to an increase in the yield of H_2, and affected the reaction path, which in turn increased the selectivities of CH_4, CO and CO_2. If the O_2 content was increased excessively, it could oxidize CH_4 and CO, and thus diminishing their selectivities; both are converted to a fully oxidized product CO_2. This excess oxygen value decreased slightly the yield of H_2.

To add, temperature is also a key parameter in this process. At low temperatures below of 300–400°C, it has been shown that acetaldehyde, acetone, and methane were formed [219] In fact, ethanol dehydrogenation to acetaldehyde took place and the acetaldehyde formed was further

decomposed to methane and carbon monoxide or was converted to acetone by condensation. CO furtherly reacted with water to produce H_2 and CO_2 through the water–gas shift reaction. As a result, at these temperaturesethanol, acetaldehyde, and acetone will entirely be reformed into H_2, CO_2, CO, and CH_4. The main reactions were dehydrogenation of ethanol to acetaldehyde and methanation due to reaction of CO and CO_2 with hydrogen. However, by increasing the temperature, selectivities to methane and acetaldehyde decreased, hydrogen production is favored and carbon formation is less favored. Other studies were performed to show the effect of reaction temperature on OSRE process [220]. $Cu_{0.93}Ni_{2.99}Zn_{0.81}Al$ catalysts were prepared by coprecipitation method and H_2O/ethanol ratio of 3 with O_2/ethanol ratio of 0.4 were used in the OSRE at temperatures between 220 °C and 300 °C. Using this catalyst, it has been shown that with increasing reaction temperature, ethanol conversion increases, the selectivity of CH_3CHO deacreases while that of CH_4 increases in parallel to ethanol conversion indicating that CH_4 is favored by increasing reaction temperature. Selectivities to CO remains unchangeable while that of CO_2 increases to a large extinct above temperatures of 270 °C.

It has also been demonstrated that the metals dispersion on the catalytic surface strongly affects the resistance of the catalyst to the carbon deposition. The size of metallic Ni particles is a main factor to prevent coking [221] . And hence, in the same pathway, it has been proved that the use of substrates capable to enlarge the support significantly improved both activity and stability of the catalytic formulation. To better understand this phenomenon the nature of active species were studied on $Cu_{1-x}Ni_xZnAl$ mixed metal oxide catalysts [222]. The existence of Cu^{2+}, Ni^{2+} and Zn^{2+} ions on calcined materials were observed by core level and valence band XPS as well as Auger electron spectroscopy. Upon reduction at certain temperatures, the Cu^{2+} is fully reduced to Cu^0, while Ni^{2+} and Zn^{2+} were partially reduced to Ni^0 and Zn^0, respectively, as well as the nature of ZnO on Cu-rich catalyst changed from crystalline to amorphous after reduction. The concentration of Ni^0 and Zn^0 increased during reduction with decreasing Cu-content. It has been shown that the density of states at Fermi level increased dramatically for Ni-rich catalysts and this influenced the products selectivity.

Both Ni and Co-based catalysts have been reported as interesting formulations for ethanol reforming, due to their capacity in promoting C–C, C–H and O–H bond cleavage [89, 223]. The performances of nickel-based catalysts could be further used by the synthesis of bimetallic formulations of catalysts [225]. In a previous study [226], it was demonstrated that bimetallic formulations supported on CeO_2-SiO_2 assured the lowest carbon formation rates among the

recent literature under oxidative reforming. In addition, interesting performances for the oxidative ethanol steam reforming process were also reported for nickel-cobalt bimetallic catalysts supported on complex/acid oxides [227-229] (including MgAl prepared from hydrotalcite precursors, $LaFeO_3$ perovskites, Al_2O_3).

It should also be noted that the way of preparation of the catalysts plays an important role in the catalytic performance. Researches have shown that among sol-gel, plasma, wet impregnation and co-precipitation method, the sol-gel process was the best one [109, 230-232]. It was also demonstrated that for nickel supported on alumina catalysts prepared by sol-gel procedure under supercritical drying achieved the highest activity and had higher nickel dispersion and thermal stability than those catalysts synthesized by conventional methods such as impregnation. This method gave a better control in the physicochemical properties of catalysts such as surface area, particle size and porosity. Many works have used plasma treatment on the preparation of catalyst at low temperature to improve the metal dispersion and the catalytic stability but in fact they prevent the growth of metal/support particles at the same time.

Regarding the catalytic ability in conversion of ethanol and the selectivity to hydrogen, first of all, it's interesting to see the influence of the support. Sato [233] used nickel (at 5 % by mass) impregnated on ceria then the same nickel is supported on a cerium modified with zirconium. The reaction took place at a particularly low temperature of 100 °C. With an $EtOH/H_2O/O_2$ ratio equal to 1:8:1 on 200 mg of catalyst, 87 % conversion of ethanol was obtained whatever the surface area was, and substantially identical hydrogen yields without and with zirconium in the support.

Another parameter that affects the catalytic reaction in the oxidative steam reforming process is the mass percentage of the active phase. It has been reported before that by increasing the percentage of active phase (in this case CuO on ceria prepared by co-precipitation method) from 10 to 40 %, hydrogen decreased in the products distribution from 39 to 32 % under a reaction temperature of 300 °C [234]. The conversion of ethanol was not mentioned, however what was interesting here was that very low amount of CO was formed which was proved by gas phase chromatography.

In the same attempt to see the effect of active phase [220], some researches were doneon CuNiZnAl catalysts with different Cu:Ni atomic ratio prepared by coprecipitation. . At 300 °C, and a reaction mixture with a ratio of $EtOH/H_2O/O_2$ equal to 1:3:0.4, up to 95 % conversion of

ethanol was obtained for a catalyst having as its active phase copper and nickel and up to to 3.7 moles of hydrogen per mole of ethanol for a catalyst composed of copper and cobalt. Kugai [207] used ceria as a carrier and nickel as the active phase. With a temperature of 300 °C, while the percentage of hydrogen is relatively the same regardless to the active phase (varying between 42 and 50 %) it resulted in up to 92 % conversion of ethanol for Ni (10 %) as an active phase. Finally, with regard to the influence of the active phase, Wang [235] was interested in the influence of the percentage of different elements in $La_xCa_{1-x}Fe_xCo_{1-x}O_3$ mixed oxides and at a temperature of 400 °C with only 75 mg of catalyst, 84 % conversion of ethanol was obtained for x = 0.7 versus 80 % for x = 0.5. On the other hand, with regard to the percentage of hydrogen, the opposite effect was observed (79 % for x = 0.5 against 76 % for x = 0.7).

The addition of a promoter has also been analyzed by different researchers. Tests were done [236, 217] using 30 % by weight of nickel, with or without addition of cobalt, copper or calcium, supported on $Ce_{0.74}Zr_{0.26}O_2$. The average crystallites sizes of NiO and of $Ce_{0.74}Zr_{0.26}O_2$ measured by XRD were of 17.3 nm and of 12.5 nm, respectively. Without addition of another element, the conversion of ethanol reached 90 % and this conversion reduced up to 30 % in case of addition of cobalt, up to 61 % in case of addition of calcium but increased by 1 % if copper was added. It should be noted, however, that in all three cases the hydrogen yield decreased. Nickel seems to be better than the other elements. The influence of potassium addition in a cerium-supported cobalt catalyst was analyzed [237]. At 420 °C, 56 % of EtOH conversion was obtained without potassium against 78 % when 2 % of potassium was added. The percentage of hydrogen increased by 10 %, from 50 to 60 % hydrogen with added potassium, after 35 hours of reaction.

In the UCCS laboratory cerium and nickel [96, 97, 210] and magnesium, aluminum and nickel based catalysts were studied [238], and in particular in their oxyhydride form. These catalysts have shown high performances with low input of energy as a very low furnace temperature of 50-60 °C could be used. With only 30 milligrams of catalyst, and an $EtOH/H_2O/O_2$ ratio of 1:3:1.6, a total conversion of ethanol and 45 % of hydrogen in the products distribution were obtained after 75 hours test.

IV.3 Autothermal steam reforming

The combination of steam reforming and partial oxidation is known as autothermal reforming (ATR). In ATR, the energy required by the reforming reactions is provided by exothermic

oxidation reactions, and thermally sustained operation is achieved together with optimized H_2 production.

This is a special case of the oxidative steam reforming of ethanol. It is the case where that the heat generated by the partial oxidation reaction is used integrally to convert ethanol into hydrogen and CO_2 and hence the enthalpy of reaction is zero (equation 13).

$$C_2H_5OH + (3\text{-}2\,\delta)\,H_2O + \delta\,O_2 \rightarrow (6\text{-}2\delta)\,H_2 + 2CO_2 \quad \Delta_rH^\circ \approx 0 \text{ kJ / mol} \qquad \text{(equation 13)}$$

The above equation displays the chemical equation for ATR of EtOH (EATR). ATR process can be achieved by controlling the molar ratio of reactants. When the value of δ is equal to 0.5, 5 mol H_2 could be produced from 1 mol EtOH, and ΔH equals to − 68.06 kJ/mol. As a result, the reaction will not require extra energy from an external environment.

The catalyst is one of the most important factors of ATR. The noble metals such as Rh [239], Ru [240, 241] and Pt [242, 243] catalysts exhibited a high activity and anti-coke capability during reforming reactions. Noble metal catalysts showed better performance than their non-noble metal counterparts [203]. Rh showed better activity in terms of ethanol conversion, selectivity and stability among other noble metals found in literature. They might be doped with other non-noble metals for capturing favorable effects [244]. However, the high price of noble-metal materials is diminishing their application.

As a reason, transition metals such as Ni, Co, Cu [183, 245, 28, 214] are becoming more used due to their affordable cost and promising properties. Typically, Ni and NiO exhibit excellent abilities for C-C, C-H and C-O bonds breaking, and dehydrogenation. However, Ni-based catalysts are easily deactivated by formation of coke, which constrains their application [246] .

It is necessary to formulate a new catalyst to overcome coke deposition. In some researches, La has been reported to increase the activity of Ni-based catalysts and increasing its lifetime. Moreover, $LaNiO_3$ formed by the interaction between La_2O_3 and NiO, favors the reactions of dehydrogenation, decomposition of hydrocarbon and water gas shift reactions [196, 221] that are very important in the ATR process. In addition, $LaNiO_3$ provides a better dispersion of Ni, and more active sites than those provided by single NiO [246].

Moreover, it has been investigated that the performance of monometallic Ni catalysts in autothermal steam reforming is less than those of bimetallic ones. Frusteri and Youn have also shown that these bimetallic and alloy catalysts are known to be highly active in the production

of H_2 and have an advantage over monometallic Ni catalysts (e.g., Ni/Al_2O_3 [28], Ni/CeO_2, Ni/MgO [214], and Ni/ZrO_2 [247, 248] in autothermal reforming of ethanol. Similarly, recent studies performed on bi metallic CuO-NiO based catalysts showed that addition of CuO provided better performance in hydrogen production and could reduce the reforming temperature used [249].

Tests have shown that CeO_2 can improve the activity of WGS reaction which is important in ATR process [245]. It has been investigated by some researchers [240] that reactions of ethanol over CeO_2 were re-combinative desorption of ethanol, dehydrogenation to acetaldehyde and dehydration to ethylene. The use of $Ru/Ce0_2$ catalyst changed the reaction direction of ceria towards ethanol, and modified the desorption products to CO, CO_2, CH_4 and H_2. Active species can change the selectivities of the catalyst with CeO_2 as its carrier.

Researchers are trying to add promoters to improve the catalyst activity in ATR process and the latest one is based on ordered mesoporous Ni-xSm-Al-O catalysts [250]. Sm was added to promote the catalyst and thus provide resistance to oxidation, sintering and coking, this improved reactivity and durability can be attributed to basic Sm oxides and ordered mesoporous framework with confinement effect. The basic sites promote the adsorption and activation of HAc, and the ordered mesoporous framework constrains the thermal agglutination of Ni metal and formation of coking.

IV.4 Poisoning of catalysts and coke formation

The stability of catalysts for reforming and partial oxidation of hydrocarbons is extremely important [159]. The deactivation and regeneration of catalysts may be caused by several chemical, thermal and mechanical factors which have been investigated by Argyle et al. [251].

The major challenge for reforming and partial oxidation is the poisoning by impurities (specially by sulfur). It has been reported that Rh/CeO_2 catalyst exhibits a higher tolerance to sulfur than Ni/CeO_2 catalyst, this is due to the existence of O^{2-} species in the former. The O^{2-} species can promote the oxidizing of sulfur into SO_x [252] .

Coking is also a problem and mainly at low oxygen partial pressure. The intermediate reactions occurring during ethanol steam reforming that can be responsible for the formation of carbon on the surface of the catalyst, and leading to deactivating are reported in equations 14-21 [28]:

$C_2H_6 \leftrightarrow 3\ H_2 + 2\ C$ (equation 14)

$C_2H_4 \rightarrow Coke \rightarrow 2\ C + H_2$ (equation 15)

$C_2H_4 \leftrightarrow 2\ H_2 + 2\ C$ (equation 16)

$CH_4 \leftrightarrow 2\ H_2 + C$ (equation 17)

$2\ CO \leftrightarrow CO_2 + C$ (equation 18)

$CO + H_2 \leftrightarrow H_2O + C$ (equation 19)

$CO_2 + 2\ H_2 \leftrightarrow 2H_2O + C$ (equation 20)

$2\ CH_3COCH_3 \rightarrow CH_2COHCH_3 + CH_3COCH_3 \rightarrow (CH_3)_2\ C\ (OH)\ CH_2COCH_3 \rightarrow (CH_3)_2C{=}CHCOCH_3$ (Mesityl Oxide) $+ H_2O$ (equation 21)

Regarding the nature of carbon deposits formed during the ethanol steam reforming process, it was reported to be of amorphous and/or filamentous forms [95, 253]. The amorphous carbon led to severe deactivation in comparison with filamentous carbon [254]. Graphitic form of carbon could be produced by direct deposition of carbon in the vapor phase or by heat treatment of amorphous carbon [255]. The formation of carbon nanotubes on the surface of reacted cobalt hydrotalcite catalyst after performing the ESR have been reported [256]. In addition, De Bokx et al. studied production of filamentous carbon from CO and CH_4 using catalysts based on iron and nickel in the 650–1000 K temperature range and showed that carbon was deposited as a metastable carbon intermediate, leading to filamentous carbon on decomposition [257]. It was reported that filamentous carbon has higher mechanical strength than others and so it has the capability to completely disintegrate the support of the catalyst [258] .

Temperature plays an important role in carbon deposition but the available information is that the carbon deposition is governed by different kinds of reactions at different temperatures and hence is not easy to consider. Low reaction temperatures favor the formation of carbon through the Boudouard reaction and reverse of carbon gasification. However, carbon formation via methane decomposition is the main route at high temperature [51, 52, 95, 164]. The mechanism of coke formation over supported Ni catalysts during steam reforming of methane is well described in the literature [29, 259, 26]. Methane dissociates on nickel surface, producing highly reactive carbon species which may undergo a number of processes, including reaction with water; encapsulation of the Ni particle surface [260], or dissolution in the Ni crystallite followed by the nucleation and growth of carbon filaments [32] (e.g., whiskers). On other hand, at high temperature Boudouard reaction reversed but carbon deposition was enhanced through decomposition of hydrocarbons [261] (Equations 14 and 17).

It has also been shown that acidic supports promote formation of coke precursors. And so, alkali (Li, Na, K and Cs) and alkaline metals (Ca, Mg and Sr) having a basic character could neutralize acid sites for an effective approach [80]. Integration of CaO and MgO has been shown to decrease the amount of coke deposition as well as affect the nature of coke formed [132, 133]

Molar ratio of ethanol and water in the feed during ethanol steam reforming can influence the yield, selectivity and deactivation of catalyst. In fact, at high temperature, water gas shift reaction leads to increase in hydrogen productivity and decreasing carbon deposition although it requires high energy consumption [262]. When the concentration of water was higher than stoichiometric quantity, it had an inhibitory effect on coke formation [263, 264] . This was also validated by the study on different molar ratio concentration over Rh catalyst for 100 h time on stream. The molar ratio of water and ethanol lower than stoichiometric ratio led to deactivation after 4 h of operation. The effect of higher ethanol to steam ratio for ESR was also experimentally approved over Ni catalyst on different support (La_2O_3, γ-Al_2O_3, La_2O_3/γ-Al_2O_3) [137].

The nature of the active phase plays an important role in enhancing the coke deposition. For example, it has been reported that noble metals were more resistant to carbon deposition than non-noble metals and among noble metals, Rh known to have high activity towards C–C and C–H bond cleavage [120] promoted hydrogenation reaction and in turn led to very low carbon deposition. Rh also had the ability to prevent carbonate formation and so oxygen vacancies could be accessible for oxidizing carbon [265]. Nevertheless, Pt catalyst supported over different oxides (CeO_2, Al_2O_3, ZrO_2) showed significant amount of carbon deposition during the ethanol steam reforming process. Au catalyst was more stable compared to Pd over SiO_2 supports [266]. Regarding Ir catalysts supported over CeO_2 and PrO_x doped CeO_2 did not show deactivation during ESR at temperatures of 623 K and 923 K, respectively [267, 268].

Preparation methods affected the dispersion of active phase and metal support interaction and thus affected coke formation during the process [269]. For example, this has been shown by Rossetti et al. who investigated the effect of support (SiO_2) preparation method on carbon deposition [270].

Good metallic dispersion and the possible formation of metallic oxide solid solutions along with strong metal-support interaction gave rise to long-lived catalysts maintaining their good activity and selectivity towards hydrogen production [120]. This phenomenon was investigated on

catalysts were Co^{2+} was incorporated into the lattice structure of the solid solution [271]. Similar effect was proved on the $Ce_{1-x}La_xO_{2-\delta}$ (CL) solid solution supported Rh catalysts, but only for the 1 % Rh/CL catalyst. The Rh species were well-dispersed on the support and formed a $Rh_2O_3//Ce_{1-x}La_xO_{2-\delta}$ interface structure. As a result, good dispersion of Rh and oxygen and hydrogen mobility were obtained on these catalysts to finally give better performances among other catalysts tested under same conditions varying x [272].

There are some techniques to remove formed carbon and regenerate the catalyst. It has been demonstrated that it is feasible to regenerate the catalyst with an air steam at around 750 °C for a Ni catalyst [273] . Montero et al. [274] reported reproducible performances of Ni catalyst in ESR under reaction-regeneration cycles. The regeneration was carried out by coke combustion with air for 2 h at 550 °C followed by the catalyst reduction at 700 °C under H_2. The reaction mechanism, catalyst modification and regeneration process have been extensively examined, however the catalytic stability remains an open issue for practical applications. In fact, the use of oxygen decreases the production of methane and coke which increases in turn the lifetime of the catalyst.

IV.5 Mechanism of oxidative steam reforming

Recently, different mechanistic schemes for ethanol reforming have been proposed over the catalyst surface [23, 28, 275-277]. The active site and mechanism are still under controversy. There are many mechanisms and reaction pathways illustrated for overall reactions taking place during steam reforming of ethanol and numerous researches are performed to find and understand the active sites with the objective to develop performant catalysts [278-283]. Therefore, an advanced knowledge of the reaction mechanism is fundamental for the improvement of catalyst formulations and processes. This is due to the complications in different catalyst's constituents and reaction conditions (such as reaction temperature, feed composition and residence time). The generally acknowledged reaction steps primarily include [28]:

Ethanol dehydrogenation to acetaldehyde: $C_2H_5OH \rightarrow C_2H_4O + H_2$ (equation 22)

Ethanol decomposition to CH_4, CO and H_2: $C_2H_5OH \rightarrow CH_4 + CO + H_2$ (equation 23)

Acetaldehyde decomposition to CH_4 and CO: $C_2H_4O \rightarrow CH_4 + CO$ (equation 24)

Methane steam reforming: $CH_4 + H_2O \rightarrow CO + 3H_2$ (equation 25)

Water gas shift: $CO + H_2O \rightarrow CO_2 + H_2$ (equation 26)

It fact, the water gas shift reaction taking place plays a key role in the oxidative steam reforming process as it has been shown that the more WGS taking place, the better the yield of hydrogen. However, despite the good WGS activity in some catalyst, it has been shown on some catalysts a deactivation due to the increased tendency in formation of soft carbonaceous residues. This is mainly due to the low bond cleavage activity of active phase and their low gasification rate [284].

Depending on the properties of the active metal and the support many other side reactions can occur, thus resulting in coke formation and decrease in hydrogen yield [58]. The possible side reactions might be: ethanol dehydration to ethylene, ethylene polymerization to coke, acetone formation via acetaldehyde condensation, followed by decarboxylation, methane cracking, Boudouard reaction and reverse of carbon gasification.

It has been already shown that the nature of the metal and the support selected greatly affected the final products distribution. The influence of active metal on the ethanol conversion pathways by temperature-programmed desorption (TPD), infrared spectroscopy (FTIR) in steady state conditions was investigated by Sheng et al. [285] and it has been investigated that adsorbed ethanol is dissociated to form ethoxide species that are then oxidized into acetaldehyde on Pt or Pd metals. However, Rh based compounds showed a deviation from this pathway. One H atom from the terminal (methyl) group of ethoxide species was lost and adsorbed in a cyclic configuration onto the surface (a five-membered-ring oxametallacycle intermediate) [286]. Further decomposition of these species led to the production of CO and CH_4. Adding Pt to Rh based catalyst promoted the hydrogen formation because Pt metal accelerated methane transformation into hydrogen. It has been elucidated that Rh had the ability to reduce the intrinsic activation barrier for C–C bond dissociation more than that of Pd or Pt [287]. In addition, the d electrons of Rh shared more antibonding orbitals of ethoxide than those of Pd and Pt, thus giving a higher capacity of C–C bond cleavage. Au/CeO_2 catalyst showed lower CO to CO_2 ratios compared to those of Pt/CeO_2 samples suggesting the WGS reaction had a higher rate over Au based catalyst. In fact, it is known that the production of CO is favored at high temperature from a thermodynamic point of view [288]. This can occur based on the following reactions:

$$CH_3CHO \rightarrow CH_4 + CO \qquad \text{(equation 22)}$$

$$CH_3CH_2OH \rightarrow CH_4 + CO + H_2 \qquad \text{(equation 23)}$$

$CH_4 + H_2O \rightarrow CO + 3H_2$ (equation 24)

It was also revealed that Rh catalysts presented the highest hydrogen selectivity and Ru promoted the formation of acetaldehyde [289]. The effect of active metals supported on the same Al_2O_3 support was studied on Ru, Pt, Rh and Pd to show that the H_2 selectivity decreased in the following order: Rh≥Pt>Ru≈Pd while acetaldehyde selectivity followed the reversed order [290].

Furthermore, a relationship between support properties and both dehydrogenation to acetaldehyde and dehydration to ethylene was revealed. In general, a high basicity of sites, Madelung potential of O anion, metal cation-oxygen anion bond energy, and high oxygen electronic polarisability of the support promoted dehydrogenation more than dehydration [287, 291, 292, 293].

Other researches have been conducted to find the mechanisms for the OSR process however it is complicated to find a global mechanism which differs from one catalyst to another and depending on conditions. Since Rh and Ni have shown best catalytic performance in bio ethanol reforming towards hydrogen production, researches aimed to search for mechanisms occurring in OSRE based on these elements [28]. Starting from Rh, some results showed that the O-H bond of adsorbed ethanol initially dissociated to form surface ethoxy (CH_3CH_2O*, * denoting an adsorbed species); [294] the C-H bond then cleaved and led to the formation of acetaldehyde (CH_3CHO*) and oxametallacycle (CH_2CH_2O*). This surface oxametallacycle could be the key intermediate for the cleavage of the C-C bond in the reforming process [295]. The surface oxygen (O*) promotes the cleavage of O-H bond of ethanol to form ethoxy and also altered the reaction path. This have been investigated on a Rh(100) surface [285].

Under high oxygen content, the key intermediates became acetaldehyde and acetate (CH_3COO*), instead of oxametallacycle. In addition, it was indicated that the surface O* can promote the oxidation of the key residue CH* in the ethanol decomposition and played a crucial role in the OSR of ethanol [296, 297].

A proposition for active site modeling has been reported previously on some mixed oxides containing Ni in UCCS laboratory [96, 97, 105, 157, 210]. It was shown that after H_2 treatment the solids contain anionic vacancies generated by elimination of H_2O (Equation 25) able to capture/receive hydrogen in the form of hydride. Hydrogen can be heterolytically dissociated on an anionic vacancy and an O^{2-} species of the solid (Equation 26).

$2OH^- \rightarrow O^{2-} + \square + H_2O$ (equation 25)

O^{2-} Mn+ □ + H_2 → OH^- Mn^+ H^- with □: anionic vacancy. (equation 26)

The dehydrogenation reaction of ethanol necessitates the abstraction of hydrogen species from ethanol, with the cleavage of C–H bond (rate determining step) [26, 31, 33, 34, 36, 37]. It was shown that the active sites involved Ni cations in strong interaction with other cations, anionic vacancies and O^{2-} species of the solid which could perform the heterolytic dissociation of ethanol (Equations 27 and 28) leading to the production of acetaldehyde and H_2 (Equation 28). At high O_2/EtOH ratios (1.6), acetaldehyde was easily transformed. Moreover, the hydride species could highly react with oxygen by an exothermic reaction that could generate hydroxyl groups (Equation 29). Since it has already been proved that OH^- groups promote CO transformation into CO_2 by water gas shift (Equation 12) [99], these hydroxyl groups could transform ethanol into CO_2 and H_2. Moreover, water could also dissociate in the presence of an anionic vacancy and an O^{2-} species of the solid (Equation 30). This could be achieved when Ni^{2+} species were stabilized in strong interaction [298]. The hydride species could react with O_2 due to their high reactivity to generate hydroxyl groups (equation 19) and then finally transformation of hydroxyls groups into the selective O^{2-} species would regenerate the active site (equation 15).

O^{2-} Mn^+ □ + C_2H_5OH → OH^- Mn^+ H^- + C_2H_4O (equation 27)

$OH^-Mn^+H^-$ + CH_3CH_2OH → $OH^-Mn^+H^-$ + CH_3CHO + H_2 (equation 28)

H^- + 0.5O_2 → OH^- (equation 29)

H_2O + O^{2-} + □ → $2OH^-$ (equation 30)

$2OH^-$ → O^{2-} + □ + H_2O (equation 31)

Based on what have been stated in this bibliographic review, several important factors emerged based on the type of material and experimental conditions used for oxidative steam reforming of ethanol. Dealing with these factors, different tendencies arise towards ethanol conversion, hydrogen production, products distribution and carbon formation.

In our UCCS laboratory, several transition metals in mixed oxides based on nickel and cerium have been studied due to their very good reactivity in hydrogenation [339] and also in partial oxidation of methane and propane [336, 351]. It has been shown that on $CeNi_1O_y$ calcined mixed oxide, oxyhydride formed by partial reduction in hydrogen allowed high performance in OSRE [96]. The solid, once treated under H_2, became a H_2 reservoir and exhibited active sites allowing catalytic activity at low temperature. The catalyst showed interesting results and high performance in OSRE under a low temperature of 60 °C (knowing that the starting temperature was 200 °C). This was explained by the chemical energy produced by the reaction between hydride species stored in the catalyst during pretreatment and oxygen. However, carbon was formed. Playing on the chemical formulation of the catalyst with different Ni/Ce molar ratios, carbon formation and products distribution could be varied [97]. The only way to drastically decrease and even eliminate carbon formation in OSRE was by optimizing the preparation method, allowing to get highly performant catalysts at 50 °C [299]. However, the total elimination of carbon formation required higher starting temperature of 265 °C which led in the meantime to reduce the percentage of hydrogen gas (34 %) in the products distribution.

The catalysts used, in this study, to reform bioethanol into hydrogen are therefore nickel and ceria based. Nickel is an inexpensive metal, and an excellent catalyst for breaking bonds C-C, but unfortunately allows for carbon formation. However, to avoid the formation of carbon it has been reported that a good dispersion of the metal can considerably reduce the carbon formation. We chose to use ceria in our catalysts for better catalytic performance with good stability and high hydrogen selectivity due to mainly to the redox properties of this support. The use of CeO_2 should allow rapid oxygen transfer as well as oxygen renewal of the defective surface. The ceria has a fluorite structure (a relatively open structure allowing easy diffusion oxygen). It is also an ionic oxide of basic character which can be obtained with great specific area with particles the size of the nanometer. The interaction of a polar molecule such as ethanol with the surface of CeO_2 can be promoted through a dipole-dipole type bond. This type of interaction is better known as an acid-base interaction, thus forming the species ethoxy and a hydroxyl species [286].

The objective of this study is to develop highly active and stable catalysts, produce H_2 at low temperature, achieve high selectivity to H_2 and CO_2 without carbon formation while maintaining high ethanol conversion and relate between catalytic performance and chemical properties of the catalyst. To achieve this, $CeNi_x(M_{0.5})O_y$ catalysts are prepared by coprecipitation method (See Annex) and doped or not with Al or Zr for this thesis work. The catalysts are treated or not at temperatures between 200-500 °C. All the catalysts prepared are analyzed by different characterization methods. Concerning the catalytic conditions, the flow rate of water-ethanol mixture is fixed at 0.1ml/min and that of nitrogen and oxygen at 60 ml/min. The water/ethanol molar ratio is fixed at 3 and the influence of that of oxygen/ethanol is studied and varied between 1.4-1.7. The temperature of the reactor oven is fixed at 50 °C after starting the reaction at 200 °C.

Chapter II: Oxidative steam reforming of ethanol

Ni and Ce based catalysts are the most attractive and extensively studied systems for oxidative steam reforming of ethanol. In our laboratory, several mixed oxides based on nickel and ceria have been studied in oxidative steam reforming of ethanol (OSRE) leading to interesting results in terms of ethanol conversion, products distribution and stability of the catalytic system [25, 96, 97, 105]. Zirconium and aluminum are also known for their good physical and chemical properties such as strength, toughness and thermal stability when considering performance in OSRE [187, 210, 229, 300]. In the present study, $CeNi_xO_y$, $CeNi_xZr_{0.5}O_y$ and $CeNi_xAl_{0.5}O_y$ catalysts where x = 0.1, 0.5, 1, 2 or 5 (dried and calcined) are prepared by co-precipitation method (See Annex) and studied in the oxidative steam reforming reaction of ethanol (OSRE). The following chapter studies these catalysts under different conditions in OSRE to analyze the influence of the nickel content, the addition of a dopant, the effect of calcination, pretreatment temperature in H_2, mass of catalyst, and oxygen over ethanol ratio. Many researchers have studied the reaction with an H_2O/EtOH ratio equal to 3 because it corresponds to the stoichiometry of the ethanol vapor reforming reaction, and this factor will be kept constant. Without precision, the mass of catalyst used is of 30 mg and the reactions are started with an oven temperature of 200 °C that is then immediately decreased and fixed at 50 °C. In all the experiments the liquid flow rate of this mixture is fixed at 0.1 ml/min. The experimental details are given in the Annex.

II.1. Oxidative steam reforming with O_2/EtOH ratio = 1.4

In the literature, a low oxygen over ethanol ratio (generally ranging from 0.3 to 0.5) is predominantly used [179, 191, 192, 207, 234, 235, 301-305,]. However, at this ratio high reaction temperatures are required. The present study focuses on low temperature OSRE, therefore higher O_2/EtOH ratio is used [202]. A ratio of O_2/Ethanol of 1.4 is used to test the performances of binary dried and calcined $CeNi_xO_y$ and $CeNi_xZr_{0.5}O_y$ catalysts *in-situ* pretreated in hydrogen over night at 250 °C. These catalysts are divided into 2 parts: dried (d) catalysts collected directly after preparation and drying process and calcined (c) catalysts subjected to a calcination at 500 °C for 5 hours in air.

II.1.1 Binary catalysts

Binary catalysts of $CeNi_xO_y$ are studied first in this section.

II.1.1.1 Binary calcined catalysts

The binary catalysts are tested in OSRE conditions at an O_2/Ethanol ratio of 1.4 to show their performance in low temperature. Figure 4 represents ethanol conversions and products distribution (%) obtained for the $CeNi_xO_{y\ (c)}$ compounds, where x = 0.5, 0.7 and 1, during 5

hours in OSRE. Conversion of O_2 not reported is total. In Figure 4-a, a weak performance is observed for $CeNi_{0.5}O_{y\,(c)}$ catalyst where this catalyst is only active for around 3 hours under these reaction conditions. The stability of the catalyst during the 3 hours is low with incomplete ethanol conversion of 87 % with unstable values for the main products (H_2 and CO_2) and the byproducts (CO, CH_4 and CH_3CHO) distribution. Similarly, for $CeNi_{0.7}O_{y\,(c)}$ catalyst shown in Figure 4-b the OSRE reaction is not stable and the catalyst deactivates after around 4.5 hours lasting slightly for more time than the $CeNi_{0.5}O_{y\,(c)}$ catalyst (Figure 4-a). Ethanol conversion is fluctuating between 80 and 94 % with 46 % H_2, 32 % CO_2, 16 % CO, 1.1 % CH_4 and 3.9 % CH_3CHO in products distribution.

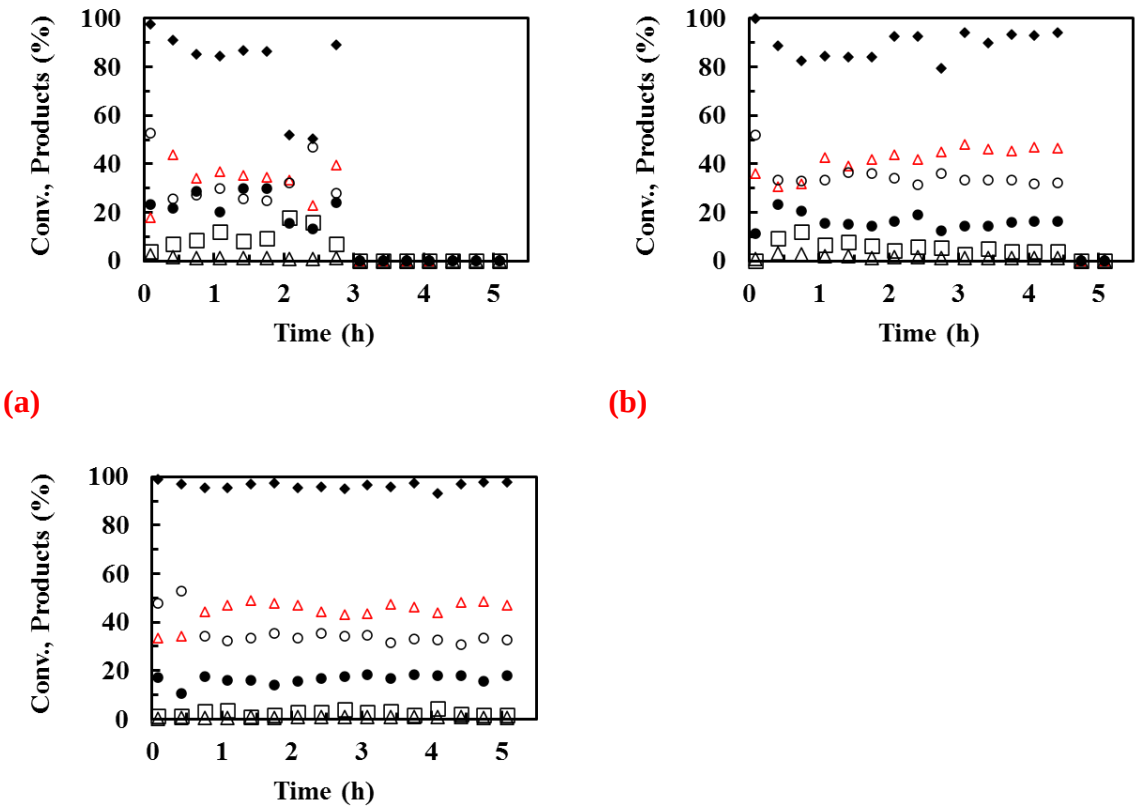

Figure 4 Ethanol conversion (◆) and products distribution (H_2 △, CO_2 ○, CO ●, CH_4 △, acetaldehyde □) on $CeNi_xO_y$ calcined catalysts *in-situ* pretreated in H_2 at 250 °C. a) x = 0.5, b) x = 0.7 and c) x = 1. Conversion of O_2 not reported is total ($EtOH/H_2O/O_2/N_2$ = 1:3:1.4:N_2).

However, with $CeNi_1O_{y\,(c)}$ catalyst (Figure 4-c), no deactivation is observed which is may be related to the higher Ni content in the compound. A more stable and higher conversion of ethanol of almost 98 % is achieved within 5 hours of reaction. Among the products distribution,

H_2 formed is of about 47 %, CO_2 is at around 32 % with 17 % CO, 2.6 % acetaldehyde and 0.7 % CH_4. Obviously, the Ni content has a major effect in the ethanol oxidative steam reforming reaction and the increase has main consequence on the catalyst stability in low temperature operation conditions in addition to considerable consequences on the products distribution and ethanol conversion.

In the literature, J. Kugai also observed on a Ni-Rh / CeO_2 catalyst an increase in conversion at 300 °C (85 % to 92 %) when the nickel content increased (5 % to 10 % by mass), but with a decrease in the formation of H_2 [207]. Here, in the used conditions, with an increased Ni content, the catalyst lasts in OSRE without deactivation.

II.1.1.2 Binary dried catalysts

OSRE studied on different $CeNi_xO_{y\,(d)}$ catalysts without previous calcination are reported in Figure 5. First, an analysis is carried out with $CeNi_{0.7}O_{y\,(d)}$ catalyst and the results are reported in Figure 5-a. With this Ni content, the reaction is deactivated after 2 hours only, in addition to the incomplete ethanol conversion during this time and the unstable products distribution of H_2, CO_2, CO, CH_4 and CH_3CHO.

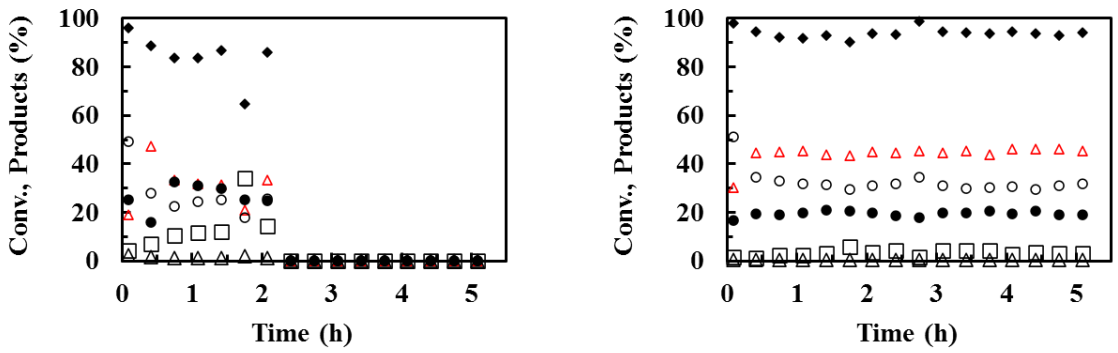

(a) **(b)**

Figure 5 Ethanol conversion (◆) and products distribution (H_2 △, CO_2 ○, CO ●, CH_4 △, acetaldehyde □) on $CeNi_xO_y$ dried catalysts *in-situ* pretreated in H_2 at 250 °C. a) x = 0.5 and b) x = 1. Conversion of O_2 not reported is total ($EtOH/H_2O/O_2/N_2$ = 1:3:1.4:N_2).

However, with $CeNi_1O_{y\,(d)}$ catalyst no deactivation is observed (Figure 5-b) in contrast to the $CeNi_{0.7}O_y$ catalyst. A good stability is achieved within time. The result of this test gives a conversion of ethanol of 94 % with a products distribution of 45.3 % H_2, 31.8 % CO_2, 19.2 % CO, 3.2 % CH_3CHO and 0.5 % CH_4. The calcined catalyst of $CeNi_1O_y$ studied in part III.1.1.1 is compared to the dried sample to show the effect of calcination under these experimental conditions (O_2/EtOH = 1.4). The numerical values of the ethanol conversion, products

distribution (%) and carbon formation (mg/h.$g_{catalyst}$) obtained for the catalyst with and without calcination are represented in Table 1. Carbon formation is highly favored for the $CeNi_1O_y$ catalyst after calcination. The amount of carbon produced in OSRE with $CeNi_1O_y$ catalyst after calcination is around 13 times greater than those of the dried catalyst. Variations in conversions of ethanol and products distribution are observed as well too along with the calcination process.

Table 1 Comparison between dried and calcined $CeNi_1O_y$ catalysts *in-situ* pretreated in H_2 at 250 °C in terms of ethanol conversion, products distribution and carbon formation. Conversion of O_2 not reported is total ($EtOH/H_2O/O_2/N_2$ = 1:3:1.4:N_2).

		Products distribution (%)					
Catalyst	**Conv. ethanol (%)**	**H_2**	**CO_2**	**CO**	**CH_4**	**CH_3CHO**	**Carbon (mg/h.$g_{catalyst}$)**
$CeNi_1O_{y\,(d)}$	94	45.3	31.8	19.2	0.5	3.2	21
$CeNi_1O_{y\,(c)}$	98	47.2	32.3	17.2	0.7	2.6	274

II.1.2 Ternary Zr based compounds

The oxidative steam reforming of ethanol using ternary $CeNi_xZr_{0.5}O_y$ **(**where x = 0.5, 1 and 2) catalysts is studied under same reaction conditions as previously reported (with $EtOH/H_2O/O_2/N_2$ = 1:3:1.4:N_2).

II.1.2.1. Calcined Zr compounds

OSRE results obtained for $CeNi_xZr_{0.5}O_{y\,(c)}$ catalysts (where x = 0.5, 1 and 2) are represented in the following section. As shown in Figure 6-a, even with a low nickel content, the catalyst shows much better stability over time in terms of ethanol conversion and products distribution which is so evident in comparison with the binary catalysts used before. The ethanol conversion reaches 89 % using $CeNi_{0.5}Zr_{0.5}O_y$ calcined catalyst with formation of 38 % H_2, 33 % CO_2, 16 % CO, 11.2 % CH_3CHO and 1.3 % CH_4. The carbon formation for this catalyst is found at 0 mg/h.$g_{catalyst}$). With a higher Ni content catalyst, $CeNi_1Zr_{0.5}O_y$, the ethanol conversion increases to around 94 % during OSRE with 42 % H_2, 31.8 % CO_2, 18.1 % CO, 6.8 % CH_3CHO and 1.4 % CH_4 in products distribution (Figure 6-b). It is important to notice here that there is a higher amount of produced carbon of about 34 mg/h.$g_{catalyst}$ (Table 2). $CeNi_2Zr_{0.5}O_y$ represented in Figure 6-c shows still even higher conversion of ethanol around 98 % with higher H_2 formation of 52 % in addition to 34.2 % CO_2, 10.4 % CO, 1.8 % CH_4 and 1.6 % CH_3CHO. The carbon

formation is of 67 mg/h.$g_{catalyst}$ so higher compared to the previous catalysts with lower Ni content (Table 2).

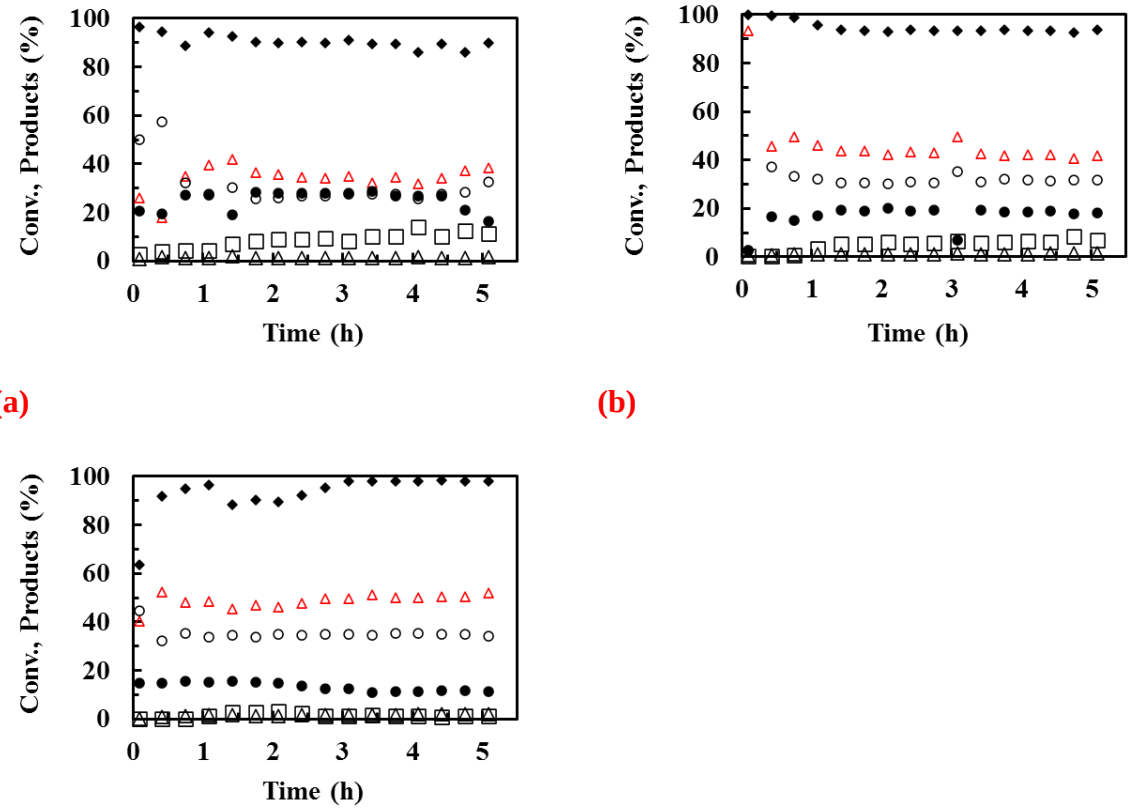

Figure 6 Ethanol conversion (◆) and products distribution (H_2 △, CO_2 ○, CO ●, CH_4 △, acetaldehyde □) on $CeNi_xZr_{0.5}O_y$ calcined catalysts *in-situ* pretreated in H_2 at 250 °C. a) x = 0.5, b) x = 1 and c) x = 2. Conversion of O_2 not reported is total ($EtOH/H_2O/O_2/N_2$ = 1:3:1.4:N_2).

Table 2 OSRE in $EtOH/H_2O/O_2/N_2$ = 1:3:1.4:N_2 on $CeNi_xZr_{0.5}O_y$ catalysts *in-situ* pretreated in H_2 at 250 °C.

		Products distribution (%)					
Catalyst	**Ethanol conv. (%)**	**H_2**	**CO_2**	**CO**	**CH_4**	**CH_3CHO**	**Carbon (mg/h.$g_{catalyst}$)**
$CeNi_{0.5}Zr_{0.5}O_{y\ (c)}$	89	38.3	32.7	16.5	1.3	11.2	0
$CeNi_1Zr_{0.5}O_{y\ (c)}$	94	41.9	31.8	18.1	1.4	6.8	34
$CeNi_2Zr_{0.5}O_{y\ (c)}$	98	52.0	34.2	10.4	1.8	1.6	67

II.1.2.2 Dried Zr compounds

In this part, the dried catalysts of $CeNi_xZr_{0.5}O_y$ are used to see their efficiency in OSRE. A comparison between dried and calcined catalyst is done along with the effect of Ni content on products distribution and ethanol conversion. Figure 7 shows the results obtained with

$CeNi_1Zr_{0.5}O_{y\,(d)}$ and $CeNi_2Zr_{0.5}O_{y\,(d)}$ catalysts under OSRE conditions with $EtOH/H_2O/O_2/N_2$ = 1:3:1.4:N_2. Under same conditions $CeNi_{0.5}Zr_{0.5}O_y$ dried catalyst are tested (not represented in the figures) but no conversion was observed in this medium. However, with x equal to 1 and 2, the reaction was functioning normally with a good stability during the 5 hours in OSRE. Taking into consideration now $CeNi_1Zr_{0.5}O_{y\,(d)}$ catalyst (Figure 7-a), 91 % conversion of ethanol is achieved during 5 hours experiment with 36.9 % H_2, 29.3 % CO_2, 24 % CO, 8.7 % CH_3CHO and 1.1 % CH_4 in products distribution. No carbon is obtained under these conditions. Moving to a higher Ni content (Figure 7-b), the conversion of ethanol is much higher of around 97 %. H_2 is of 46.7 % among the products, with 34.8 % of CO_2, 14.6 % of CO, 2.7 % of CH_3CHO and 1.2 % of CH_4. When x equal to 2, the carbon formation is of 77 mg/h.$g_{catalyst}$.

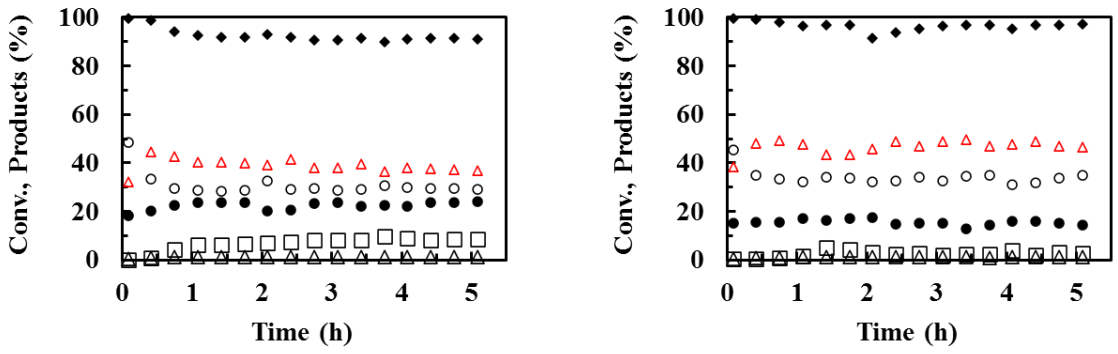

Figure 7 Ethanol conversion (◆) and products distribution (H_2 △, CO_2 ○, CO ●, CH_4 △, acetaldehyde □) on $CeNi_xZr_{0.5}O_y$ dried catalysts *in-situ* pretreated in H_2 at 250 °C. a) x = 1 and b) x = 2. Conversion of O_2 not reported is total ($EtOH/H_2O/O_2/N_2$ = 1:3:1.4:N_2)

Therefore, to summarize, at a low Ni content (x = 0.5), the reaction cannot be started unless the temperature is raised to 250 °C when considering the dried catalyst. Unlike $CeNi_{0.5}Zr_{0.5}O_{y\,(d)}$, $CeNi_{0.5}Zr_{0.5}O_{y\,(c)}$ can be started without any problems at 200 °C. Starting from x equal 1, the reaction can be started at 200 °C and both dried catalysts ($CeNi_1Zr_{0.5}O_{y\,(c)}$ and $CeNi_2Zr_{0.5}O_{y\,(c)}$) achieve a great stability overtime. In fact, the calcination process provokes better performance for catalysts at low Ni content. Moving from Ni/Ce ratio of 1 to 2, increases H_2 concentration in the products distribution from 37 % to 47 %, while CO decreases from 24 % to 15 % in addition to CH_3CHO which decreases from almost 9 % to 3 %. However, no difference is seen for CH_4.

II.1.3. Effect of adding Zr to $CeNi_xO_y$ compounds

In this part, the effect of zirconium addition to the binary compounds is investigated. For this reason, the results of the previous tests done are summarized briefly on the main effects. Using $CeNi_{0.5}O_{y\ (c)}$ (Figure 4-a) catalyst the reaction deactivates fast however by adding Zr ($CeNi_{0.5}Zr_{0.5\ (c)}$) (Figure 6-a) the test can be initiated at 200 °C maintaining good stability over time. Comparing stabilities, $CeNi_{0.5}Zr_{0.5}O_{y\ (c)}$ and $CeNi_1Zr_{0.5}O_{y\ (c)}$ (Figure 6-a and Figure 6-b) calcined catalysts have better stabilities than $CeNi_{0.5}O_{y\ (c)}$ and $CeNi_1O_{y\ (c)}$ catalysts (Figure 4--a and Figure 4--c). Moreover, adding Zr plays an important role on carbon formation as it decreases carbon formation. Table 3 summarizes the amount of carbon formed with the different binary and ternary catalysts described previously. With $CeNi_1O_y$, the amount of carbon produced is of 274 $mg/h.g_{catalyst}$ however by adding Zr the amount drastically drops to 34 $mg/h.g_{catalyst}$. Similarly for $CeNi_1Zr_{0.5}O_{y\ (d)}$ catalyst which shows no formation of carbon unlike the $CeNi_1O_{y\ (d)}$ catalyst with 21 $mg/h.g_{catalyst}$. No carbon is formed in the case of $CeNi_{0.5}Zr_{0.5}O_{y\ (c)}$. ZrO_2 improved catalytic performance with high selectivity to H_2 and low selectivity to undesirable by-products based on the reducibility [306], thermal stability[307], adsorption promotion and CO oxidation capabilities [306, 308]. Zr doping enhances oxygen mobility in ceria lattice allowing for coke gasification. Moreover, Ni-Ce-Zr catalyst has been shown to be stable at low temperature even in methane steam reforming [309].

Table 3 Effect of Zr addition to $CeNi_xO_y$ compounds *in-situ* pretreated in H_2 at 250 °C and tested in OSRE reaction with $EtOH/H_2O/O_2/N_2 = 1:3:1.4:N_2$ and oven temperature fixed at 50 °C.

	Catalyst					
	$CeNi_{0.5}O_{y\ (c)}$	**$CeNi_1O_{y(c)}$**	**$CeNi_1O_{y(d)}$**	**$CeZr_{0.5}Ni_{0.5}O_{y\ (c)}$**	**$CeZr_{0.5}Ni_1O_{y(c)}$**	**$CeZr_{0.5}Ni_1O_{y\ (d)}$**
Carbon formation ($mg/h.g_{catalyst}$)	No conversion in used conditions	274	21	0	34	0

II.1.4. Effect of O_2/ethanol ratio on $CeNi_1O_y$ catalyst

To investigate the influence of O_2/EtOH ratio on the catalytic performance in OSRE, $CeNi_1O_y$ binary catalyst is used. A binary catalyst is chosen instead of ternary, since Zr already played an important role in increasing the stability of the catalyst. For this reason, different experiments are conducted with different O_2/EtOH ratios of 1.42, 1.56 and 1.7. It is obvious that O_2/EtOH

ratio has a drastic effect on inhibition of carbon formation as shown in Figure 8. At a ratio of 1.42, the carbon formation is found to be of 274 mg/h.$g_{catalyst}$, however; this quantity drops drastically to 185 mg/h.$g_{catalyst}$ with a slight increase in O_2/EtOH ratio (1.56). Moreover, no carbon formation for this catalyst is observed at ratio of 1.7. A slight decrease of H_2 from 49 to 45 % in the products distribution is observed by the increase of the oxygen to ethanol ratio from 1.42 to 1.7 in addition to some slight variations in the products distribution of carbon dioxide, carbon monoxide and acetaldehyde.

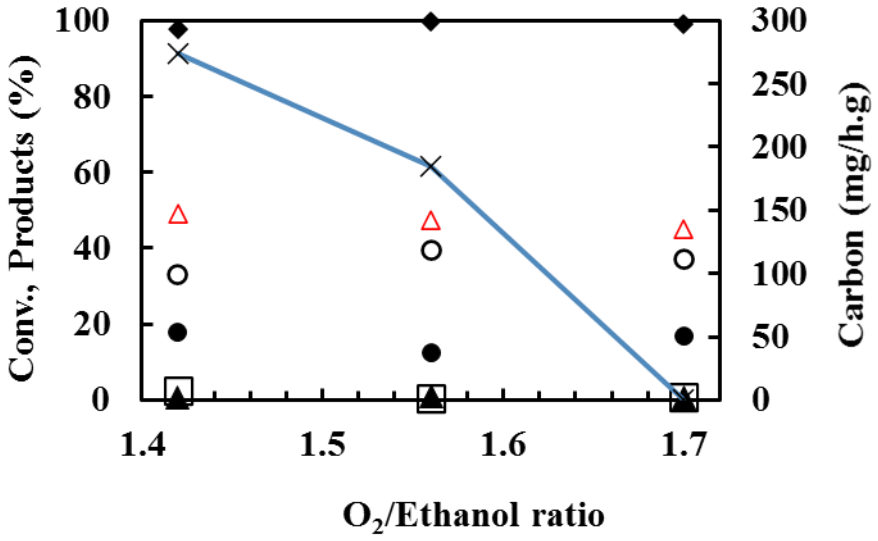

Figure 8 Effect of O_2/Ethanol ratio on conversion of ethanol, products distribution (%) and carbon formation (mg/h.g) for $CeNi_1O_y$ calcined catalyst pretreated in H_2 at 250 °C.

Similar studies performed with different oxygen/ethanol molar ratios: 0.56, 1 and 1.5 show that ethanol conversion increases more rapidly when the O_2/EtOH ratio increases. Other studies found in literature also proved the effect of O_2/EtOH ratio on OSRE. It has been found that the variation from 0.03 to 0.3 made possible to increase the conversion of ethanol from 62 to 84 % and the hydrogen yield from 15 to 47 % [201]. Previous reports in literature have shown that by feeding mixtures with higher oxygen to ethanol ratio, it was also possible to reduce coke selectivity, improving at the same time hydrogen production, similar to what has been reported in our study [310]. In addition to coke reduction, it has been proved that adding oxygen to the feed can increase the stability of the catalyst [179].

II.2. OSRE with O_2/EtOH ratio = 1.7

In this part, binary and ternary (dried and calcined) catalysts are tested in OSRE with O_2/Ethanol ratio = 1.7 since it has been shown previously (in Figure 8) that at this ratio carbon formation can be avoided. To maintain high performances the materials should be able to support high concentration of O_2.

II.2.1 Binary catalysts in OSRE

In this section, catalysts based on $CeNi_xO_y$ where x = 0.5, 1, 2 and 5 are studied in OSRE conditions with $EtOH/H_2O/O_2/N_2 = 1:3:1.7:N_2$.

II.2.1.1 Binary dried catalysts in OSRE: Influence of Ni content

Oxidative steam reforming of ethanol is studied in the present work over $CeNi_xO_{y\ (d)}$ with different Ni contents. The catalytic tests are performed under 5 hours and their corresponding results are presented in Figure 9. The complementary numerical values of ethanol conversions, products distribution and carbon formation are presented in Table 4. The conversions of ethanol in the following series ranges between 94 and 97 % for the different values of x. Globally, the reactivity order of the following compounds follows the Ni content. Starting with a low Ni content (Figure 9-a), x = 0.5, H_2 percentage in the products distribution is the least (28.9 %) compared to the catalysts with higher Ni contents. This value becomes greater (48.9 %) especially with $CeNi_5O_{y\ (d)}$ (Figure 9-d). The stability of these tests persists over the 5 hours in the OSRE process. No carbon formation is observed when x = 0.5, 2 and 5, and only negligible amount of carbon (9 $mg/h.g_{catalyst}$) is obtained when x = 1. The best catalytic result is related to the catalyst with higher Ni content, $CeNi_5O_{y\ (d)}$, where H_2 % in products distribution is the highest and the side byproducts: CO (15.8 %), CH_4 (0.4 %) and CH_3CHO (0.7 %) are the lowest.

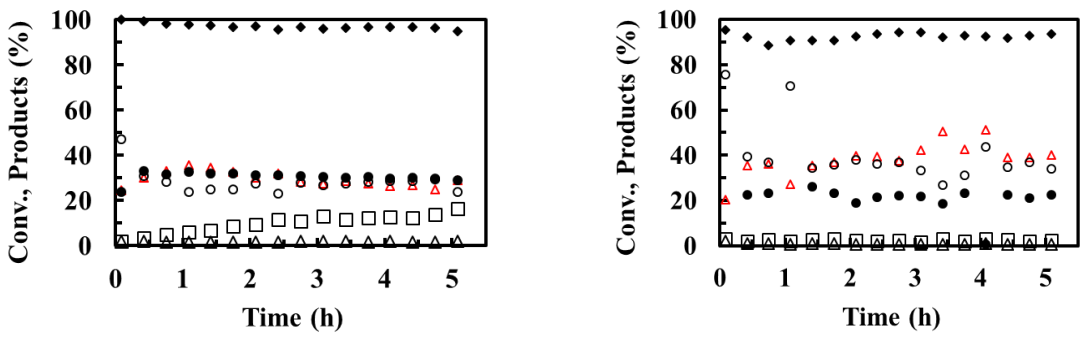

(a) **(b)**

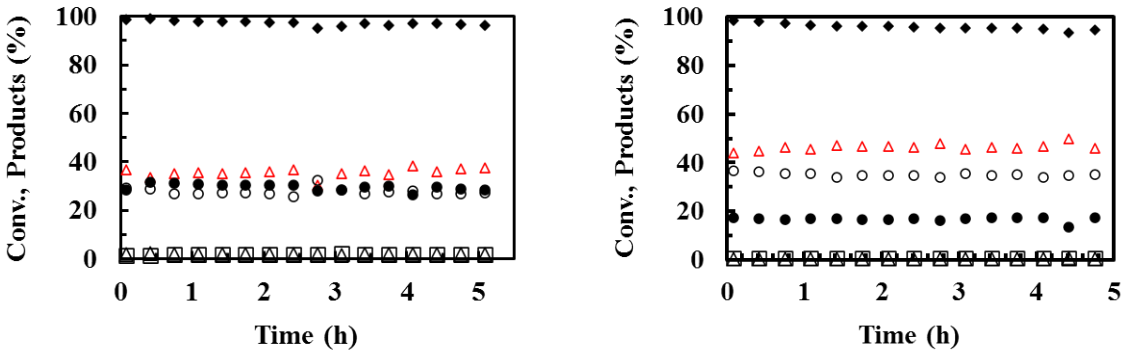

Figure 9 Ethanol conversion (◆) and products distribution (H_2 △, CO_2 ○, CO ●, CH_4 △, acetaldehyde □) on $CeNi_xO_y$ dried catalysts *in-situ* pretreated in H_2 at 250 °C. b) x = 0.5, b) x = 1, c) x = 2 and d) x = 5. Conversion of O_2 not reported is total ($EtOH/H_2O/O_2/N_2$ = 1:3:1.7:N_2).

Table 4 Conversion of ethanol, products distribution (%) and carbon formation on $CeNi_xO_y$ dried catalysts after 5 hours in OSRE process ($EtOH/H_2O/O_2/N_2$ = 1:3:1.7:N_2). Conversion of O_2 not reported is total.

		Products distribution (%)					
	Conv. of ethanol (%)	**H_2**	**CO_2**	**CO**	**CH_4**	**CH_3CHO**	**Carbon (mg/h.$g_{catalyst}$)**
$CeNi_{0.5}O_y$ (d)	94.8	28.9	23.9	29.1	1.8	16.3	0.0
$CeNi_1O_y$ (d)	97.0	40.2	34.1	22.4	0.8	2.5	9.0
$CeNi_2O_y$ (d)	96.3	37.4	27.1	28.3	1.9	5.3	0.0
$CeNi_5O_y$ (d)	94.0	48.9	34.2	15.8	0.4	0.7	0.0

In literature, under different conditions, studies were performed on Ni embedded catalysts synthesized by co-precipitation method [311]. The results showed that the more Ni embedding and the lower carbon deposits in these nickel and ceria based catalysts exhibited a more stable hydrogen production performance. Weng et al. prepared a series of Ni-substituted pyrochlore oxides of $La_2Ce_{2-x}Ni_xO_{7-\delta}$ (x = 0.0-0.45) and studied their catalytic performance in OSRE at a temperature of 500 °C and H_2O/EtOH ratio of 3 and C/O ratio between 0.4 and 0.7 [195]. They revealed that H_2 consumption in the TPR and H_2 production increases with the increased Ni content, similar to our observations. It was shown that the highest catalytic activity is obtained for the x = 0.45 sample, with a hydrogen selectivity of 80 %.

II.2.1.2 Binary calcined catalysts in OSRE: Influence of Ni content and calcination

Similarly, $CeNi_xO_y$ calcined catalysts where x = 0.5, 1, 2 and 5 are tested in OSRE conditions to investigate the effect of Ni content. Figure 10-a represents the results of $CeNi_{0.5}O_y$ calcined catalyst during 5 hours in OSRE. The conversion of ethanol is of 95.4 % with 35 % H_2, 31.9 %

CO_2, 28.2 % CO, 3.1 % CH_3CHO and 1.8 % CH_4 as products distribution after 5 h. (Table 5). It should be noted that all the ethanol conversions, using a O_2/ethanol ratio equal to 1.7, are almost total. Moving to higher Ni content (Figure 10-b) with $CeNi_1O_y$ calcined catalyst, the hydrogen gas percentage increases up to 36 %. More CO_2 (36 %) and CH_4 (3.3%) are produced and less CO (22 %) and CH_3CHO (2.5 %). At a nickel over cerium ratio of 2 (Figure 10-c), H_2 percentage increases (37.5 %). However, other competitive processes are occurring leading to higher formation of CO and CH_3CHO instead of CO_2 and CH_4 (Table 5). With an even higher Ni content using $CeNi_5O_y$ calcined catalyst *in-situ* pretreated in H_2 (Figure 10-d) at 250 °C, a much higher percentage of hydrogen is produced around 47.4 % in the products distribution with 37.4 % of CO_2, 13.5 % of CO and almost negligible amounts of CH_4 and CH_3CHO (< 2 %).

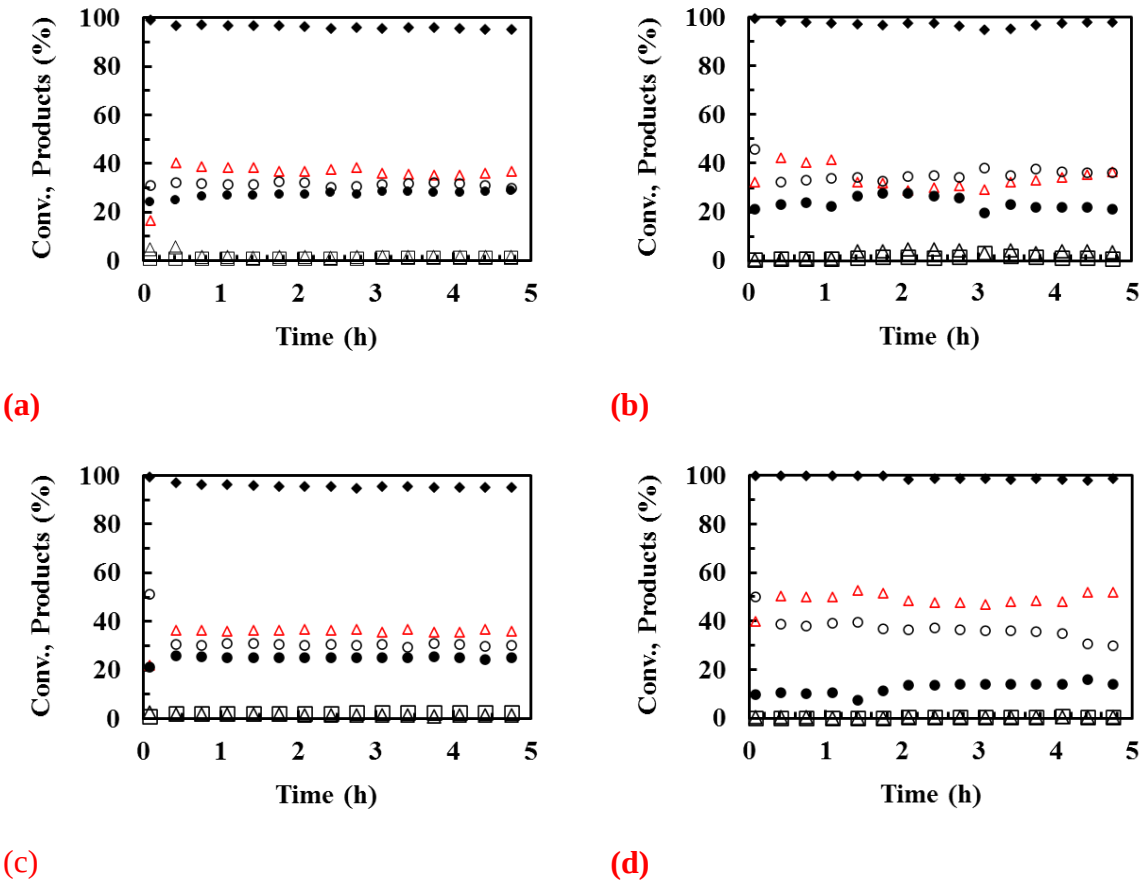

Figure 10 Ethanol conversion (◆) and products distribution (H_2 △, CO_2 ○, CO ●, CH_4 △, acetaldehyde □) on $CeNi_xO_{y\ (c)}$ catalysts *in-situ* pretreated in H_2 at 250 °C. b) x = 0.5, b) x = 1, c) x = 2 and d) x = 5. Conversion of O_2 not reported is total ($EtOH/H_2O/O_2/N_2$ = 1:3:1.7:N_2).

It is important to remark that carbon formation is avoided in all cases (x = 0.5, 1, 2 and 5) which is a confirmation of the fact that the ratio between oxygen and ethanol is an important factor

for carbon formation. A minimum of 67 % of ethanol conversion is reached and a maximum of 85 % is attained using $CeNi_5O_y$ calcined catalyst (Table 5).

Table 5 Conversion of ethanol, products distribution (%) and carbon formation on *in-situ* pretreated in H_2 at 250 °C $CeNi_xO_{y\ (c)}$ catalysts after 5 hours in OSRE process ($EtOH/H_2O/O_2/N_2$ = 1:3:1.7:N_2). Conversion of O_2 not reported is total.

		Products distribution (%)					
	Conv. of ethanol (%)	**H_2**	**CO_2**	**CO**	**CH_4**	**CH_3CHO**	**Carbon (mg/h.g)**
$CeNi_{0.5}O_{y\ (c)}$	95.4	35.0	31.9	28.2	1.8	3.1	0.0
$CeNi_1O_{y\ (c)}$	98.0	36.0	36.2	22.0	3.3	2.5	0.0
$CeNi_2O_{y\ (c)}$	95.0	37.5	31.9	26.6	1.6	2.4	0.0
$CeNi_5O_{y\ (c)}$	98.4	47.4	37.4	13.5	0.3	1.5	0.0

Figure 11 summarizes the overall trend of products distribution and ethanol conversions as a function of increasing the Ni content in the calcined catalysts. The best catalytic results based on higher conversion of ethanol, main products distribution and lower by product are obtained using $CeNi_5O_{y\ (c)}$, the catalyst with the highest Ni content. The same trend was confirmed previously on the dried $CeNi_xO_y$ catalysts. Ni based catalysts have been reported as interesting formulations for ethanol reforming, due to their capacity in promoting C–C, C–H and O–H bond cleavage [223, 224, 312].

Here, using our catalysts, it can be seen that calcination process plays an important role in OSRE process and products distribution only at low nickel contents. Comparing the results obtained after calcination to the ones obtained on dried catalysts, it is visible that at low Ni content (x = 0.5), the catalyst gives clear differences in products distribution, even if similar conversions are obtained (95.4 % ethanol conversion on $CeNi_{0.5}O_{y\ (c)}$, with 35.0 % H_2, 31.9 % CO_2, 28.2 % CO, 1.8 % CH_4 and 3.1 % CH_3CHO, compared to 94.8 % ethanol conversion on $CeNi_{0.5}O_{y\ (d)}$, with 28.9 % H_2, 23.9 % CO_2, 29 % CO, 1.8 % CH_4 and 16.3 % CH_3CHO). However, for higher Ni contents, only slight variations can be observed.

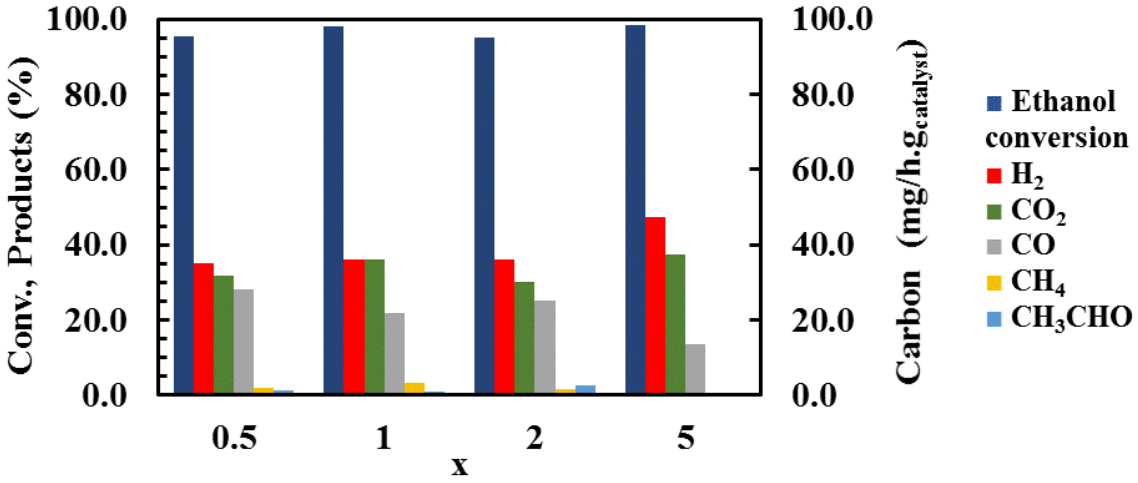

Figure 11 Conversion of ethanol, products distribution (%) and carbon formation on $CeNi_xO_{y\ (c)}$ catalysts where x = 0.5, 1, 2 or 5 after 5 hours in OSRE process ($EtOH/H_2O/O_2/N_2$ = 1:3:1.7:N_2). Conversion of O_2 not reported is total.

On some catalysts reported in literature, with high Ni/Ce ratios, only slight variations were obtained in products distribution with or without calcination or with calcination on different temperatures.[313] This is similar to our case of binary catalysts. In fact, calcination has been shown to be an important key parameter for avoiding the formation of metallic clusters, by separating the Ni crystals and thereby, metal dispersion and reducibility were enhanced [314]. However, it is not only the calcination that affects OSRE but other factors have to be considered such as for example, reaction temperature, metallic content, or metallic composition.

II.2.1.3. 31 hours run test for $CeNi_xO_y$ catalysts in OSRE with O_2/EtOH = 1.7

$CeNi_xO_y$ calcined catalysts:

In fact, many catalysts reported in literature change their performances in OSRE with time. For this reason, it is important when studying the processes occurring in OSRE to reproduce them for a long period of time. Therefore, the $CeNi_xO_y$ calcined catalysts tested before in OSRE at O_2/Ethanol ratio equal 1.7 are also tested for 31 hours to not only check their stability but also analyze carbon formation over time. Figure 12 shows the results obtained with these catalysts over time and the results obtained after 31 hours are summarized in Table 6. In general, all the conversions of ethanol and products distribution percentages are the same after 5 hours (Table 5) and after 31 hours (Table 6). No carbon formation is observed even after 31 hours in OSRE. The results obtained with *in-situ* pretreated in H_2 at 250 °C $CeNi_{0.5}O_y$ calcined catalyst during the 31 hours in OSRE are represented in Figure 12-a. The conversion of ethanol becomes better with time as it increases from 95.4 % during the first 5 hours to 100 % after 31 hours. The

distribution of products is as follows, 28.6 % H_2, 35.3 % CO_2, 27.9 % CO, 3.5 % CH_4 and finally 4.7 % CH_3CHO. The percentage of hydrogen decreases by 6 % after several hours of experiment but remains relatively stable at around this value (29 %). Figure 12-b shows the results obtained with $CeNi_1O_{y\ (c)}$ catalyst. During the first hours of experiment, some fluctuations in the products distributions are observed. Then, the catalyst stabilizes its activity giving 39.2 % H_2, 35.4 % CO_2, 20.5 % CO, 3.2 % CH_4 and 1.7 % CH_3CHO. Figure 12-c shows the results obtained on $CeNi_2O_y$ calcined catalyst in *in-situ* pretreated in H_2. Globally, the conversion of ethanol and the products distribution are constant within time. The main products are H_2 and CO_2 with 36.6 % and 31.5 % each. 26.5 % CO, 1.2 % CH_4 and 4.2 % CH_3CHO are also obtained in addition. With a higher Ni content, using $CeNi_5O_y$ calcined catalyst *in-situ* pretreated in H_2 at 250 °C, stability of ethanol conversion and products distribution are still confirmed (Figure 12-d). A much higher percentage of hydrogen is formed (47.5 %), a value higher than that obtained with x = 0.5, 1 and 2. This is in confirmation with the fact that the Ni/Ce ratio is an important factor in the OSRE. 36.2 % CO_2, 14.9 % CO are formed too in addition to negligible amounts of CH_3CHO and CH_4 (1 % and 0.4 % each respectively). $CeNi_{0.5}O_y$, $CeNi_1O_y$ and $CeNi_5O_y$ follow the same trend when increasing the Ni content. In the latter, H_2 and CO_2 percentages increase with the increase of Ni content while CO, CH_3CHO and CH_4 are decreasing. However, for $CeNi_2$, a slight difference is observed with higher CO and acetaldehyde formation.

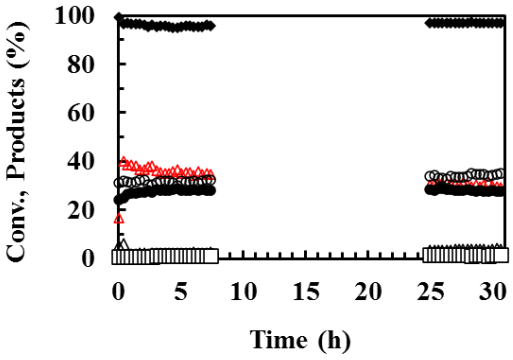

(a)

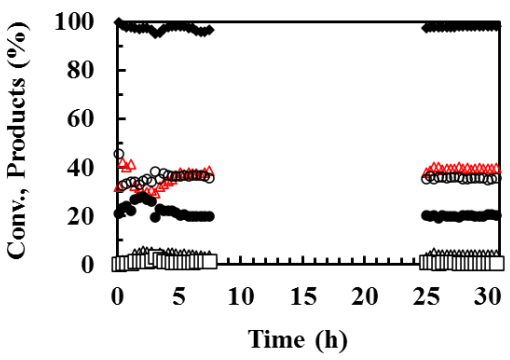

(b)

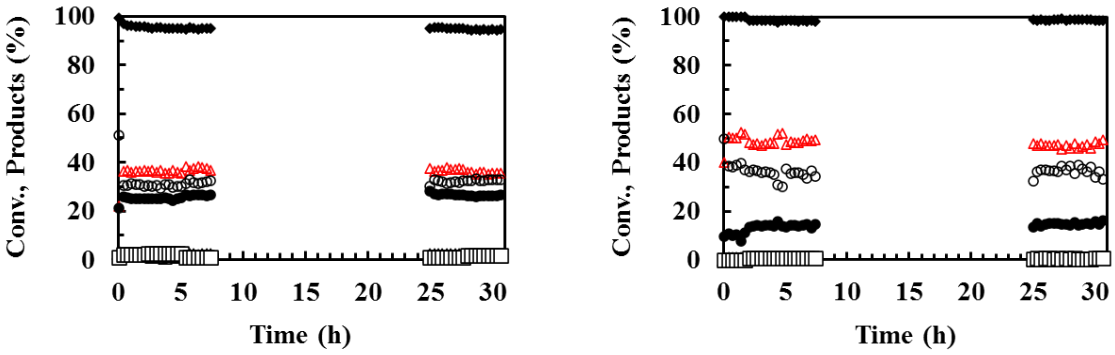

(c) **(d)**

Figure 12 Ethanol conversion (◆) and products distribution (H_2 △, CO_2 ○, CO ●, CH_4 △, acetaldehyde □) during 31 hours on $CeNi_xO_{y\ (c)}$ catalysts *in-situ* pretreated in H_2 at 250 °C. a) x = 0.5, b) x = 1, c) x = 2 and d) x = 5. Conversion of O_2 not reported is total ($EtOH/H_2O/O_2/N_2$ = 1:3:1.7:N_2).

Table 6 Conversion of ethanol, products distribution (%) and carbon formation on *in-situ* pretreated in H_2 at 250 °C $CeNi_xO_{y\ (c)}$ catalysts after 31 hours in OSRE process. Conversion of O_2 not reported is total ($EtOH/H_2O/O_2/N_2$ = 1:3:1.7:N_2).

		Products distribution (%)					
	Conv. of ethanol (%)	**H_2**	**CO_2**	**CO**	**CH_4**	**CH_3CHO**	**Carbon (mg/h.g)**
$CeNi_{0.5}O_{y\ (c)}$	100.0	28.6	35.3	27.9	3.5	4.7	0.0
$CeNi_1O_{y\ (c)}$	98.1	39.2	35.4	20.5	3.2	1.7	0.0
$CeNi_2O_{y\ (c)}$	94.5	36.6	31.5	26.5	1.2	4.2	0.0
$CeNi_5O_{y\ (c)}$	98.6	47.5	36.2	14.9	0.4	1	0.0

Figure 13 summarizes the overall trend of products distribution and ethanol conversion after 31 hours as a function of increasing the Ni content on the calcined catalysts. The best catalytic results based on higher conversion of ethanol, main products distribution and lower by products concentrations are obtained using $CeNi_5O_{y\ (c)}$, the catalyst with the higher Ni content. In fact, this trend presents no change globally with time for the different $CeNi_xO_{y\ (c)}$ catalysts. For the catalysts where x = 2 and 5, the values of conversion and products distribution remain constant within time. $CeNi_1O_{y\ (c)}$ shows even higher conversion of ethanol and better products distribution after 31 hours (Table 6) compared to those results obtained after only 5 hours (Table 5). A slight deviation of conversion towards lower values is obtained for $CeNi_{0.5}O_y$ catalyst after 31 (Table 6) hours compared to those after 5 hours (Table 5). Regardless of the Ni proportion in the catalyst, no carbon is found. In fact, this could be related to the processes occurring in parallel to OSRE.

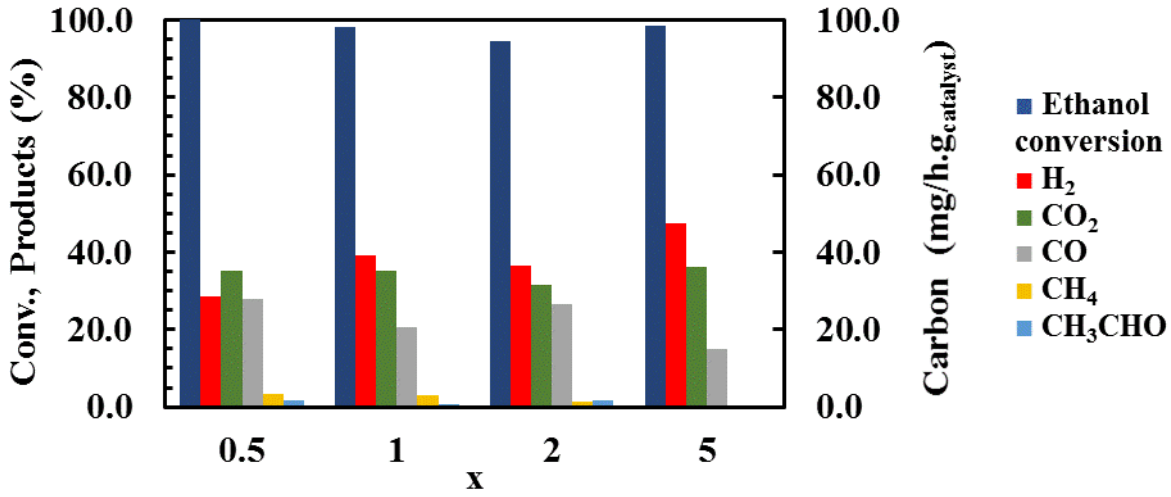

Figure 13 Conversion of ethanol, products distribution (%) and carbon formation on *in-situ* pretreated in H_2 at 250 °C $CeNi_xO_{y\ (c)}$ catalysts where x = 0.5, 1, 2 and 5 after 31 hours in OSRE process. Conversion of O_2 not reported is total ($EtOH/H_2O/O_2/N_2$ = 1:3:1.7:N_2).

$CeNi_xO_y$ dried catalysts:

Only $CeNi_1O_{y\ (d)}$ and $CeNi_5O_{y\ (d)}$ were tested under these conditions in OSRE in this series of dried binary catalysts. The corresponding figures are represented in Figure 14 and the numerical values obtained after 31 hours are represented in Table 7. Both $CeNi_1O_{y\ (d)}$ and $CeNi_5O_{y\ (d)}$ show high stability over time. $CeNi_1O_{y\ (d)}$ achieves 94.5 % ethanol conversion with 36.6 % H_2, 31.5 % CO_2, 26.5 % CO, 1.2 % CH_4 and 4.2 % CH_3CHO in products distribution. Moreover, $CeNi_5O_{y\ (d)}$ achieves 97.2 % ethanol conversion with 47.6 % H_2, 34.1 % CO_2, 17.1 % CO, 0.3 % CH_4 and 0.9 % CH_3CHO in products distribution. At this O_2/EtOH ratio of 1.7, no carbon formation is observed for both of the catalysts after 31 hours. For comparison, concerning $CeNi_1O_{y\ (d)}$, after the first 5 hours on stream, some carbon was formed (Table 4) showing that with time on stream less carbon is formed. Therefore, the rate of carbon formation varies with time, more carbon is formed at the beginning of the reaction while an amelioration of the system is obtained with time. This could be due to an evolution of the surface of the catalyst and active sites with time. The values of ethanol conversions obtained after 31 hours on calcined binary catalysts (> 98 %, Table 6) are slightly higher than those obtained on dried ones (> 94 %, Table 7). Moreover, the calcined compounds show less by products overtime than those with dried binary catalysts. So, the effect of calcination was not only visible on low Ni content but also when $5 \geq x > 0.5$ on long time on stream.

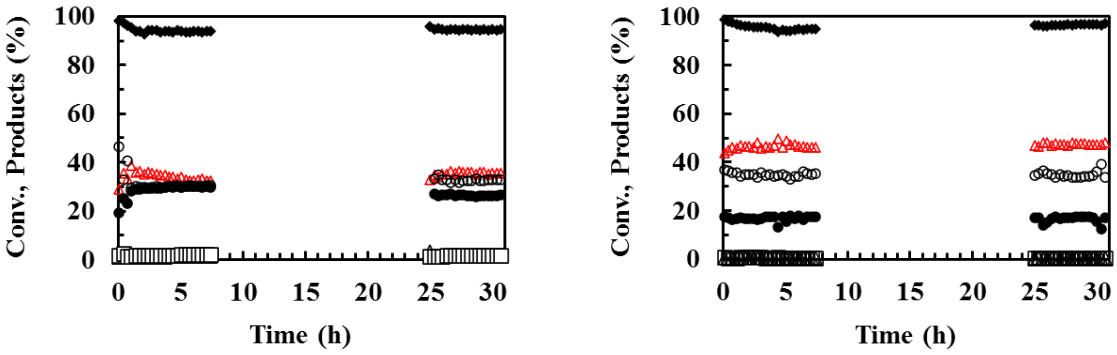

Figure 14 Ethanol conversion (◆) and products distribution (H_2 △, CO_2 ○, CO ●, CH_4 △, acetaldehyde □) during 31hours on $CeNi_xO_{y\ (d)}$ catalysts *in-situ* pretreated in H_2 at 250 °C. b) x = 1 and b) x = 5. Conversion of O_2 not reported is total ($EtOH/H_2O/O_2/N_2$ = 1:3:1.7:N_2).

Table 7 Conversion of ethanol, products distribution (%) and carbon formation on *in-situ* pretreated in H_2 at 250 °C $CeNi_xO_{y\ (d)}$ catalysts after 31 hours in OSRE process. Conversion of O_2 not reported is total ($EtOH/H_2O/O_2/N_2$ = 1:3:1.7:N_2).

		Products distribution (%)					
	Conv of ethanol (%)	**H_2**	**CO_2**	**CO**	**CH_4**	**CH_3CHO**	**Carbon (mg/h.g)**
$CeNi_1O_{y\ (d)}$	94.5	36.6	31.5	26.5	1.2	4.2	0
$CeNi_5O_{y\ (d)}$	97.2	47.6	34.1	17.1	0.3	0.9	0

II.2.2. Effect of Zr addition to catalysts in OSRE (after pretreatment in H_2 at 250 °C)

As previously shown Zr plays an important role in the activity of the catalyst in OSRE reaction. In the previous part, the effect of addition of Zr was studied with an O_2/EtOH ratio of 1.4. In this part, the same parameter is studied but using a higher O_2/EtOH ratio of 1.7. The catalysts containing Zr with different Ni/M_T ratios were studied in OSRE after *in-situ* pretreatment of the catalysts in hydrogen at 250 °C.

II.2.2.1 Dried Zr based compounds

Table 8 summarizes all the results performed for these $CeNi_xZr_{0.5}O_z$ dried catalysts in OSRE. The main products formed are hydrogen and carbon dioxide in addition to CO, CH_4 and CH_3CHO. In all these catalysts and under these conditions, no carbon is obtained after 5 hours of reaction. The corresponding schematic representations are presented in the Figure 15. Figure 15-a shows the results obtained with $CeNi_{0.5}Zr_{0.5}O_y$ dried catalyst. At 200 °C, the reaction could not be started (no conversion) and so the temperature of the oven was raised till 250 °C. After activation of the reaction, the oven was fixed back at 50 °C. 94 % conversion of ethanol is attained during the 5 hours experiment. The products are distributed as follows: 30 % H_2, 30 %

CO_2, 32 % CO, 1.4 % CH_4 and 6.8 % CH_3CHO (Table 8). $CeZr_{0.5}Ni_1O_y$ dried catalyst could start without any complications at 200 °C. During the 5 hours experiment, very good stability of ethanol conversion and products distribution are achieved within time. Ethanol conversion is found to be at 91 % with the formation of 41.7 % H_2, 28 % CO_2, 26 % CO, 1.1 % CH_4 and 1.8 % CH_3CHO. With a higher Ni content, using $CeNi_2Zr_{0.5}O_y$ dried catalyst, ethanol conversion is almost complete (99 %) with higher H_2 percentage (46 %) and CO_2 (35 %) in products distribution. In addition to other by products which are 17 % CO, 0.5 % CH_4 and 0.3 % CH_3CHO in products distribution. When the Ni content increases the percentage of the desired products increase and those of byproducts decrease. For example, CO % in products distribution drops from around 32 % when x = 0.5 to around 14 % when x is equal to 5.

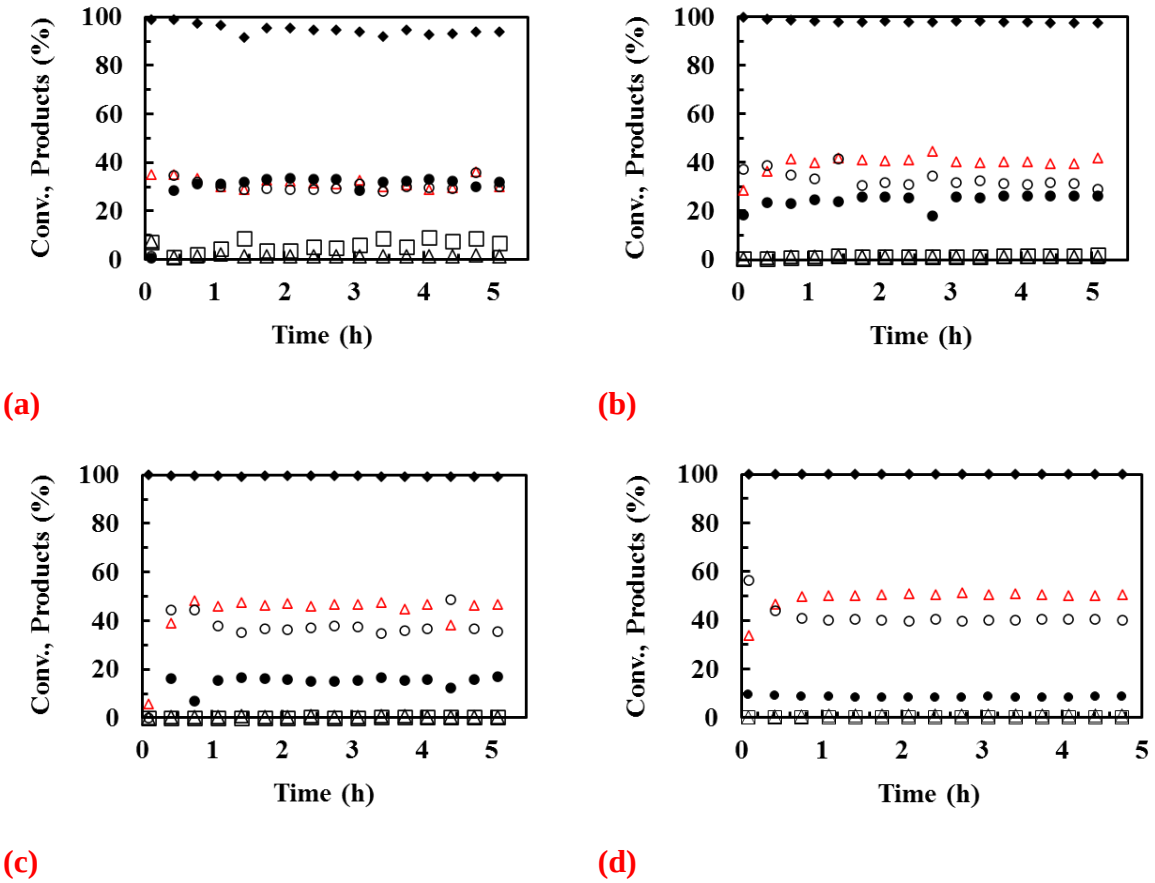

Figure 15 Ethanol conversion (◆) and products distribution (H_2 △, CO_2 ○, CO ●, CH_4 △, acetaldehyde □) during 5 hours on $CeNi_xZr_{0.5}O_{y\ (d)}$ catalysts *in-situ* pretreated in H_2 at 250 °C. a) x = 0.5, b) x = 1, c) x = 2 and d) x = 5. Conversion of O_2 not reported is total ($EtOH/H_2O/O_2/N_2$ = 1:3:1.7:N_2).

When comparing to binary compounds (Table 4), Zr addition shifts the by-products to lower values and thus increasing the percentages of H_2 and CO_2 in products distribution. The same trend is followed when considering the conversion of ethanol which is almost total with $CeNi_2Zr_{0.5}O_{y\ (d)}$ and $CeNi_5Zr_{0.5}O_{y\ (d)}$ unlike $CeNi_2O_{y\ (d)}$ and $CeNi_5O_{y\ (d)}$.

Table 8 Conversion of ethanol, products distribution (%) and carbon formation on *in-situ* pretreated in H_2 at 250 °C $CeNi_xZr_{0.5}O_{y\ (d)}$ catalysts after 5 hours in OSRE process. Conversion of O_2 not reported is total ($EtOH/H_2O/O_2/N_2 = 1:3:1.7:N_2$).

		Products distribution (%)					
	Conv. of ethanol (%)	**H_2**	**CO_2**	**CO**	**CH_4**	**CH_3CHO**	**Carbon (mg/h.g)**
$CeNi_{0.5}Zr_{0.5}O_{y\ (d)}$*	94.0	29.9	30	31.9	1.4	6.8	0.0
$CeNi_1Zr_{0.5}O_{y\ (d)}$	91.0	41.8	28.9	26.4	1.1	1.8	0.0
$CeNi_2Zr_{0.5}O_{y\ (d)}$	99.0	46.7	35.5	17.0	0.5	0.3	0.0
$CeNi_5Zr_{0.5}O_{y\ (d)}$	98.2	47.9	37.1	14.1	0.2	0.7	0.0

* Reaction started at 250°C

II.2.2.2. Calcined Zr based compounds

To see the effect of calcination on the Zr ternary compounds, $CeNi_xZr_{0.5}O_y$ catalysts with different Ni/Ce ratios were used where x= 0.5, 1, 2, and 5. The results of each experiment are represented in Figure 16 that will be explained later with the effect of calcination. Table 9 summarizes all the results after 5 hours in OSRE. As reported in the table, no carbon is formed after 5 hours of experiment on all these catalysts, as already observed with the dried catalysts. All the ethanol conversions are almost complete (≥ 97 %).

Figure 16-a is a representation of the catalytic results obtained with the calcined catalyst of $CeNi_{0.5}Zr_{0.5}O_y$. The catalyst has very good stability with time in terms of conversion of ethanol and the products distribution. Conversion of ethanol reaches 97 % after activation of the catalyst leading to 37.6 % H_2, 29.8 % CO_2, 28.5 % CO, 1.6 % CH_4 and 2.5 % CH_3CHO. Unlike the $CeZr_{0.5}Ni_{0.5}O_y$ dried catalyst, the calcined one could be started at 200 °C and there is no need to raise the temperature to 250 °C. Moreover, the formations of hydrogen and CO_2 are much higher than those on the dried catalysts with much lower concentrations of CO and CH_3CHO. Increasing the nickel content, using $CeNi_1Zr_{0.5}O_y$ calcined catalyst shown in Figure 16-b, the hydrogen percentage in products distribution increases up till 41.7 % with an increase in CO_2 percentage too (34.4 %). On another hand, other by products decrease in percentage as following: 22.2 % CO, 0.9 % CH_4 and 0.8 % CH_3CHO. Comparing this catalyst to the dried one (Table 8), the calcined catalyst produces higher percentage of CO_2 and lower percentages of CO, CH_4 and CH_3CHO. This is in coherence with the results obtained on the $CeNi_{0.5}Zr_{0.5}O_y$ catalyst for which calcination has shown an important effect on the performance of the catalyst. Using the calcined catalyst $CeNi_2Zr_{0.5}O_y$ even better hydrogen levels are obtained (Figure 16-c). A percentage of 45.1 % H_2 is reported with 36.5 % CO_2 in products distribution leading to

lower amounts of CO (17.4 %), CH_4 (0.6 %) and CH_3CHO (0.4 %). Same effect is deducted here on calcination in comparison to the dried catalyst with the same formula (Table 8), where the percentages of produced CH_4 and CH_3CHO decreased after calcination. No clear differences are noticed on the distribution of H_2, CO_2 and CO at this Ni/Ce ratio. With a nickel over cerium ratio of 5 (Figure 16-d), a complete conversion of ethanol is achieved with 51.6 % H_2 and 38.3 % CO_2 (the highest percentage among all catalysts). CH_3CHO is eliminated and trace amounts of CH_4 is formed (0.3 %). In addition to that much lower percentage of CO is reached (9.8 %) (Table 9) in comparison to all the previous catalysts. Therefore, the calcined $CeNi_5Zr_{0.5}O_y$ catalyst shows more promising results that those of the dried ones in terms of higher H_2 and CO_2 percentages and lower CO, CH_4 and elimination of CH_3CHO.

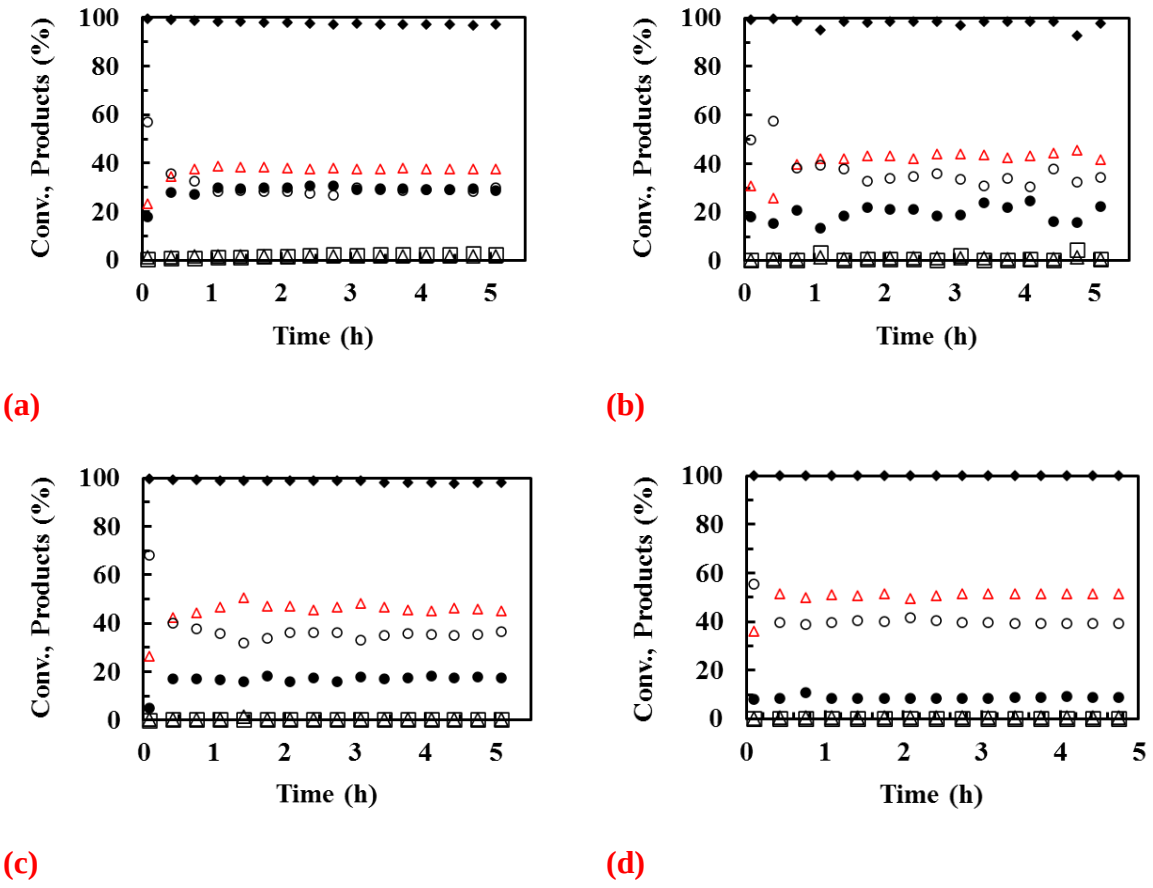

Figure 16 Ethanol conversion (◆) and products distribution (H_2 △, CO_2 ○, CO ●, CH_4 △, acetaldehyde □) during 5 hours on $CeNi_xZr_{0.5}O_{y\ (c)}$ catalysts *in-situ* pretreated in H_2 at 250 °C a) x = 0.5, b) x = 1, c) x = 2 and d) x = 5. Conversion of O_2 not reported is total ($EtOH/H_2O/O_2/N_2$ = 1:3:1.7:N_2).

Table 9 Conversion of ethanol, products distribution (%) and carbon formation on *in-situ* pretreated in H_2 at 250 °C $CeNi_xZr_{0.5}O_{y\ (c)}$ catalysts after 5 hours in OSRE process. Conversion of O_2 not reported is total ($EtOH/H_2O/O_2/N_2$ = 1:3:1.7:N_2).

		Products distribution (%)					
	Conv. of ethanol (%)	**H_2**	**CO_2**	**CO**	**CH_4**	**CH_3CHO**	**Carbon (mg/h.g)**
$CeNi_{0.5}Zr_{0.5}O_{y\ (c)}$	97.0	37.6	29.8	28.5	1.6	2.5	0.0
$CeNi_1Zr_{0.5}O_{y\ (c)}$	98.0	41.7	34.4	22.2	0.9	0.8	0.0
$CeNi_2Zr_{0.5}O_{y\ (c)}$	98.0	45.1	36.5	17.4	0.6	0.4	0.0
$CeNi_5Zr_{0.5}O_{y\ (c)}$	100.0	51.6	38.3	9.8	0.3	-	0.0

When comparing the results reported in Tables 9 and 8, calcination plays a beneficial role in the distribution of products mainly in decreasing the amounts of byproducts obtained (CO, CH_3CHO and CH_4) and thus shifting the distribution to higher percentages of hydrogen and carbon dioxide. On this series of catalysts, the best results are obtained on the $CeNi_5Zr_{0.5}O_y$ calcined catalyst with 100 % of ethanol converted and close to 52 % of hydrogen among the formed products with 38 % of CO_2 and 10 % CO.

II.2.3. 31 hours test on Zr based calcined compounds

The stabilities of the calcined Zr based catalysts are tested during 31 hours using same conditions. The results of the different *in-situ* pretreated in H_2 at 250 °C $CeNi_xZr_{0.5}O_{y\ (c)}$ catalysts where x = 0.5, 1, 2, and 5 are represented in Figure 17. The corresponding numerical values of ethanol conversion and products distribution are shown in Table 10.

Starting with the catalyst with the low Ni value, $CeNi_{0.5}Zr_{0.5}O_{y\ (c)}$, the conversion of ethanol is almost total (96.8 %) and the main products correspond to 42 % of H_2 and 29.9 % of CO_2. Therefore, not only a good stability is observed, but also an amelioration in formation of the desired gaseous products, but some carbon is formed (0.3 $mg/h.g_{catalyst}$). Unlike on $CeNi_1Zr_{0.5}O_{y\ (c)}$ where a decrease in products distribution of H_2 and CO_2 (38 and 38.9 %) is observed, when going to higher values of Ni content (x = 2 and 5), H_2 % in products distribution increases to 47.3 % and then to 51.6 %. Even if slight variations are obtained after 31 hours, the oxidative steam reforming reaction remains stable for both of these catalysts.

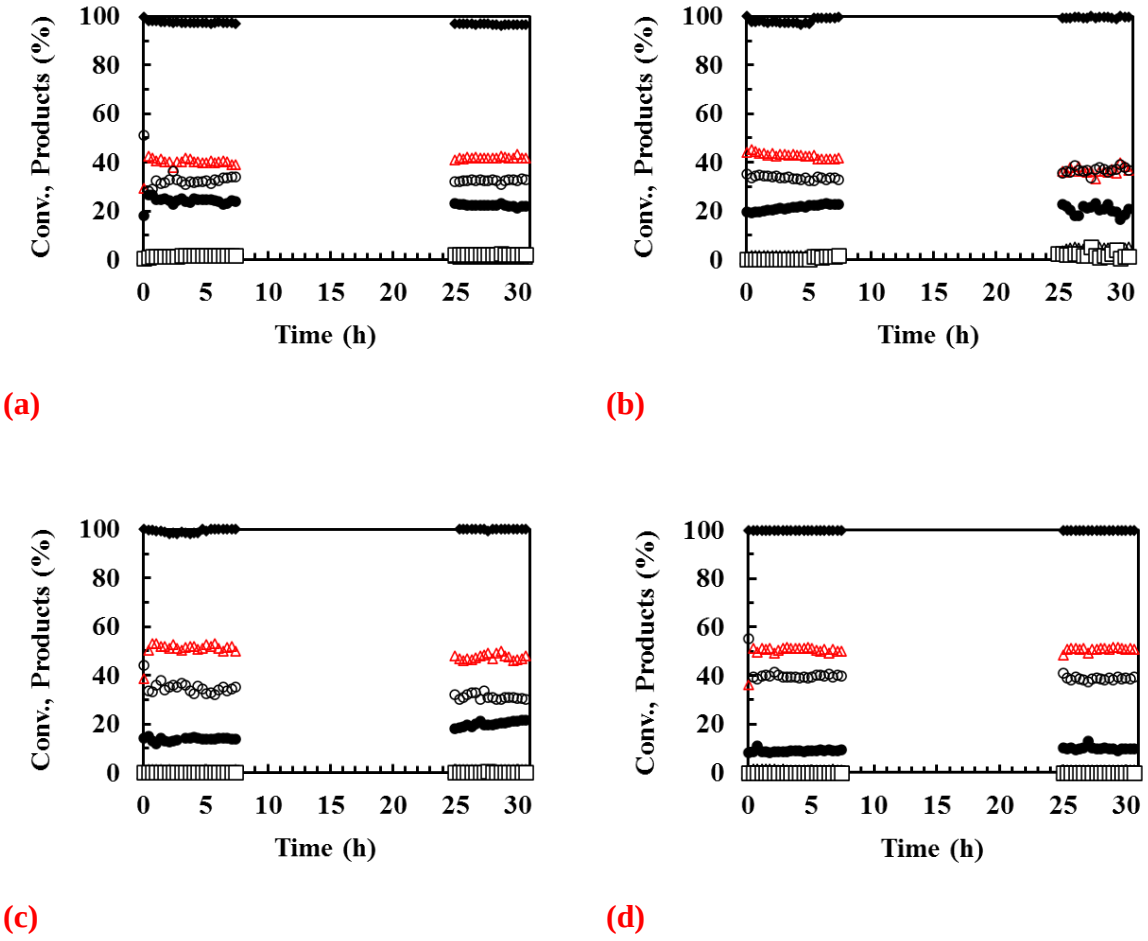

Figure 17 Ethanol conversion (◆) and products distribution (H_2 △, CO_2 ○, CO ●, CH_4 △, acetaldehyde □) during 31 hours on $CeNi_xZr_{0.5}O_{y\ (c)}$ catalysts *in-situ* pretreated in H_2 at 250 °C. a) x = 0.5, b) x = 1, c) x = 2 and d) x = 5. Conversion of O_2 not reported is total ($EtOH/H_2O/O_2/N_2$ = 1:3:1.7:N_2).

The amount of carbon obtained is negligible after 31 hours, in general, for all the Zr based calcined catalysts. Only some carbon is obtained using the lowest Ni content catalysts such as $CeNi_1Zr_{0.5}O_{y\ (c)}$ catalyst (10 mg/h.$g_{catalyst}$). However, it seems that this amount is few enough to not allow the blockage of the active sites of the catalyst and thus the deactivation. The best catalyst used under these conditions is $CeNi_5Zr_{0.5}O_{y\ (c)}$ where 100 % conversion of ethanol is reached with the highest values obtained for H_2 and CO_2 in products distribution (51.6 % and 38.3 % respectively). The only by-products obtained are CO which is obtained with a low value of 10 % and CH_4 in very low amount (at 0.3 %).

Comparing the values obtained after 31 hours in OSRE before doping (Table 6) and after doping the catalyst with Zr (Table 10), the promoting effect of Zr on the activity of the catalyst becomes visible. The conversions of ethanol increase and become 100 % (when x > 0.5) after doping with Zr. Adding Zr, the compounds become more selective to H_2 (38 % compared to 37 %, and

52 % compared to 48 % when x = 1 and 5, respectively) and CO_2 (39 % compared to 31 %, and 38 % compared to 34 % when x = 1 and 5, respectively), while maintaining absence of carbon formation for the highest Ni content catalyst.

Table 10 Conversion of ethanol, products distribution (%) and carbon formation on *in-situ* pretreated in H_2 at 250 °C $CeNi_xZr_{0.5}O_{y\ (c)}$ catalysts after 31 hours in OSRE process. Conversion of O_2 not reported is total ($EtOH/H_2O/O_2/N_2$ = 1:3:1.7:N_2).

		Products distribution (%) after 31 hours					
	Conv. of ethanol (%)	**H_2**	**CO_2**	**CO**	**CH_4**	**CH_3CHO**	**Carbon ($mg/h.g_{catalyst}$)**
$CeNi_{0.5}Zr_{0.5}O_{y(c)}$	96.8	41.9	29.9	22	1.1	2.1	0.3
$CeNi_1Zr_{0.5}O_{y(c)}$	100	38	38.9	18	4	1.1	10.8
$CeNi_2Zr_{0.5}O_{y(c)}$	100	47.3	30	21.9	0.7	0.1	0
$CeNi_5Zr_{0.5}O_{y(c)}$	100	51.6	38.3	9.8	0.3	0	0

II.2.4. Effect of Ni/M_T ratio and doping

To analyze more easily and deeply the effects of Ni/M_T ratio (Ni proportion among the metals in the compound) and doping on catalytic performance in H_2 production, all the previous results obtained under $EtOH/H_2O/O_2/N_2$ = 1:3:1.7: N_2 (5 hours) are grouped together as shown in Figure 18. The products obtained on dried and calcined catalysts are differentiated in the figure legend by the different symbols d and c respectively. The Ni/M_T ratios corresponding to each catalyst are presented in Table 11.

Table 11 Ni/M_T ratio in the different $CeNi_xZr_{0.5}O_y$ and $CeNi_xO_y$ calcined and dried catalysts.

Ni/M_T ratio	**Sample (calcined and dried)**
0.25	$CeNi_{0.5}Zr_{0.5}O_y$
0.33	$CeNi_{0.5}O_y$
0.4	$CeNi_1Zr_{0.5}O_y$
0.5	$CeNi_1O_y$
0.57	$CeNi_2Zr_{0.5}O_y$
0.66	$CeNi_2O_y$
0.76	$CeNi_5Zr_{0.5}O_y$
0.83	$CeNi_5O_y$

Among all the catalysts stated in Figure 18, the $CeNi_5Zr_{0.5}O_{y\,(c)}$ catalyst shows the best catalytic performance. The conversion of ethanol is 100 % (maximum) on $CeNi_5Zr_{0.5}O_y$ calcined catalyst (30 mg), with almost 49 % hydrogen in the products distribution without carbon or acetaldehyde formation. Clearly, ethanol conversions and distribution of H_2, CO_2, CO, CH_4 and acetaldehyde follow same tendencies with the increase in Ni content of the catalyst for both binary and ternary catalysts showing that Ni content is the main parameter influencing the results. Among ternary catalysts, the amount of acetaldehyde produced does not exceed 1 %. Considering only binary catalysts, the percentage of hydrogen increases from 36 % to 45 % when the Ni/M_T ratio is raised from 0.25 to 0.5 similarly for ternary catalysts the order of percentage of hydrogen production is as follows: $CeNi_{0.5}Zr_{0.5}O_y$ < $CeNi_1Zr_{0.5}O_y$ < $CeNi_2Zr_{0.5}O_y$ < $CeNi_5Zr_{0.5}O_y$. The same trend is followed by CO_2 for both binary and ternary catalysts as the CO_2 content produced is increasing with increasing the Ni content. In parallel, increasing this ratio leads to the formation of less CO and CH_3CHO. Therefore, increasing Ni content allows becoming closer to the unique formation of the expected products in OSRE reaction (H_2 and CO_2) diminishing the side reactions leading to byproducts like CO, acetaldehyde, carbon. If the compounds are well homogeneous (due to the preparation), increasing the nickel content increases the interactions between metals and thus favoring the number of active sites. However, as the conversion is total, one cannot afford the transformation of undesired by products (that could be formed) to desired products. Numerous different reactions could take place, and have been largely reviewed [29, 31, 33].

Similarly, the results obtained under same conditions but with only calcined compounds of $CeNi_xO_y$ and $CeNi_xZr_{0.5}O_y$ after 31 hours are reported in Figure 19. Globally, the same trend as observed before is maintained, well evidencing the good stability of the compounds with time during long test run. $CeNi_5Zr_{0.5}O_y$ still possess the best catalytic activity during the OSRE process, with the main formation of H_2 and CO_2 (51.6 % H_2 and 38.3 % CO_2 in products distribution). In addition to the great advantage that carbon, CH_3CHO and CH_4 are totally eliminated.

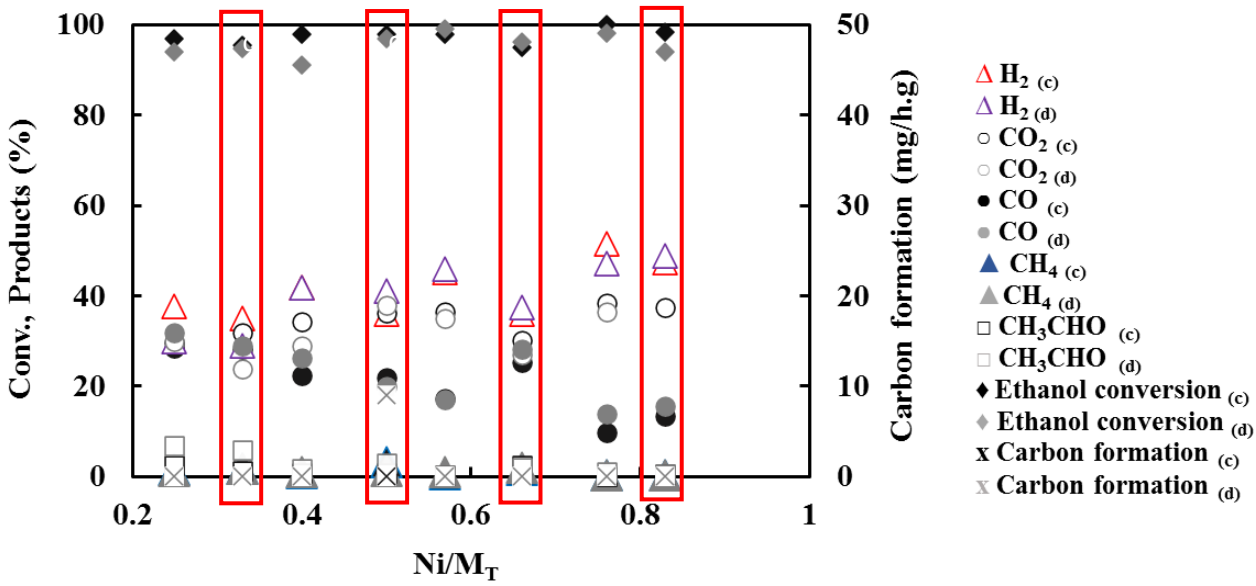

Figure 18 The effect of Ni/M_T ratio on ethanol conversion, products distribution and carbon formation using $CeNi_xZr_{0.5}O_y$ and $CeNi_xO_y$ calcined and dried catalysts pretreated previously in H_2 at 250 °C. Conversion of O_2 not reported is total ($EtOH/H_2O/O_2/N_2$ = 1:3:1.7:N_2). Results are reported after 5 hours in OSRE. Binary catalysts are placed in red columns.

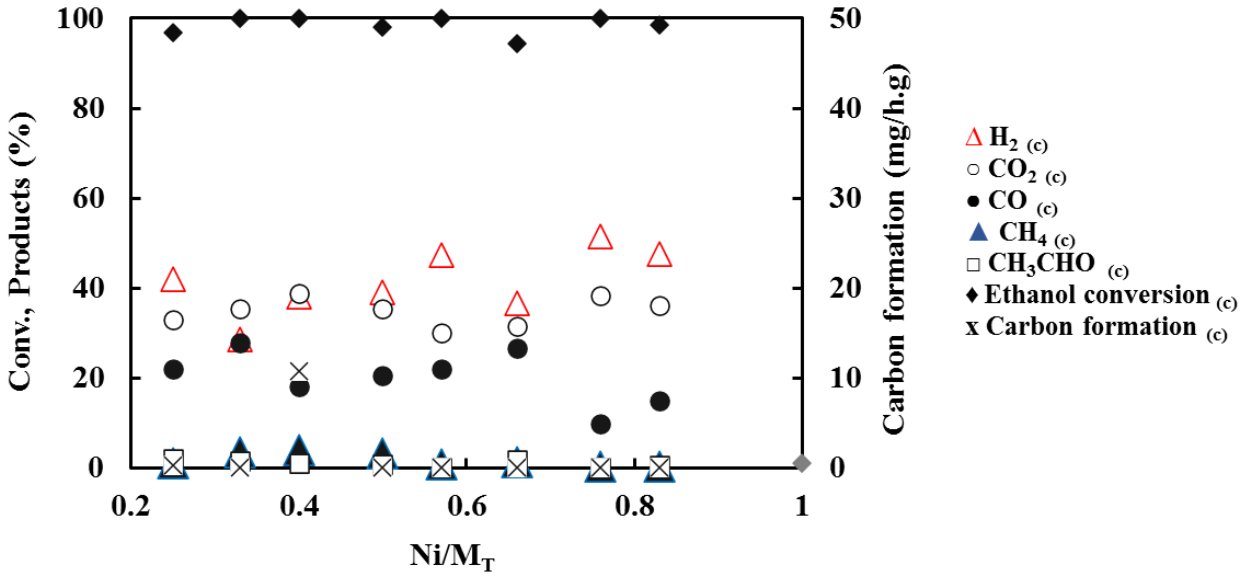

Figure 19 The effect of Ni/M_T ratio on ethanol conversion, products distribution and carbon formation using $CeNi_xZr_{0.5}O_y$ and $CeNi_xO_y$ calcined catalysts *in-situ* pretreated previously in H_2 at 250 °C. Conversion of O_2 not reported is total ($EtOH/H_2O/O_2/N_2$ = 1:3:1.7:N_2). Results are reported after 31 hours in OSRE.

Table 12 reports the measured reaction temperature at the level of the catalyst while the oven is fixed at 50 °C. These temperatures vary between 331 °C and 382 °C. The highest reaction temperature is measured for the $CeNi_5Zr_{0.5}O_{y\ (c)}$ compound (382 °C).

Table 12 Measured reaction temperature at the level of the different $CeNi_xZr_{0.5}O_y$ and $CeNi_xO_y$ calcined catalysts pretreated previously in H_2 at 250 °C and tested in OSRE at an oven temperature of 50 °C. ($EtOH/H_2O/O_2/N_2$ = 1:3:1.7:N_2).

Sample	Ni/M_T ratio	Measured reaction temperature (°C)
$CeNi_{0.5}Zr_{0.5}O_{y\ (c)}$	0.25	350
$CeNi_{0.5}O_{y\ (c)}$	0.33	353
$CeNi_1Zr_{0.5}O_{y\ (c)}$	0.4	372
$CeNi_1O_{y\ (c)}$	0.5	331
$CeNi_2Zr_{0.5}O_{y\ (c)}$	0.57	354
$CeNi_2O_{y\ (c)}$	0.66	345
$CeNi_5Zr_{0.5}O_{y\ (c)}$	0.76	382
$CeNi_5O_{y\ (c)}$	0.83	368

In general, all the catalysts presented before exhibit a very good catalytic activity in OSRE under the following conditions: $EtOH/H_2O/O_2/N_2$ = 1:3:1.7:N_2. The presence of oxygen in the gas feed has already been reported as beneficial to improve the reactions selectivity and thus increase hydrogen yields [218]. However, the excess of this oxygen ratio can decrease the selectivity to hydrogen. Moreover, as the rare earth oxides (CeO_2 or ZrO_2) possess a high redox ability and an oxygen storage capacity that allow the oxidation of the deposited coke on the surface of the catalyst, it can also explain the absence of carbon formation. It has been proposed that these types of materials improve the reducibility of the catalytic system and thus increase the activity in the reforming processes [217]. In fact, at this temperature and at this O_2/EtOH ratio, only few studies have been reported in oxidative steam reforming [96, 97, 238]. Usually lower O_2/EtOH ratios have been studied. Sato et al. reported at a particularly low temperature of 100 °C with an $EtOH/H_2O/O_2$ ratio equal to 1:8:1, with 200 mg of catalyst, 87 % conversion of ethanol on $Ni/Ce_{0.5}Zr_{0.5}O_2$ 233. Another group of scientists reported 40 % of hydrogen in the products distribution under a higher reaction temperature of 300 °C with $CuO\text{-}CeO_2$ catalyst [213]. Here, the oven temperature is fixed at 50 °C, however the reaction temperature measured at the level of the catalysts lies in this range (Table 12). $Ni\text{-}Co/ZnO\text{-}Al_2O_3$ allowed total conversion of ethanol with a H_2 selectivity at about 50 % when feeding a mixture of $EtOH/H_2O/O_2/N_2$ = 1/3/0.4/1.2. Some $CoZn_{2.4}Al_{1.9}$ ex-hydrotalcite mixed oxides were used under $EtOH/H_2O/O_2/\ N_2$ = 1/2.28/0.36/N_2 ratio and a total flow of 120 ml/min to obtain total conversion of ethanol with a H_2 formation around 60 mol % at 575 °C. $La_{0.9}Ce_{0.1}NiO_3$

perovskite-type oxide (performing at $EtOH/H_2O/O_2/N_2$ = 2.5/7.5/1.25/88.75 ratio) gave almost same conversion and product distribution of hydrogen but at 500 °C 212. Therefore, the present catalysts show high performance for OSRE reaction while using high concentration of ethanol (14 %), low mass of catalyst and in particular with an oven fixed at room temperature.

II.2.5. Effect of *in-situ* pretreatment in H_2

To study the effect of pretreatment in H_2 on OSRE process, $CeNi_2Zr_{0.5}O_y$ catalyst is chosen as an intermediate between low and high Ni content. The catalyst is pretreated over night at different temperatures (200, 250, 400 or 500 °C) or not pretreated at all. Figure 20 shows that the pretreatment in H_2 has a drastic effect. Without pretreatment in H_2, the reaction doesn't start at 200 °C and it requires a temperature of 250 °C to get activated and to obtain total conversions. Moreover, without pretreatment a much higher carbon formation is observed with 163 mg/hg. Concerning the gas phase products obtained when the reaction is started at 250 °C, 45 % of H_2, 37 % of CO_2, 17 % of CO, 0.6 % of CH_4 and 0.4 % of acetaldehyde are obtained. In the cases where the catalyst is pretreated in H_2, no carbon formation is observed at all. The conversions are always almost total, and close results are obtained on almost all products formed. H_2 formation varying between 45 % and 51 %, CO_2 between 36 % and 38 %, CO between 10 and 18 %, while the sum of CH_4 and acetaldehyde is lower than 1 %. Therefore, there is only a variation in CO formation when varying the pretreatment in H_2 between 200 °C and 500 °C. So, as a general estimation, a pretreatment in H_2 at 200 °C and 250 °C could be the optimal pretreatment temperatures to be used at the level of conversions (total), products distribution (49 % of H_2, 38 % of CO_2, 12 % of CO, and less than 1 % of CH_4 and acetaldehyde) and energy consumption. As there is a little difference of 50 °C between these 2 pretreatment temperatures, it is important to check the variations in OSRE occurring also at 200 °C

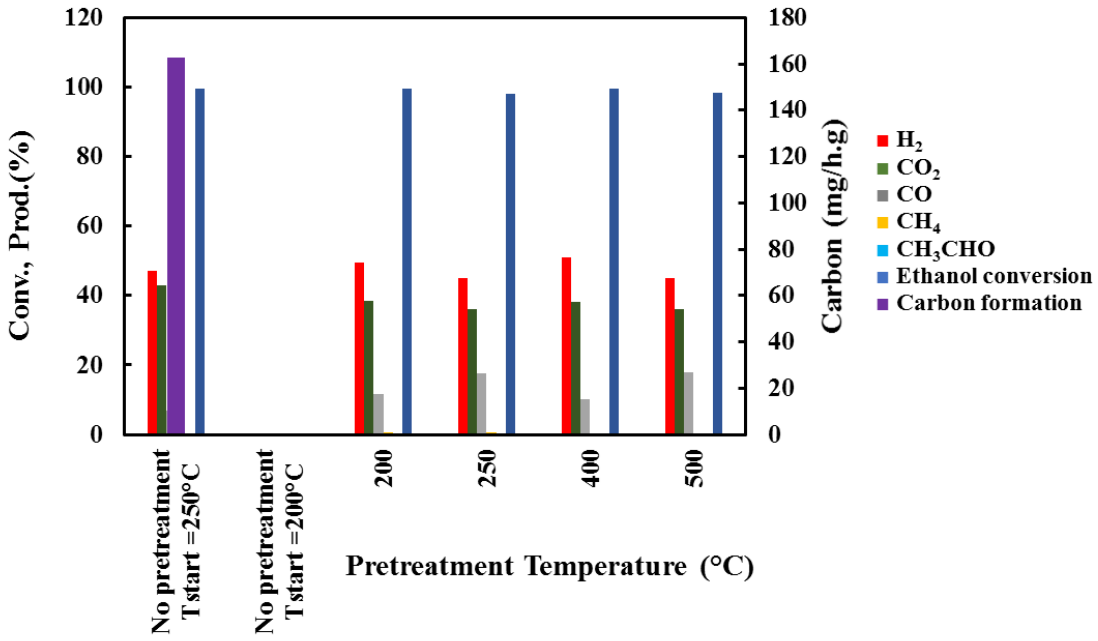

Figure 20 Products distribution and conversion of ethanol with a T_{oven} = 50 °C on the $CeNi_2Zr_{0.5}O_y$ calcined catalyst pretreated at different temperatures in H_2. O_2 conversion is total. Without pretreatment, the reaction started at 250 °C, with pretreatment the reaction starts at 200 °C. $EtOH/H_2O/O_2/N_2$ = 1:3:1.7: N_2. Each result after 5 hours of test.

II.3. OSRE with pretreatment in hydrogen at a temperature of 200 °C

As just seen before on $CeNi_2Zr_{0.5}O_y$ calcined catalyst, a pretreatment temperature of 200 °C could be considered as optimal. For this reason, the other calcined and dried $CeNi_xZr_{0.5}O_y$ catalysts of the same series are tested in same conditions. The results below are divided into 2 parts: the calcined and the dried Zr based catalysts.

II.3.1. Zr based calcined compounds

The calcined compounds of $CeNi_xZr_{0.5}O_y$ series are tested in OSRE conditions ($EtOH/H_2O/O_2/N_2$ = 1:3:1.7:N_2) after previous *in-situ* pretreatment in hydrogen at 200 °C. Table 13 shows the values of ethanol conversions and products distributions obtained on these catalysts after 5 hours experiment. Figure 21 shows the graphs obtained for ethanol conversions and products distributions in percentages for each of these catalysts. Figure 21-a shows the results obtained with $CeNi_{0.5}Zr_{0.5}O_y$ calcined catalyst, the obtained conversion and products distribution are stable over time. 96.8 % conversion of ethanol is achieved under these conditions. The products are distributed as follows: 40 % H_2, 30 % CO_2, 26.1 % CO, 1.2 % CH_4 and 2.1 % CH_3CHO. No solid carbon is formed during this process. With a pretreatment

temperature of 200 °C, this catalyst exhibits higher percentages of hydrogen and CO_2 (Table 13) than those at 250 °C (Table 9) where these ratios were at 37.6 % and 29.8 %. CO, CH_4 and CH_3CHO were higher in percentage when this catalyst was pretreated at 250 °C (Table 9). Similarly, $CeNi_1Zr_{0.5}O_y$ calcined catalyst (Figure 21-b) shows a high stability over the 5 hours experiment. 98.3 % conversion of ethanol is obtained after testing similar to the value obtained with a pretreatment temperature of 250 °C. The products are distributed as follows: 41.3 % H_2, 31.4 % CO_2, 25.2 % CO, 1.2 % CH_4 and 0.9 % CH_3CHO. No carbon is formed. On $CeNi_2Zr_{0.5}O_y$ calcined catalyst (Figure 21-c) a good stability over time with complete conversion of ethanol is observed, with 49.5 % of H_2, 38.3 % of CO_2 in addition to 11.6 % CO, 0.5 % CH_4 and 0.1 % CH_3CHO. In comparison to the same catalyst pretreated at 250 °C (Table 9), higher values are obtained for hydrogen and CO_2 in products distribution and lower values are obtained for the by-products. Conversion of ethanol is not affected by this change of pretreatment temperature. At a nickel/cerium ratio of 5 (Figure 21-d), using the $CeNi_5Zr_{0.5}O_y$ calcined catalyst *in-situ* pretreated in H_2 at 200 °C, total conversion is achieved similar to when the catalyst was pretreated at 250 °C. The percentage of formed hydrogen is of 50.1 %, with 39.1 % of CO_2, 10.3 % of CO and 0.5 % of CH_4. No traces of acetaldehyde are observed. Almost very similar results were obtained with a pretreatment temperature of 250 °C (Table 9) in terms of ethanol conversion and products distribution. At this higher nickel content, a difference of 50 °C in pretreatment temperature is no more noticeable and only slight variations of around 1 % are observed. On all the studied series of calcined catalysts, no carbon is collected after 5 hours (Table 13).

The conversion of ethanol is the same when pretreating the catalysts ($CeNi_xZr_{0.5}O_y$ calcined) at 250 °C or 200 °C. $CeNi_2Zr_{0.5}O_y$ and $CeNi_{0.5}Zr_{0.5}O_y$ calcined catalysts show better activity, in terms of higher percentage of H_2 and CO_2 and lower percentages of by-products, when pretreated at 200 °C compared to 250 °C. However, for $CeNi_1Zr_{0.5}O_y$ and $CeNi_5Zr_{0.5}O_y$ hydrogen percentage is the same using both pretreatment temperatures. Only slight variations are induced on the by-products.

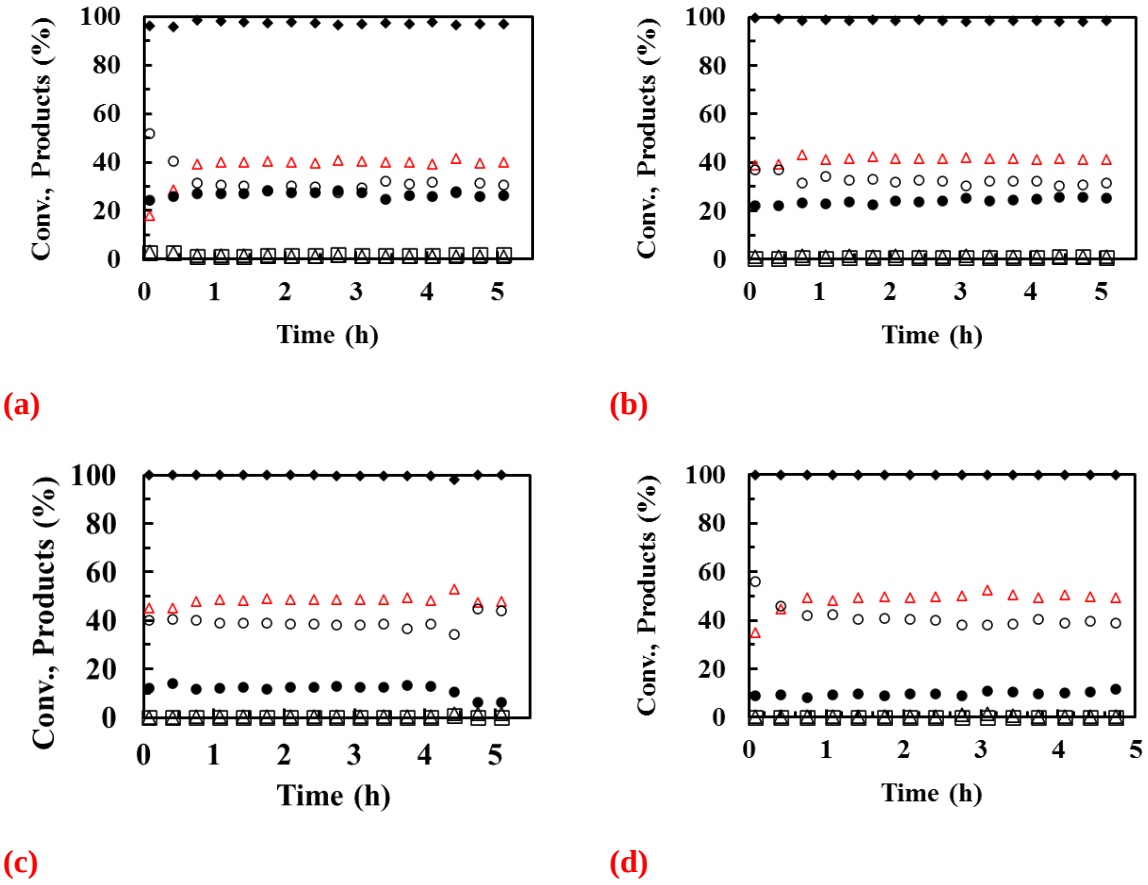

Figure 21 Ethanol conversion (◆) and products distribution (H_2 △, CO_2 ○, CO ●, CH_4 △, acetaldehyde □) on $CeNi_xZr_{0.5}O_y$ calcined catalyst *in-situ* pretreated in H_2 at 200 °C. a) x = 0.5, b) x = 1, c) x = 2 and d) x = 5. Conversion of O_2 not reported is total ($EtOH/H_2O/O_2/N_2$ = 1:3:1.7:N_2).

Table 13 Ethanol conversions, products distribution and carbon formation in OSRE on $CeNi_xZr_{0.5}O_y$ calcined catalysts *in-situ* pretreated in H_2 at 200 °C. Results reported after 5 hours in $EtOH/H_2O/O_2/N_2$ = 1:3:1.7: N_2.

		Products distribution (%)					
	Conv. of ethanol (%)	H_2	CO_2	CO	CH_4	CH_3CHO	Carbon (mg/h.g)
$CeNi_{0.5}Zr_{0.5}O_y$ (c)	96.8	40.2	30.4	26.1	1.2	2.1	0.0
$CeNi_1Zr_{0.5}O_y$ (c)	98.3	41.3	31.4	25.2	1.2	0.9	0.0
$CeNi_2Zr_{0.5}O_y$ (c)	99.5	49.5	38.3	11.6	0.5	0.1	0.0
$CeNi_5Zr_{0.5}O_y$ (c)	100.0	50.1	39.1	10.3	0.5	0.0	0.0

It is obvious that with the increase of Ni content the conversion of ethanol is increasing in addition to the percentages of hydrogen and carbon dioxide in products distribution. Moreover, the amount of byproducts CO, CH_4 and CH_3CHO drops from 26.1 %, 1.2 % and 2.1 % respectively with Ni/Ce ratio of 0.5 till 10.3 %, 0.5 % and 0 % respectively using Ni/Ce ratio

of 5. This is in good conformation of what have been observed before regarding the effect of Ni content on performance in OSRE.

II.3.2. Zr based dried compounds

In this part, the dried compounds of $CeNi_xZr_{0.5}O_y$ are studied after a pretreatment in H_2 at 200 °C and compared to the previous results obtained with a pretreatment of 250 °C. Table 14 summarizes the results obtained after 5 hours experiment in OSRE. A very good stability is obtained on the catalysts in terms of conversion of ethanol and distribution of products (Figure 21). Similar to the values obtained at pretreatment of 250 °C (Table 8), no carbon is collected after 5 hours of experiment (Table 14). Starting with $CeNi_{0.5}Zr_{0.5}O_{y\ (d)}$ catalyst (Figure 22-a), 93 % conversion of ethanol is obtained. This conversion is the same whether pretreating the catalyst at 250 °C or 200 °C. The dominating by-product here is CO filling around 33 % of the products distribution. Almost equal percentages of H_2 (31 %) and CO_2 (30 %) are obtained among the products. The other by-products are distributed as follows: 1.3 % CH_4 and 5.8 % CH_3CHO. At a higher Ni content, on $CeNi_1Zr_{0.5}O_{y\ (d)}$ catalyst (Figure 22-b), the conversion of ethanol reaches 97 % and is higher than that on the pretreated at 250 °C compound (91 %) shown in Table 14. The products are distributed as follows: 41.8 % H_2, 29.1 % CO_2, 26.6 % CO, 1.2 % CH_4 and 1.3 % CH_3CHO. With this Ni content and with a pretreatment temperature of 250 °C, the percentages of products tend to be slightly higher (around 2 %). Similar to the $CeNi_{0.5}Zr_{0.5}O_y$ dried catalyst, no great difference in products distribution is obtained by decreasing the pretreatment temperature by 50 °C even higher conversion of ethanol is obtained.

Figure 22-c describes the results obtained with $CeNi_2Zr_{0.5}O_y$ dried catalyst and complete conversion is obtained under these conditions (99.6 %) with 47.9 % H_2, 36.9 % CO_2, 14.7 % CO and trace amounts of CH_4 and CH_3CHO (0.4 % and 0.1 % respectively). The values of H_2 and CO_2 percentages are higher than those obtained with a pretreatment temperature of 250 °C (2% difference). As a consequence, lower percentages of undesired products are obtained with a pretreatment temperature of 200 °C on $CeNi_5Zr_{0.5}O_y$ dried catalyst.

Figure 22-d shows similar results to other experiments performed on the zirconium series, with pretreatment temperature of 200 °C or 250 °C. The conversion of ethanol is almost complete over time. The highest percentage of produced H_2 is obtained here in this series where it reaches around 51 % with 41 % CO_2. The other products are distributed as follows: 6.9 % CO, 0.9 % CH_4 and 0.5 % CH_3CHO. In comparison to the experiment done at a pretreatment temperature of 250 °C, these conditions gave higher production of hydrogen and CO_2 with only 8 %

undesired products. For comparison, at a pretreatment temperature of 250 °C, around 15 % of undesired products were obtained. Thus, 7 % of byproducts are diminished when pretreating the $CeNi_5Zr_{0.5}O_y$ dried catalyst at 200 °C.

Finally, it can be noticed that at a pretreatment temperature of 200 °C, all the dried catalysts in this series (except $CeNi_1Zr_{0.5}O_y$ dried which showed slightly lower H_2 and CO_2 percentages) have better distribution of products in terms of higher hydrogen and carbon dioxide percentages. In general, at both pretreatment temperatures 250 °C and 200 °C, all catalysts show very good catalytic performance in OSRE.

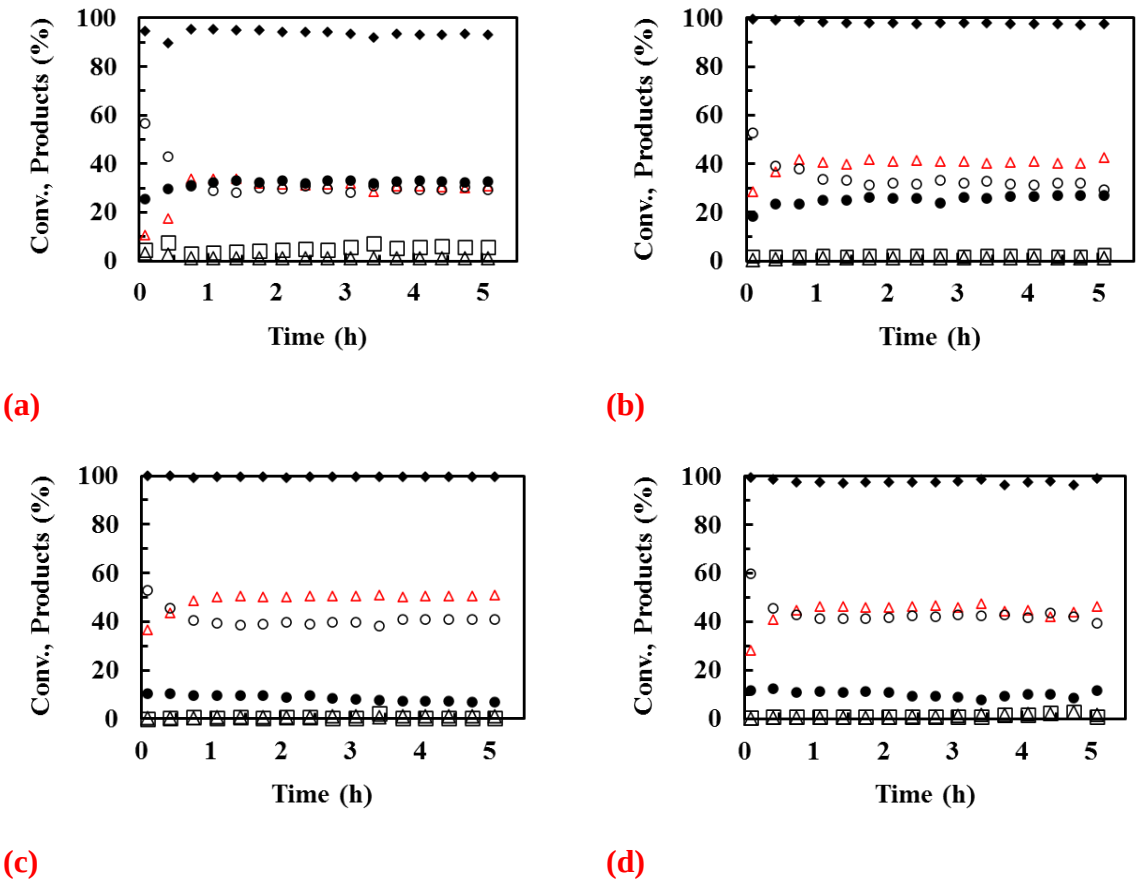

Figure 22 Ethanol conversion (◆) and products distribution (H_2 △, CO_2 ○, CO ●, CH_4 △, acetaldehyde □) after 5 hours in OSRE on $CeNi_xZr_{0.5}O_{y\ (d)}$ catalyst *in-situ* pretreated in H_2 at 200 °C. a) x = 0.5, b) x = 1, c) x = 2 and d) x = 5. Conversion of O_2 not reported is total ($EtOH/H_2O/O_2/N_2$ = 1:3:1.7:N_2).

Table 14 Ethanol conversions, products distribution and carbon formation in OSRE on $CeNi_xZr_{0.5}O_y$ dried catalysts pretreated in H_2 at 200 °C. Results reported after 5 hours in $EtOH/H_2O/O_2/N_2$ = 1:3:1.7: N_2.

		Products distribution (%)					
	Conv of ethanol (%)	**H_2**	**CO_2**	**CO**	**CH_4**	**CH_3CHO**	**Carbon (mg/h.$g_{catalyst}$)**
$CeNi_{0.5}Zr_{0.5}O_{y\ (d)}$	93.1	30.8	29.4	32.7	1.3	5.8	0.0
$CeNi_1Zr_{0.5}O_{y\ (d)}$	97.4	41.8	29.1	26.6	1.2	1.3	0.0
$CeNi_2Zr_{0.5}O_{y\ (d)}$	99.6	47.9	36.9	14.7	0.4	0.1	0.0
$CeNi_5Zr_{0.5}O_{y\ (d)}$	99.7	50.9	40.8	6.9	0.9	0.5	0.0

Now, comparing the dried catalysts to the calcined ones of the $CeNi_xZr_{0.5}O_y$ series pretreated at 200 °C, it can be revealed that calcination has a very important role in the performance of the catalysts specially at low Ni contents. More by-products are obtained on catalysts without previous calcination in particular acetaldehyde and carbon monoxide. This phenomenon is more evident on lowest Ni content catalyst ($CeNi_{0.5}Zr_{0.5}O_y$). CH_4 formation is not affected by the calcination step as it is obtained in the same amounts in the presence and absence of the calcination.

II.3.3. 31 hours test on Zr based calcined compounds

Several papers existing in literature report the activity, selectivity and stability of Ni based catalysts over time in OSRE [189, 190, 315-317]. Based on the previous tests showing the good activities in OSRE after 5 hours of $CeNi_xZr_{0.5}O_{y\ (c)}$ previously pretreated in H_2 at 200 °C, it is interesting to perform long test runs of 31 hours. The results of ethanol conversion and products distribution are shown in Figure 23 and Table 15). It is clear that the conversion of ethanol is complete in all the cases of x. Based on the graphs of Figure 23, the conversion of ethanol and products distribution are stable overtime for all the $CeNi_xZr_{0.5}O_{y\ (c)}$. During the first 2 hours in OSRE, the temperature of the oven stabilizes at 50 °C and thus the main variations lye in the first 1 or 2 hours of the reaction. However, analyzing deeply into the table, some slight variations take place compared to the results obtained in the 5 hours. Globally, when x increases, ethanol conversion and H_2 and CO_2 formations increase, while the by-products decrease, in particular CO (from 20 % down to 10 %) while CH_4 and acetaldehyde are lower or equal to 1 % (Table 15). When comparing the 31 hours test (Table 15) to 5 hours test (Table 12), H_2 percentage in products distribution increases from 41 % to 46 % and from 42 % to 48 % on $CeNi_{0.5}Zr_{0.5}O_{y\ (c)}$ and $CeNi_1Zr_{0.5}O_{y\ (c),}$ respectively. Moreover, on the same catalysts, the percentages of CO and CH_3CHO drop after 31 hours compared to the results obtained after 5 hours (Table 13). On the contrast, a slight decrease in H_2 products distribution is followed by

the long time on stream with $CeNi_2Zr_{0.5}O_{y\ (c)}$ in addition to the increase in CO and CH_3CHO %. However, regardless of this slight decrease the results are still considered in the range of stability and mainly satisfactory. Few amounts of carbon are found only on $CeNi_2Zr_{0.5}O_{y\ (c)}$. $CeNi_5Zr_{0.5}O_{y\ (c)}$ leads to the best results among the calcined Zr based catalysts pretreated in H_2 at 200 °C. The conversion of this catalyst remains at 100 % all over the process with high stability and good selectivity on the main products.

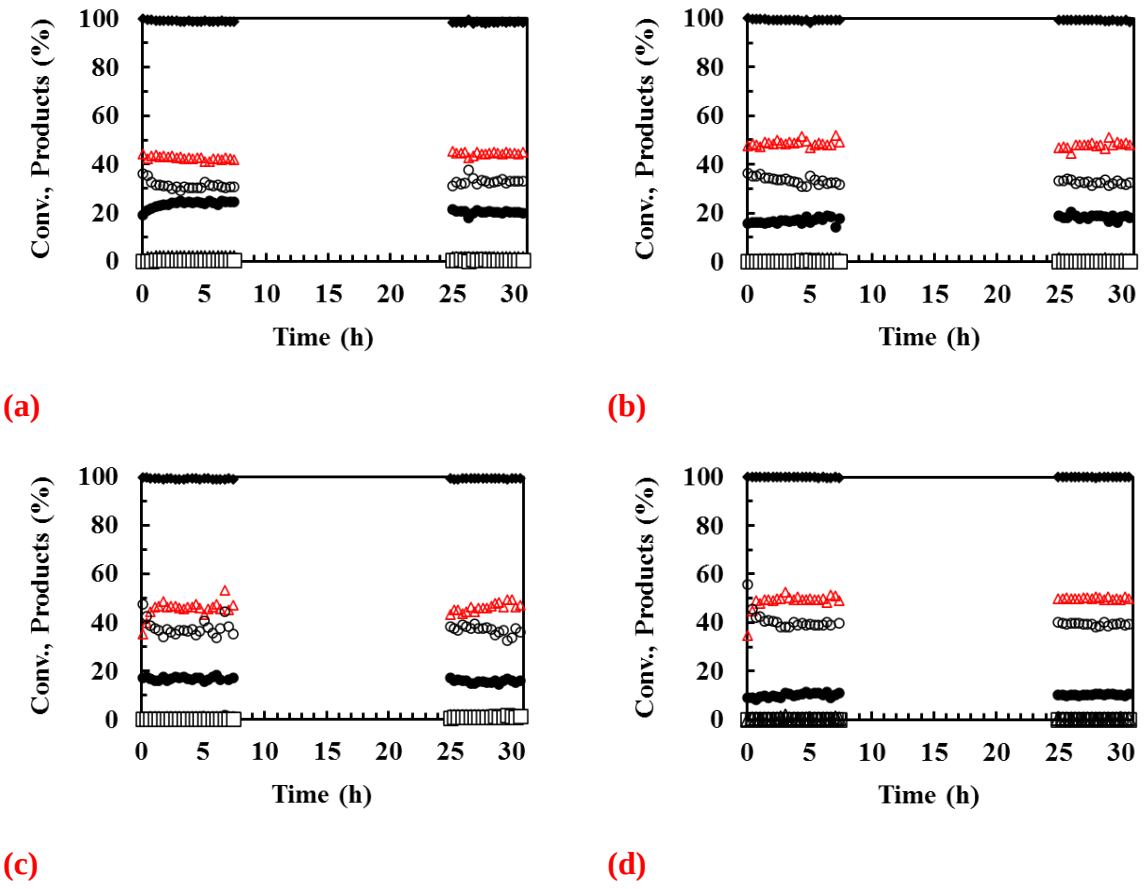

Figure 23 Ethanol conversion (◆) and products distribution (H_2 △, CO_2 ○, CO ●, CH_4 △, acetaldehyde □) after 31 hours in OSRE on $CeNi_xZr_{0.5}O_y$ calcined catalyst *in-situ* pretreated in H_2 at 200 °C. a) x = 0.5, b) x = 1, c) x = 2 and d) x = 5. Conversion of O_2 not reported is total ($EtOH/H_2O/O_2/N_2$ = 1:3:1.7:N_2).

Table 15 Ethanol conversions, products distribution and carbon formation in OSRE on $CeNi_xZr_{0.5}O_y$ calcined catalysts pretreated in H_2 at 200 °C. Results reported after 31 hours in $EtOH/H_2O/O_2/N_2$ = 1:3:1.7: N_2.

		Products distribution (%)					
	Conv. of ethanol (%)	**H_2**	**CO_2**	**CO**	**CH_4**	**CH_3CHO**	**Carbon (mg/h.$g_{catalyst}$)**
$CeNi_{0.5}Zr_{0.5}O_{y\ (c)}$	98.2	46.2	31.7	19.9	1.4	0.8	0.0
$CeNi_1Zr_{0.5}O_{y\ (c)}$	98.7	48.2	33.2	17.4	0.8	0.4	0.0
$CeNi_2Zr_{0.5}O_{y\ (c)}$	99.2	46.8	35.6	15.5	1.0	1.1	16.0
$CeNi_5Zr_{0.5}O_{y\ (c)}$	100.0	50.1	39.0	10.3	0.6	0.0	0.0

II.3.4. 31 hours test on dried Zr based compounds

In the following section, dried compounds of $CeNi_xZr_{0.5}O_y$ will be studied in similar conditions to what has been reported before on the calcined catalysts. This will allow to investigate the stability of these compounds after 31 hours in addition to the effect of calcination. The dried and calcined compounds containing Zr will be compared finally to determine the best Zr based catalysts in OSRE. Figure 24 and Table 16 represent the results obtained after 31 hours in OSRE for dried compounds. In general, the conversions of ethanol obtained with these catalysts after the long test run are almost complete (≥ 95 %). Regardless of any fluctuations that are normal at the very first steps in OSRE, this conversion remains the same as reported before with 5 hours (Table 14). H_2 percentage increases with the increase in Ni content from around 36 % to 47 %, going higher from x = 0.5 to x = 5. These percentages change slightly with time with a deviation of maximum 5 % from what has been recorded after 5 hours. Even though these dried catalysts show good performances in OSRE with pretreatment temperature of 200 °C, the calcined catalysts under same conditions still show better performances in terms of ethanol conversion and selectivity to products. Only with $CeNi_2Zr_{0.5}O_{y\ (d)}$, carbon is obtained after 31 hours with an estimation of about 8 mg/h.$g_{catalyst}$. This catalyst presents few amounts of carbon only after 31 hours in both cases with previous calcination at 500 °C or without previous calcination. The best catalyst performing in this series is contributed to $CeNi_5Zr_{0.5}O_{y\ (d)}$ which gives the highest conversion of ethanol (about 100 %) and the maximal main products distribution (48 % H_2 and 39 % CO_2, 10 % CO, 1 % CH_4, and 1 % acetaldehyde, no carbon) among the other catalysts. The order of better performance, under $EtOH/H_2O/O_2/N_2$ = 1:3:1.7:N_2 and pretreatment temperature of 200 °C, could be as follows: $CeNi_5Zr_{0.5}O_{y\ (d)}$ > $CeNi_2Zr_{0.5}O_{y\ (d)}$ > $CeNi_1Zr_{0.5}O_{y}$ > $_{(d)}$ $CeNi0._5Zr_{0.5}O_{y\ (d)}$. In comparison to the calcined Zr series presented in Table 15, $CeNi_5Zr_{0.5}O_{y\ (c)}$ is still the best (with 100 % EtOH conv., 50 % H_2, 39 % CO_2, 10 % CO, 0.6 %

CH_4, no acetaldehyde, no carbon) among the Zr based compounds performing in OSRE after pretreatment in H_2 at 200 °C. However, one can remark that the results obtained on the dried and calcined $CeNi_5Zr_{0.5}O_y$ compounds are relatively small, while the dried compound requires much less energy to be prepared.

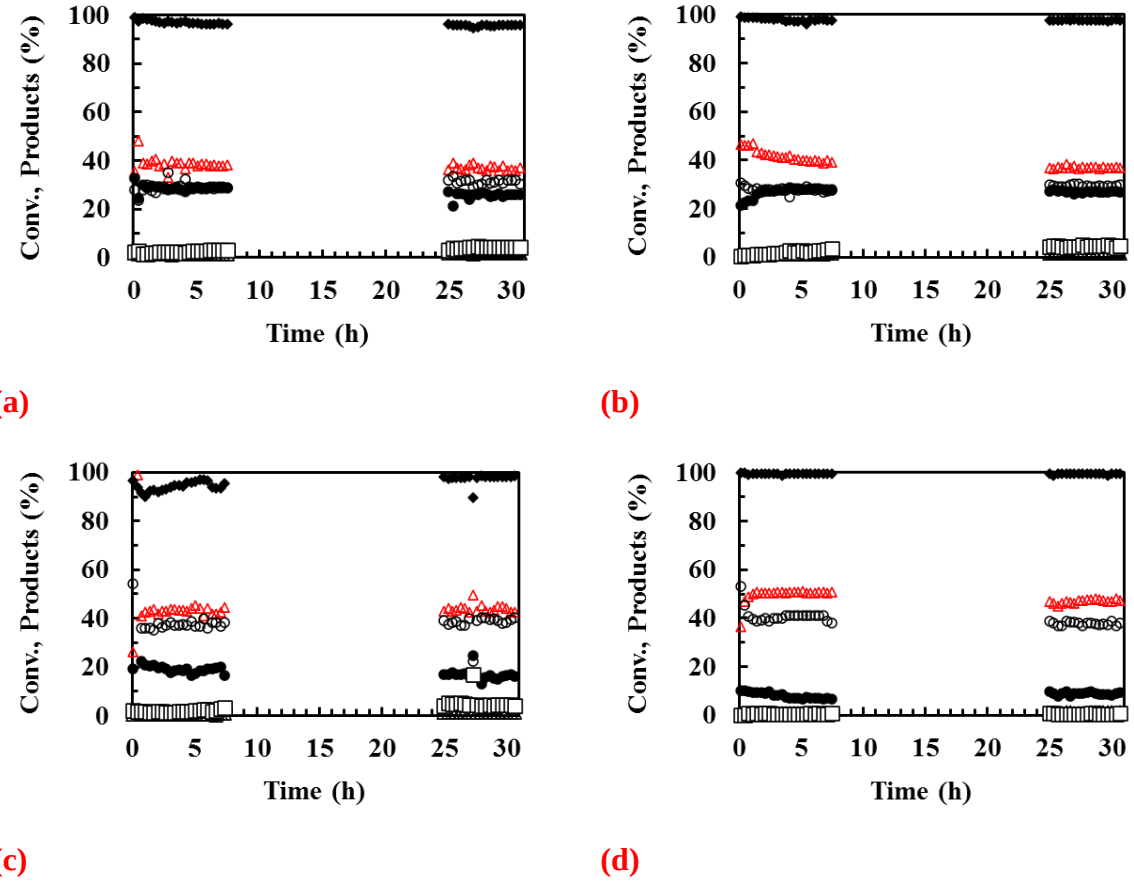

Figure 24 Ethanol conversion (◆) and products distribution (H_2 △, CO_2 ○, CO ●, CH_4 △, acetaldehyde □) after 31 hours in OSRE on $CeNi_xZr_{0.5}O_y$ dried catalyst *in-situ* pretreated in H_2 at 200 °C. a) x = 0.5, b) x = 1, c) x = 2 and d) x = 5. Conversion of O_2 not reported is total ($EtOH/H_2O/O_2/N_2$ = 1:3:1.7:N_2).

Table 16 Ethanol conversions, products distribution and carbon formation in OSRE on $CeNi_xZr_{0.5}O_y$ dried catalysts pretreated in H_2 at 200 °C. Results reported after 31 hours in $EtOH/H_2O/O_2/N_2$ = 1:3:1.7: N_2.

		Products distribution (%)					
	Conv. of ethanol (%)	**H_2**	**CO_2**	**CO**	**CH_4**	**CH_3CHO**	**Carbon (mg/h.$g_{catalyst}$)**
$CeNi_{0.5}Zr_{0.5}O_y$ (d)	95.1	36.3	31.6	25.1	2.1	4.9	0.0
$CeNi_1Zr_{0.5}O_y$ (d)	97.5	37.1	29.3	26.9	1.8	4.9	0.0
$CeNi_2Zr_{0.5}O_y$ (d)	98.5	41.2	38.8	15.6	1.2	3.2	8.25
$CeNi_5Zr_{0.5}O_y$ (d)	99.7	47.7	39.4	10.3	1.3	1.3	0.0

II.3.5. Effect of mass of catalyst

To study the effect of mass of catalyst on the OSRE process, 2 different masses (30 mg and 60 mg) are used to test $CeNi_2Zr_{0.5}O_{y\ (c)}$ and $CeNi_5Zr_{0.5}O_{y\ (c)}$ under the same conditions as before but during 31 hours (with a previous pretreatment of these catalysts in hydrogen at 200 °C).

Figure 25 shows the progression of the different products and that of ethanol over time for $CeNi_2Zr_{0.5}O_{y\ (c)}$ with 30 mg (-a) and 60 mg (-b). The corresponding numerical values after 31 hours on stream are represented in Table 17 . The conversions of ethanol are always complete no matter what the mass of catalyst used is. Increasing the mass of catalyst from 30 mg to 60 mg is responsible for the high amounts of carbon produced at the end of the process. On the contrary, CO percentage in products distribution drop while using 60 mg of the catalyst which can be seen as an advantage. The same effect is observed on $CeNi_5Zr_{0.5}O_{y\ (c)}$ (Table 18 and Figure 26) where an increase of the mass of the catalyst leads to the formation of 9.2 $mg/h.g_{catalyst}$. Moreover, the percentage of H_2 in products distribution drops from 50 to 45 %. On the other side, the percentage of CO drops by 4 %.

To finally conclude, increasing the mass of the catalyst is not the best option to optimize the OSRE process. It is shown that this only leads to the formation of more carbon which could later block the activity of the catalyst with time.

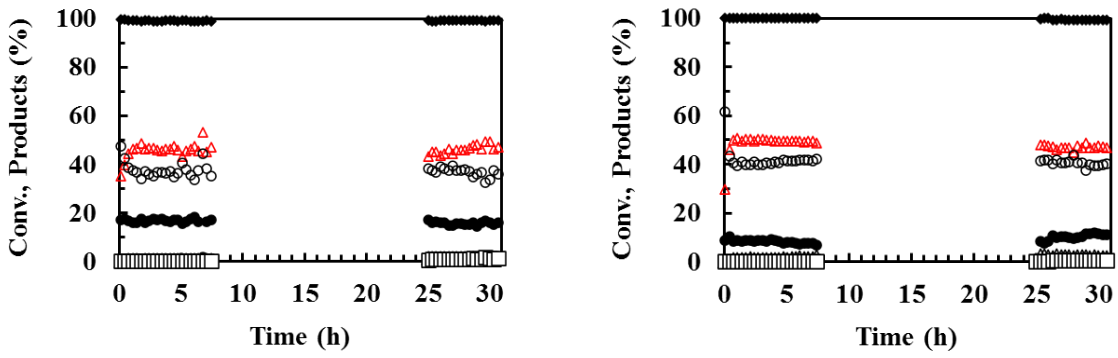

(a) **(b)**

Figure 25 Ethanol conversion (◆) and products distribution (H_2 △, CO_2 ○, CO ●, CH_4 △, acetaldehyde □) after 31 hours OSRE on a) 30 mg and b) 60 mg $CeNi_2Zr_{0.5}O_y$ calcined catalyst *in-situ* pretreated in H_2 at 200 °C. Conversion of O_2 not reported is total ($EtOH/H_2O/O_2/N_2$ = 1:3:1.7:N_2).

Table 17 Effect of mass of catalyst on the conversion of ethanol and products distribution after 31 hours on $CeZr_{0.5}Ni_2O_y$ calcined catalyst *in-situ* pretreated in H_2 at 200 °C.

		Products distribution (%)					
Mass of $CeNi_2Zr_{0.5}O_{y(c)}$ (mg)	**Conv. of ethanol (%)**	**H_2**	**CO_2**	**CO**	**CH_4**	**CH_3CHO**	**Carbon ($mg/h.g_{catalyst}$)**
30	99.2	46.9	35.7	15.7	0.8	0.9	16.0
60	99.7	47.2	40.1	10.7	1.7	0.3	68.4

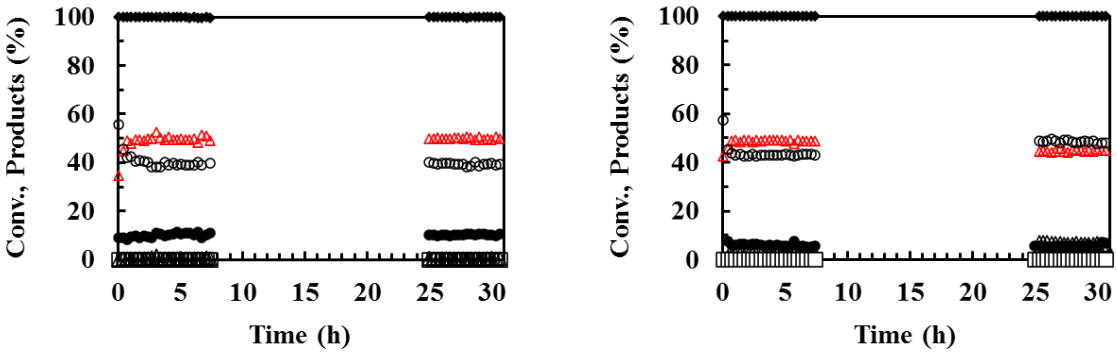

(a) **(b)**

Figure 26 Ethanol conversion (◆) and products distribution (H_2 △, CO_2 ○, CO ●, CH_4 △, acetaldehyde □) after 31 hours in OSRE on a) 30 mg and b) 60 mg $CeNi_5Zr_{0.5}O_y$ calcined catalyst *in-situ* pretreated in H_2 at 200 °C. Conversion of O_2 not reported is total ($EtOH/H_2O/O_2/N_2$ = 1:3:1.7:N_2).

Table 18 Effect of mass of catalyst on the conversion of ethanol and products distribution after 31 hours on $CeNi_5Zr_{0.5}O_y$ calcined catalyst *in-situ* pretreated in H_2 at 200 °C.

		Products distribution (%)					
Mass of $CeNi_5Zr_{0.5}O_{y\ (c)}$ (mg)	**Conv. of ethanol (%)**	**H_2**	**CO_2**	**CO**	**CH_4**	**CH_3CHO**	**Carbon ($mg/h.g_{catalyst}$)**
30	100.0	50.1	39.0	10.3	0.6	0.0	0.0
60	100.0	44.8	48.2	6.1	0.8	0.1	9.2

II.4. OSRE on Al based compounds

In this part Zr is substituted by Al to see the effect of doping with this element on OSRE results under same conditions. Al has been previously studied in literature and previous works in our lab. It is interesting to check its performance in OSRE with these ratios: $EtOH/H_2O/O_2/N_2$ = 1:3:1.7: N_2 as they have already shown better performances than other ratios used on the binary catalysts. Only calcined compounds of $CeNi_xAl_{0.5}O_y$ where x = 0.5, 1 and 2 are studied. These compounds are tested after *in-situ* pretreatment in H_2 at 250 °C and also 300 °C.

II.4.1 OSRE on Al based compounds pretreated in H_2 at 250 °C

In this section the catalysts were previously pretreated in H_2 at 250 °C. Same as previously, the reaction is started with an oven temperature of 200 °C and then it is decreased and fixed at 50 °C when the reaction is stabilized. Figure 27 reports the results versus time, Table 19 summarizes all the results for this series of catalysts illustrating the evolutions of products distribution and conversion of ethanol after 5 hours in OSRE. During the first hour of OSRE with $CeNi_{0.5}Al_{0.5}O_y$ calcined catalyst (Figure 27-a), the conversion of ethanol is around 95 %. However, this value drops down to 83 % as soon as the temperature of the oven started to stabilize (knowing that the reaction is started at 200 °C and then fixed at 50 ˚C). The ethanol conversion remains stable during the rest 4 hours of OSRE. This trend is also followed by the products that also remains stable for the other 4 hours of experiment. The percentage of hydrogen and CO_2 reach 34.9 % and 37.2 % respectively. 20.9 % CO is produced in addition with 6.1 % acetaldehyde and trace amounts of CH_4 (0.9 %). No carbon formation is observed after the test. At Ni/Ce ratio of 1 ($CeNi_1Al_{0.5}O_y$, Figure 27-b) the conversion of ethanol and products distribution are not affected by the change of temperature at the beginning of the test. The conversion of ethanol remained stable at about 97 %. This value is higher than that obtained with the $CeNi_{0.5}Al_{0.5}O_y$ calcined catalyst (Figure 27-a), The percentage of hydrogen reaches 42.7 % during 5 hours experiment higher than that produced with a Ni ratio of 0.5. The other products are distributed as follows: 38.6 % CO_2, 15.4 % CO, 2.1 % CH_3CHO and 1.2 % CH_4 (Table 19). However, after 5 hours experiment 24 mg/h.$g_{catalyst}$ of carbon are collected which is still not a high value. On $CeNi_2Al_{0.5}O_y$ compound (Figure 27-c) very good stability of ethanol conversion and products distribution is attained over time. The conversion of ethanol is around 96 % during the 5 hours of experiment. The products are distributed as follows: 40 % H_2, 34.1 % CO_2, 22.1 % CO, 1.5 % CH_4 and 2.3 % CH_3CHO. No carbon is obtained with this $CeNi_2Al_{0.5}O_y$ calcined catalyst.

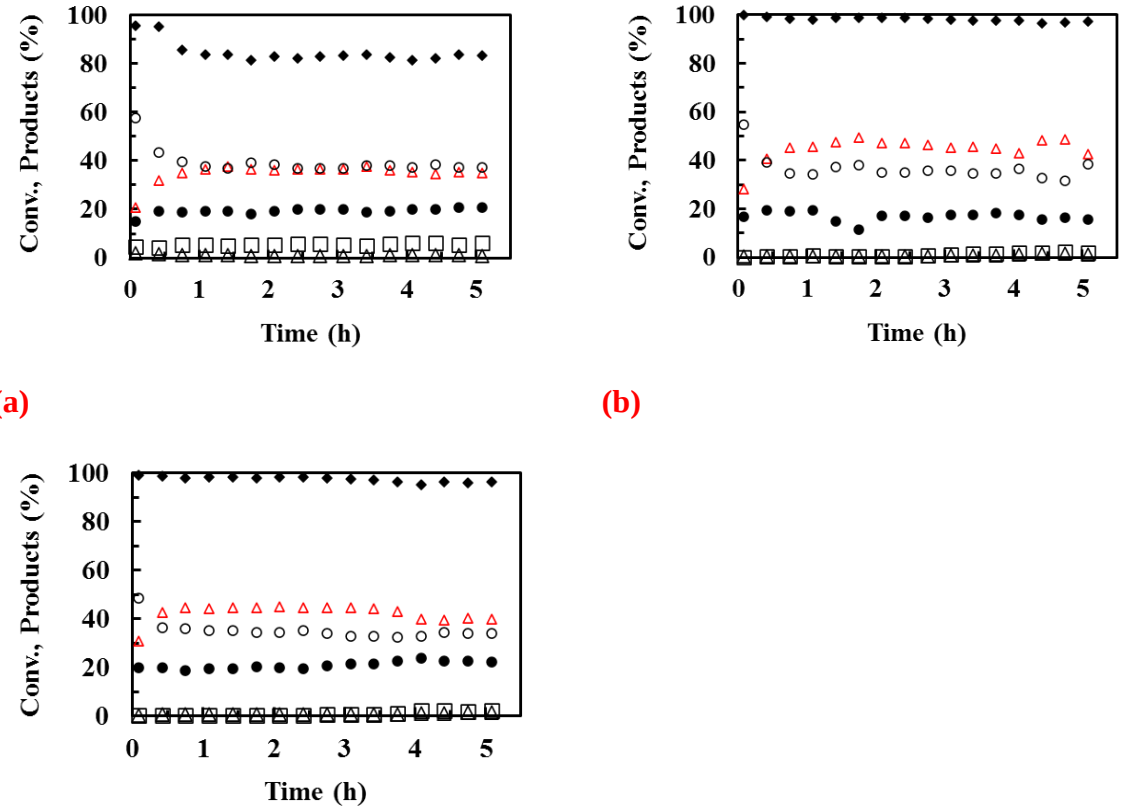

Figure 27 Ethanol conversion (◆) and products distribution (H_2 △, CO_2 ○, CO ●, CH_4 △, acetaldehyde □) during 5 hours in OSRE on $CeNi_xAl_{0.5}O_y$ catalysts *in-situ* pretreated in H_2 at 250 °C. a) x = 0.5, b) x = 1 and c) x = 2. Conversion of O_2 not reported is total ($EtOH/H_2O/O_2/N_2$ = 1:3:1.7:N_2).

Table 19 Ethanol conversions, products distribution and carbon formation in OSRE on $CeNi_xAl_{0.5}O_y$ calcined catalysts *in-situ* pretreated in H_2 at 250 °C. Results reported after 5 hours in $EtOH/H_2O/O_2/N_2$ = 1:3:1.7: N_2.

		Products distribution (%)					
	Conv. of ethanol (%)	H_2	CO_2	CO	CH_4	CH_3CHO	Carbon (mg/h.g)
$CeNi_{0.5}Al_{0.5}O_y$ (c)	83	34.9	37.2	20.9	0.9	6.1	0
$CeNi_1Al_{0.5}O_y$ (c)	97	42.7	38.6	15.4	1.2	2.1	24
$CeNi_2Al_{0.5}O_y$ (c)	96	40	34.1	22.1	1.5	2.3	0

Comparing $CeNi_1Al_{0.5}O_y$ (c) to $CeNi_1Zr_{0.5}O_y$ (c) catalyst, $CeNi_1Zr_{0.5}O_y$ can be considered as having a better performance in OSRE since no carbon formation is recorded compared to 24 mg/h.$g_{catalyst}$. The conversion of ethanol (97 - 98 %) and hydrogen percentage (41.7 - 42.7 %) are almost similar but the CH_4 and CH_3CHO values are much lower (0.9 % CH_4 and 0.8% CH_3CHO) on Zr based catalysts (Table 9, Figure 16) compared to Al catalysts (1.2 % CH_4 and 2.1% CH_3CHO). Similar trend is observed on $CeNi_2Zr_{0.5}O_y$ (c) catalyst in terms of lower

CH_3CHO (0.4 %), CH_4 (0.6 %) values in addition to CO (17.4 %) when compared to the Al compound of same Ni/Ce ratio (2.3 % CH_3CHO, 1.5 % CH_4 and 22.1 % CO). Moreover, $CeNi_2Zr_{0.5}O_{y\ (c)}$ catalyst gives higher H_2 concentration (51.6 % H_2) in the products distribution than $CeNi_2Al_{0.5}O_{y\ (c)}$ catalyst (40 % H_2).

As an overall, doping the catalyst with Zr is better than doping with Al, since this can decrease the amounts of byproducts obtained and eliminate the possible carbon formation that could be produced from Al compounds. Al compounds can be considered better when using low Ni/Ce ratio (0.5) since it can be started at lower temperatures unlike the Zr compound with low Ni/Ce ratio. Doping $CeNi_xO_y$ catalysts with Zr leads to higher conversions of ethanol (97-100 %) compared to that doped with Al (83 – 96 %) and higher H_2 percentage with lower acetaldehyde percentage when considering x values higher than 0.5. The $CeNi_{0.5}Al_{0.5}O_y$ calcined catalyst can be started at 200 °C after pretreating it overnight at 250 °C however the $CeNi_{0.5}Zr_{0.5}O_{y\ (c)}$ cannot be started at 200 °C under same conditions and it requires a temperature of 250 °C to be launched. $CeNi_1Zr_{0.5}O_{y\ (c)}$ and $CeNi_2Zr_{0.5}O_{y\ (c)}$ catalysts are started normally at 200 °C same with $CeNi_1Al_{0.5}O_{y\ (c)}$ and $CeNi_2Al_{0.5}O_{y\ (c)}$ catalysts.

III.4.2. OSRE on Al based compounds pretreated in H_2 at 300°C

In this part, $CeNi_xAl_{0.5}O_{y\ (c)}$ catalysts are studied in OSRE after pretreating them in H_2 at 300 °C overnight. Table 20 and Figure 28 summarize the results obtained on this series of calcined Al based catalysts. All the catalysts discussed in this part show no formation of carbon after 5 hours. Figure 28-a shows the results obtained on $CeNi_{0.5}Al_{0.5}O_{y\ (c)}$. At the beginning of the experiment (during the first half hour), the conversion is almost complete and then it starts to decrease to reach 82 % after 1 hour, when the reaction temperature stabilizes (the time between temperature stabilization when switching the oven temperature from 200 °C to 50 °C). This conversion is almost the same with the one obtained when pretreating the catalyst at 250 °C. Regarding the products distribution, they are definitely affected by the change of treatment temperature. The percentages of products after 5 hours in OSRE are as follows: 32.8 % H_2, 38.2 % CO_2, 22.2 % CO, 1.5 % CH_4 and 5.3 % CH_3CHO. At pretreatment temperature of 250 °C, a higher H_2 percentage is obtained (34.9 %) with lower CH_4 (0.9 %) and CO (20.9 %) (Table 19). However, a slight decrease of acetaldehyde percentage is observed by changing the pretreatment temperature from 250 °C (6.1 %) to 300 °C (5.3 %). Figure 28-b shows a very good stability of ethanol conversion and products distribution over time on $CeNi_1Al_{0.5}O_{y\ (c)}$ catalyst unlike the $CeNi_{0.5}Al_{0.5}O_{y\ (c)}$ catalyst that is affected by the slight change in temperature

(Figure 28-a). With a pretreatment temperature of 300 °C, this catalyst gets higher stability compared to when pretreating the catalyst at 250 °C. The conversion of ethanol is almost 91 % during 5 hours of experiment, lower than that obtained when pretreating the catalyst at 250 °C. 38.2 % H_2 and 34.1 % CO_2 are obtained which are also lower than the values obtained at a pretreatment temperature of 250 °C (42.7 % and 38.6 %). The other products obtained are distributed as follows: 24.1 % CO, 2.6 % CH_3CHO and 1 % CH_4. With pretreatment temperature of 300 °C, higher percentages of CO and CH_3CHO (24.1 and 2.6 %, respectively) are obtained than those with pretreatment temperature at 250 °C (15.4 % and 2.1 %, respectively). CH_4 levels at both pretreatment temperatures are almost the same (0.2 % difference only). Finally, it is important to notice that no carbon is formed when this catalyst is pretreated at this temperature in contrast to the 24 $mg/h.g_{catalyst}$ obtained at a pretreatment temperature of 250 °C.

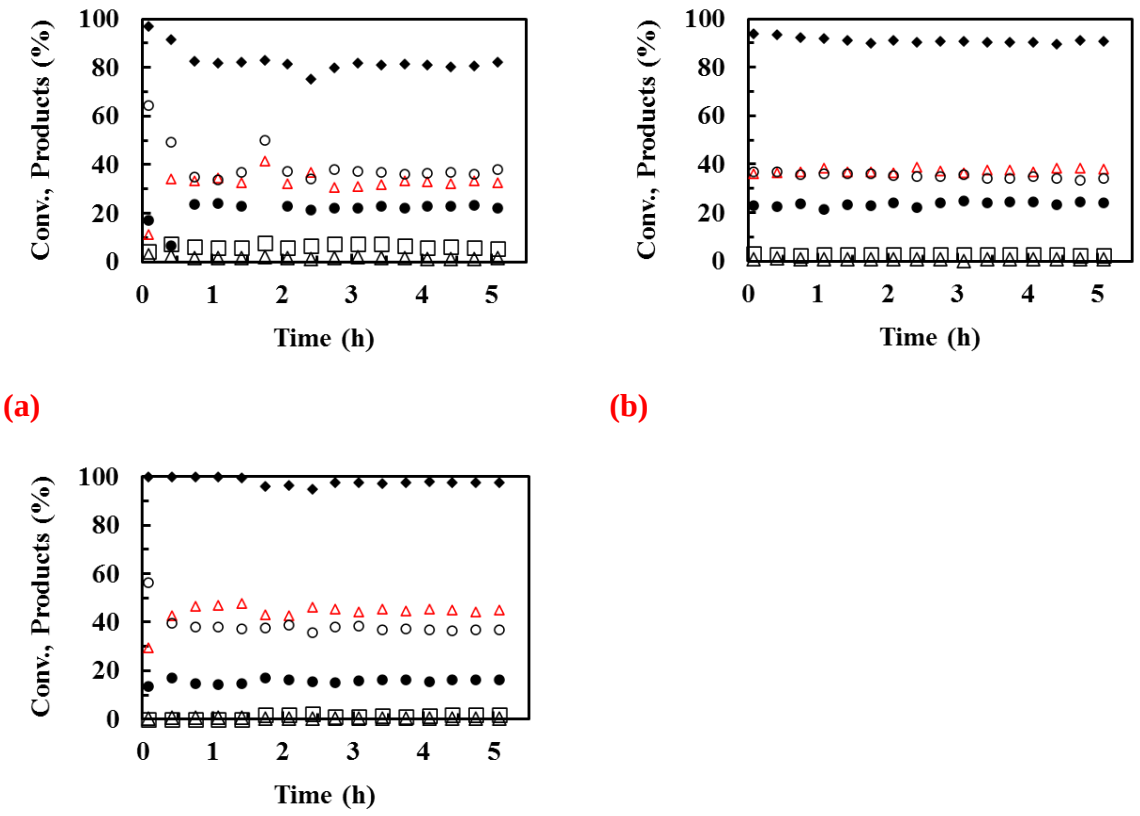

Figure 28 Ethanol conversion (◆) and products distribution (H_2 △, CO_2 ○, CO ●, CH_4 △, acetaldehyde □) during 5 hours in OSRE on $CeNi_xAl_{0.5}O_y$ catalysts *in-situ* pretreated in H_2 at 300 °C. a) x = 0.5, b) x = 1 and c) x = 2. Conversion of O_2 not reported is total ($EtOH/H_2O/O_2/N_2$ = 1:3:1.7:N_2).

Table 20 Ethanol conversion, products distribution and carbon formation in OSRE on $CeNi_xAl_{0.5}O_y$ calcined catalysts *in-situ* pretreated in H_2 at 300 °C. Results reported after 5 hours in $EtOH/H_2O/O_2/N_2$ = 1:3:1.7: N_2.

		Products distribution (%)					
	Conv. of ethanol (%)	**H_2**	**CO_2**	**CO**	**CH_4**	**CH_3CHO**	**Carbon (mg/h.g)**
$CeNi_{0.5}Al_{0.5}O_{y\ (c)}$	82	32.8	38.2	22.2	1.5	5.3	0
$CeNi_1Al_{0.5}O_{y\ (c)}$	91	38.2	34.1	24.1	1	2.6	0
$CeNi_2Al_{0.5}O_{y\ (c)}$	98	44.8	36.8	16.1	0.6	1.7	0

Finally, it can be said that a pretreatment temperature of 300 °C is better when considering high Ni/Ce ratios (2). However, at a lower Ni/Ce ratio (0.5 and 1), 250 °C is a better choice. Among the 2 series of experiments (at 250 and 300 °C), the best performance is attributed to the $CeNi_2Al_{0.5}O_{y\ (c)}$ catalyst pretreated in H_2 at 300 °C in terms of higher main products and lower by products.

II.5. OSRE without pretreatment of the catalyst

It has been previously shown that pretreatment is an important step in OSRE process as well as the choice of the pretreatment temperature is important in order to obtain an active and selective compound. This process takes time, consumes gases and requires some energy even if it is still low at 200 °C or 250 °C. The lack of this pretreatment might result in carbon formation, low selectivity for the catalyst and most of all catalysts could require temperatures higher than 200 °C to start. Nevertheless, it is interesting to investigate the resulting values obtained for ethanol conversion and products distribution for catalysts without previous pretreatment in hydrogen. For this reason, $CeNi_xO_{y\ (c)}$ and $CeNi_xZr_{0.5}O_{y\ (c\ \&\ d)}$ catalysts are selected to see their performance in OSRE without pretreatment and to estimate the minimum temperature required for each catalyst to be able to perform in OSRE under these conditions of $EtOH/H_2O/O_2/N_2$ = 1:3:1.7: N_2. The results are presented in the next section.

II.5.1. $CeNi_xO_{y\ (c)}$ catalysts without pretreatment in H_2

Figure 29 and Table 21 represent the results obtained with $CeNi_xO_{y\ (c)}$ in OSRE without previous pretreatment in hydrogen. Without pretreatment, the test cannot be started at 200 °C (as previously mentioned). The test can be started (conversion is observed) when the temperature of the catalyst reaches 250 °C. After this activation, the temperature of the oven is reduced to 50 °C. The results reported in the following part are therefore obtained in a different procedure compared to what has been reported previously in Table 5. The conversion of ethanol is between 97 and 98% in all the cases with x equal to 0.5, 1, 2 or 5. $CeNi_{0.5}O_{y\ (c)}$ gives around

38 % H_2, 30 % CO_2, 27.7 % CO and 2.8 % CH_3CHO in products distribution after 5 hours. However, when the Ni content increases in $CeNi_1O_{y\ (c)}$, these values are ameliorated to be 44.7 % H_2, 33.4 % CO_2, 18.9 % CO, 1.9 % CH_4 and 1.1 % CH_3CHO. Yet with $CeNi_2O_{y\ (c)}$ and even if this nickel content is still higher than the two previous catalysts mentioned, the percentages of the main products drop (34% H_2 and 34% CO_2) giving rise to more by products (24.6 % CO, 3.5 % CH_4 and 2.9 % CH_3CHO). $CeNi_5O_{y\ (c)}$, the catalyst with the highest nickel content, gave the best catalytic results in this series and under these conditions. Using this catalyst, around 40 % H_2 and 36 % CO_2 are obtained in products distribution with 12 % CO, 0.6 % CH_4 and 1.7 % CH_3CHO. But, at this high ratio, 14 mg/h.$g_{catalyst}$ of carbon are produced. It can be recalled that when pretreating $CeNi_5O_{y\ (c)}$ catalyst in H_2 at 250 °C (Table 5), no carbon is reported even after 31 hours in OSRE (Table 6) unlike this case where 14 mg/h.$g_{catalyst}$ of carbon are produced with $CeNi_5O_{y\ (c)}$.

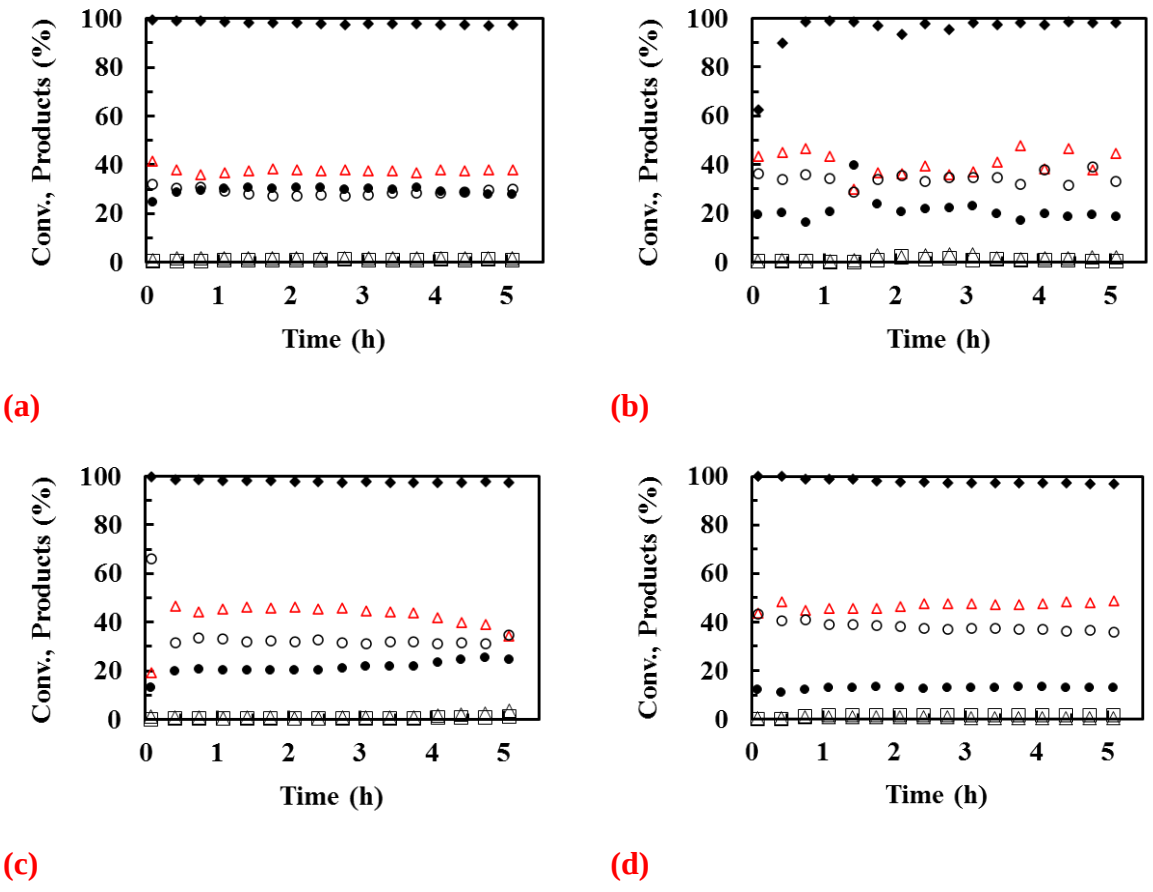

Figure 29 Conversion of ethanol and distribution of products at T_{oven} = 50˚C and T_{start} = 250 ˚C during 5 hours test under $EtOH/H_2O/O_2/N_2$ = 1:3:1.7: N_2 using the $CeNi_xO_y$ calcined catalysts without *in-situ* pretreatment in H_2. a) x = 0.5, b) x = 1, c) x = 2 and d) x = 5. Ethanol conversion ♦, H_2 △, CO_2 ○, CO •, CH_4 Δ, acetaldehyde □.

Table 21 Ethanol conversions, products distribution and carbon formation in OSRE on $CeNi_xO_y$ calcined catalysts without pretreatment in H_2. Results reported after 5hours in $EtOH/H_2O/O_2/N_2$ = 1:3:1.7: N_2.

		Products distribution (%)					
	Conv. of ethanol (%)	**H_2**	**CO_2**	**CO**	**CH_4**	**CH_3CHO**	**Carbon (mg/h.$g_{catalyst}$)**
$CeNi_{0.5}O_{y\ (c)}$	97.0	37.9	30	27.7	1.6	2.8	0.0
$CeNi_1O_{y\ (c)}$	98.3	44.7	33.4	18.9	1.9	1.1	0.0
$CeNi_2O_{y\ (c)}$	97.6	34.3	34.7	24.6	3.5	2.9	0.0
$CeNi_5O_{y\ (c)}$	96.9	48.9	36.0	12.8	0.6	1.7	14.0

II.5.2 $CeNi_xZr_{0.5}O_{y\ (c)}$ catalysts without pretreatment in H_2

In this part, the results corresponding to $CeNi_xZr_{0.5}O_{y\ (c)}$ without pretreatment are presented. Complete conversion is almost achieved on all the $CeNi_xZr_{0.5}O_{y\ (c)}$ catalysts where x = 0.5, 1, 2 and 5 (Figure 30 and Table 22). The conversions can be observed only when the temperature is raised to 250 °C (the minimal temperature required for the activation of OSRE without pretreatment in H_2). During the 5 hours process in OSRE, the conversion of ethanol and the stability of products remain constant Figure 30. Globally, the percentage of hydrogen in products distribution increases with the increase in Ni content (Table 22). With $CeNi_{0.5}Zr_{0.5}O_{y\ (c)}$, the products distribution obtained is as follows: 43 % H_2, 32 % CO_2, 23 % CO and 1.4 % CH_3CHO. The H_2 and CO_2 percentages become even higher (48 % and 34 %, respectively) while CO, CH_4 and CH_3CHO percentages (17 %, 0.7 % and 0.4 %, respectively) becomes less using the catalyst $CeNi_1Zr_{0.5}O_{y\ (c)}$. With $CeNi_2Zr_{0.5}O_{y\ (c)}$, 47 % H_2 are obtained in products distribution, a value which is almost similar to that obtained with $CeNi_1Zr_{0.5}O_{y\ (c)}$. However, the CO_2 percentage obtained is higher (43 %), and CO and CH_3CHO percentages are lower (7 % and 0.2 % respectively). Finally, using $CeNi_5Zr_{0.5}O_{y\ (c)}$ in OSRE without pretreatment gives the most promising results among this series in terms of hydrogen formation. The total conversion of ethanol reached by this catalysis leads to the formation of 52 % H_2, 37 % CO_2, 11 % CO and trace amounts of CH_4 and CH_3CHO (0.2 and 0.1 %). The conversion of ethanol and the products distribution on $CeNi_5Zr_{0.5}O_{y\ (c)}$ are always the same regardless of the presence (200 °C or 250 °C) or absence of pretreatment in hydrogen. However, for the other catalysts with different Ni contents, the values of ethanol conversions remain the same with slight deviations in products distribution when they are started without pretreatment in hydrogen. Concerning the hydrogen percentage obtained with calcined Zr catalysts with

x = 0.5, 1 and 2, it is higher than those obtained when pretreating with a temperature of 200 °C or 250 °C. The percentages of CO obtained after 5 hours are less than those obtained previously with a pretreatment temperature of 200 °C or 250 °C. $CeNi_1Zr_{0.5}O_{y\ (c)}$ produces 19 mg/h.$g_{catalyst}$ of carbon and $CeNi_2Zr_{0.5}O_{y\ (c)}$ produces a much higher quantity of 163 mg/h.$g_{catalyst}$ of carbon. Although, on these catalysts, the products distribution is better, this high amount of carbon is not advantageous with time. Finally, it can be concluded that $CeNi_{0.5}Zr_{0.5}O_{y\ (c)}$ performs better when it is used without previous pretreatment in hydrogen since it gives better distribution for the products with zero carbon formation. $CeNi_5Zr_{0.5}O_{y\ (c)}$ is still the best among these catalysts performing without pretreatment in hydrogen.

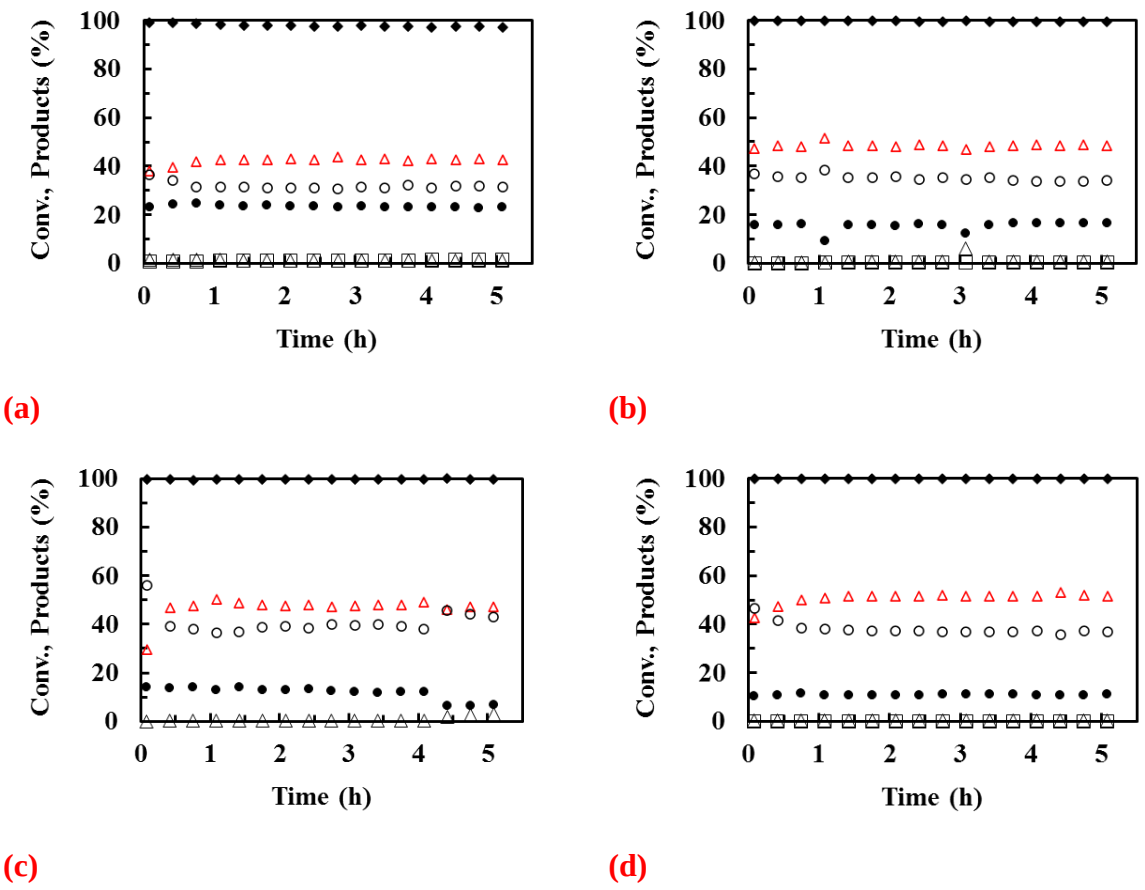

Figure 30 Ethanol conversion (◆) and products distribution (H_2 △, CO_2 ○, CO ●, CH_4 △, acetaldehyde □) during 5 hours on $CeNi_xZr_{0.5}O_{y\ (c)}$ without *in-situ* pretreatment in H_2 , a) x = 0.5, b) x = 1, c) x = 2 and d) x = 5. Conversion of O_2 not reported is total ($EtOH/H_2O/O_2/N_2$ = 1:3:1.7:N_2).

Table 22 Ethanol conversions, products distribution and carbon formation in OSRE on $CeNi_xZr_{0.5}O_y$ calcined catalysts without *in-situ* pretreatment in H_2. Results reported after 5hours in $EtOH/H_2O/O_2/N_2$ = 1:3:1.7: N_2.

		Products distribution (%)					
	Conv. of ethanol (%)	**H_2**	**CO_2**	**CO**	**CH_4**	**CH_3CHO**	**Carbon (mg/h.$g_{catalyst}$)**
$CeNi_{0.5}Zr_{0.5}O_{y\ (c)}$	97.3	42.7	31.6	23.1	1.2	1.4	0.0
$CeNi_1Zr_{0.5}O_{y\ (c)}$	99.5	48.2	34.1	16.6	0.7	0.4	19.0
$CeNi_2Zr_{0.5}O_{y\ (c)}$	99.6	47	42.9	6.9	3.0	0.2	163.0
$CeNi_5Zr_{0.5}O_{y\ (c)}$	99.7	52	36.8	10.9	0.2	0.1	0.0

The starting temperature to set under these catalysts is at minimum of 250 °C. Under which, without pretreatment, the catalyst can be activated under only ethanol-water flow. To our best knowledge, this is the lowest temperature reported in literature as a starting temperature for catalysts used in OSRE without previous reduction in H_2. For example, it has been reported before on Pt-Ni/CeO_2-SiO_2 catalyst in OSRE only 80 % ethanol conversion. Moreover, in this recent publication, only 20 % and 10 % yield of H_2 and CO_2 were obtained [316]. Other studies were performed under catalysts and certain conditions to obtain the lowest activation temperature that they could reach (300 ºC). However, in that study, to achieve 100 % ethanol conversion, it was necessary to raise the activation temperature until 700 ºC.

II.5.3. $CeNi_xZr_{0.5}O_{y\ (d)}$ catalysts without pretreatment in H_2

The results obtained on $CeNi_xZr_{0.5}O_{y\ (d)}$ catalysts without previous pretreatment in hydrogen are presented in Figure 31 and Table 23. It is important to mention here that the catalysts cannot be started (no conversion observed) at a temperature of 200 °C and not even at 250 °C (the temperature at which the calcined catalysts without pretreatment are started), however, they can be started when the temperature reaches 280 °C. Generally, all the following graphs from a to d show great stability over time for conversion of ethanol, and products distribution (H_2, CO_2, CO, CH_4 and CH_3CHO). Starting with $CeNi_{0.5}Zr_{0.5}O_{y\ (d)}$, the conversion of ethanol is around 95 % after 5 hours. The distribution of the products is not very satisfactory with low Ni content. The products are distributed as follows: 26.8 % H_2, 33 % CO_2, 29 % CO, 5 % CH_4 and 6.5 % CH_3CHO. With this Ni content, an *in-situ* pretreatment in H_2 at 200 °C or 250 °C previously mentioned in this work is better in terms of ethanol conversion and products distribution compared to those without pretreatment in hydrogen. With $CeNi_1Zr_{0.5}O_{y\ (d)}$, 97.1 % conversion of ethanol is obtained and with a products distribution as follows: 43.1 % H_2, 32 % CO_2, 22.4

% CO, 0.9 % CH_4 and 1.7 % CH_3CHO. With a higher Ni/Ce ratio, $CeNi_2Zr_{0.5}O_{y\ (d)}$, conversion of ethanol reaches almost 100 % with 50 % H_2 in products distribution, higher than that obtained with a pretreatment value of 200 °C and 250 °C. The $CeNi_5Zr_{0.5}O_{y\ (d)}$ catalyst shares almost same values with the latter $CeNi_2Zr_{0.5}O_{y\ (d)}$. In fact, under these conditions, CH_4 percentage is almost negligible for x = 1, 2 and 5. Moreover, CO concentration obtained is lower on catalysts where x = 1, 2 and 5 when no pretreatment is done. As a conclusion, pretreatment is required when x = 0.5 to get higher concentrations of H_2 and CO_2. Under these conditions, catalysts with x = 2 and 5 are considered the best.

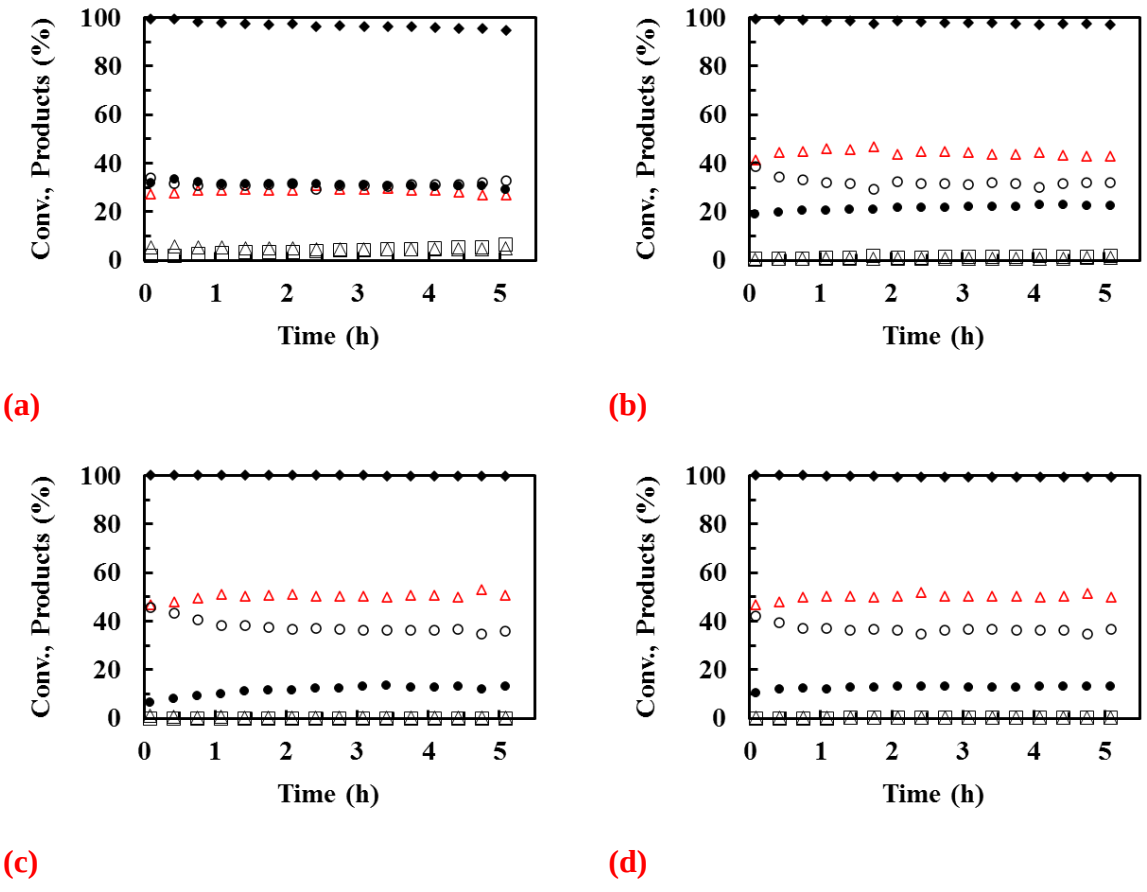

Figure 31 Ethanol conversion (◆) and products distribution (H_2 △, CO_2 ○, CO ●, CH_4 △, acetaldehyde □) during 5 hours on $CeNi_xZr_{0.5}O_{y\ (d)}$ without *in-situ* pretreatment in H_2 , a) x = 0.5, b) x = 1, c) x = 2 and d) x = 5. Conversion of O_2 not reported is total ($EtOH/H_2O/O_2/N_2$ = 1:3:1.7:N_2).

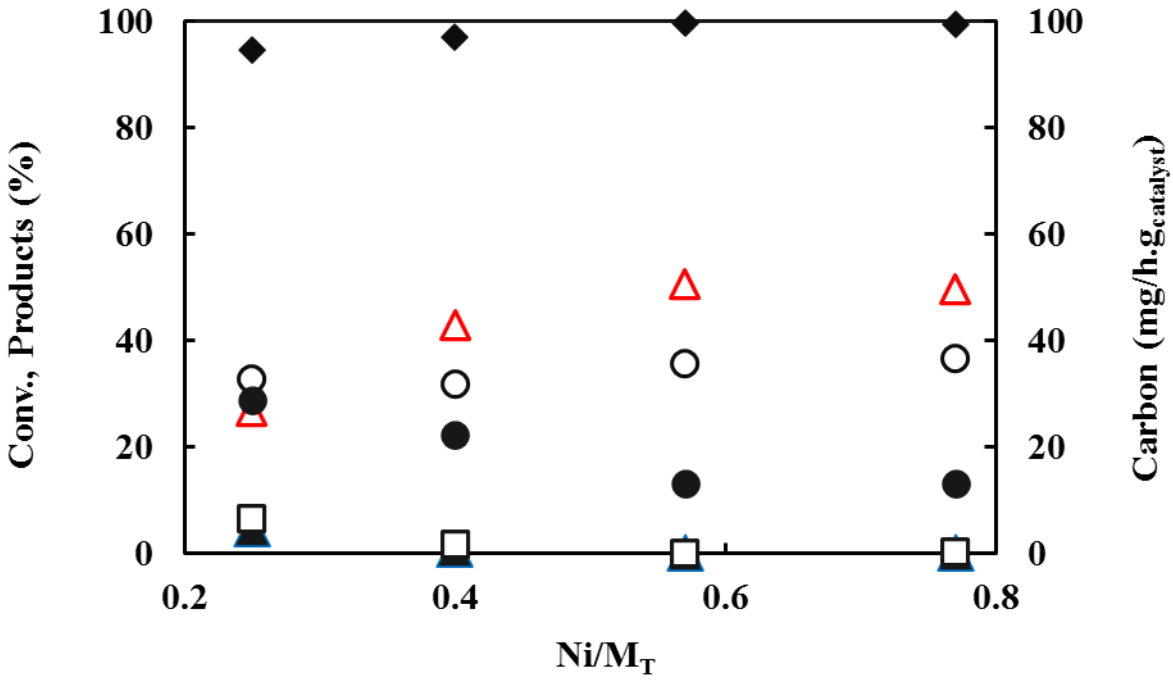

Figure 32 summarizes the conversion of ethanol, products distribution (%) and carbon formation as a function of Ni/M_T ratio in $CeNi_xZr_{0.5}O_y$ dried catalysts without previous pretreatment in H_2. Clearly, with the increase of Ni/M_T, the conversion of ethanol increases as well as the percentage of H_2 and CO_2. The percentages of acetaldehyde and CO decrease with the increase of Ni/M_T ratio. This trend is also followed by the binary and ternary catalysts mentioned before operating after a pretreatment in hydrogen at 200 °C and 250 °C.

Table 23 Ethanol conversions, products distribution and carbon formation in OSRE on $CeNi_xZr_{0.5}O_y$ dried catalysts without pretreatment in H_2. Results reported after 5 hours in $EtOH/H_2O/O_2/N_2$ = 1:3:1.7: N_2.

		Products distribution (%)					
	Conv. of ethanol (%)	**H_2**	**CO_2**	**CO**	**CH_4**	**CH_3CHO**	**Carbon (mg/h.g$_{catalyst}$)**
$CeNi_{0.5}Zr_{0.5}O_y$ (d)	94.7	26.8	32.9	29.0	4.8	6.5	0.0
$CeNi_1Zr_{0.5}O_y$ (d)	97.1	43.1	31.9	22.4	0.9	1.7	0.0
$CeNi_2Zr_{0.5}O_y$ (d)	99.8	50.6	35.8	13.2	0.3	0.1	0.0
$CeNi_5Zr_{0.5}O_y$ (d)	99.5	49.8	36.6	13.2	0.2	0.2	0.0

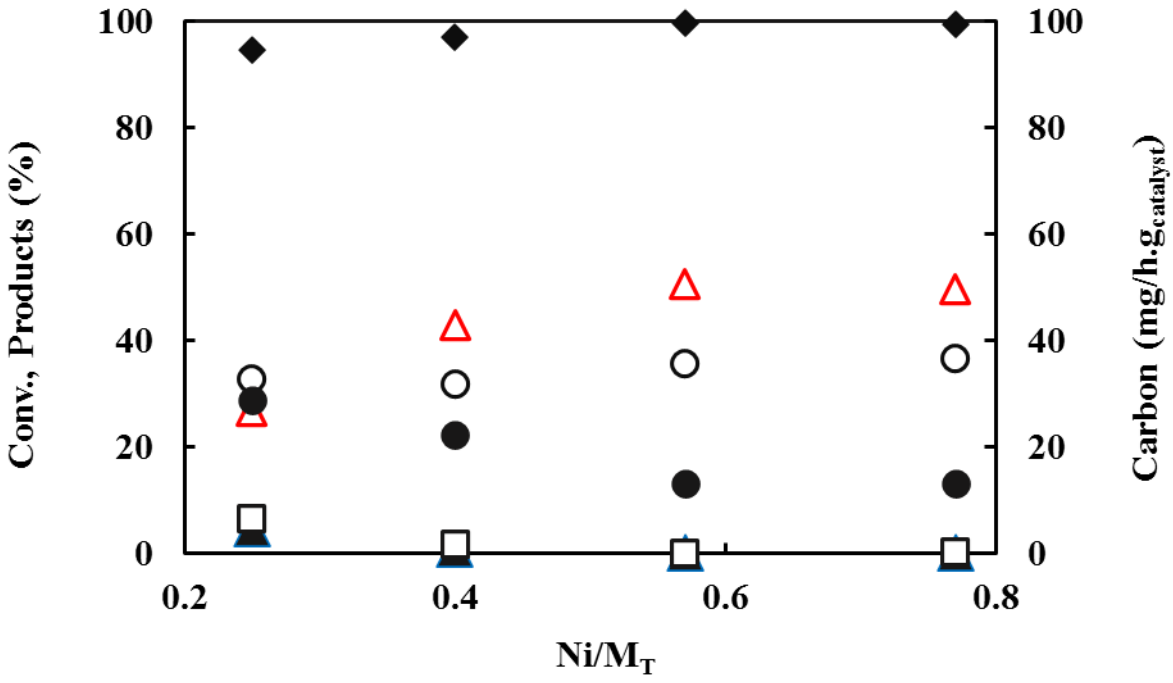

Figure 32 Ethanol conversion, products distribution (%) and carbon formation as a function of Ni/M_T ratio in $CeNi_xZr_{0.5}O_y$ dried catalysts without previous pretreatment in H_2. Ethanol conversion ♦, H_2 △, CO_2 ○, CO •, CH_4 △, carbon formation ×, acetaldehyde □.

II.5.4. Effect of Ni/M_T ratio on calcined catalysts without pretreatment in H_2

A seen before on catalysts pretreated in hydrogen at 250 °C, the Ni/M_T ratio plays an important role in OSRE such that with the increase in Ni content, the main products increase and that of byproducts decrease. To check if this trend is valid when no pretreatment is performed on the binary and ternary (Zr) catalysts, Figure 33 summarizes the effect of Ni/M_T ratio on the conversion of ethanol, products distribution and carbon formation in OSRE. When no pretreatment is applied on the catalysts, globally the same trend as before can be seen on the gas phase products variation versus Ni/M_T ratio, but with some discrepancies (H_2 between 40 and 50 %, CO_2 at about 30 %, CO varying between 20 and 10 %). However, it can be remarked that here binary and ternary catalysts are reported together. The main discrepancy is observed on carbon formation. The obtained results evidence that the main effect observed can be attributed to the Ni content, as globally on all the series of catalysts, the expected products (H_2 and CO_2) are favored on high Ni content compounds. Finally, clearly, the $CeNi_5Zr_{0.5}O_{y\ (c)}$ catalyst presents the best performance among all other catalysts with different Ni/Ce whether doped with Zr or not, and without pretreatment in H_2.

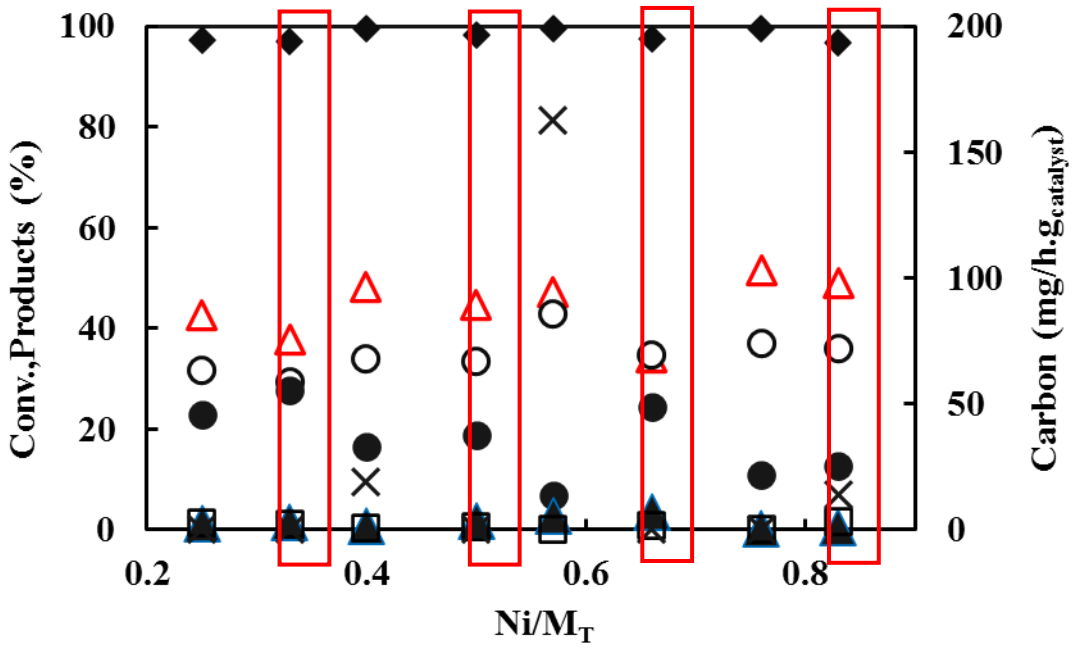

Figure 33 Conversion of ethanol, products distribution (%) and carbon formation as a function of Ni/M_T content in $CeNi_xZr_{0.5}O_{y\ (c)}$ and $CeNi_xO_{y\ (c)}$ catalysts without previous *in-situ* pretreatment in H_2. H_2 △, ethanol conversion ♦, CO_2 ○, CO •, CH_4 △, carbon formation ×, acetaldehyde □. Binary catalysts in red column.

II.6. Stability tests (80 hours)

In this section, the catalysts presenting the best catalytic results under different conditions are checked under a long test run stability test of 80 hours. $CeNi_5Zr_{0.5}O_{y\ (c)}$ is among the catalysts showing good catalytic performance and thus was tested for an 80 hours stability test. The test was performed with prior pretreatment in hydrogen at 250 °C. The corresponding results are represented in Figure 34-a. The test is started at an oven temperature of 200 °C and then fixed at 50 °C. The catalyst performance is extremely stable over time on stream. The conversion of ethanol is of 100 % with the products distribution as follows: 51 % H_2, 36 % CO_2 and 12.6 % CO, 0.4 % CH_4 and 0.1 % CH_3CHO.

The second test chosen for 80 hours stability test is $CeNi_5Zr_{0.5}O_{y\ (d)}$ (Figure 34-b). It has shown previously good results under the same conditions with $CeNi_5Zr_{0.5}O_{y\ (c)}$ discussed lately in Figure 34-a Similarly, great stability is achieved over time for ethanol conversion and products distribution. The conversion of ethanol and oxygen consumption are complete over the 80 hours time on stream. The products distribution is as follows: 47.2 % H_2, 34.7 % CO_2, 15.6 % CO, 1.8 % CH_4 and 0.7 % CH_3CHO. In the 2 cases studied before for the $CeNi_5Zr_{0.5}O_y$ (calcined and dried), no carbon is collected after the 80 hours on the stream.

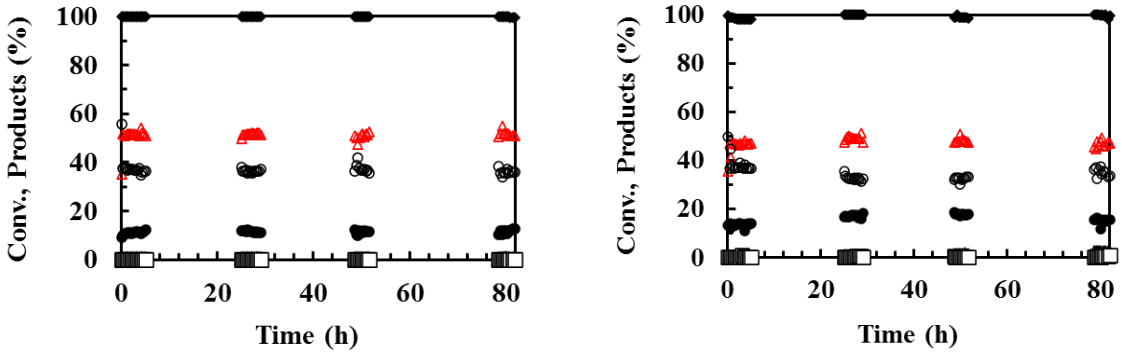

(a) **(b)**

Figure 34 Ethanol conversion (◆) and products distribution (H_2 △, CO_2 ○, CO ●, CH_4 △, acetaldehyde □) during *80* hours on $CeNi_5Zr_{0.5}O_y$ with *in-situ* pretreatment in H_2 at 250 °C, a) calcined catalyst b) dried catalyst. Conversion of O_2 not reported is total ($EtOH/H_2O/O_2/N_2$ = 1:3:1.7:N_2).

This dried catalyst shows good performance in OSRE when used without previous pretreatment in hydrogen. For, this reason it is also selected to check its efficiency over time. The test is started at an oven temperature of 280 °C since 200 °C is not enough to activate the catalyst which has not been treated before in hydrogen. The conversion of ethanol remains complete over the 80 hours in OSRE (Figure 35). Similarly, the hydrogen percentage in products distribution remains constant at 50 %. A slight deviation of 2 % in CO_2 is observed at the beginning of the test and after 80 hours. After 80 hours, the percentage of CO_2 in products distribution is reported as 34 %. Trace amounts of CH_3CHO and CH_4 are recorded (0.2 % and 0.5 % respectively). Moreover, it is important to declare that no carbon is reported at the end of the process.

Finally, the last catalyst chosen for a long test run of 80 hours is $CeNi_2Al_{0.5}O_y$ calcined presented in Figure 36. This catalyst is pretreated in hydrogen at 300 °C. The results obtained are very stable over time. 100 % conversion of ethanol is achieved with the formation of the following products: 43.9 % H_2, 34.7 % CO_2, 18.8 % CO, 1.3 % CH_3CHO and 1.3 % CH_4.

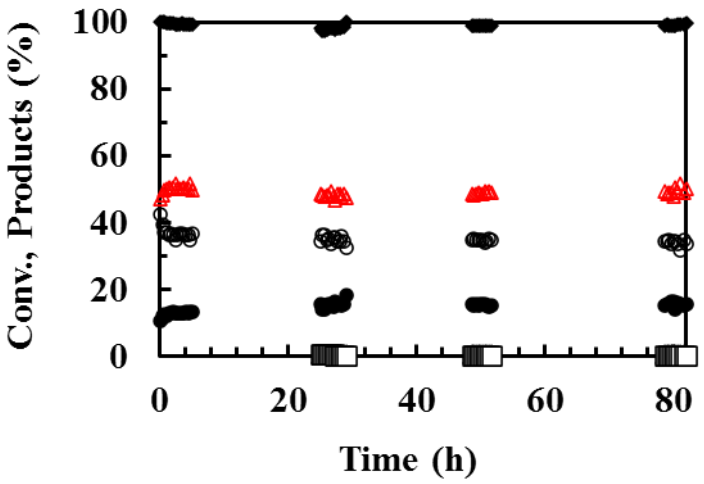

Figure 35 Ethanol conversion (◆) and products distribution (H_2 △, CO_2 ○, CO ●, CH_4 △, acetaldehyde □) during 80 hours on $CeNi_5Zr_{0.5}O_{y\ (d)}$ without *in-situ* pretreatment in H_2. Conversion of O_2 not reported is total ($EtOH/H_2O/O_2/N_2$ = 1:3:1.7:N_2).

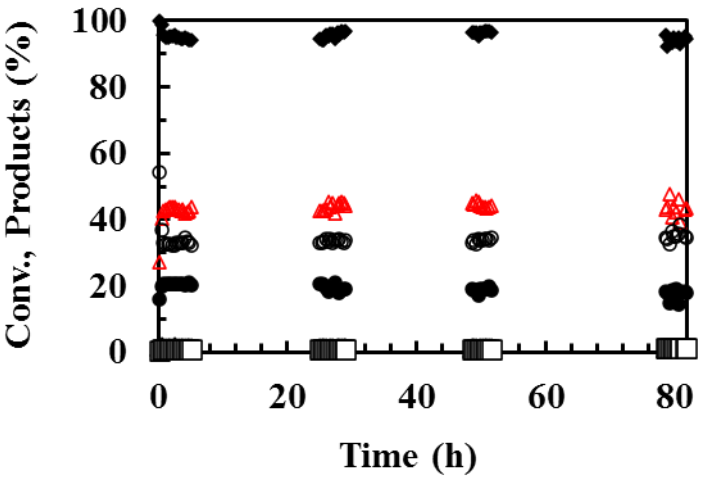

Figure 36 Ethanol conversion (◆) and products distribution (H_2 △, CO_2 ○, CO ●, CH_4 △, acetaldehyde □) during 80 hours on $CeNi_2Al_{0.5}O_y$ (c) with *in-situ* pretreatment in at 300 °C, a) x = 0.5, b) x = 1, c) x = 2 and d) x = 5. Conversion of O_2 not reported is total ($EtOH/H_2O/O_2/N_2$ = 1:3:1.7:N_2)

Similar studied have been reported before but with higher temperature of 550 °C under H_2O/EtOH/O_2 ratio of 3/1/0.5 [318]. Lima et al also observed stability over 50 hours in the stability tests done OSR under H_2O/ethanol molar ratio = 3.0 and O_2/ethanol molar ratio = 0.5 (mass of catalyst = 20 mg) associated to water production in the hydrogen production in OSR reactions but this necessitated high temperatures of in the stability tests done OSR under H_2O/ethanol molar ratio = 3.0 and O_2/ethanol molar 500 °C [319]. However, Passos et al. also reported decrease in ethanol conversion and hydrogen production after 80 hours in OSRE using Ni based catalysts

at a temperature of 300 °C under OSR condition with a water/ethanol/oxygen at a molar ratio of 6/1/0.3.

Conclusion

The oxidative steam reforming of ethanol (OSRE) is studied on catalysts based on nickel and cerium ($CeNi_xO_y$ with $0.5 \leq x \leq 5$), dried and calcined, and doped with another element, mainly aluminum or zirconium ($CeNi_xM_{0.5}$ Oy, with $0.5 \leq x \leq 5$ and M = Al or Zr) and varying the nickel content of the catalyst. OSRE is performed under $EtOH/H_2O/O_2/N_2$ mixture with a H_2O/EtOH molar ratio of 3. The reaction is started at a temperature of 200 °C (unless specified) and then the oven temperature is decreased to 50 °C. The influence of several parameters on catalysts performances and reaction products are analyzed such as: the influence of the reaction mixture by varying O_2/EtOH ratios, pretreatment in hydrogen, mass of catalyst, and reaction duration with stability tests in OSRE over time (5 h, 31 h and 80 h on some chosen samples).

With an O_2/EtOH molar ratio of 1.42, $CeNi_xO_y$ dried and calcined catalysts, *in-situ* pretreated in H_2 at 250 °C, could only possess stability in OSRE over time when $x \geq 1$. Doping with zirconium ($CeNi_xZr_{0.5}O_y$ where x = 0.5, 1 and 2) makes it possible to obtain more stable results over 5 hours in gas stream. The best results obtained under these conditions are with $CeNi_1O_{y\ (c)}$ (47 % H_2, 32 % CO_2, 17 % CO, 0.7 % CH_4, 2.6 % CH_3CHO in products distribution and 274 $mg/h.g_{catalyst}$ carbon formation) and $CeNi_2Zr_{0.5}O_{y\ (c)}$ (52 % H_2, 34.2 % CO_2, 10.4 % CO, 1.8 % CH_4, 1.6 % CH_3CHO in products distribution and 67 $mg/h.g_{catalyst}$ carbon formation) compounds giving total ethanol and oxygen conversions. At this O_2/EtOH ratio, high amounts of carbon are formed specially when increasing Ni content in case of the binary catalysts. Zr addition allows the drastic decrease in carbon formation which is recorded on the binary catalysts. For example, with $CeNi_1O_{y\ (c)}$ the amount of carbon formed after 5 hours is of 274 $mg/h.g_{catalyst}$, while with $CeNi_1Zr_{0.5}O_{y\ (c)}$, this amount drops to 34 $mg/h.g_{catalyst}$. $CeNi_{0.5}Zr_{0.5}O_{y\ (d)}$ requires to start the reaction at 250 °C unlike on all the other catalysts.

To ameliorate the previous results obtained, different O_2/EtOH ratios of 1.42, 1.56 and 1.7 are adjusted and used under same conditions mentioned before with the calcined $CeNi_1O_y$ catalyst. The main effect obtained is on carbon formation such that a little change in this ratio (from 1.4 to 1.56 to 1.7) allows the carbon amounts to drop from 274 $mg/h.g_{catalyst}$ to 185 $mg/h.g_{catalyst}$ and finally to 0 $mg/h.g_{catalyst}$ respectively after 5 hours in OSRE. This change does not affect the conversion of ethanol as it is already complete, on the other hand, it gives some variations in the products distribution.

The O_2/EtOH ratio is then fixed at 1.7 to minimize the carbon formation and the study is performed on $CeNi_xO_y$ and $CeNi_xZr_{0.5}O_y$ dried and calcined catalysts where x = 0.5, 1, 2 and 5. Under these conditions, almost total ethanol conversions are obtained in all the series of catalysts. Considering binary dried compounds, acetaldehyde level is decreasing with the increase in nickel content. The optimal OSRE results are obtained with the catalyst with highest Ni content, $CeNi_5O_{y\ (d)}$, where an ethanol conversion of 94 % is achieved with formation of 49 % H_2, 34 % CO_2 and 15 % CO. Similar results are obtained on $CeNi_5O_{y\ (c)}$ which are also considered the best among the calcined binary series. The study on $CeNi_xZr_{0.5}O_y$ dried catalysts shows different abilities for hydrogen production starting with 30 % in products distribution with x = 0.5 till 47.9 % when x = 5. Main products percentages increase with the increase in nickel content while CO and CH_4 decrease. Same trend is investigated on the calcined zirconium-based catalysts and shows even more promising results. 100 % conversion of ethanol is obtained when testing $CeNi_5Zr_{0.5}O_{y\ (c)}$ as well as higher hydrogen percentage is obtained (52 %) among all other binary and ternary catalysts. Moreover, the only by product is CO which is obtained with a low value of 10 %. In general, the calcination of the compounds shows a beneficial effect in terms of good distribution of products and minimizing CO, CH_3CHO and CH_4. The experiments performed on calcined catalysts are then reproduced after 31 hours to check their stability over time as a first approach and show great constancy. These catalysts preparations and the used reaction conditions allow the elimination of carbon formation after 5 hours. Similarly, no carbon is formed after 31 hours in stream, except for $CeNi_1Zr_{0.5}O_{y\ (c)}$, however, it is low enough not to cause any deactivation of the catalyst.

The effect of pretreatment in hydrogen is also investigated on $CeNi_2Zr_{0.5}O_{y\ (c)}$ under the same experimental conditions. The temperatures of pretreatment are chosen based on the TPR profiles since the main approach is to obtain partially reduced compounds. The results show that without pretreatment in H_2 of the compound, the activation temperature of the catalyst (temperature at which reaction starts) must be raised till 250 °C instead of 200 °C in addition to some carbon formation. With *in-situ* pretreatment in H_2 at 200 °C, 250 °C, 400 °C or 500 °C, only slight variations are obtained in products distribution and in none of them carbon is recorded, on the studied compound. As the objective of this study is to minimize the energetic consumption, some further studies are conducted with a low pretreatment temperature in hydrogen of 200 °C and without pretreatment in hydrogen at all.

To this purpose, the zirconium-based catalysts with x = 0.5, 1, 2 and 5 are chosen to be studied with a pretreatment in hydrogen at a temperature of 200 °C. When $x \leq 2$, better results are obtained with pretreatment temperature of 200 °C than that of 250 °C in terms of products distribution in the calcined series. However, at a higher Ni content (x = 5), this difference is no more noticeable and only slight variations are obtained with this little change in temperature. Conversion of ethanol is at 97 % with x = 0.5 and approaches 100% when Ni content increases to x = 5. In fact, the same trend is observed concerning Ni content, ethanol conversion and products distribution. Similar results are obtained on the dried catalysts after pretreatment in H_2 at 200 °C. $CeNi_5Zr_{0.5}O_{y\ (d)}$ gives the best results among the dried series. 100% ethanol conversion is obtained using this catalyst with 51 % H_2, 41 % CO_2, 7 % CO and almost 1 % of CH_4 and 0.5 % of CH_3CHO in products distribution. Calcination allows to get better catalytic results on catalysts with low Ni content however with higher nickel content, no evident variation is observed. The stability of these compounds is also analyzed under same conditions but during 31 hours and proves great steadiness. Even after 31 hours, no carbon formation is measured, except with $CeNi_2Zr_{0.5}O_y$ (dried and calcined). This is only evident after 31 hours and not after 5 hours, however, this amount does not exceed 12 mg/h.$g_{catalyst}$.

The influence of mass of catalyst is investigated on $CeNi_2Zr_{0.5}O_y$ and $CeNi_5Zr_{0.5}O_y$ calcined catalysts and reveals that an increase of mass from 30 mg to 60 mg leads to the formation of more carbon. The amount of carbon formed increases from 16 to 68 mg/h.$g_{catalyst}$ with $CeNi_2Zr_{0.5}O_{y\ (c)}$ and from 0 to 9.2 mg/h.$g_{catalyst}$ with $CeNi_5Zr_{0.5}O_{y\ (c)}$, when doubling the mass of catalyst

The influence of doping the catalyst with Al instead of Zr is also studied under same experimental conditions ($EtOH/H_2O/O_2/N_2$ = 1:3:1.7: N_2 with is situ pretreatment of the catalyst in hydrogen at 250 °C). Doping $CeNi_xO_y$ catalyst with Zr shows much higher conversion of ethanol compared to doping with Al (83-96%) and higher H_2 percentage and lower acetaldehyde percentage in the products distribution. However, the $CeNi_{0.5}Al_{0.5}O_y$ calcined catalyst can be started at a reaction temperature of 200 °C while the $CeNi_{0.5}Zr_{0.5}O_{y\ (c)}$ requires higher temperature (250 °C). On this basis, the pretreatment temperature in hydrogen for the Al compounds is raised to 300 °C. This study shows that at low Ni/Ce ratios where x = 0.5 and x = 1, higher ethanol conversions (83 % and 97 % respectively) as well as higher hydrogen percentage (34.9 and 42.7 %, respectively) are obtained in comparison to results obtained with pretreatment in H_2 at 250 °C. However, at higher value of x (x = 2), pretreatment temperature

in H_2 of 300 °C promises better results as the hydrogen percentage in products distribution increases from 40 % to 44.8 % when this temperature increases from 250 °C to 300 °C.
Furthermore, the study of $CeNi_xO_{y\ (c)}$ and $CeNi_xZr_{0.5}O_{y\ (c)(d)}$ without pretreatment in hydrogen is conducted. The calcined catalysts require an activation temperature of 250 °C to initiate the OSRE process and the dried ones require a higher temperature of 280 °C. The calcined binary compounds without pretreatment shows better performance in OSRE when $x \leq 2$ in terms of higher formation of hydrogen and carbon dioxide compared to those with pretreatment in hydrogen. However, at high Ni content where x = 5, 14 $mg/h.g_{catalyst}$ of carbon are formed. Similarly, on the calcined catalysts doped with Zr, a pretreatment step would be more recommended at a higher Ni/Ce ratio of x=5 for the same reasons. However, on the dried catalysts doped with zirconium, pretreatment step would be better recommended when x = 0.5 as it gives better conversion and higher H_2 and CO_2 percentages in products distribution.
Finally, some of the catalysts showing the best results are conducted for 80 hours in OSRE to check their stability under a long time reaction ($EtOH/H_2O/O_2/N_2$ = 1:3:1.7: N_2 and D_L = 0.1 ml/min). One of the selections is $CeNi_5Zr_{0.5}O_{y\ (c)}$ pretreated in H_2 at 250 °C which gives the following results: 100 % conversion of ethanol with formation of 51 % H_2, 36 % CO_2 and 12.6 % CO, 0.1 % CH_3CHO and 0.4 % CH_4. The 80 hours stability test on $CeNi_5Zr_{0.5}O_{y\ (d)}$ pretreated in hydrogen at 250 °C leads to 100 % ethanol conversion, with 47.2 % H_2, 34.7 % CO_2, 15.6 % CO, 1.8 % CH_4 and 0.7 % CH_3CHO in products distribution. The same catalyst in same conditions without pretreatment in hydrogen shows stable results as reported before after 5 hours. $CeNi_2Al_{0.5}O_y$ compound *in-situ* pretreated in hydrogen at 300 °C allows 100 % conversion of ethanol with the formation of the following products: 43.9 % H_2, 34.7 % CO_2, 18.8 % CO, 1.3 % CH_3CHO and 1.3 % CH_4 after 80 hours in OSRE. All these studied compounds show high stability over 80 hours in OSRE with almost no carbon formation during the process.

Chapter III: Preparation and characterization of fresh and spent catalysts

In this chapter, the preparation and characterization of $CeNi_xO_y$ (binary) and $CeNi_xM_{0.5}O_y$ (ternary) catalysts, where M = Al or Zr, dried and calcined catalysts previously mentioned in chapter II, are investigated. On the fresh catalysts, the physico-chemical characterizations of the catalysts are analyzed by the following techniques: BET, XRD, TPR, TPO, Raman, XPS and XRF. The details of these different techniques are presented in the Appendix. This chapter also focuses on the characterizations of spent catalysts after test with Raman and XPS analysis to study the surface and bulk of the catalyst before and afer test.

III.1. Preparation of catalysts

To prepare the $CeNi_xO_y$ or $CeNi_xM_{0.5}O_y$, catalysts where M = Al or Zr, precursors based on nitrates were used. Zirconium and aluminum oxide are known to have good physical and chemical properties such as strength, toughness and thermal stability [320]. For this reason, zirconium and aluminum were chosen to be doped in the catalyst expecting better performance under the same conditions as those used previously for binary catalysts. The preparation of these catalysts was carried out by coprecipitation with triethylamine. The coprecipitation method has been widely used before since it has a desired effect in allowing the strong interactions in the catalyst that can have a beneficial effect on active sites and also limiting the sintering effect of metallic particles. The compounds were then filtered and dried at 100 °C. A part of the dried catalyst is collected and the other part is then calcined in air at 500 °C for 4 hours. The preparation method is more detailed in the Annex section

III.2. Characterizations of $CeNi_xO_y$ fresh catalysts

The physico-chemical properties of fresh $CeNi_xO_y$ catalysts are studied in this section. Different characterizations are done on these catalysts with different values of x. The $CeNi_xO_y$ catalysts are studied in the dried and calcined forms, the dried compounds are noted as $CeNi_xO_{y\ (d)}$ and the calcined ones are noted as $CeNi_xO_{y\ (c)}$.

III.2.1. Elemental analysis of $CeNi_xO_y$ catalysts

The binary $CeNi_xO_y$ compounds are analyzed by micro-X-Ray Fluorescence (XRF) (Table 25). For each catalyst, the proportion of Ni in the compound is presented by the Ni/M_T ratio, corresponding to the ratio of the quantity of nickel (noted Ni) to the total quantity of metal present in the solid (noted M_T). This ratio is calculated by equation 32:

Equation 32: $Ni/M_T = Ni / \Sigma metals = x/(x+1)$, where 1 refers to Ce.

Table 24 Theoretical values of Ni/M_T content in bulk and weight percentage of $CeNi_xO_y$ (calcined and dried).

		Theoretical wt%		
Theoretical formula	**Ni/M_T ratio theo.**	**O**	**Ni**	**Ce**
$CeNi_{0.5}O_{2.5}$	0.3	19.1	14.0	66.9
$CeNi_1O_3$	0.5	19.4	23.8	56.8
$CeNi_2O_4$	0.7	19.9	36.5	43.6
$CeNi_5O_7$	0.8	20.5	53.8	25.7

Table 25 XRF analysis, experimental values of metallic contents, Ni/M_T ratio in $CeNi_xO_y$ calcined and dried catalysts.

	Experimental formula				
	$Ce_xNi_yO_m$			Experimental mass %	
Theoretical formula	**x**	**y**	**Ni/M_T ratio**	**Ni**	**Ce**
$CeNi_{0.5}O_{y\ (c)}$	1.0	0.5	0.3	13.6	67.3
$CeNi_1O_{y\ (c)}$	1.0	0.9	0.5	22.0	58.6
$CeNi_2O_{y\ (c)}$	1.1	2.0	0.7	35.5	44.6
$CeNi_5O_{y\ (c)}$	1.0	5.0	0.8	53.1	26.4
$CeNi_{0.5}O_{y\ (d)}$	1.1	0.5	0.3	13.7	67.2
$CeNi_1O_{y\ (d)}$	1.0	0.9	0.5	22.0	58.6
$CeNi_2O_{y\ (d)}$	1.0	2.0	0.7	36.2	44.0
$CeNi_5O_{y\ (d)}$	1.0	5.1	0.8	53.7	25.8

The experimental and theoretical values of metal content, the percentage weight of each metal and Ni/M_T ratio of the Ce-Ni based catalysts are presented in Table 25 and Table 24 respectively. The results obtained experimentally match with the theoretical values in all the binary catalysts. This insures the good preparation of catalysts and the good incorporation of Ni into the catalyst.

III.2.2. BET surface areas for $CeNi_xO_y$ catalysts

The specific surface areas of $CeNi_xO_y$ catalysts (dried and calcined) where x = 0.1, 0.5, 1, 2 and 5 are presented in Table 26 and Figure 37. The dried catalysts have an average specific surface area between 81 and 198 m^2/g. Whereas, for the calcined catalysts, this value is between 60 and 134 m^2/g. The calcined catalysts in comparison to the dried ones have a lower specific surface area except for $CeNi_2O_y$ catalyst where they both have almost similar specific surface areas. In general, the catalysts with low Ni content (x = 0.5 and 1) have higher surface areas than those

with higher Ni content (x = 2 and 5). These values of specific surface areas lie in the same range of values found in literature for $CeNi_xO_y$ catalysts [97].

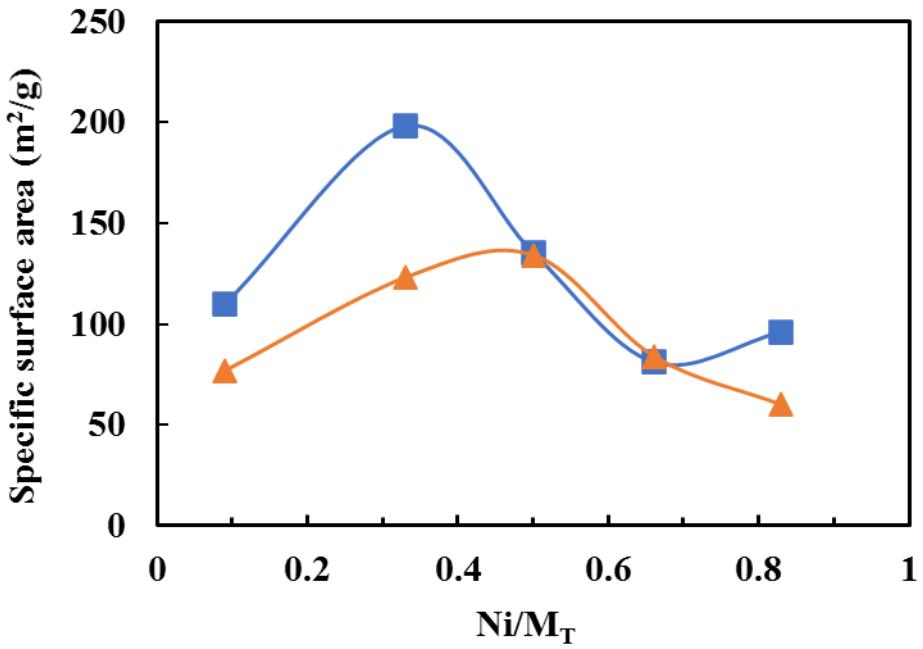

Figure 37 BET specific surface area of $CeNi_xO_y$ dried (■) and calcined (▲) catalysts as a function of Ni/M_T ratio.

Table 26 BET specific surface areas obtained for $CeNi_xO_y$ catalysts.

	Specific surface area (m^2/g)	
Catalyst	**Dried (d)**	**Calcined (c)**
$CeNi_{0.1}O_y$	110	77
$CeNi_{0.5}O_y$	198	123
$CeNi_1O_y$	135	134
$CeNi_2O_y$	81	84
$CeNi_5O_y$	96	60

III.2.4. XRD studies for $CeNi_xO_y$ catalysts

Figure 38 and Figure 39 show the X-Ray diffraction patterns obtained for $CeNi_xO_y$ calcined and dried catalysts respectively (where x = 0.1, 0.5, 1, 2, and 5). The ceria like phase (34-0394 JCPDS file) having the fluorite structure, presents diffraction patterns with the main one at around 28.5° (2θ°) clearly visible in all the calcined samples whatever the ratio of Ni is. The position of the main ceria peaks in each catalyst are exactly precised in Table 27 and 28. The average crystallites size of NiO and CeO_2 in $CeNi_xO_y$ calcined catalysts, measured using the

Scherrer equation are presented in Table 27. The simple CeO_2 and NiO oxides are reported for comparison. The average crystallites size are found between 11 and 14 nm for NiO and between 5 - 7 nm for CeO_2 in $CeNi_xO_{y\,(c)}$. The NiO crystalline phase (4-0835 JCPDS file) is not apparent in all the $CeNi_xO_y$ calcined samples. This phase is visible at high Ni content when $x \geq 1$. The diffraction peaks of the crystallized NiO become more intense with the increasing Ni content. CeO_2 phase becomes broader due to the decrease of average crystallite size of CeO_2. Moreover, the ceria peak position shifts to higher 2 θ values when adding Ni compared to simple CeO_2, showing a compression of the lattice. This is attributed to the substitution of Ce^{4+} cations by Ni^{2+} cations (smaller in size) inside the CeO_2 lattice and so to the formation of Ce-Ni-O solid solution. The presence of smaller NiO nano-crystallites which are not visible by XRD cannot be denied as a reduction signal can still be detected previously with TPR on samples with low Ni content. In fact, crystallites with a size smaller than 2 nm could be difficult to detect by XRD (because of the limits of detection). These nano-crystallites could be well dispersed in the presence of ceria phase [311]. The average crystallites size of NiO and CeO_2 in $CeNi_xO_y$ calcined catalysts, measured using the Scherrer equation are presented in Table 27. The simple CeO_2 and NiO oxides are reported for comparison. The average crystallites sizes are found between 11 and 14 nm for NiO and between 5 - 7 nm for CeO_2 in $CeNi_xO_{y\,(c)}$.

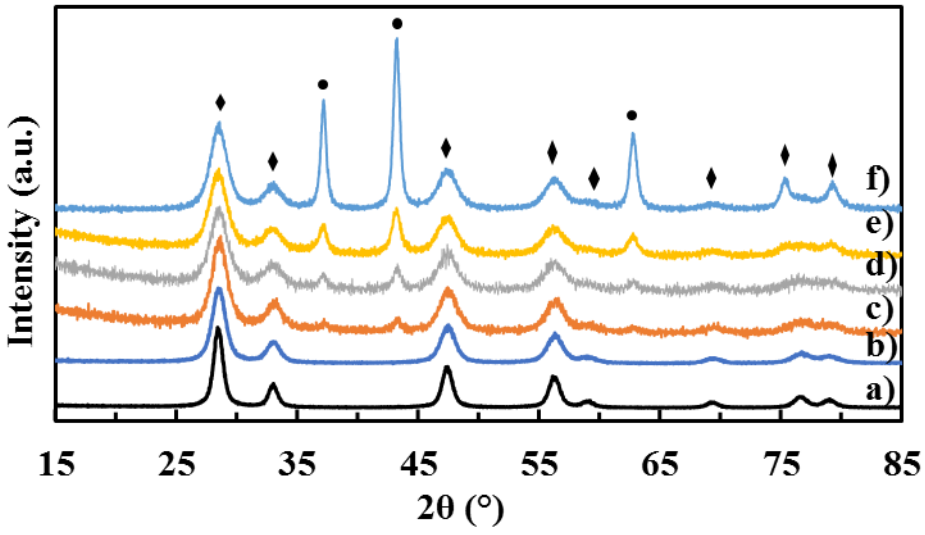

Figure 38 XRD patterns of $CeNi_xO_y$ calcined catalysts: a) CeO_2, b) x = 0.1, c) x = 0.5, d) x = 1, e) x = 2 and f) x = 5 . CeO_2 phase (♦), NiO phase (●).

Table 27 Average crystallites size (nm) of NiO & CeO_2 phases in $CeNi_xO_y$, CeO_2 and NiO calcined samples with the position of the main peak of ceria (2θ°).

Sample	Position of main peak of ceria (2θ°)	Average crystallites size	
		d NiO (nm)	d CeO_2 (nm)
$CeO_{2\ (c)}$	28.4	-	9
NiO*$_{(c)}$	-	> 20	-
$CeNi_{0.1}O_{y\ (c)}$	28.4	-	7
$CeNi_{0.5}O_{y\ (c)}$	28.7	12	5
$CeNi_1O_{y\ (c)}$	28.6	12	5
$CeNi_2O_{y\ (c)}$	28.5	11	5
$CeNi_5O_{y\ (c)}$	28.6	14	5

*from Phys. Chem. Chem. Phys., 2000, 2, 303-312

The structure and crystalline phases of $CeNi_xO_{y\ (d)}$ catalysts are investigated by XRD technique too. Figure 39 shows the XRD patterns obtained for these catalysts with various Ni contents. CeO_2 phase is visible in all the $CeNi_xO_{y\ (d)}$ catalysts. The position of the main ceria XRD pattern of these catalysts is presented in Table 28. $Ni(OH)_2$ phase is observed on some compounds, and only visible when $x \geq 0.5$. To better see the $Ni(OH)_2$ phase when hardly visible (0.5 and 2), a magnification of the XRD patterns is presented in Figure 40. Broadening of the CeO_2 peaks is observed in agreement with the decrease of measured average crystallites size of CeO_2 [321-323].

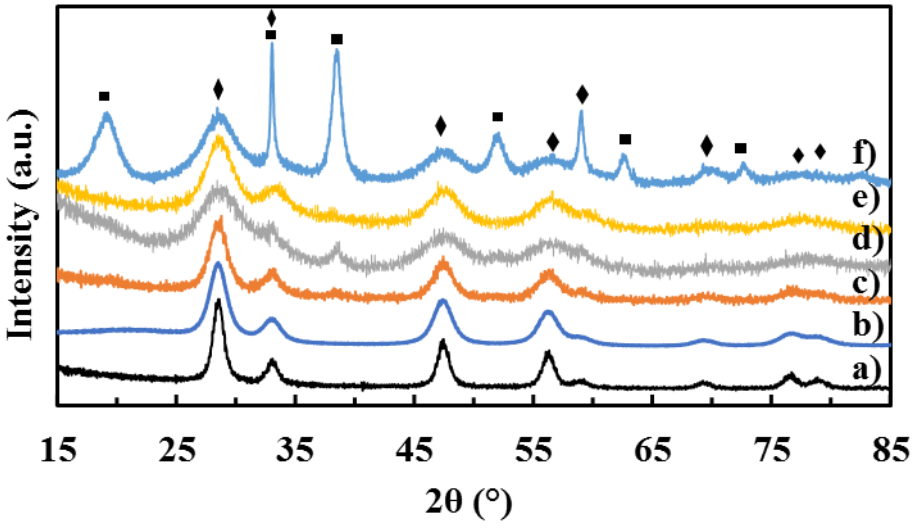

Figure 39 XRD patterns of $CeNi_xO_{y\ (d)}$ catalysts: a) CeO_2, b) x = 0.1, c) x = 0.5 , d) x = 1, e) x = 2 and f) x = 5 . CeO_2 phase (♦), $Ni(OH)_2$ phase (■).

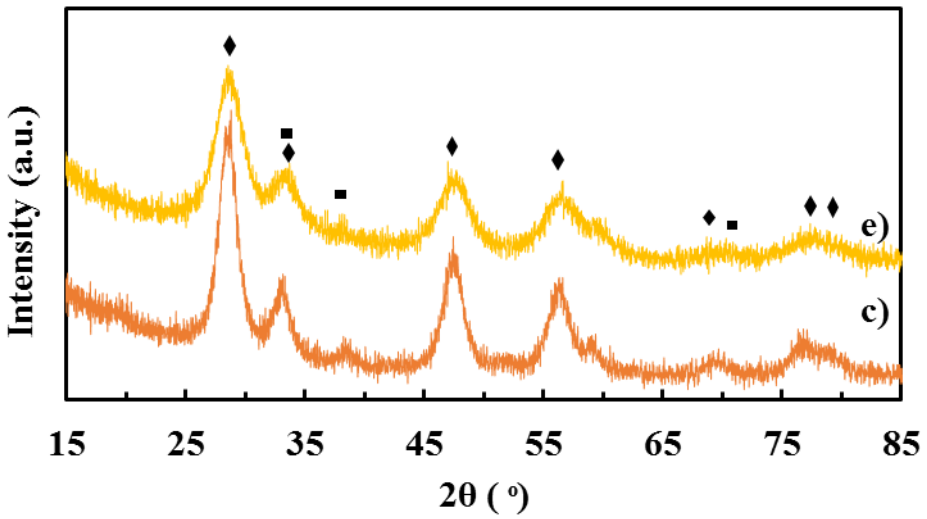

Figure 40 Magnification on XRD patterns of c) $CeNi_{0.5}O_y$ and e) $CeNi_2O_{y\ (d)}$ catalysts.

The average crystallites sizes of $Ni(OH)_2$ and CeO_2 phases in $CeNi_xO_{y\ (d)}$ were measured using the Scherrer equation and presented in Table 28. The average crystallites size of $Ni(OH)_2$ is found at 9 nm in all $CeNi_xO_{y\ (d)}$ catalysts. The average crystallites size of CeO_2 ranges between 3-5 nm in the mixed oxides. These sizes are lower than those of pure CeO_2 (8 nm) and relatively stable with the Ni content of the solid. Moreover, the ceria peak position shifts to higher 2 θ values for highest Ni content compounds when comparing to simple CeO_2, showing a compression of the lattice. This can be linked to the formation of a cerium nickel solid solution.

Table 28 Average crystallites size (nm) of $Ni(OH)_2$ & CeO_2 phases in dried $CeNi_xO_y$ and CeO_2 samples with the position of the main peak of ceria (2θ°).

Sample	Position of main peak of ceria (2θ°)	Average crystallites size (nm)	
		d $Ni(OH)_2$	d CeO_2
$CeO_{2\ (d)}$	28.6	-	8
$CeNi_{0.1}O_{y\ (d)}$	28.5	-	5
$CeNi_{0.5}O_{y\ (d)}$	28.6	9	5
$CeNi_1O_{y\ (d)}$	28.7	9	3
$CeNi_2O_{y\ (d)}$	28.7	9	4
$CeNi_5O_{y\ (d)}$	28.7	9	3

III.2.5. Raman studies on $CeNi_xO_y$ catalysts

The Raman results obtained for calcined and dried $CeNi_xO_y$ catalysts are shown in Figure 41 and

Figure 42, respectively. In fact, this technique permits to have an idea about the structure and oxygen vacancy defects. The Raman spectra show different signals noted here as signal 1 (S_1), signal 2 (S_2) and signal 3 (S_3) along with the F_{2g} ceria peak. A magnification of the spectra of dried $CeNi_{0.1}O_y$ and $CeNi_{0.5}O_y$ catalysts is done in Figure 43 to show the presence of signal S_1 and S_2. The positions of these signals are precised in Table 29 and Table 30 for the calcined and dried binary catalysts, respectively. On nano-crystallized ceria, prepared in similar conditions, the first-order (F_{2g}) CeO_2 peak is found to be located near 460 cm^{-1} [97, 324]. Analyzing cerium compounds is quite complicated due to numerous initial and final 4f electronic configurations. The F_{2g} first order ceria peak is visible in all the samples and is correlated to fluorite nano-crystalline CeO_2 [325, 326]. This agrees with the low average crystallites size previously shown by XRD. For comparison, the position of the F_{2g} ceria peak of crystallized ceria has been reported at the position of 466 cm^{-1} [327]. Moreover, there is a shift and broadening effect, that could be explained by the incorporation of nickel species in the ceria phase, in agreement with the presence of a solid solution [328]. This has been shown in the case of catalysts supported over CeO_2 with the formation of additional bands due to supported molecular species and crystalline phases [329]. This shift is higher when x = 0.5 and 1. The peaks visible in the range between 500 and 700 cm^{-1} correspond to local vibrations due to the doping of the catalyst [330]. Signal S_1 at around 550 cm^{-1}, is related to an extrinsic defect mode induced by oxygen vacancies that can be increased in case of the substitution of Ce^{4+} by lower valence cations in a solid solution. As a matter of fact, it has been reported on a Ni/CeO_2 catalyst that the significant band observed in the 500-630 cm^{-1} region, could be decomposed in two contributions at 547 cm^{-1} and 615 cm^{-1} and the component observed at 547 cm^{-1} was assigned to an extrinsic defect mode induced by oxygen vacancies [331]. Signal S_2 existing between 619 and 630 cm^{-1} assumes the existence of Ce^{3+} complexes in the ceria structure [328]. This peak cannot be well identified when x = 5. It has been reported that the region 590-670 cm^{-1} may be attributed to the oxygen vacancies defect in the CeO_2 lattice, induced by the Ce^{3+} ion, and that the interconversion of Ce^{4+} to Ce^{3+} concomitantly leads to the generation of oxygen vacancies [332]. A peak at around 520 cm^{-1} assigned to NiO could exist but cannot be clearly visible due to the shadowing effect by the long tail of the first-order CeO_2 F_{2g} peak [333]. Signal S_3 visible at around 220 cm^{-1} is assigned to ceria nanostructures [334]. This peak is not visible on the dried samples. The intensity of the signals S_1 and S_2 in the calcined catalysts is higher than those appearing in the catalyst without previous calcination. The F_{2g} ceria peak position is shifted more to lower values on the

dried catalysts than those of calcined catalysts. Moreover, S_1 and S_2 cannot be well separated in the dried catalysts.

As a matter of fact, the Raman-active mode in CeO_2 corresponding to the frequency of $\omega_R = 466\ cm^{-1}$, which is attributed to the symmetrical stretching mode of Ce-O8 vibrational unit, is easily affected by disorders in the oxygen sublattice and/or grain size induced non-stoichiometry. It has also been shown that the line shifts and broadens with decreasing grain size and increasing lattice defects [335]. All the obtained results agree with the presence of small nanoparticles and the solubility of Ni^{2+} into CeO_2 creating anionic vacancies.

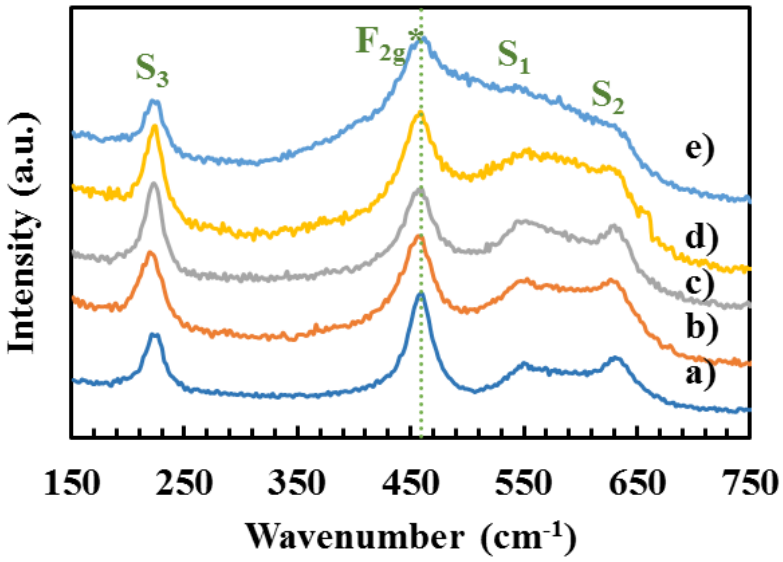

Figure 41 Raman spectra of $CeNi_xO_y$ calcined catalysts: a) x = 0.1, b) x = 0.5, c) x = 1, d) x = 2 and e) x = 5. (F_{2g}*: ceria peak position).

Table 29 Raman signal positions for $CeNi_xO_{y\ (c)}$ where x = 0.1, 0.5, 1, 2 and 5.

x	F_{2g} ceria peak position (cm^{-1})	S_1 (cm^{-1})	S_2 (cm^{-1})	S_3 (cm^{-1})
0.1	460.1	549.3	630	226
0.5	456.6	552	626.8	219
1	456.6	551	626.8	222.7
2	458.3	554	619.7	224.5
5	461.9	545	shoulder	220.8

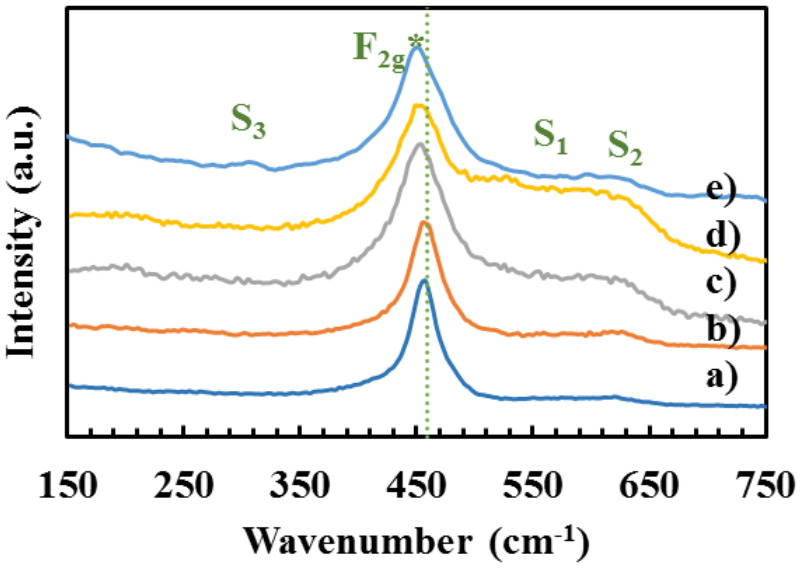

Figure 42 Raman spectra of dried $CeNi_xO_{y\ (d)}$ catalysts: a) x = 0.1, b) x = 0.5, c) x = 1, d) x = 2 and e) x = 5.

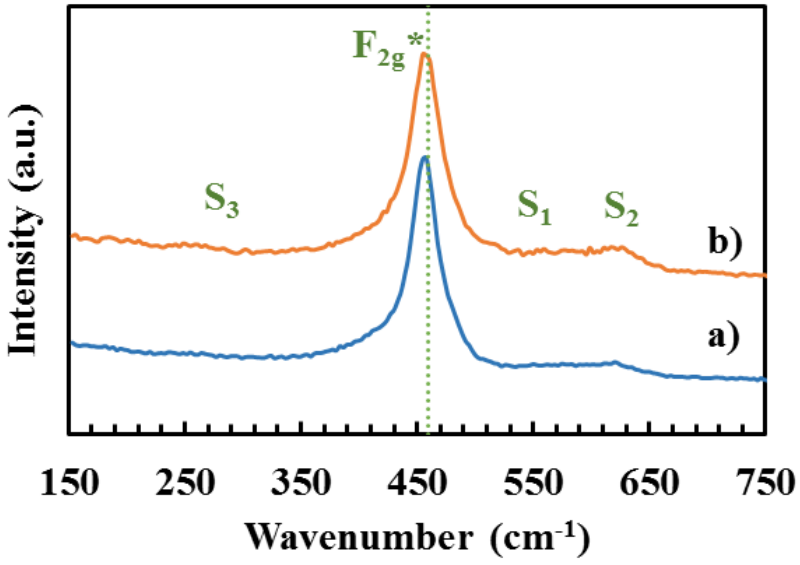

Figure 43 Raman spectra magnification of a) $CeNi_{0.1}O_{y\ (d)}$ and b) $CeNi_{0.5}O_{y\ (d)}$ catalysts.

Table 30 Raman signal positions for $CeNi_xO_{y\ (d)}$ where x = 0.1, 0.5, 1, 2 and 5.

x	F_{2g} ceria peak position (cm^{-1})	$S_1 + S_2$ (cm^{-1})
0.1	457	500-670
0.5	454.8	500-670
1	457.8	500-670
2	454.8	500-670
5	450.2	500-670

III.2.3. TPR profiles for $CeNi_xO_y$ catalysts

The temperature programmed reduction (TPR) under hydrogen makes it possible to study the reduction of the different phases present in a solid. This technique allows measuring the hydrogen consumption of a solid as a function of temperature. This allows to investigate the strength of metal-support interactions through the reduction temperature of Ni species in the catalyst. The reduction temperature profile in H_2 of the $CeNi_xO_y$ calcined catalysts is shown in Figure 44. The reduction of these catalysts takes place in different range of temperatures as this can be verified from the presence of several peaks. The presence of two peaks shows the presence of two types of nickel species, that could correspond to Ni species in two different environments. The reduction temperatures will be divided into 2 zones: zone 1 and zone 2. represents the positions of these reduction zones along with the positions of the main reduction peaks if possible to detect (Table 31 and Table 32). A first reduction temperature peak is observed at low temperatures (between 250 and 283 °C) and has been related to the reducibility of Ni species in solid solution and/or small NiO nanoparticles [336]. These species could also be easily oxidized and as a matter of fact, some redox processes have already been demonstrated between Ce^{4+}, Ce^{3+}, Ni^0 and Ni^{2+} [321]. In addition, it is possible to see a slight displacement of the peaks towards higher or lower temperatures by increasing Ni content. In general, it appears at higher temperatures (283 °C) for low Ni content (x = 0.1) and at lower temperatures (258 °C) for high Ni content (x = 5). The second reduction zone appearing at higher temperature between 277 °C and 480 °C for x = 0.5, 1, 2 and 5. This reduction zone was previously assigned to the reduction of larger NiO nanoparticles (visible by XRD) [336]. The small shoulder observed on this peak could be assigned to reductions of subsurface Ni species and of surface Ce^{4+}, obtained from weak metal-support interaction of Ni species with ceria [337]. This temperature zone is not observed for a very low Ni content (x = 0.1). However, the second reduction stage (between 360-615 °C) observed on $CeNi_{0.1}O_{y\ (c)}$ can be assigned to the reduction of surface oxygen species of CeO_2 [338]. This stage could exist in all other catalysts but not visible due to overlapping. The TPR peak for the simple NiO oxide prepared in similar conditions has been reported at about 400 °C [339]. During calcination, the $Ni(OH)_2$ phase and/or some nickel species can migrate and generate NiO nanoparticles, with a reducibility slightly different when compared to the reduction temperature reported for pure NiO (393 °C) [339, 340]. The reduction behaviour of Ni based catalyst supported on pure CeO_2 has also been reported before with a two-step reduction process [341]. Therefore, the stages of reduction being in the temperature range

of 300–550°C can be assigned to the reduction of NiO eventually interacting with the support when some shifts in temperature are observed and also of Ce^{4+} cations of CeO_2 to non-stoichiometric oxides CeO_{2-x}.

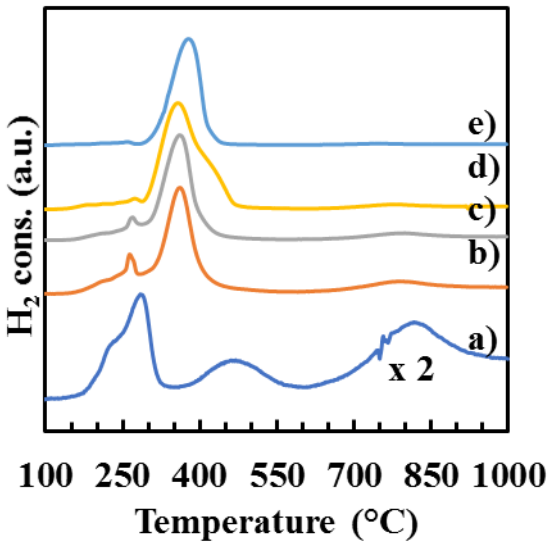

Figure 44 TPR profiles for $CeNi_xO_{y\ (c)}$ catalysts: a) x = 0.1, b) x = 0.5, c) x = 1, d) x = 2 and e) x = 5.

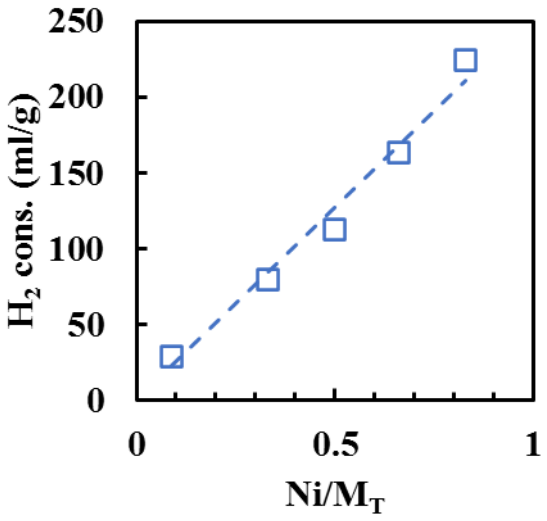

Figure 45 Hydrogen consumption in TPR as a function of Ni content of $CeNi_xO_{y\ (c)}$ catalysts $Ni/M_T = x/(x+1)$.

Table 31 Temperature reduction zones and main peak positions in TPR for $CeNi_xO_{y\ (c)}$ catalysts.

	Zone (peak position) (°C)	
Catalyst	**1st zone**	**2nd zone**
$CeNi_{0.1}O_{y\ (c)}$	155-330 (283)	360 - 615 (468.5)
$CeNi_{0.5}O_{y\ (c)}$	155-276 (263)	277- 470 (360.8)
$CeNi_1O_{y\ (c)}$	170-285 (268.4)	285 - 470 (359.9)
$CeNi_2O_{y\ (c)}$	150-300 (274.6)	300 - 480 (359)
$CeNi_5O_{y\ (c)}$	190-285 (258)	285 - 450 (378.6)

Similar to the calcined $CeNi_xO_y$ catalysts, the dried $CeNi_xO_y$ catalysts show the presence of 2 main reduction peaks. However, the first reduction zone exists at higher temperature ranges than that of the calcined ones. Moreover, this peak is sharper and more intense. However, the second peak is broader than that of the calcined catalysts. In addition, it appears at lower temperatures than that of the calcined ones.

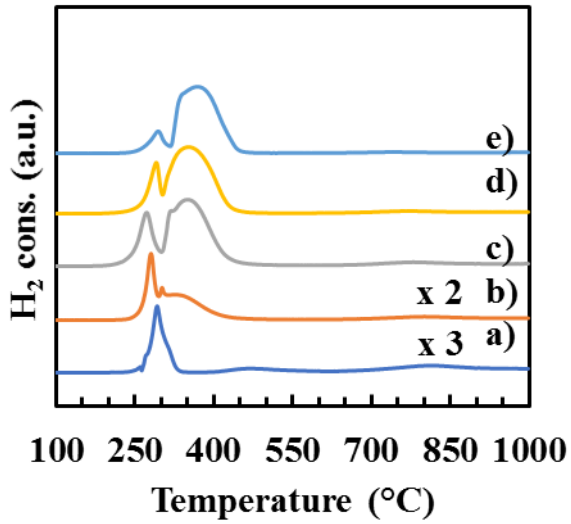

Figure 46 TPR profiles for $CeNi_xO_{y\ (d)}$ catalysts: a) x = 0.1, b) 0.5, c) , d) 2 and e) 5.

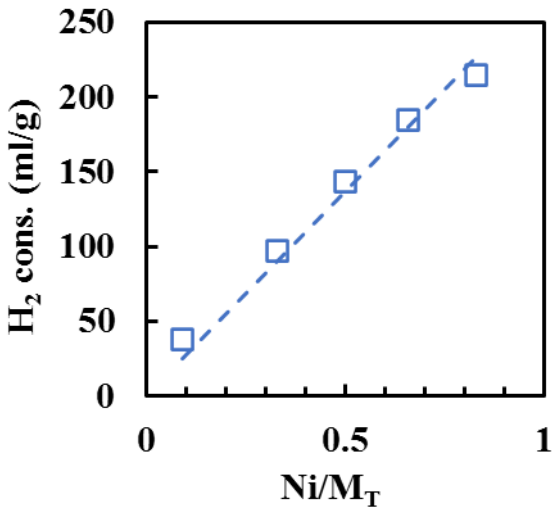

Figure 47 Hydrogen consumption in TPR as a function of Ni content of $CeNi_xO_{y\ (d)}$ catalysts $Ni/M_T=x/(x+1)$.

Table 32 Temperature reduction zones and main peak positions in TPR for $CeNi_xO_{y\ (d)}$ catalysts.

	Zone (peak position) (°C)	
Catalyst	**1st zone**	**2nd zone**
$CeNi_{0.1}O_{y\ (d)}$	230-270 (264)	-
$CeNi_{0.5}O_{y\ (d)}$	230-290 (279.9)	290-420 (300.6)
$CeNi_1O_{y\ (d)}$	200-300 (270.6)	300-450 (347)
$CeNi_2O_{y\ (d)}$	230-300 (290)	300-450 (352)
$CeNi_5O_{y\ (d)}$	240-320 (294)	320-450 (370)

The first peak can be attributed to nickel in solid solution in the ceria phase or to the reduction of very small nanoparticles of a Ni related phase also visible in XRD for low content of nickel. At high Ni contents, the second peak could correspond to the transformation of $Ni(OH)_2$ (phase which could be amorphous in XRD). It is also possible that $Ni(OH)_2$ (present in amorphous form) is converted into NiO and then reduced to metallic Ni as a function of the temperature leading to the formation of two peaks. So, whatever the nickel content is, the second peak corresponds to the reduction of the oxide of nickel (NiO).

The amount of H_2 consumed is in good linearship with the Ni amount of the catalysts (Figure 45 and Figure 47). This can be illustrated in where the amount hydrogen consumed is presented as a function of the Ni content. The quantity of consumed H_2 is in good agreement with the Ni content of the solids for both the dried and calcined $CeNi_xO_y$ catalysts. The amount of hydrogen

consumed corresponds to the reduction of Ni species in different surrounding environments. This good linear relationship proves the good incorporation of Ni inside the compound and thus a good preparation process of the catalyst.

III.2.6. XPS studies for $CeNi_xO_y$ catalysts

XPS (X-ray Photoelectron Spectroscopy) technique performed on $CeNi_xO_y$ catalysts allows analyzing the binding energies corresponding to Ce, Ni, O and C species (Tables 33 and 34). Figure 48 and Figure 49 represent XPS spectra for the different calcined and dried binary catalysts with different Ni contents. The binding energies corresponding to Ce, Ni, O and carbon are presented below in Table 33 and Table 34. Previous studies performed on CeO_2 simple oxide show the presence of doublets denoted by (u, v), (u', v'), (u'', v'') and (u''', v''') [322, 342]. In Ce 3d XPS characterizations (Figure 48-1 and Figure 49-1), these doublets, which are ascribed to Ce^{4+} ions in CeO_2, are easily noticed regardless of the content of Ni. Different signals can be observed for Ce 3d mainly at the following positions close to 882, 898, 901 and 917 eV. The positions of these signals vary slightly from one catalyst to another. These band shapes are less broad and more intense when the Ni loading is low in the catalyst. The Ce species bind along with oxygen species present in the solid, and through oxygen bonds with other cations like Ni species when forming a solid solution. Previous studies performed in our lab stated that some of the Ni^{2+} specieswe inserted in the solid solution with ceria and with ceria–zirconia [321]. The peak appearing at around 917 eV is the characteristic peak of Ce^{4+} [343].
Ni 2p XPS spectra (Figure 48-2 and Figure 49-2, Tables 33 and 34) reveal the presence of a main Ni $2p_{3/2}$ emission with, for dried and calcined compounds, binding energies between 854.7 - 855.3 eV and for calcined compounds, when $x > 0.1$ also a peak at 853.6 - 853.8 eV. The satellite peak at around 860.7 - 860.8 eV can be observed on both calcined and dried catalysts. It has been interpreted by a plasmon loss on the surface related to a two hole loss $c3d^9 4s^2$ final state effect as a characteristic presence of Ni^{2+} species [344]. The change of binding energies than those found in literature (861 eV) for the simple NiO oxide proves the strong interactions between the cations in the solid. It has to be noted that on the dried catalysts, the absence of the peak at around 853 eV is probably due to the fact of dominance of metallic hydroxides at this step before calcination. Ni $2p_{1/2}$ peaks can also be seen at around 881eV. The Ni $2p_{3/2}$ bands exhibit line broadening effect as the Ni content increases giving an indication of the existence of different Ni species interacting with other metallic cations.

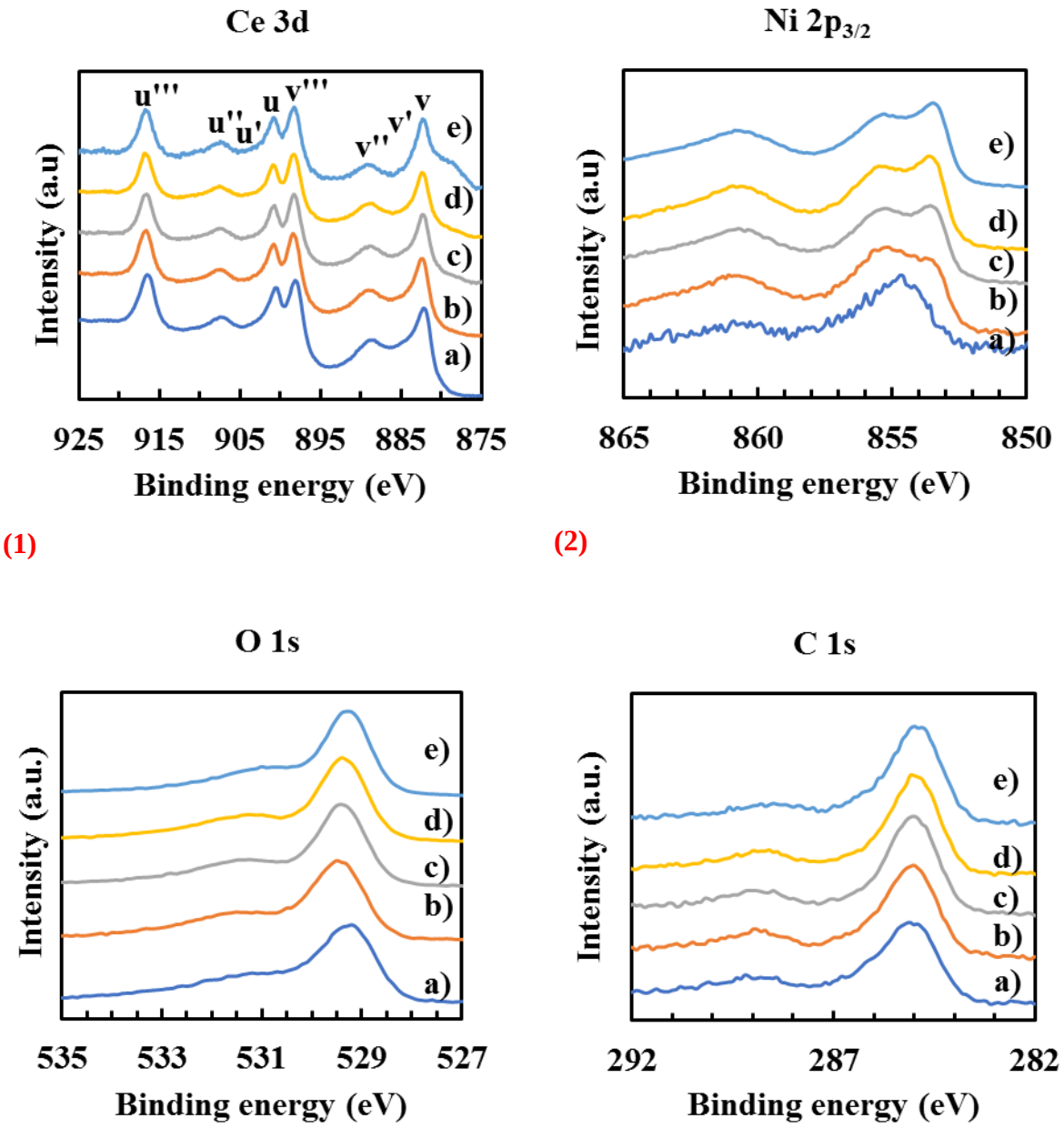

Figure 48 XPS spectra of a) $CeNi_{0.1}O_y$, b) $CeNi_{0.5}O_y$, c) $CeNi_1O_y$, d) $CeNi_2O_y$ and e) $CeNi_5O_y$ calcined catalysts. 1) Ce 3d, 2) Ni $2p_{3/2}$, 3) O 1s and 4) C 1s.

As reported in Figure 48-3 and Figure 49-3 and Tables 33 and 34, two peaks exist at 529 and 531 eV for O1s core level. The peak at 529 ± 1 eV corresponds to typical O^{2-} lattice oxygen in oxides of NiO and CeO_2. This peak (existing between 529.2 eV and 529.5eV) appears more intense on the calcined catalysts than those of the dried ones. On the dried catalysts, this peak is more evident at lower nickel content when x is equal to 0.1 and 0.5. The latter, at 531 eV, can be assigned to oxygen species in the form of OH^{-1} group. This is the fact why this peak

appears more intense on non-calcined compounds and more intense going to higher Ni ratios (x = 2 and 5). It has to be noted that carbon is always present on dried and calcined compounds. This is due to adventitious carbon that cannot be avoided while performing XPS analysis, and used as a reference (at 285 eV). Signals produced due to C-C bonding are found at around 285 eV and those of C-O bonding at 286 eV [345].

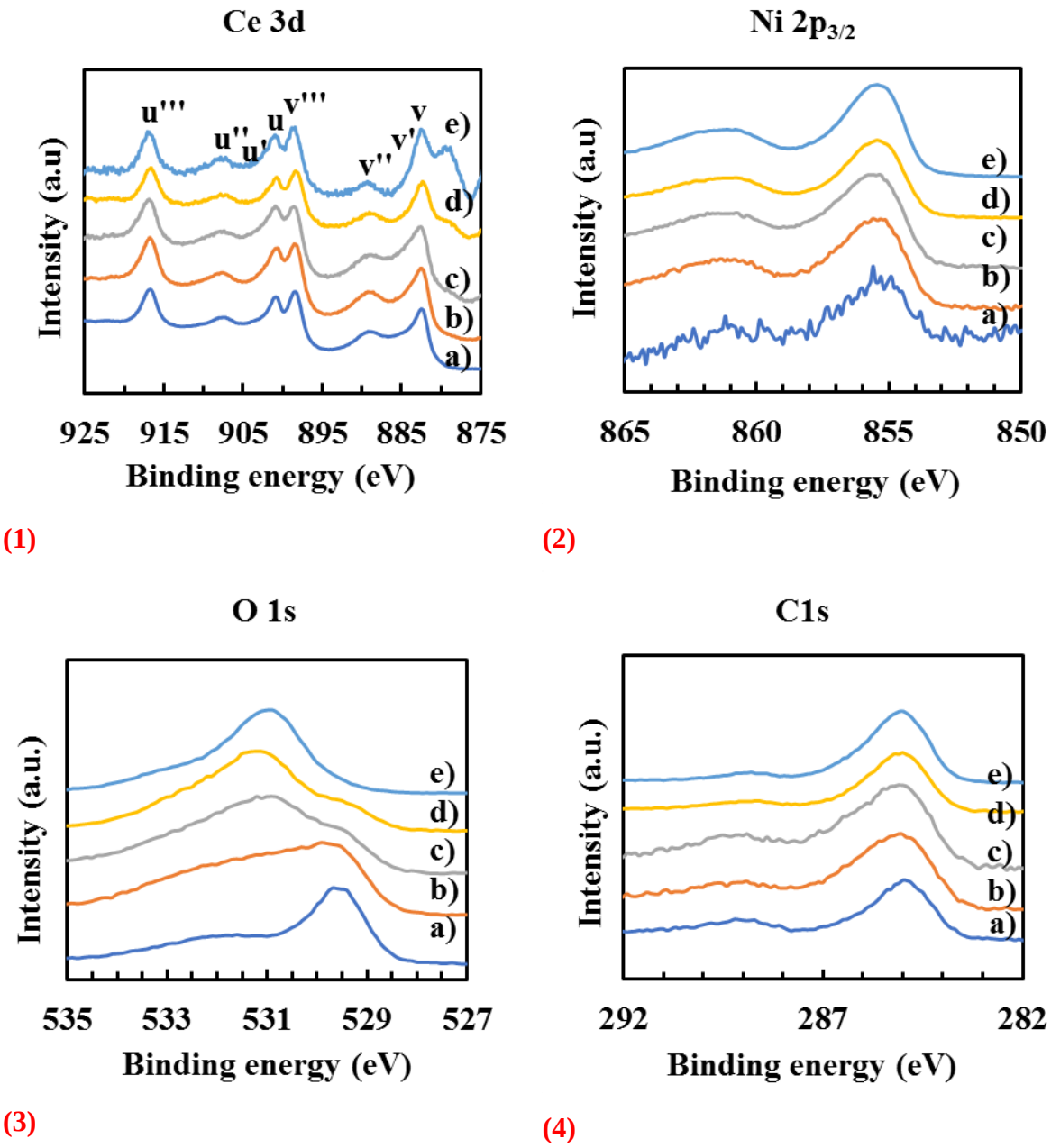

Figure 49 XPS spectra of a) $CeNi_{0.1}O_y$, b) $CeNi_{0.5}O_y$, c) $CeNi_1O_y$, d) $CeNi_2O_y$ and e) $CeNi_5O_y$ dried catalysts. 1) Ce 3d, 2) Ni $2p_{3/2}$, 3) O 1s and 4) C 1s.

Table 33 Binding energies for the different XPS signals obtained for $CeNi_xO_{y\ (c)}$ catalysts.

	Binding energy (eV)				
Catalyst (c)	**Ni $2p_{3/2}$**	**Ni $2p_{3/2}$ satellite**	**O 1s**	**Ce 3d**	**C 1s**
$CeNi_{0.1}O_y$	854.7	860.7	529.2/531.2	882.2/898.2/900.5/916.5	285
$CeNi_{0.5}O_y$	855.2/853.8	860.7	529.5/531.5	882.3/898.4/900.8/916.6	285
$CeNi_1O_y$	855.3/853.6	860.7	529.4/531.3	882.4/898.3/900.7/916.6	285
$CeNi_2O_y$	855.3/853.6	860.7	529.4/531.1	882.4/898.3/900.9/916.8	285
$CeNi_5O_y$	855.3/853.6	860.7	529.3/531	882.4/898.3/900.9/916.8	285

Table 34 Binding energies for the different XPS signals obtained for $CeNi_xO_{y\ (d)}$ catalysts.

	Binding energy (eV)				
Catalyst (d)	**Ni $2p_{3/2}$**	**Ni $2p_{3/2}$ satellite**	**O 1s**	**Ce 3d**	**C 1s**
$CeNi_{0.1}O_y$	854.7	860.8	529.2/531.2	882.2/898.3/900.5/916.5	285
$CeNi_{0.5}O_y$	855.2	860.8	529.5	882.3/898.3/900.8/916.6	285
$CeNi_1O_y$	855.3	860.8	531.1	882.4/898.3/900.7/916.6	285
$CeNi_2O_y$	855.3	860.8	531.1	882.4/898.4/900.9/916.8	285
$CeNi_5O_y$	855.3	860.8	530.9	882.4/898.2/900.9/916.8	285

XPS allows quantitative analysis of the different atomic species present in the solid samples. Table 35 and Table 36 represent the quantitative data obtained in both calcined and dried catalysts respectively. All Ni $2p_{3/2}$ spectra correspond to Ni^{2+} contributions. 70 – 80 % of cerium is found on the form of Ce^{4+} with a small percentage attributed to the presence of Ce^{3+} cations. Concerning oxygen, O^{2-} and OH species exist in almost equal proportions with the calcined catalysts of $CeNi_xO_y$. However, on the dried catalysts, the OH species dominate and reach almost 90 % of the total contribution to atomic percentage of O in $CeNi_5O_{y\ (d)}$, in good agreement with the presence in high proportion of $Ni(OH)_2$ in this compound, as shown by XRD in Figure 39. XPS provides additional information on the structure of the catalysts. Figure 50 compares the surface Ni molar ratio determined by XPS to the bulk molar ratio obtained from XRF. The 45° diagonal line represents the ideal case of a homogeneous distribution of nickel inside the solid. The series of calcined and dried catalysts of $CeNi_xO_y$ present a good homogeneous and a well dispersed system as they follow well the ideal case of distribution. This is in agreement with a maximal Ni^{2+} incorporation inside the ceria lattice [8].

Table 35 Quantification data for atomic percentage in $CeNi_xO_y$ calcined catalysts obtained from XPS.

	% at						
	Ni 2p3/2		Ce 3d		O 1s		
Catalyst (c)	Ni^0	Ni^{2+}	Ce^{4+}	Ce^{3+}	O^{2-}	OH	O'
$CeNi_{0.1}O_y$	0	100	82	18	44	55	-
$CeNi_{0.5}O_y$	0	100	85	15	49	50	-
$CeNi_1O_y$	0	100	86	14	54	46	-
$CeNi_2O_y$	0	100	70	30	61	39	-
$CeNi_5O_y$	0	100	82	18	50	50	-

Table 36 Quantification data for atomic percentage in $CeNi_xO_y$ dried catalysts obtained from XPS.

	% at						
	Ni 2p3/2		Ce 3d		O 1s		
Catalyst (d)	Ni^0	Ni^{2+}	Ce^{4+}	Ce^{3+}	O^{2-}	OH	O'
$CeNi_{0.1}O_y$	0	100	86	14	45	55	-
$CeNi_{0.5}O_y$	0	100	87	13	40	60	-
$CeNi_1O_y$	0	100	73	27	30	70	-
$CeNi_2O_y$	0	100	85	15	18	81	-
$CeNi_5O_y$	0	100	68	32	10	90	-

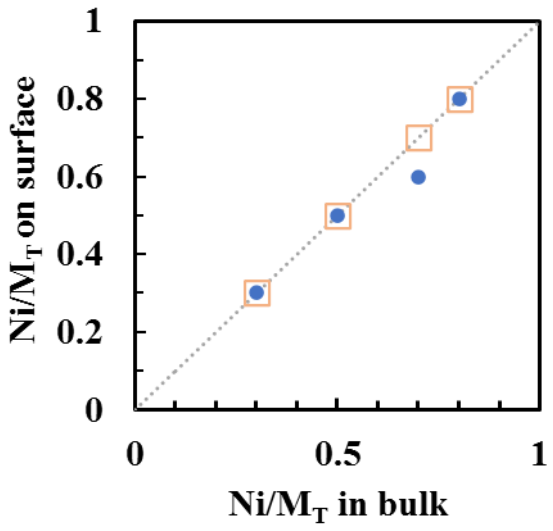

Figure 50 variation of surface Ni/M_T ratio as a function of bulk Ni/M_T ratio. $CeNi_xO_{y\ (c)}$ catalysts (●). $CeNi_xO_{y\ (d)}$ catalysts (□).

III.3. Characterizations of $CeNi_xZr_{0.5}O_y$ catalysts

Similar to the binary catalysts, the calcined zirconium-based ternary catalysts $CeNi_xZr_{0.5}O_y$ are analyzed by different physico-chemical characterization methods.

III.3.1. Elemental Analysis and textural properties of $CeNi_xZr_{0.5}O_y$ catalysts

To get the weight percentage of each metallic element in the different catalysts of $CeNi_xZr_{0.5}O_y$, XRF technique is used in the same conditions mentioned previously. The experimental and theoretical mass percentage values of metal and Ni/M_T content in bulk of $CeNi_xZr_{0.5}O_y$ calcined and dried catalysts are summarized in table 37 and 38 respectively. The expected theoretical weight percentage of Ni and Ce are truly validated experimentally. However, the experimental wt% of Zr obtained are less than that of the expected value. The atomic ratio of Zr in all the ternary catalysts was 0.3 instead of 0.5. However, this ratio does not change in all the series of catalysts which means that the preparation process is successful and similar in all the cases. This could be due to some undissolved zirconium based starting material added during the preparation (even if the solution has been warmed), or that the mixing time during preparation is not enough to precipitate all hydrates or due to uncertainty in the XRF technique on low weight percentages. This value will still be noted as 0.5 in the nomenclature of the catalysts.

Table 37 Experimental values of metallic mass percentages and Ni/M_T content in bulk of $CeNi_xZr_{0.5}O_y$ calcined and dried catalysts.

	Experimental formula $Ce_xNi_yZr_zO_m$				**Experimental mass %**		
Theoretical formula	**x**	**y**	**z**	**Ni/M_T ratio bulk**	**Ni**	**Zr**	**Ce**
$CeNi_{0.5}Zr_{0.5}O_{y\ (c)}$	1.0	0.5	0.3	0.3	11.8	10.9	57.3
$CeNi_1Zr_{0.5}O_{y\ (c)}$	1.0	1.0	0.3	0.4	20.7	9.6	49.4
$CeNi_2Zr_{0.5}O_{y\ (c)}$	1.0	2.0	0.3	0.6	32.3	7.6	39.6
$CeNi_5Zr_{0.5}O_{y\ (c)}$	1.0	5.0	0.3	0.8	50.4	4.6	24.2
$CeNi_{0.5}Zr_{0.5}O_{y\ (d)}$	1.0	0.5	0.3	0.3	11.7	11.1	57.0
$CeNi_1Zr_{0.5}O_{y\ (d)}$	1.0	1.0	0.3	0.4	20.8	9.7	49.2
$CeNi_2Zr_{0.5}O_{y\ (d)}$	1.0	2.0	0.3	0.6	32.7	8.1	38.7
$CeNi_5Zr_{0.5}O_{y\ (d)}$	1.0	5.0	0.3	0.8	50.7	4.7	23.8

$Ni/M_T = x/(x + 1.5)$

Table 38 Theoretical values of Ni/M_T content in bulk and weight percentage of $CeNi_xZr_{0.5}O_y$ (calcined and dried) catalysts.

		Theoretical wt%			
Theoretical formula	**Ni/M_T ratio theo.**	**O**	**Ni**	**Zr**	**Ce**
$CeNi_{0.5}Zr_{0.5}O_{3.5}$	0.3	19.1	10.8	16.8	51.7
$CeNi_1Zr_{0.5}O_4$	0.4	19.4	19.0	14.8	45.4
$CeNi_2Zr_{0.5}O_5$	0.6	19.9	30.6	11.9	36.6
$CeNi_5Zr_{0.5}O_8$	0.8	20.5	48.3	7.5	23.1

III.3.2. BET surface areas for $CeNi_xZr_{0.5}Oy$ catalysts

The surface areas of the different $CeNi_xZr_{0.5}O_y$ calcined and dried catalysts are presented in Table 39 and Figure 51 respectively. The dried catalysts have specific surface areas ranging between 186 and 112 m^2/g. These specific surface areas are higher than those presented by the calcined catalysts (between 71 and 130 m^2/g). This phenomenon can be explained by the thermal treatment of 500 °C applied for calcination. The specific surface areas of the dried catalysts decrease when the Ni content increases. The same trend is followed by the calcined catalysts however this applies when $x \geq 1$. Moreover, when $x \geq 1$, the binary catalysts have lower surface areas than that of those doped with Zr (For x = 1, both binary and ternary catalysts have same specific surface areas in the presence or absence of calcination. The trend followed by specific surface area as a function of Ni/M_T ratio is relatively the same for compounds including and missing Zr element (Table 39 and Figure 51). Similar catalytic compositions were reported in literature having much lower specific surface areas between 6 and 9 m^2/g [346].

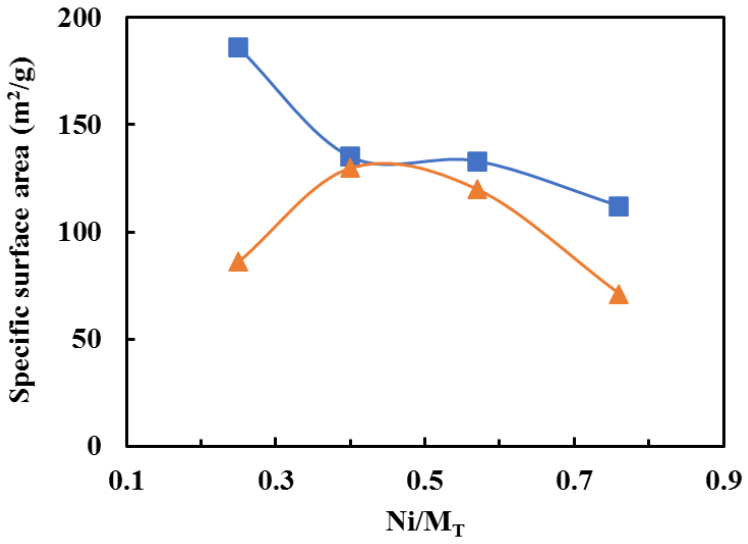

Figure 51 BET specific surface areas of $CeNi_xZr_{0.5}O_y$ dried (■) and calcined (▲) catalysts as a function of Ni/M_T

ratio.

Table 39 BET specific surface areas obtained for $CeNi_xZr_{0.5}O_y$ catalysts where x = 0.5, 1, 2 or 5.

	Specific surface area (m^2/g)	
Catalyst	**Dried (d)**	**Calcined (c)**
$CeZr_{0.5}Ni_{0.5}O_y$	186	86
$CeZr_{0.5}Ni_1O_y$	135	130
$CeZr_{0.5}Ni_2O_y$	133	120
$CeZr_{0.5}Ni_5O_y$	112	71

III.3.3. XRD studies for $CeNi_xZr_{0.5}O_y$ catalysts

Figure 52 and Figure 53 group together the diffractograms of the $CeNi_xZr_{0.5}O_y$ ternary calcined and dried catalysts respectively. Starting from $CeNi_xZr_{0.5}O_{y\ (c)}$ lets us observe two different phases: ceria phase is always observed, that could correspond to a solid solution of ceria-zirconia and a phase corresponding to NiO. As with binary catalysts, the NiO phase is increasingly intensified when the nickel content increases. Both phases, CeO_2 and NiO, appear even when the nickel content is low (in the studied series). The position of the main peak of ceria in each of simple $CeO_{2\ (c)}$ and $CeNi_xZr_{0.5}O_{y\ (c)}$ are precised in Table 40. The main XRD diffraction pattern of ceria lies at around 28° (2θ°). The average crystallites size of CeO_2 is found at 4 nm in the ternary compounds which is almost half the size obtained for the simple CeO_2 (9 nm). The average crystallites size of NiO is found at 13 nm. All these values are calculated using Scherrer equation.

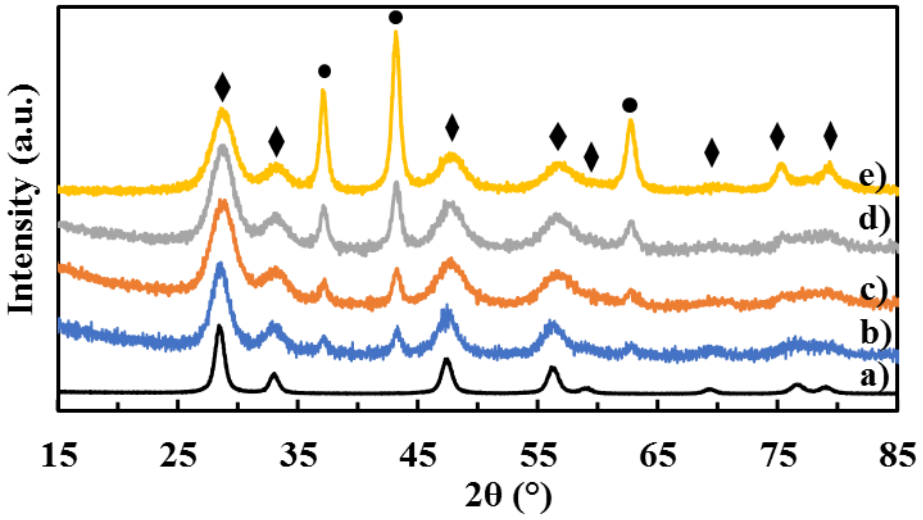

Figure 52 XRD patterns of $CeNi_xZr_{0.5}O_y$ calcined catalysts: a) CeO_2, b) x = 0.5, c) x = 1, d) x = 2 and e) x = 5 . CeO_2 phase (♦), NiO phase (●).

Table 40 Average crystallites size for $CeNi_xZr_{0.5}O_{y\ (c)}$ (taking into account the main XRD patterns of $CeO_{2\ (c)}$, $NiO_{(c)}$).

Sample	Position of main peak of ceria (2θ°), plane (111)	Average crystallite size (nm)	
		d NiO	d CeO_2
$CeO_{2\ (c)}$	28.4	-	9
NiO*$_{(c)}$	-	>20	-
$CeNi_{0.5}Zr_{0.5}O_y$ (c)	28.6	13	4
$CeNi_1Zr_{0.5}O_y$ (c)	28.5	13	4
$CeNi_2Zr_{0.5}O_y$ (c)	28.6	13	4
$CeNi_5Zr_{0.5}O_y$ (c)	28.6	12	4

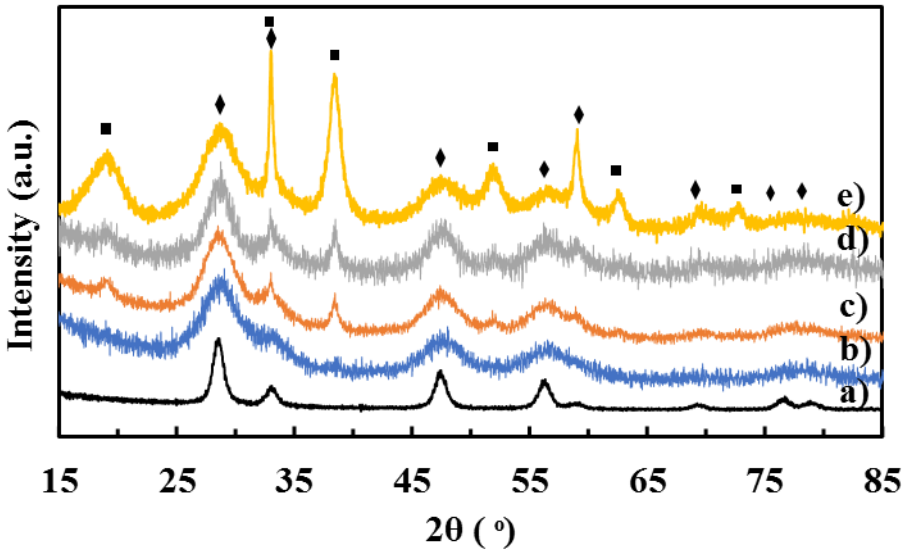

Figure 53 XRD patterns of $CeNi_xZr_{0.5}O_{y\ (d)}$ catalysts: a) CeO_2, b) x = 0.5, c) x = 1, d) x = 2 and e) x = 5. CeO_2 phase (♦), $Ni(OH)_2$ phase (■).

Table 41 Average crystallites size of $CeZr_{0.5}Ni_xO_{y\ (d)}$ (taking into account the main XRD patterns of $Ni(OH)_2$ and CeO_2).

Sample	Position of main peak of ceria (2θ°), plane (111)	Average crystallites size (nm)	
		d $Ni(OH)_2$	d CeO_2
$CeO_{2\ (d)}$	28.6	-	8
$Ni(OH)_2$*$_{(d)}$	-	10	-
$CeNi_{0.5}Zr_{0.5}O_{y\ (d)}$	28.6	12	3
$CeNi_1Zr_{0.5}O_{y\ (d)}$	28.5	12	3
$CeNi_2Zr_{0.5}O_{y\ (d)}$	28.6	13	4
$CeNi_5Zr_{0.5}O_{y\ (d)}$	28.6	8	3

On the dried ternary catalysts, similarly to the binary dried catalysts, the $Ni(OH)_2$ phase increases with the increase in Ni content. The average crystallites size of $Ni(OH)_2$ and CeO_2 calculated from XRD are shown in Table 41. The average crystallites size of $Ni(OH)_2$ is of 12 nm for x < 5. However, at x = 5, the size becomes smaller at 8 nm. The average crystallites size of $CeO_{2\ (d)}$ is found at 4 nm. The average crystallites size of CeO_2 is affected by the presence of Ni even if it is at a very low ratio. However, this size is still much lower than that of simple CeO_2 oxide which is probably due to the fact of the presence of different cations in the same material. The coprecipitation method have been proved to be more efficient in obtaining smaller

average crystallites size, for both NiO and CeO_2 [347]. This has also been reported by Bueno-Ferrer by studying the relationship between surface area and crystal size of pure and doped cerium oxide solids [348].

It has been previously shown that the larger the NiO crystal, the reduction occurs at higher temperatures becoming closer to simple NiO, while if nickel (II) oxide crystals are small, or in solid solution, H_2 is consumed at lower temperature, so they could be transformed to nickel(0) at lower temperatures [349]. However, this is not so obvious, due to the strong interactions between different cations it has been shown previously, that a redox process can allow the Ni^{2+} species that could be reduced to stay oxidized while Ce^{4+} species in strong interaction are reduced to Ce^{3+} cations.

III.3.4. Raman studies for $CeNi_xZr_{0.5}O_y$ catalysts

Figure 54 shows Raman analysis for $CeNi_xZr_{0.5}O_{y\ (c)}$ catalysts. It can be recalled that the position of the main peak F_{2g} is located at 460 cm^{-1} for CeO_2 simple oxide prepared in similar way. Even if the signal is broad and present an uncertainty, it seems that the position of this peak deviates globally to higher values on calcined compounds, as shown in Table 42. For the highest Ni content, this peak shifts to the highest value (483.4 cm^{-1}). This peak becomes wider than that obtained on the nano-crystallized CeO_2, as also observed on binary compounds. This agrees with the solubility of nickel in ceria, and with the formation of the solid solution of Ce-Ni-Zr-O. F_{2g} ceria peak shift to higher energy (482.5 cm^{-1}) has been already reported and attributed to the formation of ceria-zirconia solid solution [332]. These values are slightly different than those of the binary catalysts whose range was between 456 and 461 cm^{-1}. This is explained by the modification of the ceria phase by the insertion of the zirconium inside it. Other signals S_1, S_2 and S_3 are presented in the Table 42. S_3 at around 220 cm^{-1} is a characteristic of nanostructure of the ceria phase. S_1 as S_2 signals appear as a shoulder due to the broadness of these signals and the presence of different environments for the oxygen vacancies present in the lattice. These defects produced create the signal between 500 and 730 cm^{-1} and a peak at 567 cm^{-1} seems to emerge but all the peaks in this range correspond to oxygen deficient complexes in the structure of the catalyst, due to the creation of anionic vacancies related to the insertion of the Ni and Zr species in the lattice and to the formation of a solid solution of Ce-Zr-Ni-O. For low Ni contents, several peaks are more observable. However, when the Ni content increases, the signal becomes very broad and complex. As for binary compounds, at

520 cm^{-1}, could exist a peak corresponding to NiO located near the peak of ceria, difficult to see on all samples due to the tail created by the CeO_2 F_{2g} peak.

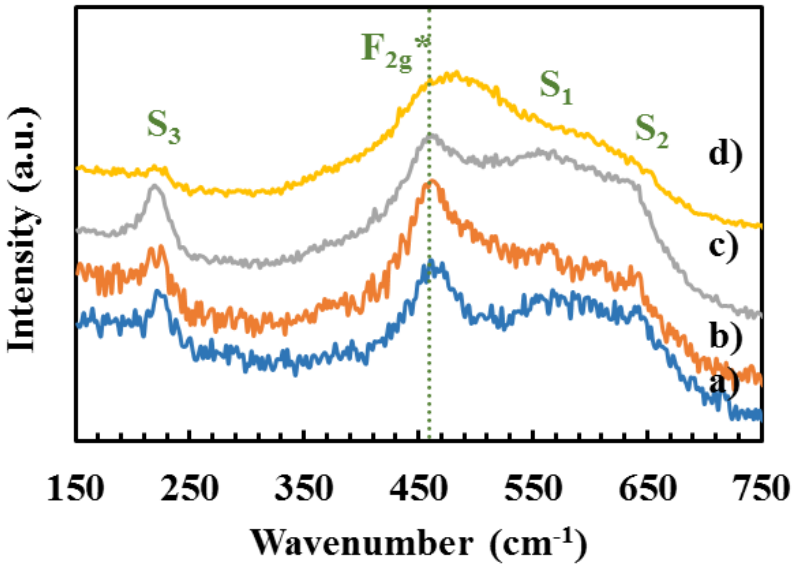

Figure 54 Raman spectra for $CeNi_xZr_{0.5}O_y$ calcined catalysts: a) x = 0.5, b) x = 1, c) x = 2 and d) x = 5.

Table 42 Raman signal positions for $CeNi_xZr_{0.5}O_y$ calcined catalysts.

x	F_{2g} ceria peak position (cm^{-1})	$S_1 + S_2$ (cm^{-1})	S_3 (cm^{-1})
0.5	460.1	500-730	220
1	462	500-730	224.5
2	462	500-730	219
5	483.4	500-730	219

The Raman spectra for dried $CeNi_xZr_{0.5}O_y$ catalysts are shown in Figure 55. The F_{2g} peak appears for all the samples in a range between 451 and 460 cm^{-1} which agrees with the presence of nano-crystallized ceria. However, for the dried ternary Zr based compounds, this peak is shifted mainly to lower values compared to CeO_2, as it was observed on binary Ce-Ni compounds. The peak shifts the most when the Ni content increases to x = 5 (451 cm^{-1}) which supports the fact that the Ni species are being inserted in the form of a solid solution with ceria and thus creating a wavenumber shift. The wavenumbers of the signals created by the different dried and ternary samples are presented in Table 43.

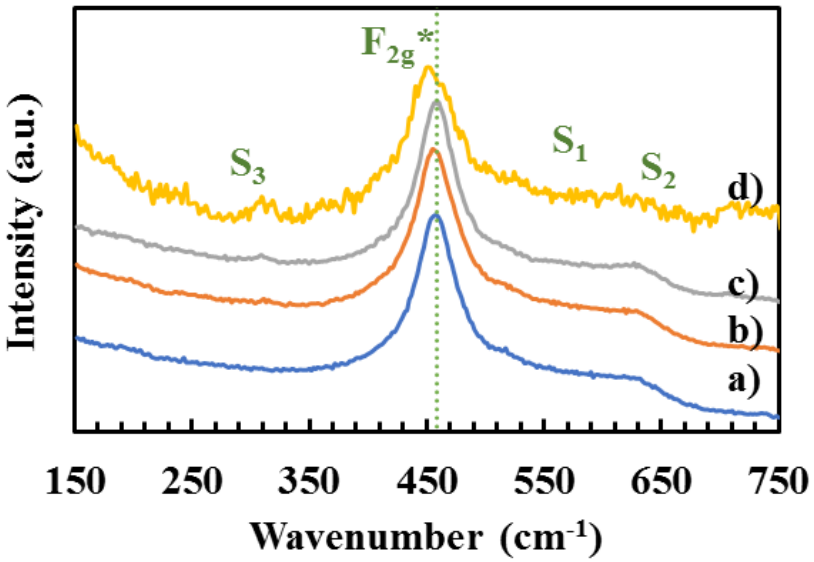

Figure 55 Raman spectra for $CeNi_xZr_{0.5}O_y$ dried catalysts: a) x = 0.5, b) x = 1, c) x = 2 and d) x = 5.

Weak shoulders shown by S_1 and S_2 are obtained at around 580 and 630 cm^{-1} related to the local vibrations of different oxygen vacancy (Vo) complexes. Signal S_2 at about 630 cm^{-1} is more visible up to x = 2 and assumes the existence of Ce^{3+} complexes in the ceria structure. It has been reported that the vibrational mode obtained at around 600 cm^{-1} corresponds to the presence of Ce^{3+} - Vo complexes in the ceria lattice. A weak band for the highest Ni content compounds in the region of 300 - 315 cm^{-1} could be related to the displacement of the oxygen atoms from their ideal positions in the fluorite lattice [350].

Table 43 Raman signal positions for $CeNi_xZr_{0.5}O_y$ dried catalysts.

x	F_{2g} ceria peak position (cm^{-1})	$S_1 + S_2$ (cm^{-1})
0.5	458	490-690
1	454	490-690
2	460	490-690
5	451	490-690

All these vibrational modes, mentioned before, are more visible compared to the binary catalysts, in agreement with the Zr introduction inside the CeO_2 lattice, with more oxygen vacancies formed and thus vibration modes appear in the Raman spectra with higher intensities.

With the increase in Ni content, these peaks become broader, less intense and less resolved. All these data, gives a proof for the presence of a Ce-Zr-Ni-O solid solution present in the catalysts.

III.3.5. TPR profiles for $CeNi_xZr_{0.5}O_y$ catalysts

Figure 56 shows the results of the temperature programmed reduction (TPR) performed on the calcined catalysts of $CeNi_xZr_{0.5}O_y$. Two reduction zones can be reported and are reported in Figure 56. The first reduction zone appearing between 110 and 320 °C depends on each catalyst. The position of the main peak in this zone (low temperature) varies with the different Ni contents of the solid. It should be noted that the first peak (286 – 295 °C) is observed at slightly higher temperatures compared to binary catalysts (264 – 294 °C) (Table 44). As for binary compounds, this peak can probably be attributed to the reduction of Ni^{2+} species of small NiO nano-particles, or Ni species localized in solid solution in ceria (or ceria-zirconia). It is possible, as for the binary catalysts, to see that this peak decreases in favor of the second peak, which can be attributed to the reduction of larger NiO nanoparticles (visible by XRD), since it increases with the content in Ni. Thus, both of the reduction peaks appear at a higher temperature. The second reduction zone appears between 290 and 576 °C with peaks varying between 370 °C and 390 °C and can be compared to the reduction temperature of simple NiO at about 390 °C [97, 339]. The peaks corresponding to this zone are more intense and clearly correspond mainly to the reduction of Ni^{2+} species from NiO particles, well shown by the linear relationship between H_2 consumed and Ni content (Figure 57). However, as already pointed before for binary compounds the reduction of CeO_2 surface species to non-stoichiometric oxides CeO_{2-x} can also be obtained.

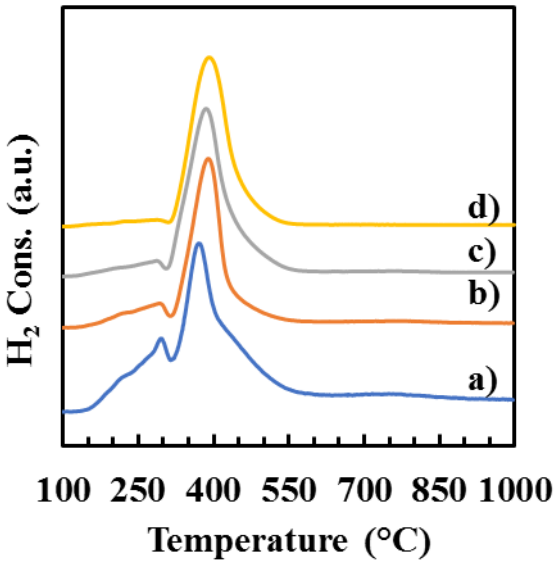

Figure 56 TPR profiles for $CeNi_xZr_{0.5}O_{y\ (c)}$ catalysts: a) x = 0.5, b) x = 1), c) x = 2 and d) x = 5.

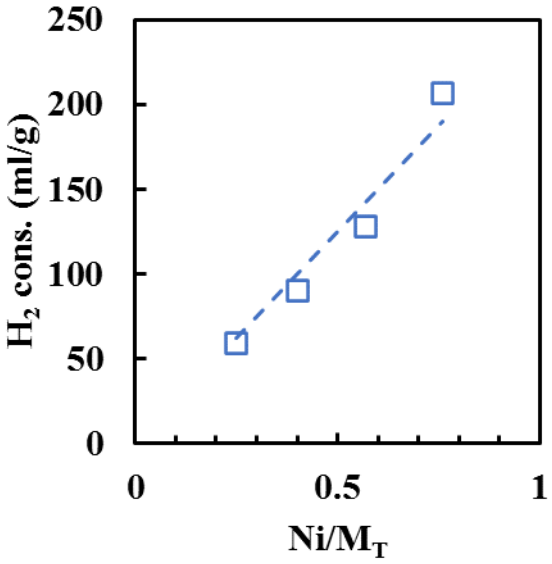

Figure 57 Hydrogen consumption in TPR as a function of Ni content of $CeNi_xZr_{0.5}O_{y\ (c)}$ catalysts Ni/M_T = x/(x+1).

Table 44 Reduction zone and peak positions in TPR for $CeNi_xZr_{0.5}O_{y\ (c)}$.

	Zone (peak position) (°C)	
Catalyst	**1st zone**	**2nd zone**
$CeZr_{0.5}Ni_{0.5}O_{y\ (c)}$	145 - 320 (295)	320 - 576 (370)
$CeZr_{0.5}Ni_1O_{y\ (c)}$	145 - 290 (293.5)	290 - 512 (390)
$CeZr_{0.5}Ni_2O_{y\ (c)}$	145 - 317 (285.7)	317 - 533 (385.4)
$CeZr_{0.5}Ni_5O_{y\ (c)}$	110 - 305 (290)	315 - 545 (389)

Similarly, two reduction zones appear for the dried catalysts of $CeNi_xZr_{0.5}O_y$ with the first reduction zone appearing between 200 and 320 °C (Table 45). The peak corresponding to this zone shifts to higher reduction temperatures along with the increase in Ni content. It appears at a temperature of 294 °C for $CeNi_5Zr_{0.5}O_{y\ (d)}$ while it is at 269 °C for $CeNi_{0.5}Zr_{0.5}O_{y\ (d)}$. This reduction zone is less broad than those appearing on the calcined catalysts. The other reduction zone which is the main zone corresponding to the reduction of Ni^{2+} species in larger particles appear between 300 and 550 °C. A noticeable shift of this peak appears with the change in Ni content. In fact, the positions of these peaks appear at lower temperature (352 – 366 °C) than those of catalysts with calcination (370 – 390 °C), corresponding to the presence in dried samples of $Ni(OH)_2$ phase visible by XRD.

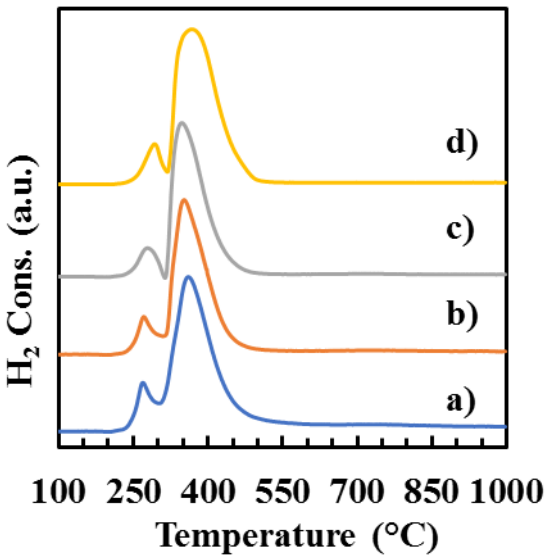

Figure 58 TPR profiles for $CeNi_xZr_{0.5}O_{y\ (d)}$ catalysts: a) x = 0.5, b) x = 1), c) x = 2 and d) x = 5.

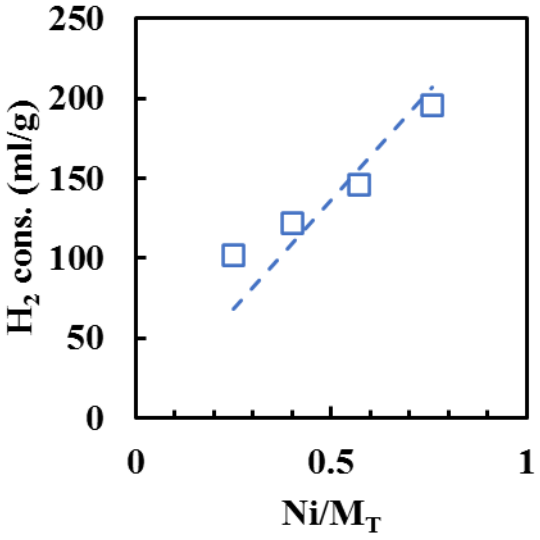

Figure 59 Hydrogen consumption in TPR as a function of Ni content of $CeNi_xZr_{0.5}O_{y\ (d)}$ catalysts Ni/M_T = x/(x+1).

Table 45 Reduction zone and peak positions in TPR for $CeNi_xZr_{0.5}O_{y\ (d)}$.

	Zone (peak position) (°C)	
Catalyst	**1st zone**	**2nd zone**
$CeZr_{0.5}Ni_{0.5}O_{y\ (d)}$	200 - 300 (268.9)	300 - 550 (359.5)
$CeZr_{0.5}Ni_1O_{y\ (d)}$	200 - 310 (270)	310 - 500 (352)
$CeZr_{0.5}Ni_2O_{y\ (d)}$	200 - 313 (278.7)	313 - 510 (347.8)
$CeZr_{0.5}Ni_5O_{y\ (d)}$	200 - 320 (293.5)	320 - 515 (366.2)

Furthermore, figures 59 and 61 show the linear relationship obtained between total hydrogen consumption and the Ni content of the calcined and dried catalysts respectively. Both series of calcined and dried catalysts of $CeNi_xZr_{0.5}O_y$ exhibit a good linear relationship between the nickel content and hydrogen consumption.

III.3.6. XPS studies for $CeNi_xZr_{0.5}O_y$ catalysts

Similar to the binary catalysts, Zr compounds are also analyzed by XPS to check any difference in elemental distribution and environment of these elements. Figure 60 represents the XPS spectra of all the elements present in $CeNi_xZr_{0.5}O_{y\ (c)}$ catalysts. The corresponding binding energies are presented in Table 46 For the Ce 3d core level, three spin-orbits doublets $3d_{3/2}$-$3d_{5/2}$ denoted by (u, v), (u'', v'') and (u''', v''') are present in all cases. The position of the main cerium signal lies between 916.8 and 916.6 eV. Other characteristics signals for cerium are present at around 901, 898 and 882 eV. This has also been shown previously on Zr

compounds [351]. For O 1s, intense peaks appearing at around 529.5 eV are related to O^{2-} species present in the metallic oxides. Another peak at around 531 eV is assigned to oxygen bonded as hydroxides. Those peaks increase clearly on both calcined and dried catalysts with the increase in Ni content. This is in good agreement with XRD and Raman, where the peaks related to metallic oxides are increasing with Ni content. The intensity of these 2 signals do not change with respect to each other and with respect to the different nickel content present in these Zr doped catalysts. Regarding Zr 3d core levels, 2 asymmetric bands appear at 182 and 184 eV related to Zr $3d_{5/2}$ and Zr $3d_{3/2}$ energy levels showing well the presence of Zr^{4+} cations. A doublet peak appears in the region of Ni $2p_{3/2}$ core level due to Ni^{2+} species present in the calcined catalysts [354]. One of them appearing at 855 eV and the second at 853 eV are characteristics of the different Ni^{2+} species present at the surface of the catalyst. The main satellite peak is located at 860.8 around eV. The positions of these signals do not change with nickel content.

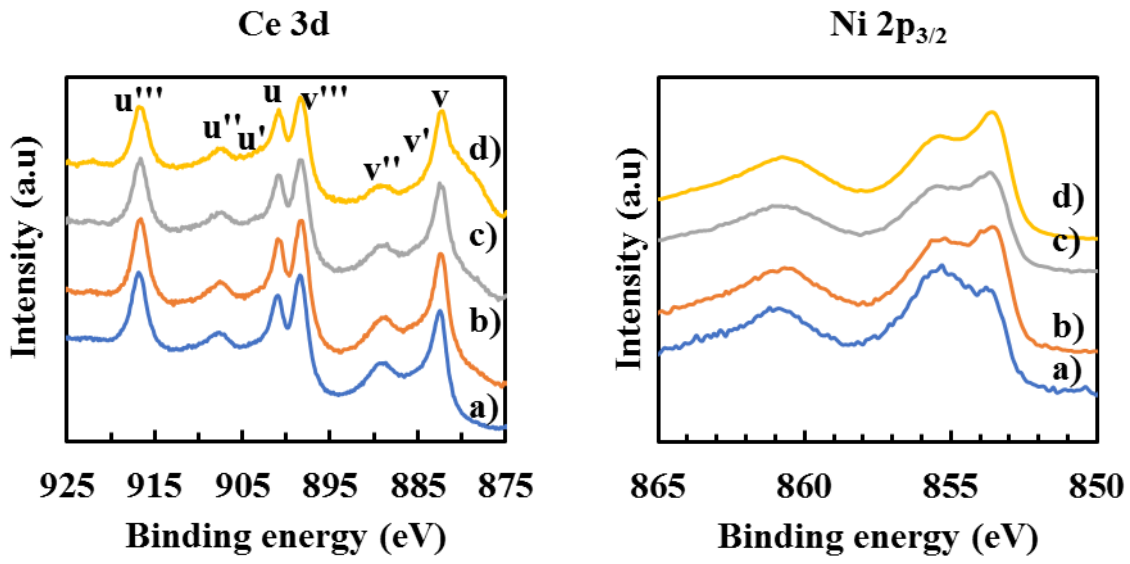

(1) **(2)**

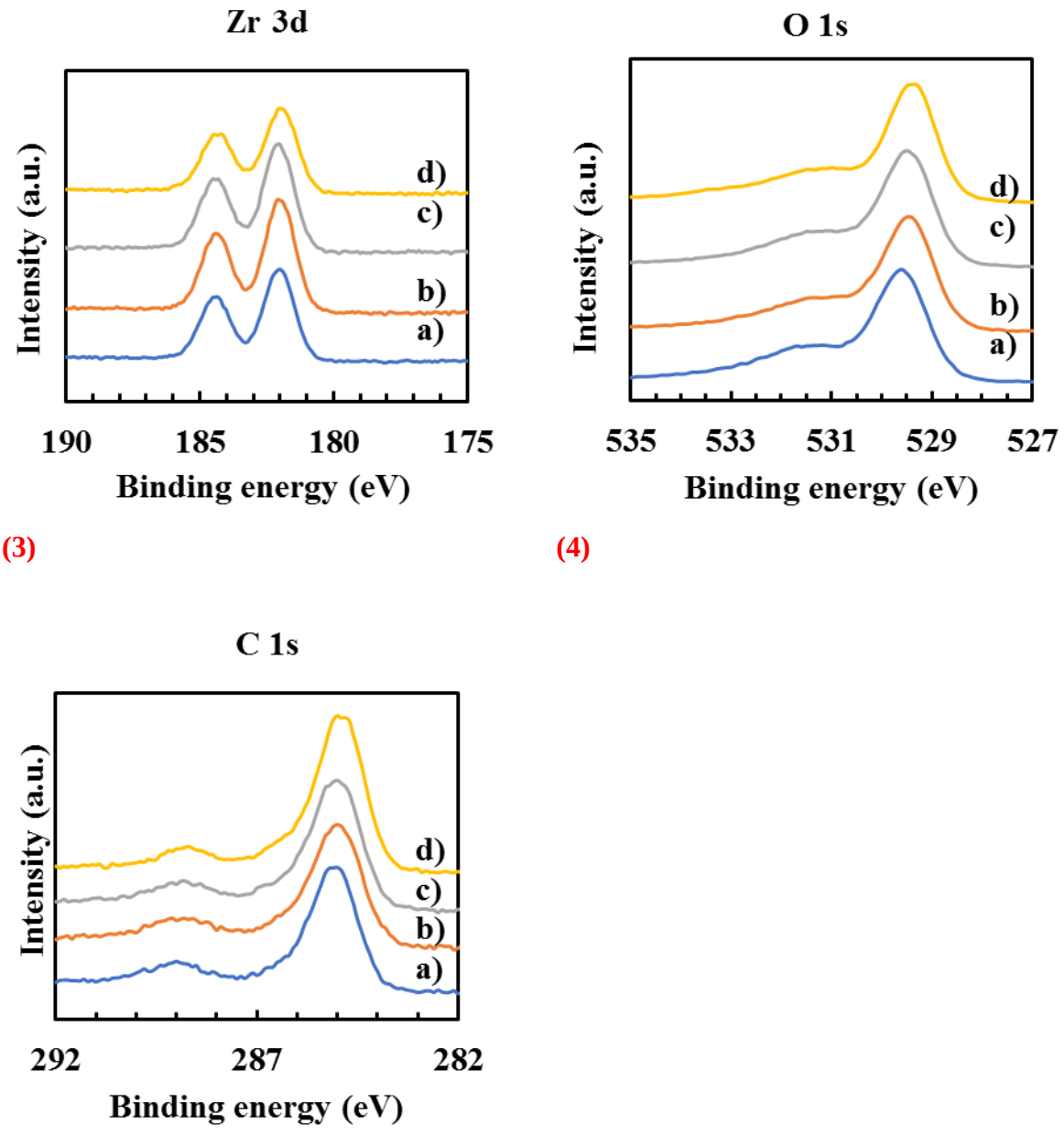

Figure 60 XPS spectra of a) $CeNi_{0.5}Zr_{0.5}O_y$, b) $CeNi_1Zr_{0.5}O_y$, c) $CeNi_2Zr_{0.5}O_y$ and d) $CeNi_5Zr_{0.5}O_y$ calcined catalysts. 1) Ce 3d, 2) Ni $2p_{3/2}$, 3) Zr 3d, 4) O 1s and 5) C 1s.

Table 46 Binding energies for the different XPS signals obtained for $CeNi_xZr_{0.5}O_y$ calcined catalysts.

	Binding energy (eV)					
Catalyst	**Ni $2p_{3/2}$**	**Ni $2p_{3/2}$ satellite**	**Zr 3d**	**O 1s**	**Ce 3d**	**C 1s**
$CeNi_{0.5}Zr_{0.5}O_{y\ (c)}$	855.3/853.8	860.8	184.3/182	531.2/529.6	916.8/900.9/898.4/882.4	285
$CeNi_1Zr_{0.5}O_{y\ (c)}$	855.2/853.6	860.7	184.4/182.1	531.4/529.5	916.6/901/898.3/882.4	285
$CeNi_2Zr_{0.5}O_{y\ (c)}$	855.5/853.7	860.8	184.3/182.1	531/529.5	916.6/900.9/898.4/882.5	285
$CeNi_5Zr_{0.5}O_{y\ (c)}$	855.4/853.6	860.8	184.2/182	531/529.4	916.8/900.9/898.5/882.3	285

Quantification data obtained from XPS (Table 47) shows that at the surface of this catalyst, 100 % of atomic Ni $2p_{3/2}$ is present in the form of Ni^{2+}. The majority of Ce 3d core level atoms appear in the form of Ce^{4+} (around 70 %). This atomic percentage reaches up to 80 % with $CeNi_5Zr_{0.5}O_{y\ (c)}$. O 1s splits to be almost in equivalence between 47 % OH and 53 % O^{2-}.

Table 47 Quantification data for atomic percentage in $CeNi_xZr_{0.5}O_y$ calcined catalysts obtained from XPS.

	% at						
	Ni $2p_{3/2}$		Ce 3d		O 1s		
Catalyst	**Ni^0**	**Ni^{2+}**	**Ce^{4+}**	**Ce^{3+}**	**O^{2-}**	**OH**	**O'**
$CeNi_{0.5}Zr_{0.5}O_{y\ (c)}$	0	100	68	32	47	53	-
$CeNi_1Zr_{0.5}O_{y\ (c)}$	0	100	73	27	54	46	-
$CeNi_2Zr_{0.5}O_{y\ (c)}$	0	100	73	27	54	46	-
$CeNi_5Zr_{0.5}O_{y\ (c)}$	0	100	82	18	52	48	-

XPS spectra of $CeNi_xZr_{0.5}O_{y\ (d)}$ are represented in Figure 61. The Ni $2p_{3/2}$ spectra of the fresh catalysts prepared by co precipitation method show the main peak at 855.8 eV and peaks of shake-up satellites at 861.6 eV (Table 48). These satellites are typical for Ni^{2+} cations [352, 353, 354] originating from multielectron processes [355]. According to the literature, the broadness appearing in the peak at 855.5 eV arises due of the strong interaction between NiO_x species and the support [356] or the formation of Ni-Ce-Zr-O solid solution due to diffusion of Ni^{2+} cations into the fluorite lattice.

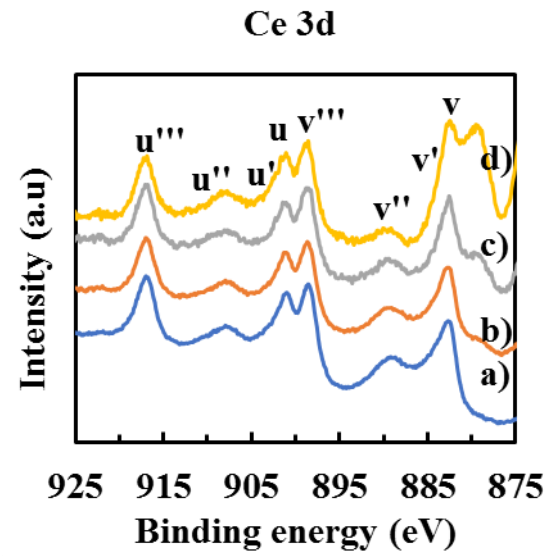
Ce 3d
u'''
u''
u'
u
v'''
v''
v'
v
d)
c)
b)
a)
Intensity (a.u)
925
915
905
895
885
875
Binding energy (eV)

(1)

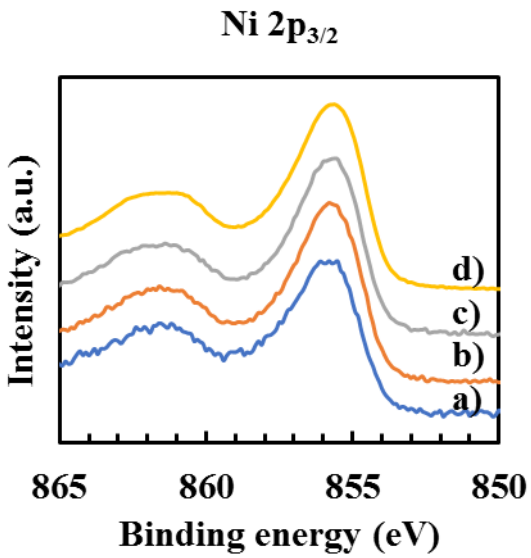
Ni 2p3/2
d)
c)
b)
a)
Intensity (a.u.)
865
860
855
850
Binding energy (eV)

(2)

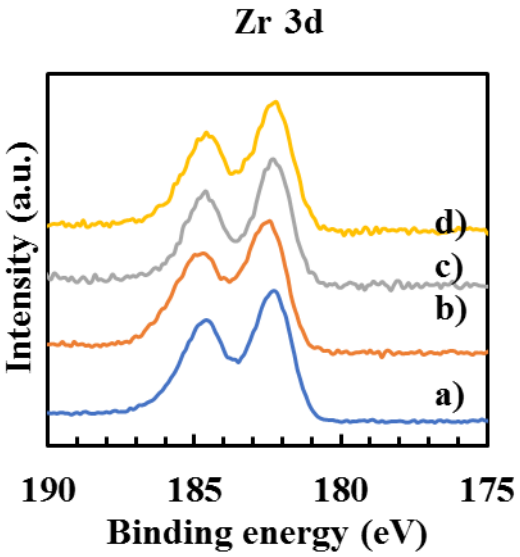
Zr 3d
d)
c)
b)
a)
Intensity (a.u.)
190
185
180
175
Binding energy (eV)

(3)

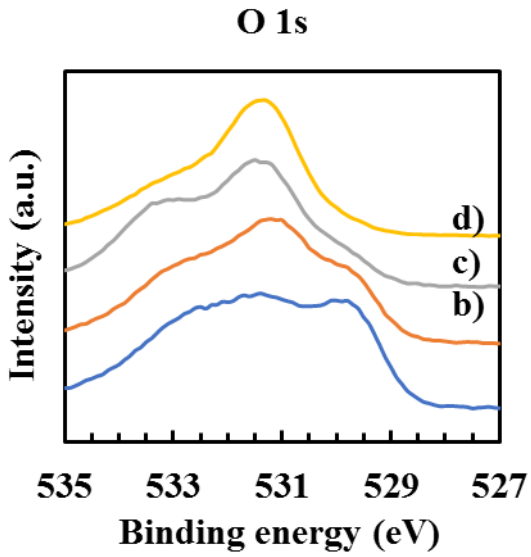
O 1s
d)
c)
b)
Intensity (a.u.)
535
533
531
529
527
Binding energy (eV)

(4)

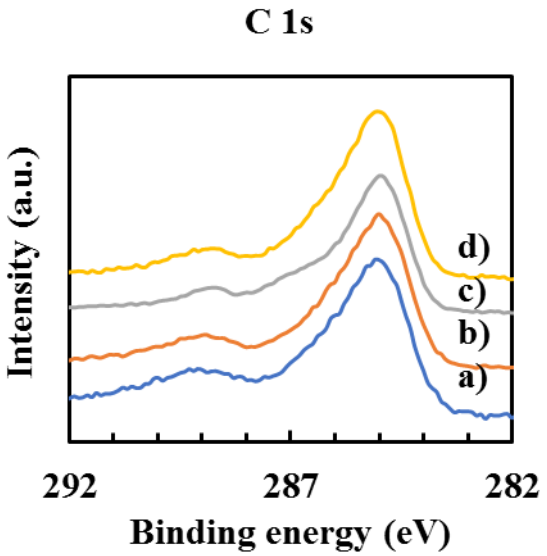

(5)

Figure 61 XPS spectra of a) $CeNi_{0.5}Zr_{0.5}O_y$, b) $CeNi_1Zr_{0.5}O_y$, c) $CeNi_2Zr_{0.5}O_y$ and d) $CeNi_5Zr_{0.5}O_{y\ (d)}$ catalysts. 1) Ce 3d, 2) Ni $2p_{3/2}$, 3) Zr 3d, 4) O 1s and 5) C 1s.

Concerning O1s core level, a triplet can be observed on Zr dried compounds originating from OH groups, O^{2-} and other oxygen species (O') deposited on the surface that could be organic species coming from preparation method, or due to water. The majority of O1s species are of OH nature (Table 49) in agreement with the presence of $Ni(OH)_2$ phase observed by XRD. The position of the main O 1s signal is at around 531 eV for all the dried $CeNi_{0.5}Zr_{0.5}O_y$ catalysts.

Figure 62 compares the surface Ni molar ratio determined by XPS to the bulk molar Ni ratio measured by XRF. A slight variation between surface and bulk can be observed. The Ni/M_T ratio on the surface appears higher than the one of bulk in $CeNi_1Zr_{0.5}O_y$ and $CeNi_2Zr_{0.5}O_y$ calcined and dried catalysts. At lower and higher ratios of Ni, the 45° diagonal line is well followed by the catalysts indicating a very good homogeneous distribution of Ni inside the catalysts, in good agreement with XRD and Raman analysis.

Table 48 Binding energies for the different XPS signals obtained for $CeNi_xZr_{0.5}O_{y\ (d)}$ catalysts.

	Binding energy (eV)					
Catalyst	**Ni $2p_{3/2}$**	**Ni $2p_{3/2}$ satellite**	**Zr 3d**	**O 1s**	**Ce 3d**	**C 1s**
$CeNi_{0.5}Zr_{0.5}O_{y\ (d)}$	855.8	861.6	184.6/182.3	531.4	917/900.1/898.8/882.7	285
$CeNi_1Zr_{0.5}O_{y\ (d)}$	855.8	861.6	184.6/182.4	531.2	916.9/901.3/898.7/882.6	285
$CeNi_2Zr_{0.5}O_{y\ (d)}$	855.6	861.6	184.6/182.3	531.5	917.1/901.5/898.8/882.7	285
$CeNi_5Zr_{0.5}O_{y\ (d)}$	855.6	861.7	184.6/182.2	531.5	916.9/901.1/898.6/882.5	285

Table 49 Quantification data for atomic percentage in $CeNi_xZr_{0.5}O_{y\ (d)}$ catalysts obtained from XPS.

	% at						
	Ni $2p_{3/2}$		Ce 3d		O 1s		
Catalyst	**Ni^0**	**Ni^{2+}**	**Ce^{4+}**	**Ce^{3+}**	**O^{2-}**	**OH**	**O'**
$CeNi_{0.5}Zr_{0.5}O_{y\ (d)}$	0	100	65	35	20	63	17
$CeNi_1Zr_{0.5}O_{y\ (d)}$	0	100	80	20	17	43	40
$CeNi_2Zr_{0.5}O_{y\ (d)}$	0	100	82	18	10	47	43
$CeNi_5Zr_{0.5}O_{y\ (d)}$	0	100	88	12	2	70	28

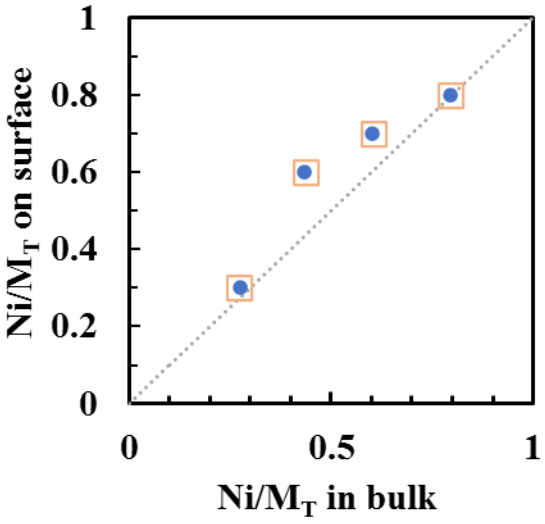

Figure 62 variation of surface Ni/M_T ratio as a function of bulk Ni/M_T ratio. $CeNi_xZr_{0.5}O_y$ calcined catalysts (●). $CeNi_xZr_{0.5}O_y$ dried catalyst (□).

III.4. Characterizations of $CeNi_xAl_{0.5}O_y$ catalysts

Only the calcined catalysts of this series are used for catalytic tests. Below are all the characterizations done on the series of calcined catalysts of $CeNi_xAl_{0.5}O_y$ (where x = 0.5, 1 or 2) prepared by co-precipitation method.

III.4.1. BET surface areas for $CeNi_xAl_{0.5}O_y$ catalysts

The specific surface areas obtained for the $CeNi_xAl_{0.5}O_y$ are presented below in Table 50. The calcined catalysts have a surface area between 125 and 154 m^2/g. It can be seen that the amount of Ni in the catalysts enhances the surface area. Figure 63 represents the BET specific surface area of each catalyst as a function of Ni/M_T ratio. On the calcined Al catalysts, a trend of increased surface area is followed by the increase in Ni/M_T ratio.

Table 50 Specific surface areas of $CeNi_xAl_{0.5}O_y$ calcined catalysts.

Catalyst	Specific surface area (m^2/g)
$CeAl_{0.5}Ni_{0.5}O_y$ (c)	125.6
$CeAl_{0.5}Ni_1O_y$ (c)	136
$CeAl_{0.5}Ni_2O_y$ (c)	154.4

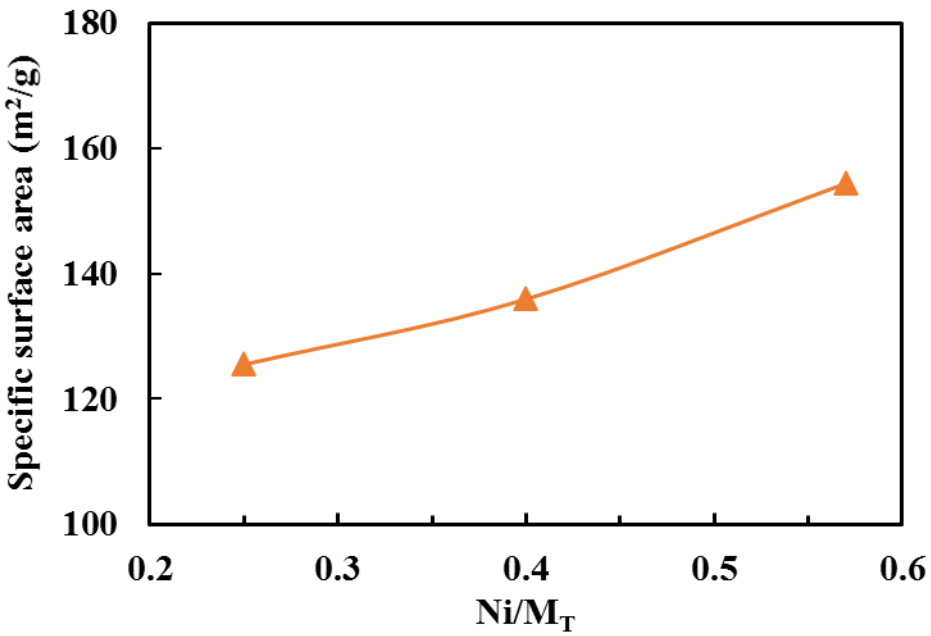

Figure 63 BET specific surface area of $CeNi_xAl_{0.5}O_y$ calcined (▲) catalysts as a function of Ni/M_T ratio.

III.4.2 XRD patterns for $CeNi_xAl_{0.5}O_y$ calcined catalysts

Figure 64 shows the analysis carried out by X-Ray diffraction of the calcined $CeNi_xAl_{0.5}O_y$ calcined catalysts. The ceria (CeO_2) phase is present in all catalysts. The NiO phase, which was well present for the $CeNi_xO_y$ (where $x \geq 1$) and all $CeNi_xZr_{0.5}O_y$ calcined catalysts, is not present for the catalyst with the lower nickel content ($CeNi_{0.5}Al_{0.5}O_y$). However, for $CeNi_1Al_{0.5}O_y$ and $CeNi_2Al_{0.5}O_y$ catalyst, the phase corresponding to NiO can be distinguished clearly. It is therefore likely that when NiO crystallites are not detected, the Ce^{4+} species inside the ceria phase are replaced by Ni^{2+} or Al^{3+} cations with formation of a solid solution of cerium nickel (and aluminum). However, by XRD the presence of an amorphous phase cannot be detected even if present.

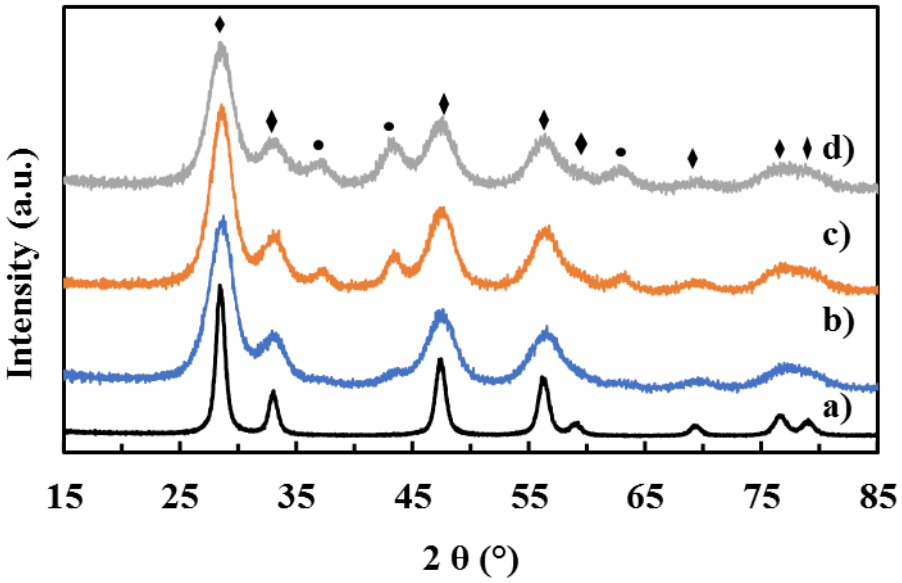

Figure 64 XRD patterns for $CeNi_xAl_{0.5}O_y$ where a) CeO_2, b) x = 0.5, c) x = 1 and d) x = 2.

The positions of main peak of ceria as well as the average crystallites size of NiO and CeO_2 in $CeAl_{0.5}Ni_xO_{y\ (c)}$ catalysts are presented below in Table 51. NiO phase tends to increase with increasing Ni content. Indeed, these diffraction patterns become more intense when Ni content increases. A phase related to Al is not observed. The average crystallites size is estimated to be of 4 nm for CeO_2 and between 5-9 nm for NiO crystallites, based on Scherrer's formula.

Table 51 positions of main peak of ceria, average crystal size (nm) of NiO and CeO_2 crystals in $CeNi_xAl_{0.5}O_{y\,(c)}$.

Sample	Position of main peak of ceria (20°), plane (111)	Average crystallites size (nm)	
		d NiO	d CeO_2
$CeO_{2\,(c)}$	28.4	-	9
NiO*$_{(c)}$	-	>20	-
$CeAl_{0.5}Ni_{0.5}O_{y\,(c)}$	28.6	9	4
$CeAl_{0.5}Ni_1O_{y\,(c)}$	28.6	7	4
$CeAl_{0.5}Ni_2O_{y\,(c)}$	28.6	5	3

III.4.3. Raman studies of $CeNi_xAl_{0.5}O_y$ catalysts

Figure 65 represents the Raman analysis of ternary catalysts containing aluminum. The position of the main peak, attributed to ceria phase is at 452.9 cm^{-1} for $CeNi_{0.5}Al_{0.5}O_y$ and $CeNi_1Al_{0.5}O_y$ and at 456.5 cm^{-1} for $CeNi_2Al_{0.5}O_y$ (Table 52). The nano-crystallized ceria has been reported previously at 460 cm^{-1} so a deviation to lower wavenumbers appears on all catalysts. The peaks at this position for $CeNi_xAl_{0.5}O_y$ are wider than those of simple ceria. These two phenomena are in agreement with the solubility of nickel (and Al) in ceria, i.e. with the formation of a Ce-Ni-Al-O solid solution [357]. The values of these peak positions are slightly different from those of the binary and ternary Zr based catalysts.

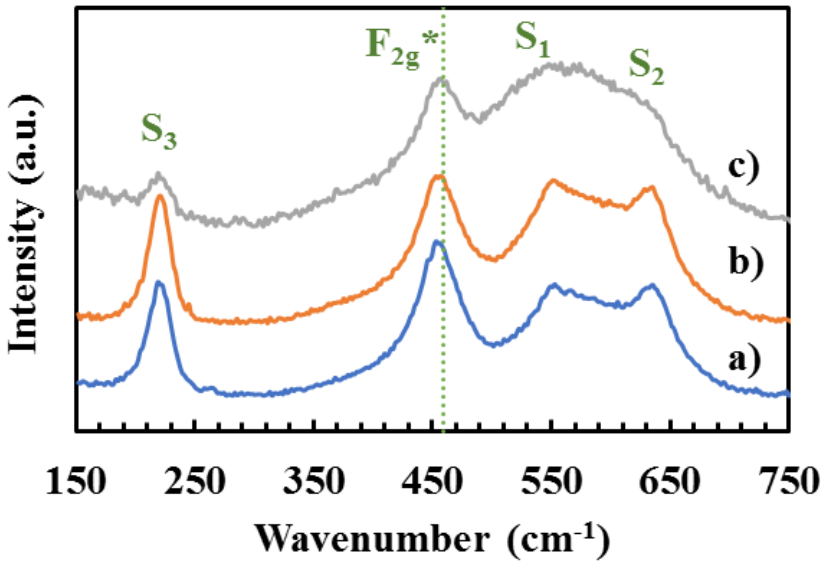

Figure 65 Raman spectra of $CeNi_xAl_{0.5}O_y$ calcined catalysts where x = 0.5 (a), 1 (b) and 2 (c).

However, in both cases a deviation from the original F_{2g} peak of single ceria is observed. This can indicate the presence of modifications in ceria structure and crystallinity in the presence of Al. Signal S_3 visible at about 230 cm^{-1} is characteristic of ceria phase nanostructures. Between 500 and 700 cm^{-1}, a very wide peak appears for $CeNi_2Al_{0.5}O_y$ catalyst. This wide peak in fact is the summation of signal S_1 and S_2 that can appear in the catalysts $CeNi_{0.5}Al_{0.5}O_y$ and $CeNi_1Al_{0.5}O_y$ catalysts. Signal S_1 at 552 cm^{-1} and S_2 at 635.5 cm^{-1} assigned to local vibrations of the various oxygen deficiency complexes. In fact, these vibrations increase in case of Al compounds compared to binary ones due to the incorporation of Ni^{2+} and Al^{3+} cations into CeO_2 phase which increases the number of defects. A peak at 570 cm^{-1} still exists and is precisely an indicative of the presence of oxygen vacancies in the ceria structure [358].

Table 52 Raman signal positions for $CeNi_xAl_{0.5}O_y$ (c) catalysts.

x	F_{2g} ceria peak position (cm^{-1})	S_1 (cm^{-1})	S_2 (cm^{-1})	S_3 (cm^{-1})
0.5	452.9	552.8	635.5	219
1	452.9	551.1	635.5	220
2	456.5	558.1	(shoulder)	219

III.4.4. TPR analysis for $CeNi_xAl_{0.5}O_y$ catalysts

Figure 66 represents the results of TPR analysis of $CeNi_xAl_{0.5}O_y$ calcined catalysts and 3 temperature reduction zones appear as reported in. The TPR spectra are complex but 2 peaks appear clearly at about 300 and 500 °C (Table 53). The first reduction zone could be assigned to easily reducible Ni species in solid solution Ce-Ni-O-Al and/or small NiO nanoparticles similarly to those of binary and Zr based catalysts mentioned before. However, this peak appears at a much higher temperature (314 – 333 °C) compared to binary compounds due to the insertion of Al into the structure. A shoulder appearing before the peak at 300 °C, indicates the presence of Ni in different environment. This could be related to the presence of Ce-Ni-O solid solution as well similar to the case of the binary catalysts. Therefore, it could be concluded that part of Ce-Ni-O solid solution is replaced by Ce-Ni-Al-O solid solution. At higher temperatures (407 – 500 °C) larger NiO nanoparticles are reduced. This peak becomes more intense and shifts to higher temperature when x increases. These reduction temperatures are much higher than those of binary catalysts and higher that TPR peak of simple NiO (390 °C), indicating that there are very strong interactions between Ni cations and other cations in the

solid. Then, the peak in the third zone at around 930 °C, could be assigned to the reduction of bulk Ce^{4+} into Ce^{3+} cations but could be also related to Al^{3+} cations, as it is obtained at much higher temperature than before.

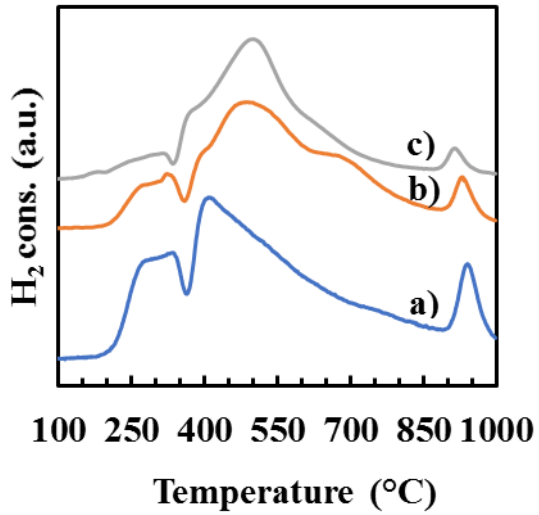

Figure 66 TPR profiles for $CeNi_xAl_{0.5}O_y$ calcined catalysts: a) x = 0.5, b) x = 1) and c) x = 2.

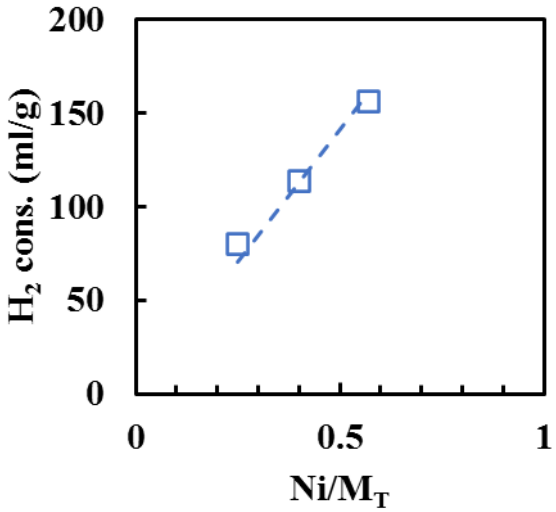

Figure 67 Hydrogen consumption in TPR as a function of Ni content of $CeNi_xAl_{0.5}O_y$ calcined catalysts, $Ni/M_T = x/(x+1)$.

Figure 67 proves that a linear relationship exists between the total hydrogen consumed and the Ni content in the catalyst. It is notable that in TPR analysis, H_2 molecules merely consume oxygen species present on the surface of the catalyst. As a result, the positions and the intensities of hydrogen consumption peaks can be linked to the oxygen mobility on the surface of these catalysts. As previously said, high Ni content leads to higher reduction temperature too. Finally, it can be deduced that a higher Ni content means higher reduction temperatures and thus lower oxygen mobility/oxidizing ability for a metal oxide [359].

Table 53 TPR reduction temperature zones for $CeNi_xAl_{0.5}O_{y\ (c)}$.

	Zone (peak position) (°C)		
Catalyst	**1st zone**	**2nd zone**	**3rd zone**
$CeNi_{0.5}Al_{0.5}O_y$ (c)	185-360 (333.5)	365-855 (407.4)	875-980 (940)
$CeNi_1Al_{0.5}O_y$ (c)	185-360 (322.6)	365-855 (481.8)	870-1000 (930)
$CeNi_2Al_{0.5}O_y$ (c)	185-360 (314)	365-855 (499.6)	885-1000 (913)

III.4.5. XPS analysis for $CeNi_xAl_{0.5}O_y$ calcined catalysts

In this part, the XPS analysis of the $CeNi_xAl_{0.5}O_y$ catalysts are presented, in particular the regions of Ce 3d, Al 2p, Ni $2p_{3/2}$ and O 1s. The results are represented in Figure 68. Al 2p that has a binding energy very close to Ni 3p is reported together to show the eventual perturbation (Figure 68-3). The Al^{3+} species are present at the surface as shown by the Al 2p peak found at around 74 eV. Analysis of Ni $2p_{3/2}$ spectra reveal the presence of 2 different environments for Ni^{2+}, either in solid solution (or strong interactions) or in NiO. The binding energies corresponding to each are represented in Table 54. The satellite peak for nickel appears at 861.2 – 861.6 eV and the other signal appears at around 855.5 – 855.7 eV for the different calcined Al catalysts.

Concerning O 1s, in Figure 68-4, two different environments exist verified by the presence of 2 peaks. The first peak exists at a position between 529.3 – 529.8 eV, corresponds to the presence of O^{2-} species, in agreement with the presence of an oxide and with the ceria phase observed in XRD. The second peak at 531.3 eV for catalysts with x = 0.5 and 1 and at 532 eV when x = 2 corresponds to the presence of oxygen species in connection with the presence of OH^- groups on the surface of the catalyst. The spectra of Ce 3d can be divided into 3 spin orbitals as mentioned before on binary and ternary Zr based compounds. These orbitals are denoted by (u, v), (u'', v'') and (u''', v''').

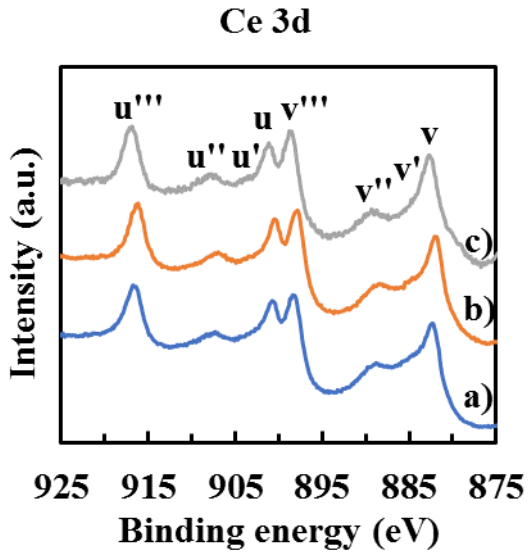

(1)

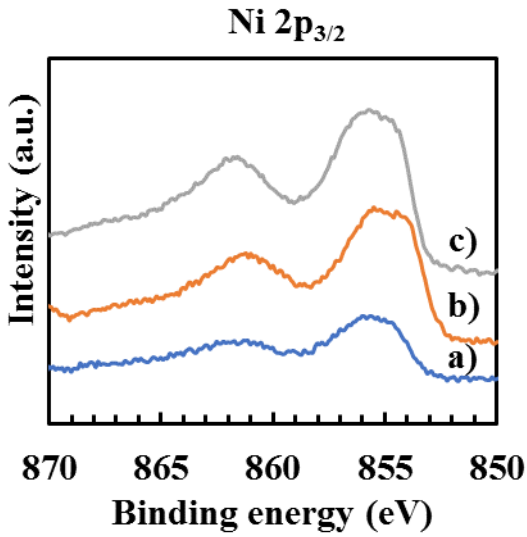

(2)

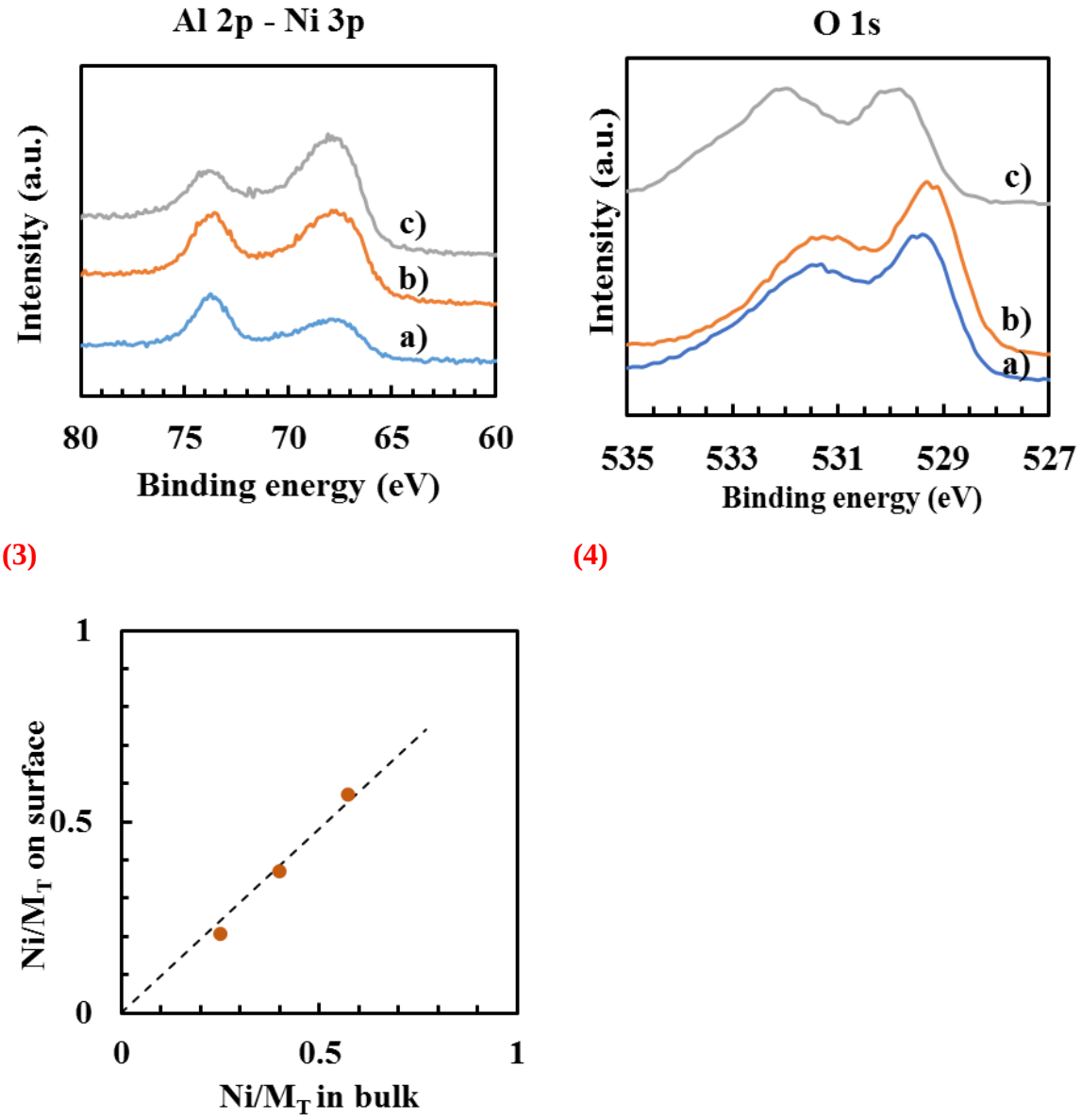

Figure 68 XPS spectra of a) $CeNi_{0.5}Al_{0.5}O_y$, b) $CeNi_1Al_{0.5}O_y$ and c) $CeNi_2Al_{0.5}O_y$ calcined catalysts. 1) Ce 3d, 2) Ni $2p_{3/2}$, 3) Al 2p and Ni 3p, 4) O 1s and 5) Ni/M_T in bulk versus Ni/M_T on surface.

Table 55 shows the values obtained from XPS for atomic percentage of species found in Ni $2p_{3/2}$, Ce 3d and O 1s. Therefore, XPS results show the presence of Ni^{2+} cations presenting strong interactions with other cations (Ce^{4+}, Ce^{3+}, Al^{3+}), together with the presence of O^{2-} species and hydroxyl groups at the surface [360]. The Ni /M_T ratio on the surface as a function of Ni /M_T in mass shown in Figure 68-5 shows that the obtained points follow the dotted line. This is an indication that the amount of Ni on the surface is very close to the amount of Ni in the bulk of the catalysts and thus a homogeneous distribution of Ni in the solid is obtained.

Table 54 Binding energies for the different XPS signals obtained for $CeNi_xAl_{0.5}O_{y\ (c)}$ catalysts.

	Binding energy (eV)				
Catalyst	**Ni $2p_{3/2}$**	**Ni $2p_{3/2}$ satellite**	**Al 2p**	**O 1s**	**Ce 3d**
$CeNi_{0.5}Al_{0.5}O_y$	855.6	861.2	73.8	529.4/ 531.3	916.7/ 900.7/ 898.4/ 882.3
$CeNi_1Al_{0.5}O_y$	855.5	861.6	73.8	529.3/ 531.3	916.1/ 900.4/ 897.8/ 882.0
$CeNi_2Al_{0.5}O_y$	855.7	861.5	74.1	529.8/ 532.0	916.8/ 901.1/ 898.7/ 882.6

Table 55 Quantification data for atomic percentage in $CeNi_xAl_{0.5}O_{y\ (c)}$ catalysts obtained from XPS.

	%at						
	Ni $2p_{3/2}$		Ce 3d		O 1s		
Catalyst	**Ni^0**	**Ni^{2+}**	**Ce^{4+}**	**Ce^{3+}**	**O^{2-}**	**OH**	**O'**
$CeNi_{0.5}Al_{0.5}O_y$	0	100	83	17	40	55	5
$CeNi_1Al_{0.5}O_y$	0	100	87	13	51	42	7
$CeNi_2Al_{0.5}O_y$	0	100	94	6	35	54	11

III.5. Characterizations of spent $CeNi_xO_y$ catalysts

The $CeNi_xO_y$ catalysts tested in OSRE at 50 °C for 31 hours with a starting temperature of 200 °C and after *in-situ* pretreatment in H_2 at a temperature of 250 °C are collected and analyzed by Raman and XPS.

III.5.1 Raman analysis for spent $CeNi_xO_y$ catalysts

With the spent binary calcined catalysts, broad peaks are observed, a high uncertainty is observed on the position of the F_{2g} ceria peak in particular when x = 0.5 and 2, while it is more visible when considering x = 1 and 5 (Figure 69). On these last catalysts, this peak is observed at lower values than those of the fresh catalysts. When x = 1, this peak deviates from 456.6 cm^{-1} to 450.5 cm^{-1} and when x = 5, the shift is observed clearly from 461.9 cm^{-1} to 452.3 cm^{-1} (Table 56). Therefore, it appears that globally the nano-crystallites and Ce-Ni solid solution seem to be maintained however with inducing more oxygen vacancies. Indeed, ceria presents the ability to easily and reversibly change between its Ce^{3+} and Ce^{4+} oxidation states and to accommodate oxygen vacancies in its fluorite-type crystal structure and thus leading to the broadness in S_1 and S_2 signals (due to oxygen vacancies), thus acting as an efficient oxygen buffer [361-365]. This ability for oxygen storage capacity allows to obtain this shift [366]. In the same direction, the presence and the availability of mobile active oxygen species play a fundamental

role in the ceria oxidation activity [367-369]. This effect has already been investigated on ceria compounds where it has been shown that the reduction and oxidation state of the doped material affect the intensity of the vibrational modes between 550 cm^{-1} and 570 cm^{-1} [370, 371].

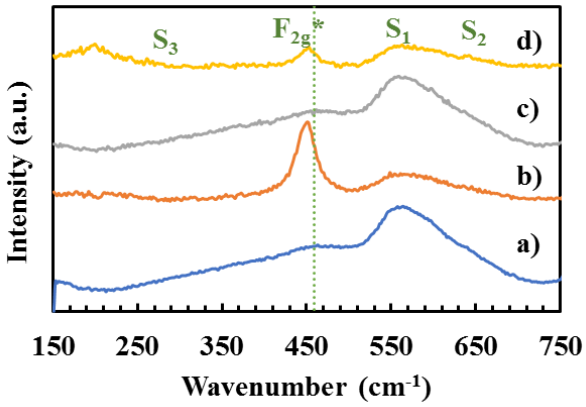

Figure 69 Raman spectra for $CeNi_xO_y$ calcined catalysts after 31 hours test with a pretreatment in H_2 at 250 °C: a) x = 0.5, b) x = 1, c) x = 2 and d) x = 5.

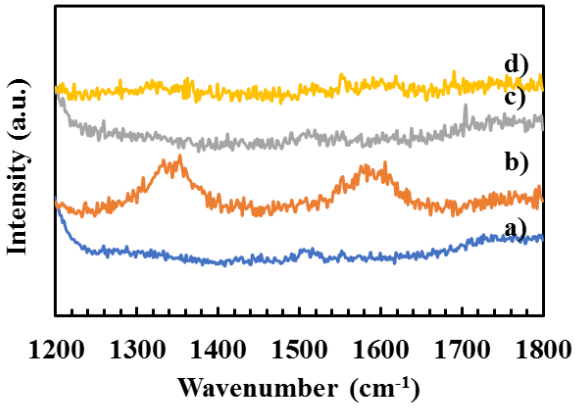

Figure 70 Raman spectra in the carbon region for $CeNi_xO_y$ calcined catalysts after 31 hours test with a pretreatment in H_2 at 250 °C: a) x = 0.5, b) x = 1, c) x = 2 and d) x = 5.

Figure 70 shows no evidence for carbon formation in all the binary catalysts after test except on $CeNi_1O_{y\,(c)}$ catalyst, for which graphitic carbon is evidenced by the presence of the D band (vibration of sp^3-hybridized carbon atom in the disordered carbonaceous species) and G band (stretching mode of sp^2-hybridized carbon atom in the ordered graphite), observed at 1352 cm^{-1} and at 1605 cm^{-1}, respectively [372, 373]. The obtained values are very close (in particular, when taking into account the uncertainty) to those previously obtained after ethanol steam reforming on $Ni_XMg_2AlO_Y$ nanocomposites (1349 cm^{-1} and 1592 cm^{-1}) [374]. The G band is observed at a higher frequency than in some studies (1580 cm-1), this could be explained by the fact that another D' band exists at 1620 cm^{-1} and caused by sufficient concentration of defects and thus merging with the G band [375-378]. It must be noted that the signal is weak, and to allow the observation of the peaks, the intensity (reported in arbitrary units) has been multiplied, as seen by the signal to noise. Knowing that no evidence of carbon was detected by applying the mass variation method to calculate carbon formation, only scarce carbon formation is observed and as shown here by Raman it corresponds to graphitic type carbon materials [374, 379].

Table 56 Raman signal positions for $CeNi_xO_y$ calcined catalysts after test of 31 hours with a pretreatment in H_2 at 250 °C: a) x = 0.5, b) x = 1, c) x = 2 and d) x = 5.

X	F_{2g} ceria peak position (cm^{-1})	S_1 (cm^{-1})	S_2 (cm^{-1})	S_3 (cm^{-1})	Carbon (cm^{-1})
0.5	463	564	636	199.6	-
1	450.5	561	-	-	1352, 1605
2	464.8	559	-	-	-
5	452.3	562	-	-	-

III.5.2. XPS on spent $CeNi_xO_y$ catalysts after 31 hours in OSRE

The same $CeNi_xO_y$ discussed before are analyzed by XPS to investigate the changes at the level of the catalyst before and after the process. The corresponding data obtained are presented in Figure 71 exhibiting the binding energies of the different elemental compositions. The exact positions of the binding energies, as well the atomic percentage of each element after test are reported in Table 57 and 58. As carbon can be formed during the test, Ce^{4+} at 917 eV is taken as a reference for XPS analysis after test [343].

Globally, the main emission peak of Ni $2p_{3/2}$ is observed on the compounds after test at higher binding energies than those of fresh catalysts, meaning that the Ni^{2+} cations are well present after test and these cations that are present after test are those in strong interaction with other cations. The doublet peak of Ni $2p_{3/2}$ originally present in the fresh catalyst becomes undifferentiated at low values of x (x = 0.5 and 1). This peak position related to Ni^{2+} species is close (855.2 eV - 855.4 eV) on $CeNi_{0.5}O_{y\ (c)}$, and varies from 855.3 eV to 856.7 eV on $CeNi_1O_{y\ (c)}$. Similarly, the peaks appearing at BE of 855.3/853.6 eV on $CeNi_2O_{y\ (c)}$ and $CeNi_5O_{y\ (c)}$ before test appear at BE of 856/854.2 eV and 856.3/853.1 eV after test. When x= 5, low contributions of Ni^0 could be evidenced at round 852.6 appearing as a small shoulder due to the main Ni $2p_{3/2}$ peak. The characteristic peaks corresponding to cerium cations, mainly Ce^{4+}, are still well observed after test. For O 1s, globally, the peak appearing at BE around 529.5 eV is related to O^{2-} species present in the metallic oxides, the BE around 531 eV corresponds to oxygen bonded as hydroxides and could be also related to NiO [380], while higher values of BE can be related to adsorbed water or organic compounds [158]. The BE vary from 529.4/531.3 to 529.9/532.6 eV on $CeNi_1O_{y\ (c)}$, from 529.4/531.1 eV to 530.1/531.4 eV on $CeNi_2O_{y\ (c)}$, and from 529.3/531 eV to 530/532.3 eV on $CeNi_2O_{y\ (c)}$, when comparing before and after test, respectively, showing a higher presence of hydroxyl groups and adsorbed water and/or organic compounds after test. This result can be explained by the reactants used (EtOH-H_2O) and the

stopping of the reaction under these reactants. A significant change in intensities and broadness is observed on $CeNi_{0.5}O_{y\ (c)}$, for which the values of BE vary from 529.5/531.5 eV to 532.4/ 533.3 eV after test. At low nickel over cerium molar ratio, x = 0.5, no changes in C 1s spectra can be revealed after test and this signal being correlated to adventitious carbon. However, starting from x = 1, a small shoulder starts to appear in the spectra and can be differentiated into a peak at 286.1 eV on $CeNi_2O_{y\ (c)}$. This corresponds to graphitic carbon and has been reported previously on similar type of materials [374]. This is in agreement with the Raman analysis previously shown (Figure 70).

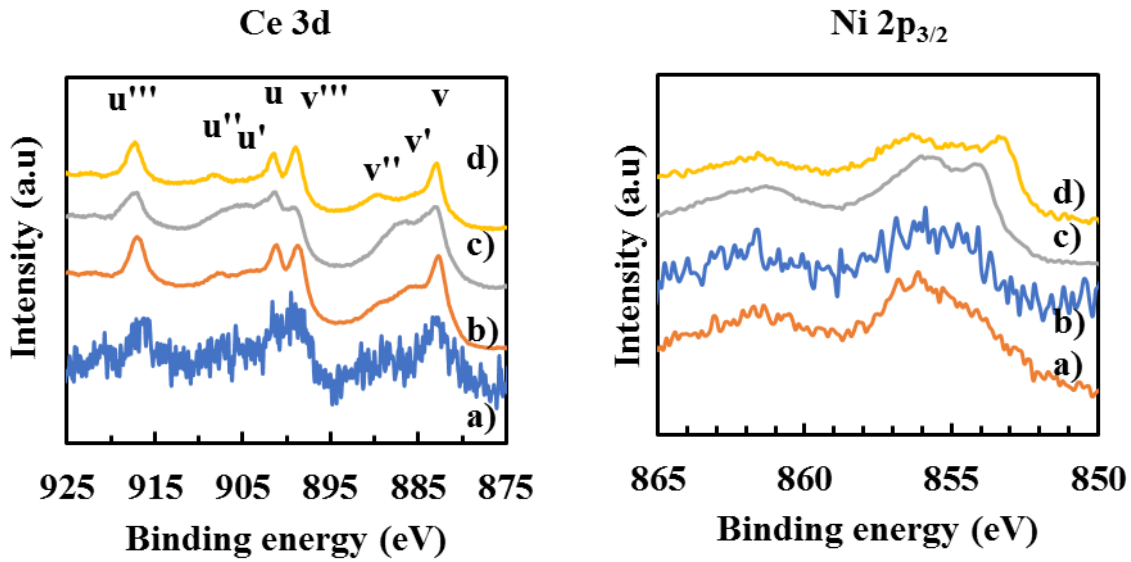

(1) **(2)**

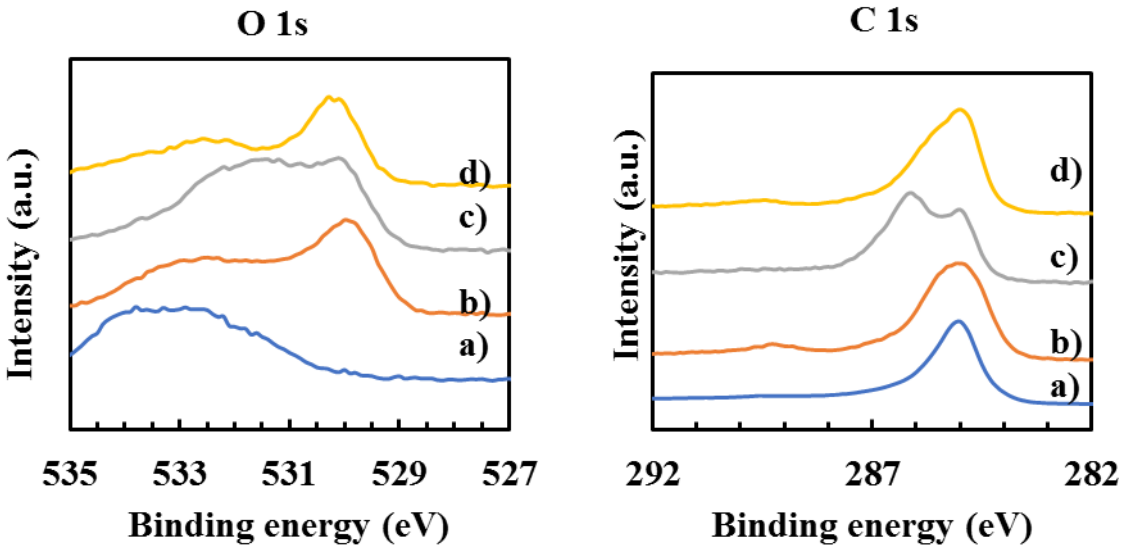

(3) **(4)**

Figure 71 XPS spectra for $CeNi_xO_y$ calcined catalysts after test of 31 hours with a pretreatment in H_2 at 250 °C: a) x = 0.5, b) x = 1, c) x = 2 and d) x = 5.

Table 57 Binding energies for the different XPS signals obtained for $CeNi_xO_{y\ (c)}$ catalysts after test (Fig. 73).

	Binding energy (eV)				
Catalyst	**Ni $2p_{3/2}$**	**Ni $2p_{3/2}$ satellite**	**O 1s**	**Ce 3d**	**C 1s**
$CeNi_{0.5}O_{y\ (c)}$	855.4	861.1	533.3/532.4	917/901.1/899/882.3	284.5
$CeNi_1O_{y\ (c)}$	856.7	861.3	532.65/ 529.9	917/901.1/898.8/882.7	284.9
$CeNi_2O_{y\ (c)}$	856/ 854.2	861.3	531.4/ 530.1	917/901.4/899/883.1	286.1/285
$CeNi_5O_{y\ (c)}$	856.3/ 853.1	861.3	532.3/530	917/901.2/898.7/882.7	284.7

The additional features supported by XPS allows to reveal the atomic changes happening at the surface of the catalyst. These are investigated in Table 58 that summarizes the quantification data obtained on the spent catalysts of $CeNi_xO_{y\ (c)}$. Starting with cerium, the elemental distribution between Ce^{4+} and Ce^{3+} changes clearly after OSRE for $CeNi_1O_{y\ (c)}$ and $CeNi_5O_{y\ (c)}$. The distribution of cerium cations at the surface of $CeNi_1O_{y\ (c)}$ becomes 75 % Ce^{4+} and 25 % Ce^{3+} (before test: 86 % Ce^{4+} and 14 % Ce^{3+}) evidencing a higher amount of Ce^{3+} cations, and so a slightly more reduced compound after test. However, on all compounds the Ce^{4+} cations remain the main species in presence, after test. Similarly, with nickel, although all contributions correspond to Ni^{2+} cations and that some evidence of Ni^0 is reported only when x = 5 (however cannot be calculated), the environment of these nickel species changes after test proved by the shifting of binding energies. As a matter of fact, some XPS signals appearing on fresh catalyst

are no more visible on the spent catalysts. The previous changes in binding energies of O 1s signals before and after test can be also quantified. Starting with $CeNi_{0.5}O_{y\ (c)}$, the distribution of oxygen becomes distributed among 11 % OH species and 89 % O' species that could be related to organic species deposited on the catalyst after test. These O' species are mostly evident on this catalyst with low Ni content. However, it is around 8 % on $CeNi_1O_{y\ (c)}$ and $CeNi_2O_{y\ (c)}$ after test and 4 % on $CeNi_5O_{y\ (c)}$ after test. The amount of O^{2-} species decreases with respect to OH species after test. These distributions become as follows: 33% O^{2-} and 59% OH on $CeNi_1O_{y\ (c)}$ after test (previously 49 % O^{2-} and 50 % OH), 12 % O^{2-} and 80 % OH on $CeNi_2O_{y\ (c)}$ after test (previously 61 % O^{2-} and 39 % OH) and 38 % O^{2-} and 57 % OH on $CeNi_2O_{y\ (c)}$ after test (previously 50 % O^{2-} and 50 % OH).

Table 58 Quantification data from XPS for atomic percentage in $CeNi_xO_y$ calcined catalysts after test (Fig. 73).

	% at						
	Ni $2p_{3/2}$		Ce 3d		O 1s		
Catalyst	**Ni^0**	**Ni^{2+}**	**Ce^{4+}**	**Ce^{3+}**	**O^{2-}**	**OH**	**O'**
$CeNi_{0.5}O_{y\ (c)}$	0	100	88	12	0	11	89
$CeNi_1O_{y\ (c)}$	0	100	75	25	33	59	8
$CeNi_2O_{y\ (c)}$	0	100	73	27	12	80	8
$CeNi_5O_{y\ (c)}$	0	100	76	24	38	57	4

III.6. Characterizations of $CeNi_xZr_{0.5}O_y$ calcined spent catalysts

III.6.1 $CeNi_xZr_{0.5}O_y$ calcined catalysts after test with pretreatment of 250 °C

III.6.1.1 After 31 hours in OSRE

III.6.1.1.1. Raman analysis

Raman spectra for $CeNi_xZr_{0.5}O_y$ calcined catalysts after test (50 °C) with a pretreatment in H_2 at 250 °C for 31 hours are presented in Figure 72 and Figure 73. Table 59 summarizes the positions of each Raman signal obtained. The F_{2g} ceria peak mainly present at 460 cm^{-1} becomes at a position of around 477 cm^{-1} in $CeNi_{0.5}Zr_{0.5}O_{y\ (c)}$. This peak is observed at 468 cm^{-1}, 477 and 470 cm^{-1} for the catalysts $CeNi_1Zr_{0.5}O_{y\ (c)}$, $CeNi_2Zr_{0.5}O_{y\ (c)}$ and $CeNi_5Zr_{0.5}O_{y\ (c)}$, respectively (which were previously present at 462, 462 and 483 cm^{-1} respectively). The F_{2g} peak shift to higher energy (482.5 cm^{-1}), has been attributed to the formation of ceria-zirconia solid solution [372, 381]. Therefore, all these results show the well maintain of the solid solution after test. As a

consequence of these changes in the lattice and due to the defects created (oxygen vacancies) and loss of electrons, the vibrational modes occurring between 500 and 650 cm^{-1} (S_1) becomes more intense with respect to S_2 signal and F_{2g} ceria peak. Before test, S_1 and S_2 peak couldn't be differentiated, appearing as broad peaks occurring between 500 and 730 cm^{-1} for all these catalysts. However, after test, a peak becomes well positioned and visible at 564, 561, 564 and 564 cm^{-1} for $CeNi_{0.5}Zr_{0.5}O_{y\ (c)}$, $CeNi_1Zr_{0.5}O_{y\ (c)}$, $CeNi_2Zr_{0.5}O_{y\ (c)}$ and $CeNi_5Zr_{0.5}O_{y\ (c)}$ respectively. Vibrations situated between 400 and 450 cm^{-1} are reported previously to be responsible of Ce-O longitudinal stretching of atoms in the outermost layers and the latter to a transversal Ce−O stretching vibration [382, 383]. The oxygen vacancies and defects in the structure of ceria increase clearly after test as a proof of the continuous redox processes occurring in OSRE reaction leading to the good performance and stability over time. Two bands corresponding to carbon (D and G bands) can be observed on the catalysts with x values equal to 1 and 2. However with $CeNi_5Zr_{0.5}O_y$ and $CeNi_{0.5}Zr_{0.5}O_{y\ (c)}$, no signals could be observed at all, indicating that carbon formation is totally eliminated using these compounds. Nevertheless, even if very low signals of C can be observed on some catalysts, all catalysts have good stability over time. This type of carbon could be related to graphitic carbon as previously mentioned.

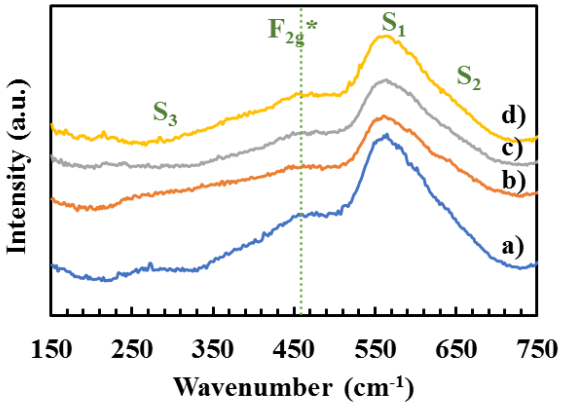

Figure 72 Raman spectra for $CeNi_xZr_{0.5}O_y$ calcined catalysts after 31 hours test with a pretreatment in H_2 at 250 °C: a) x = 0.5, b) x = 1, c) x = 2 and d) x = 5.

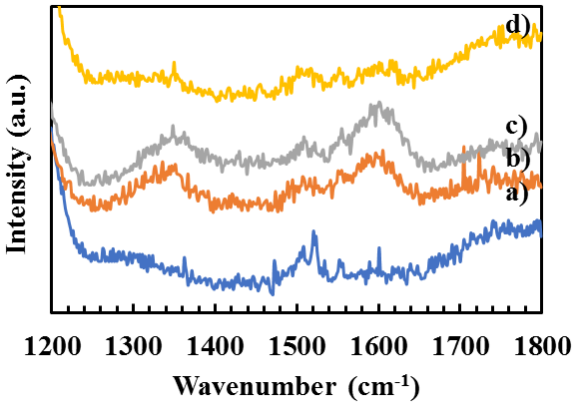

Figure 73 Raman spectra in the carbon region for $CeNi_xZr_{0.5}O_y$ calcined catalysts after 31 hours test with a pretreatment in H_2 at 250 °C: a) x = 0.5, b) x = 1, c) x = 2 and d) x = 5.

Table 59 Raman signal positions for $CeNi_xZr_{0.5}O_y$ calcined catalysts after test with a pretreatment in H_2 at 250 °C: a) x = 0.5, b) x = 1, c) x = 2 and d) x = 5.

X	F_{2g} ceria peak position (cm^{-1})	S_1 (cm^{-1})	Carbon (cm^{-1})
0.5	477.4	564.5	-
1	468.4	561	1335, 1605
2	477.4	564.5	1348, 1600
5	470.2	564.5	-

III.6.1.1.2. XPS analysis

On the $CeNi_xZr_{0.5}O_{Y\ (c)}$ compound after pretreatment in H_2 at 250 °C followed by OSRE ($EtOH/H_2O/O_2/N_2$ = 1:3:1.7:N_2) at 50 °C, XPS (Figure 74) reveals the main presence of Ni^{2+} cations on the surface. Quantification data obtained from XPS for atomic percentage in these $CeNi_xZr_{0.5}O_y$ calcined catalysts after are presented in table 61. A main Ni $2p_{3/2}$ peak at about 856.0 eV is observed with a shoulder at about 854 eV due to the different environment surrounded by nickel, with the binding energy of the satellite peak observed at around 861 eV. Those main emission peaks appear around 855 – 856 and 853 – 854 eV. The values of these binding energies remain very close before and after test for all these catalysts. These results demonstrate that the strong interactions between Ni^{2+} cations with other cations are well preserved after test at 50 °C after 31 hours (Table 60). Ce 3d spectra, show the main presence of Ce^{4+} cations (to note that Ce has been taken as a reference to analyze C). An increase of Ce^{4+} percentages with respect to Ce^{3+} percentages is followed after test for the $CeNi_{0.5}Zr_{0.5}O_{Y\ (c)}$, $CeNi_1Zr_{0.5}O_{Y\ (c)}$ and $CeNi_2Zr_{0.5}O_{Y\ (c)}$ catalysts showing that more cerium is being oxidized during OSRE in these samples. However, with $CeNi_5Zr_{0.5}O_{Y\ (c)}$, the catalyst that showed the best catalytic performance under these conditions in OSRE, the percentage of Ce^{4+} decreases from 82 % to 77 % and that of Ce^{3+} changes from 18 % to 23 %. As a reason, the u' signal is more visible in the XPS spectra of spent catalysts than those of fresh ones. It can be seen that the distribution of oxygen species present on the surface of the catalysts change after test. Before test, the O 1s core level presents two major oxygen species at around 529 and 532 eV with the presence of O^{2-} species and oxygen species in hydroxyl groups (OH^-). After test, a third group of oxygen species appears represented as O' which could be due to organic compound or water deposit on the surface of the catalyst after test. These species are more evident at higher Ni/Ce ratios when x = 1, x = 2 and x = 5. With x = 0.5, these O' species are not present even after test. The only detected species are O^{2-} and OH of 53 % and 47 %

respectively being reported as one peak at 530 eV in inverse to what have been reported before test (47 % O^{2-} and 53 % OH reported in the signals at 531.2/529.6 eV). However, with x = 5, the spectra of oxygen changes clearly after test from signals obtained at 521/529.4 to signals with much higher binding energies (533.5/532.2 eV). This is due to the change in oxygen environments after test leading to the dominance of OH species (45 %) with respect to O^{2-} (12 %) species (which were almost in equivalent percentages on fresh catalysts). Finally, the big shoulder appearing at around 533 eV is due to the O' species deposited at the surface of the catalyst and clearly more evident with large nickel contents in the catalyst. C1s spectra reveals a small shoulder appearing at higher BE similar to what has been reported in the previous results due to C–O bonding which could have increased due to deposits of ethanol on the surface of catalyst however still in agreement with the absence of carbon measured after test by mass variation method and dealing with the fact that these peaks are only related to adventitious carbon [345]. Regarding Zr 3d core levels, (184.7 and 182.3 eV) r are almost similar to those of fresh catalysts (184.4/182.2 eV) indicating that zirconium cations (Zr^{4+}) are maintaining stable after test.

In fact, it has been shown on similar formulation of catalysts that the combination of oxygen with nickel, cerium, and zirconium provided a bridge among them which prevented sintering and a reduction in grain size and therefore allowed to establish great stability of catalysts and catalytic activity over time [384]. This feature allows these catalysts to reserve good conversion of ethanol of 100 % over time. The Ce and Ni cations change in percentages on the surface of the catalyst due to the redox processes occurring between them. Zr has a role according to Di Monte [385], when ZrO_2 was added to CeO_2, the oxygen vacancies were increased, and more reduction of Ce-Zr composite was also observed. Moreover, Ni improved the catalytic activity [386, 387]. Furthermore, the oxygen storage capacity of CeO_2 on its surface was limited, whereas for Ce-Ni-Zr mixed oxides, there was participation of bulk oxygen in the storage process and thus allowing these redox processes to maintain and as an overall gave good catalytic results [388].

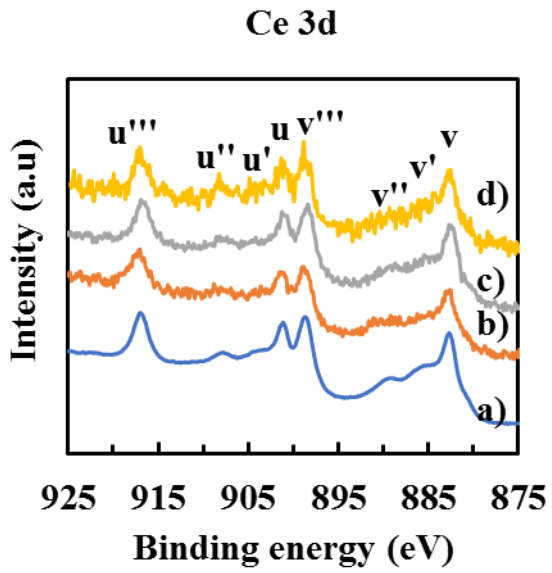
Ce 3d
u'''
u''
u'
u
v'''
v''
v'
v
d)
c)
b)
a)
Intensity (a.u)
925
915
905
895
885
875
Binding energy (eV)

(1)

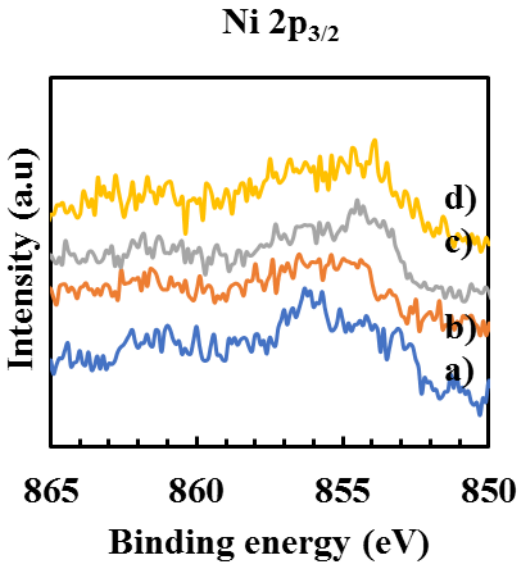
Ni 2p3/2
d)
c)
b)
a)
Intensity (a.u)
865
860
855
850
Binding energy (eV)

(2)

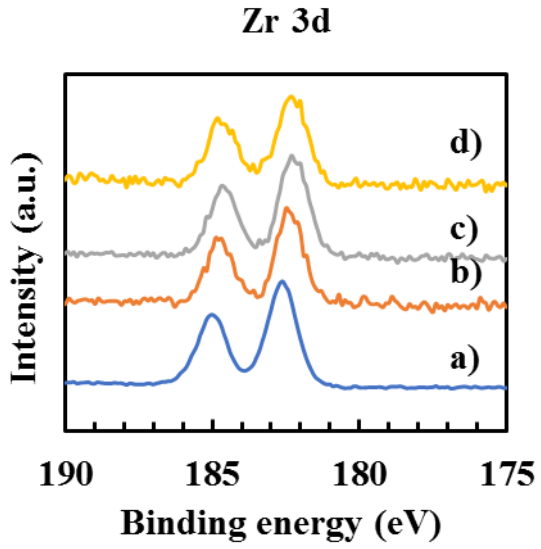
Zr 3d
d)
c)
b)
a)
Intensity (a.u.)
190
185
180
175
Binding energy (eV)

(3)

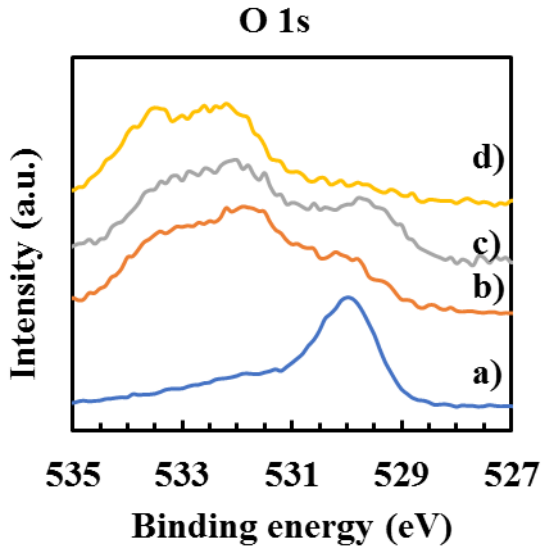
O 1s
d)
c)
b)
a)
Intensity (a.u.)
535
533
531
529
527
Binding energy (eV)

(4)

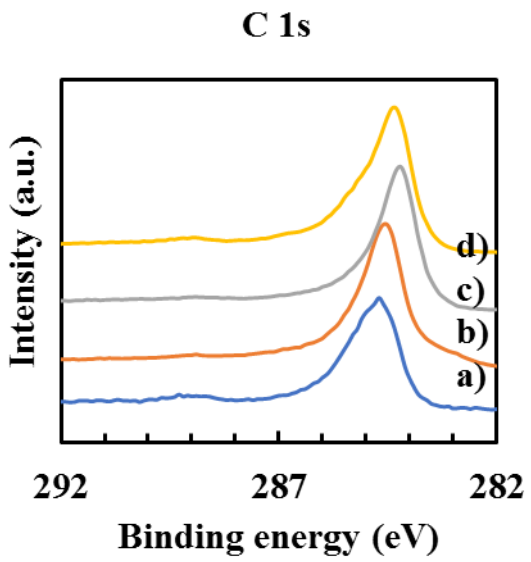

(5)

Figure 74 XPS spectra for $CeNi_xZr_{0.5}O_y$ calcined catalysts after test for 31 hours with a pretreatment in H_2 at 250 °C: a) x = 0.5, b) x = 1, c) x = 2 and d) x = 5. 1) Ce 3d, 2) Ni $2p_{3/2}$, 3) Zr 3d, 4) O 1s and 5) C 1s.

Table 60 Binding energies for the different XPS signals obtained for $CeNi_xZr_{0.5}O_y$ calcined catalysts after test for 31 hours with a pretreatment in H_2 at 250 °C: a) x = 0.5, b) x = 1, c) x = 2 and d) x = 5.

	Binding energy (eV)					
Catalyst	**Ni $2p_{3/2}$**	**Ni $2p_{3/2}$ satellite**	**Zr 3d**	**O 1s**	**Ce 3d**	**C 1s**
$CeNi_{0.5}Zr_{0.5}O_y$ (c)	856/853.9	861.1	185/182.6	530	917/901.2/898.7/882.7	284.7
$CeNi_1Zr_{0.5}O_y$ (c)	855.7/853.46	860.7	184.7/182.3	531.7/530	917/901.1/898.6/882.3	284.2
$CeNi_2Zr_{0.5}O_y$ (c)	855.5/853.7	861	184.7/182.3	532/529.6	917/901.3/898.4/882.5	284.2
$CeNi_5Zr_{0.5}O_y$ (c)	856.1/853.2	861	184.8/182.3	533.5/532.2	917/901.3/898.8/882.5	284.3

Table 61 Quantification data obtained from XPS for atomic percentage in $CeNi_xZr_{0.5}O_y$ calcined catalysts after test for 31 hours with a pretreatment in H_2 at 250 °C.

	% at						
	Ni $2p_{3/2}$		Ce 3d		O 1s		
Catalyst	**Ni^0**	**Ni^{2+}**	**Ce^{4+}**	**Ce^{3+}**	**O^{2-}**	**OH**	**O'**
$CeNi_{0.5}Zr_{0.5}O_y$ (c)	0	100	84	16	53	47	0
$CeNi_1Zr_{0.5}O_y$ (c)	0	100	78	22	19	47	32
$CeNi_2Zr_{0.5}O_y$ (c)	0	100	81	19	26	44	28
$CeNi_5Zr_{0.5}O_y$ (c)	0	100	77	23	12	45	43

III.6.1.2 After 80 hours in OSRE

III.6.1.2.1. Raman analysis

The spectra obtained after 80 hours OSRE with $CeNi_5Zr_{0.5}O_{y\ (c)}$ catalysts after test of 80 hours with a pretreatment in H_2 at 250 °C after 80 hours is represented in Figure 75. The signal corresponding to F_{2g} ceria peak is mainly hidden by the S_1 signal. Therefore, it appears as a very broad single peak at 542 cm^{-1}. After 80 hours of test, carbon formation can be evidenced by Raman, (even if not evidenced by mass variation method), due to the two peaks appearing at 1306 and 1601 cm^{-1} (Table 62). The D band at 1306 cm^{-1} due to disordered carbon is much higher in intensity compared to the G band. The D band is sensitive to disorders is the fact why it appears at lower wavenumbers than carbon normally at 1330 cm^{-1}. The D band has several activation phonons going from 1240 to 1390 cm^{-1} (hence a spectral range of 150 cm^{-1}) [389]. It can be seen that with increasing the duration of the test from 31 hours to 80 hours, a small evolution of carbon can be detected since after 31 hours in OSRE no carbon signal was detected by Raman. Moreover, The F_{2g} ceria peak was still visible in the test after 31 hours (at 470.2 cm^{-1}) unlike that of 80 hours indicating that with time even more oxygen vacancies and more defects in the structure of the catalyst are being formed. CeO_2 species are much easier to reduce than other species allowing to see great changes in terms of intensities of peaks and in turn leading to the changes in percentages between Ce^{3+} and Ce^{4+} species observed by XPS [390, 391, 392].

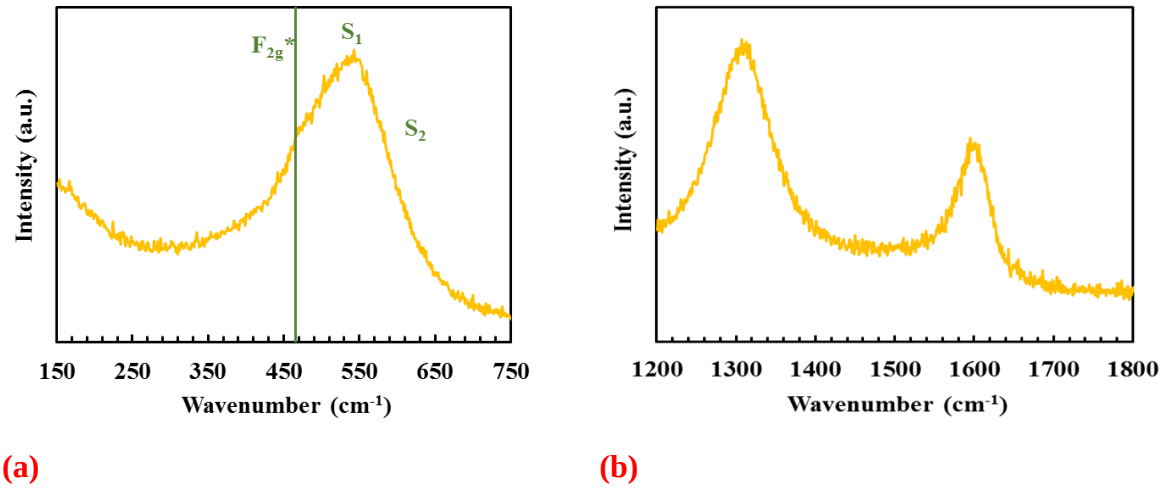

Figure 75 Raman spectra for $CeNi_5Zr_{0.5}O_{y\ (c)}$ catalysts after test of 80 hours with a pretreatment in H_2 at 250 °C in a) ceria region and b) carbon region.

Table 62 Raman signal positions for $CeNi_5Zr_{0.5}O_y$ fresh calcined and spent catalysts after test of 80 hours with a pretreatment in H_2 at 250 °C.

F_{2g} ceria peak position (cm^{-1})		**S_1 +S_2(cm^{-1})**		**Carbon (cm^{-1})**
fresh	**spent**	**fresh**	**spent**	**spent**
483.4	unresolved	500-730	542	1306, 1601

III.6.1.2.1. XPS analysis

$CeNi_5Zr_{0.5}O_y$ calcined catalysts after test for 80 hours with a pretreatment in H_2 at 250 °C are analyzed by XPS (Figure 76). Ce 3d spectra show that the presence of Ce^{4+} and Ce^{3+} cations are well maintained after test. However, Ce^{4+} cations are reduced into Ce^{3+} and thus the percentage of Ce^{4+} decreases from 8 2% to 64%. The positions of Zr 3d BE do not change (Table 63). The Ni $2p_{3/2}$ signals are still present after 80 hours however the peaks are broader than those of fresh catalysts. slight deviations of the main BE are observed from 855.4/853.6 eV to 855.7/853.1 eV. 13 % of Ni species corresponds to Ni^0 and 87 % are Ni^{2+} (Table 64). Concerning oxygen, a broad signal at 530.9 eV can be observed related to O^{2-} and OH species which are well separated (531/529.4 eV respectively) for each of these oxygen species on fresh compound. Moreover, these oxygen species are quantified as 42 % O^{2-} and 53 % OH. As the catalyst achieves more time on stream (from 31 hours to 80 hours in OSRE), the positions of Ni $2p_{3/2}$, Ce 3d and Zr 3d signals almost do not change however that of oxygen appears as a single peak after 80 hours. Even, if the signals remain at same position the quantification of these species vary with time in OSRE test. After 31 hours in OSRE, no metallic nickel is observed, unlike after 80 hours 13 % of Ni^0 is found (with 87 % of Ni^{2+}). The distribution of Ce^{4+} and Ce^{3+} species changes between 77 % and 23 % respectively, after 31 hours to become 64 % and 36 % after 80 h, respectively (thus the quantity of Ce^{3+} species increase after time on stream). Therefore, the solid becomes more reduced under stream even with the presence of a large amount of hydroxyl groups at the surface.

The big variation in oxygen analysis goes to the fact that the oxygen storage capacity and redox property of the CeO_2-ZrO_2 support greatly influenced the reaction intermediates by tuning the reaction pathway in addition to the fact of formation of solid solution [393, 394]. It was reported by Ocampo et al. that the incorporation of ZrO_2 increases the oxygen mobility and promotes the formation of vacancies [395]. It was reported by Iglesias et al. that the oxygen vacancy rate and utilization rate over the Ni/CeO_2-ZrO_2 catalyst were higher than those over the binary Ni/CeO_2

catalysts [396]. They proposed that the promoting effect of the incorporated Zr on the catalytic properties was ascribed to higher oxygen mobility.

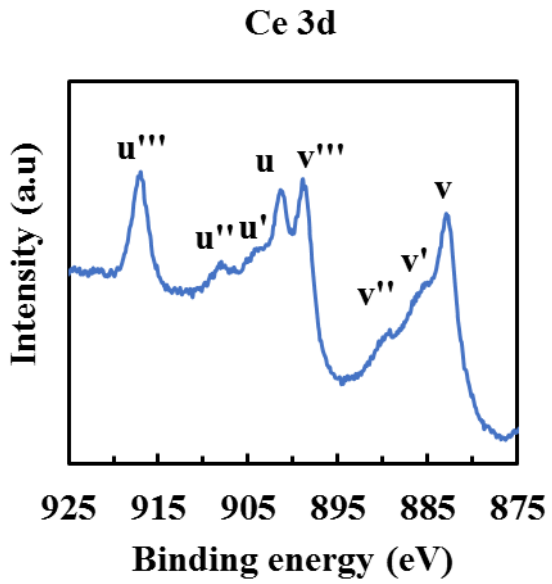

(1)

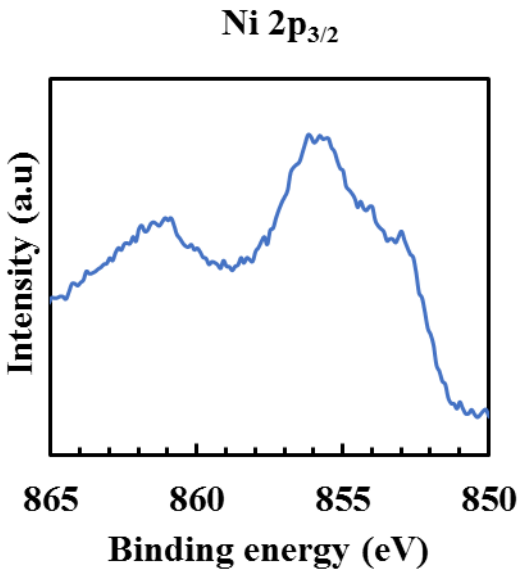

(2)

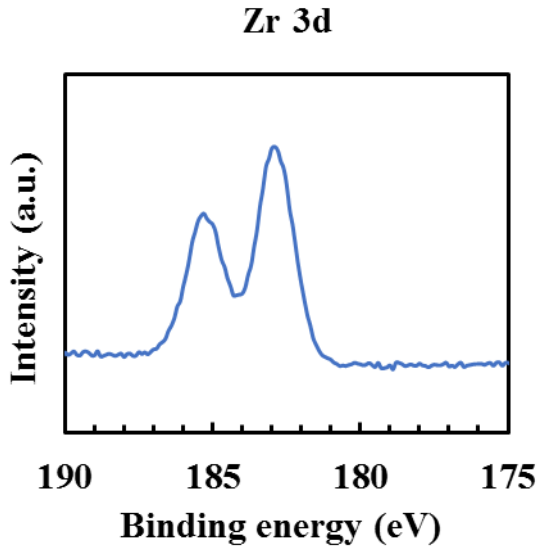

(3)

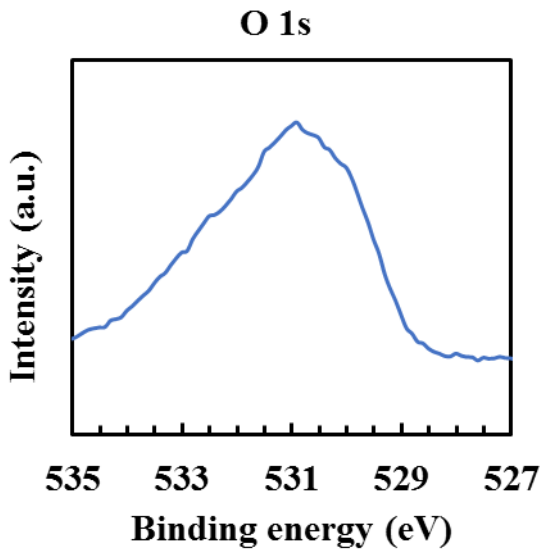

(4)

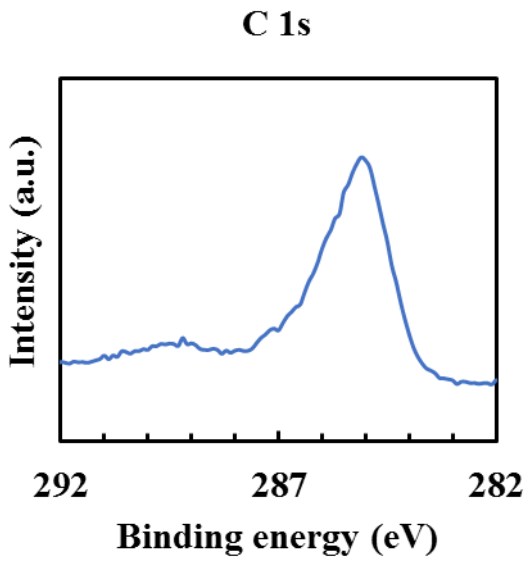

Figure 76 XPS spectra for $CeNi_5Zr_{0.5}O_y$ calcined catalyst after test for 80 hours with a pretreatment in H_2 at 250 °C. 1) Ce 3d, 2) Ni $2p_{3/2}$, 3) Zr 3d, 4) O 1s and 5) C 1s.

Table 63 Binding energies for the different XPS signals obtained for $CeNi_5Zr_{0.5}O_y$ calcined catalyst after test for 80 hours with a pretreatment in H_2 at 250 °C.

	Binding energy (eV)					
Catalyst	**Ni $2p_{3/2}$**	**Ni $2p_{3/2}$ satellite**	**Zr 3d**	**O 1s**	**Ce 3d**	**C 1s**
$CeNi_5Zr_{0.5}O_y$ (c)	855.7/853.1	861.3	185.3/182.9	530.9	917/901.4/899/882.9	285.1

Table 64 Quantification data obtained from XPS for atomic percentage in $CeNi_5Zr_{0.5}O_y$ calcined catalyst after test for 80 hours with a pretreatment in H_2 at 250 °C.

	% at						
	Ni $2p_{3/2}$		Ce 3d		O 1s		
Catalyst	**Ni^0**	**Ni^{2+}**	**Ce^{4+}**	**Ce^{3+}**	**O^{2-}**	**OH**	**O'**
$CeNi_5Zr_{0.5}O_y$ (c)	13	87	64	36	42	53	5

III.6.2 $CeNi_xZr_{0.5}O_y$ calcined catalysts after test with pretreatment of 200 °C

III.6.2.1. Raman analysis

The Raman spectra obtained for the different $CeNi_xZr_{0.5}O_y$ calcined catalysts after test with a pretreatment in H_2 at 200 °C after 31 hours are presented in Figure 77 (ceria region) and Figure 78 (carbon region) with the positions of these signals presented in Table 65. The signal of the main ceria F_{2g} peak is low, mainly due to the high intensity of the S_1 signal, and so the position of the position of the F_{2g} peak presents a high uncertainty, however, it seems to change with

respect to the position of the peak on the fresh catalysts. Clearly, the ceria F_{2g} peak becomes broader after test in all the cases (x = 0.5, 1, 2 and 5). All the obtained results indicate that oxygen vacancies have been formed in addition to those vacancies present after the preparation of the catalyst. With a low nickel content (x = 0.5), this peak is positioned at 473 cm^{-1} a much higher value than that on the fresh catalyst (460.1 cm^{-1}). With $CeNi_5Zr_{0.5}O_{y\ (c)}$, the F_{2g} ceria peak shifts greatly to lower positions from 483.4 cm^{-1} (on fresh catalyst) to 461.3 cm^{-1} (spent catalyst). For x = 1 and x = 2, this ceria F_{2g} peak do not vary (peak at 462.2 cm^{-1} and 464.8 cm^{-1}, respectively). Signals S_1 and S_2 increase in intensity and become amplified compared to the F_{2g} ceria peak, due to the redox capacity of the doped material that affect the intensity of the vibrational modes between 550 cm^{-1} and 570 cm^{-1} [370, 371]. Concerning carbon, it can be seen that no signal is observed in the carbon zone when the value of x is of 0.5 and 1. At higher values of x, 2 and 5, only a small signal (high noise/signal ratio) at around 1340 cm^{-1} and 1600 cm^{-1} can be observed corresponding to the D band and G band signals of C. This could be related to filamentous carbon that could not be detected by mass variation method because it is produced in a very low amount. These Raman results obtained after test with *in-situ* pretreatment of the solid at 200 °C in H_2 do not only vary from those obtained on fresh catalysts, they vary also compared to results obtained with temperature of pretreatment in H_2. The F_{2g} ceria peak previously present at 477.4 cm^{-1} for $CeNi_{0.5}Zr_{0.5}O_{y\ (c)}$, 468.4 cm^{-1} for $CeNi_1Zr_{0.5}O_{y\ (c)}$, 477.4 cm^{-1} for $CeNi_2Zr_{0.5}O_{y\ (c)}$ and 470.2 cm^{-1} for $CeNi_5Zr_{0.5}O_{y\ (c)}$ when the pretreatment in hydrogen was of 250 °C is now shifted to 473 cm^{-1}, 462.2 cm^{-1}, 464.8 cm^{-1} and 461.3 cm^{-1}, respectively after test with pretreatment in hydrogen at 200 °C. Similarly, the S1 signal shifts to different positions specially with the $CeNi_1Zr_{0.5}O_{y\ (c)}$ catalyst where it appears at 561 cm^{-1} after pretreatment temperature in hydrogen at 250 °C and at 574.5 cm^{-1} after pretreatment temperature in hydrogen at 200 °C. With all the other catalysts this peak is found at 564.5 cm^{-1} and 562.8 cm^{-1} after test with pretreatment temperatures in hydrogen of 250 °C and 200 °C, respectively.

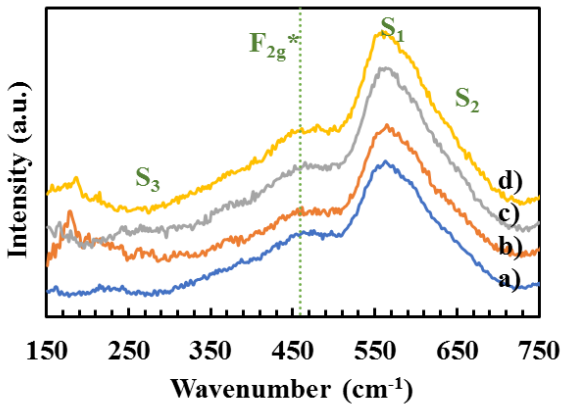

Figure 77 Raman spectra for $CeNi_xZr_{0.5}O_y$ calcined catalysts after 31 hours test with a pretreatment in H_2 at 200 °C: a) x = 0.5, b) x = 1, c) x = 2 and d) x = 5.

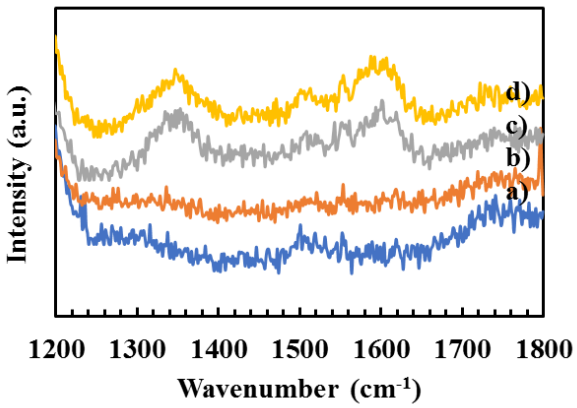

Figure 78 Raman spectra in the carbon region for $CeNi_xZr_{0.5}O_y$ calcined catalysts after 31 hours test with a pretreatment in H_2 at 200 °C: a) x = 0.5, b) x = 1, c) x = 2 and d) x = 5.

Table 65 Raman signal positions for $CeNi_xZr_{0.5}O_y$ calcined catalysts after 31 hours test with a pretreatment in H_2 at 200 °C: a) x = 0.5, b) x = 1, c) x = 2 and d) x = 5.

X	F_{2g} ceria peak position (cm^{-1})	S_1 (cm^{-1})	Carbon (cm^{-1})
0.5	473	562.8	-
1	462.2	574.5	-
2	464.8	562.8	1346, 1600
5	461.3	562.8	1346, 1587

III.6.2.2. XPS analysis

Calcined $CeNi_xZr_{0.5}O_Y$ catalysts previously studied are also analyzed by XPS but after pretreatment in H_2 at 200 °C followed by OSRE ($EtOH/H_2O/O_2/N_2$ = 1:3:1.7:N_2) at 50 °C for 31 hours and the corresponding data are presented in Figure 79 and Table 66. Ni $2p_{3/2}$ main peak no more appears clearly as a doublet due to the increased broadness between the signals. The main emission peak seems to shift to different positions that can be estimated at 855.9, 855.3, 855 and 855.6 eV for $CeNi_{0.5}Zr_{0.5}O_{y\ (c)}$, $CeNi_1Zr_{0.5}O_{y\ (c)}$, $CeNi_2Zr_{0.5}O_{y\ (c)}$ and $CeNi_5Zr_{0.5}O_{y\ (c)}$ respectively which were previously appearing as a doublet positioned at around 855.3 and 853.6 eV on the fresh Zr catalysts. Ni $2p_{3/2}$ satellite peaks become also less intense. u' and v' signals in Ce 3d core level become more visible after test. The Zr 3d core levels are not affected after test (at 184 and 182 eV). However, with O 1s changes occur in the distribution of these species and thus the positions of the peaks vary from 531/529.5 and 531/529.4 eV for each of $CeNi_2Zr_{0.5}O_{y\ (c)}$ and $CeNi_5Zr_{0.5}O_{y\ (c)}$ respectively (fresh catalysts) to 529.9/532.5 eV and 529.9/532 eV respectively. For the catalysts with low nickel content, only one signal is obtained

in the O 1s spectra at 530 eV (compared to 531/529.5 eV on fresh catalysts). Concerning the atomic distribution of the atoms on the surface of the catalyst after this OSRE test with pretreatment in at 200 °C, no evidence for Ni^0 is observed after 31 hours. The distribution of Ce^{4+} and Ce^{3+} species varies compared to the fresh catalysts (Table 67). The percentages of Ce^{4+} species increase after test to 83 % (68 % on fresh catalyst) with $CeNi_{0.5}Zr_{0.5}O_{y\ (c)}$ spent catalyst and Ce^{3+} species decrease from 27 % to 17%. However, the opposite evolution is obtained with Ce^{3+} species increase on catalysts where x = 1, 2 and 5. This is more induced on $CeNi_5Zr_{0.5}O_{y\ (c)}$ leading to an increase of these species from 18 % (on fresh catalysts) to 32% (after test), O' species appear when $x \geq 2$ and have a larger contribution on $CeNi_2Zr_{0.5}O_{y\ (c)}$ (40 %). After test, the oxygen species attribute a different distribution leading to slight changes between OH and O^{2-} percentages.

The variation of pretreatment temperature in hydrogen between 200 °C and 250 °C does not change the positions of the Ni $2p_{3/2}$, Zr 3d and Ce 3d signals after OSRE. However, with pretreatment in hydrogen at 200 °C, the doublet peak for Ni $2p_{3/2}$ core level becomes too broad to be differentiated into two separate peaks unlike that with pretreatment temperature in hydrogen of 250 °C where the two peaks are still possible to be distinguished. Concerning O 1s level, when x = 0.5 and 1 a single signal is observed at around 530 eV after test corresponding to about 50-50 % of OH and O^{2-} species (Table 67), in similar proportions compared to before test (Table 47), while when x = 2 or 5, OH and O^{2-} species are still found in similar proportions but with the appearance of O' species (with the highest amount when x = 2). Globally, the Ce^{3+} cations are found between 17 and 36 % after this series of test (Table 67) compared to 18 - 32 % before test (Table 47) and 16 - 23 % after test with pretreatment in H_2 at 250 °C (Table 61). That means that globally the main Ce cations (Ce^{4+}, Ce^{3+}) are well maintained before and after tests. Quantification data obtained with XPS on spent $CeNi_{0.5}Zr_{0.5}O_{y\ (c)}$ remain the same after pretreatment in hydrogen of 200 and 250 °C. However by increasing the nickel content ($x \geq 1$), these quantifications vary for O 1s and Ce 3d species. Surprisingly, Ce^{4+} species decrease with respect to the Ce^{3+} species in spent catalysts obtained after test with pretreatment in hydrogen at 200 °C compared to those with pretreatment in hydrogen at 250 °C. Even if it must be recalled that an uncertainty exists in the estimation of Ce^{3+} cations from XPS, some precise analysis can be further done. It appears that on the solids *in-situ* pretreated in H_2 at 250 °C, the presence of Ce^{4+} is well maintained under reaction stream and even better compared to those pretreated in H_2 at 200 °C. The percentages of Ce^{4+} cations are higher in the case when the

catalysts are pretreated in H_2 at 250 °C than those of pretreatment temperature in H_2 of 200 °C. Thus, the pretreatment temperature plays a role in the OSRE process as previously reported in the tests using different pretreatment temperature.

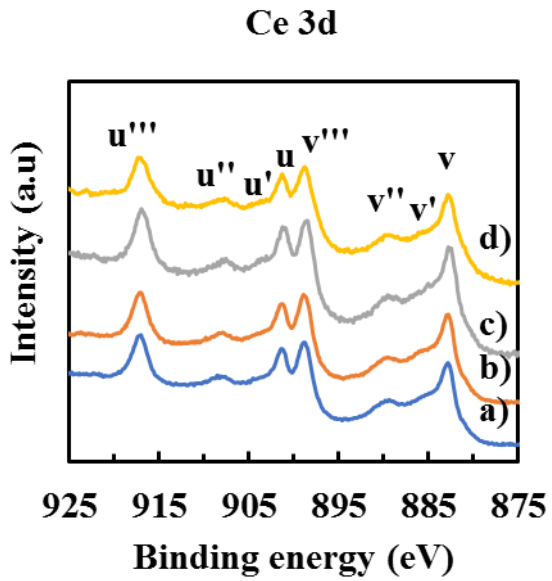

(1)

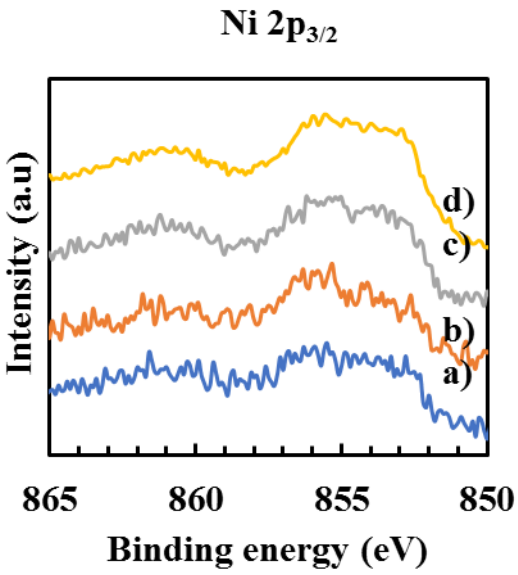

(2)

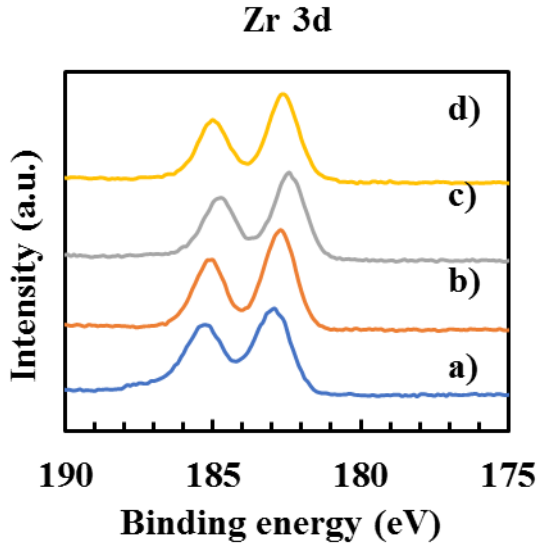

(3)

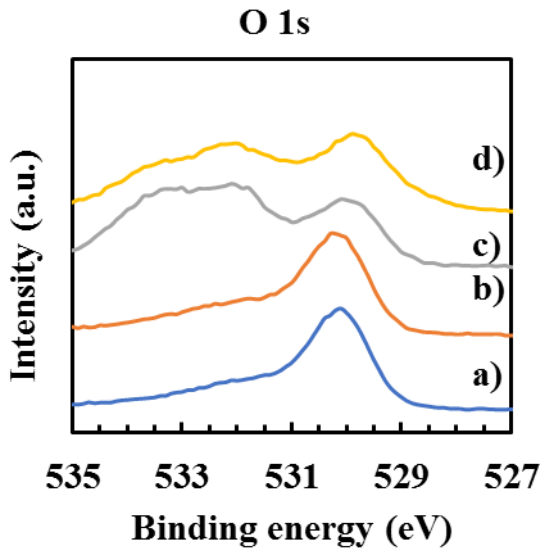

(4)

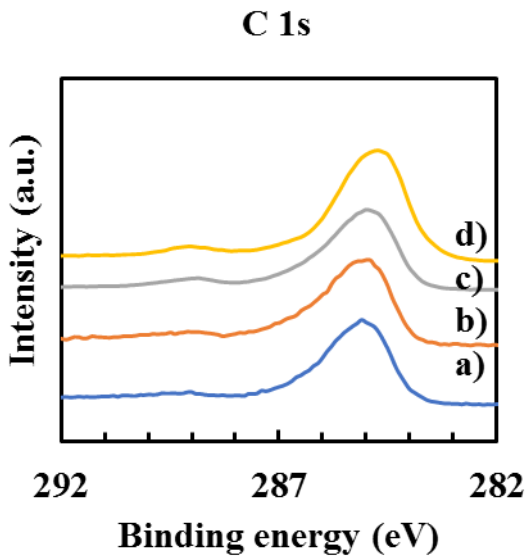

Figure 79 XPS spectra for $CeNi_xZr_{0.5}O_y$ calcined catalysts after test for 31 hours with a pretreatment in H_2 at 200°C: a) 0.5, b) x=1, c) x=2 and d) x=5. 1) Ce 3d, 2) Ni $2p_{3/2}$, 3) Zr 3d, 4) O 1s and 5) C 1s.

Table 66 Binding energies for the different XPS signals obtained $CeNi_xZr_{0.5}O_y$ calcined catalysts after test for 31 hours with a pretreatment in H_2 at 200 °C: a) x = 0.5, b) x = 1, c) x = 2 and d) x = 5.

	Binding energy (eV)					
Catalyst	**Ni $2p_{3/2}$**	**Ni $2p_{3/2}$ satellite**	**Zr 3d**	**O 1s**	**Ce 3d**	**C 1s**
$CeNi_{0.5}Zr_{0.5}O_y$ (c)	855.9	855.9	185.2/182.9	530.1	917/901.4/898.8/882.8	285.1
$CeNi_1Zr_{0.5}O_y$ (c)	855.3	855.3	185.1/182.7	530.3	917/901.3/898.9/882.8	285
$CeNi_2Zr_{0.5}O_y$ (c)	855	855	184.7/182.4	532.5/529.9	917/901.3/898.5/882.8	285
$CeNi_5Zr_{0.5}O_y$ (c)	855.6	855.6	185/182.6	532/529.9	917/901.2/898.7/882.8	284.7

Table 67 Quantification data obtained from XPS for atomic percentage in $CeNi_xZr_{0.5}O_y$ calcined catalysts after test for 31 hours with a pretreatment in H_2 at 200 °C.

	% at						
	Ni $2p_{3/2}$		Ce 3d		O 1s		
Catalyst	**Ni^0**	**Ni^{2+}**	**Ce^{4+}**	**Ce^{3+}**	**O^{2-}**	**OH**	**O'**
$CeNi_{0.5}Zr_{0.5}O_y$ (c)	0	100	83	17	54	46	0
$CeNi_1Zr_{0.5}O_y$ (c)	0	100	70	30	51	49	0
$CeNi_2Zr_{0.5}O_y$ (c)	0	100	64	36	29	30	40
$CeNi_5Zr_{0.5}O_y$ (c)	0	100	68	32	42	40	18

III.7. Characterizations of $CeNi_xZr_{0.5}O_y$ dried spent catalysts

III.7.1 $CeNi_xZr_{0.5}O_y$ dried catalysts after test with pretreatment of 250 °C after 80 hours

III.7.1.1. Raman analysis

Raman results obtained for $CeNi_5Zr_{0.5}O_{y\ (d)}$ catalysts after test of 80 hours with a pretreatment in H_2 at 250 °C are presented in Figure 80 and Table 68. The signal over noise is very poor and a high uncertainty is therefore present on this result that should be checked. However, it seems that a deviation of the F_{2g} ceria peak from a position of 451 cm^{-1} to 470 cm^{-1} occurs on the spent catalyst. The noisy signal and difficulty to observe the F_{2g} ceria lead to not be able to analyze the region between 500 and 700 cm^{-1}. Even if the signal is poor, the Raman analysis in the carbon region shows the presence of 2 peaks at 1309 cm^{-1} and 1590 cm^{-1}, that can be attributed to highly disordered graphitic type carbon.

With the spent $CeNi_5Zr_{0.5}O_y$ calcined catalyst tested under same conditions, the F_{2g} peak couldn't be resolved from S_1 and S_2 signals that appear between 500 and 730 cm^{-1}, while here with dried catalyst the F_{2g} peak seems visible and the S_1 and S_2 signals are not evident. Both of these catalysts, the dried and the calcined $CeNi_5Zr_{0.5}O_y$, show the presence of carbon by Raman which is in a very low amount not detected previously by mass variation method.

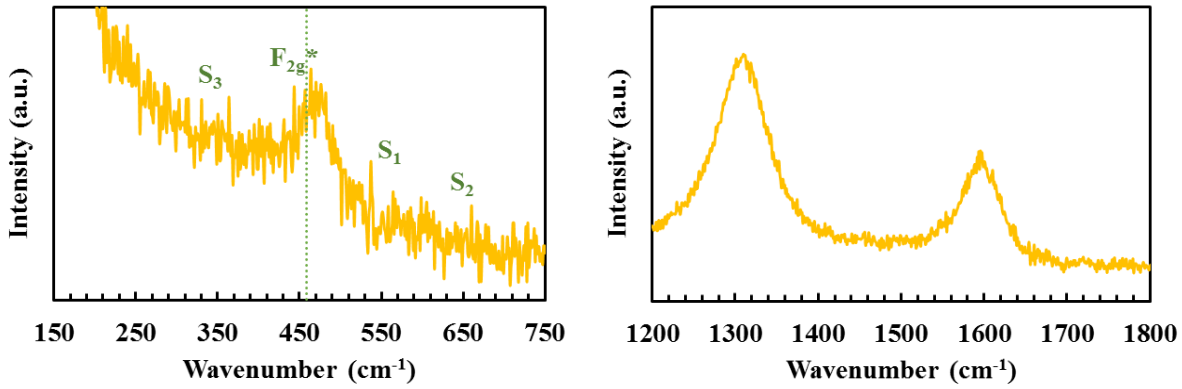

(a) **(b)**

Figure 80 Raman spectra for $CeNi_5Zr_{0.5}O_{y\ (d)}$ catalysts after test of 80 hours with a pretreatment in H_2 at 250 °C in a) ceria region and b) carbon region.

Table 68 Raman signal positions for $CeNi_5Zr_{0.5}O_y$ fresh dried and spent catalysts after test of 80 hours with a pretreatment in H_2 at 250 °C.

F_{2g} ceria peak position (cm^{-1})		**S_1 +S_2(cm^{-1})**		**Carbon (cm^{-1})**
fresh	**spent**	**fresh**	**spent**	**spent**
451	470	490-690	unresolved	1309-1590

III.7.1.2. XPS analysis

XPS analysis for the $CeNi_5Zr_{0.5}O_{y\ (d)}$ catalysts after test of 80 hours with a pretreatment in H_2 at 250 °C (tables 69 and 70) shows the presence of 2 main emission peaks for Ni $2p_{3/2}$ at 856.1 and 853.4 eV (Figure 81) in addition to the satellite peak at 861.4 eV. The signal at 853.4 eV was not observed on the fresh catalyst, moreover, the other signal was appearing at lower binding energy of 855.6 eV with the fresh $CeNi_5Zr_{0.5}O_{y\ (d)}$ catalyst. Ce 3d core level XPS spectra evidences well the presence of C^{4+} and Ce^{3+} cations, however, v' and u' signals become more intense than when the catalyst is fresh. No changes occur at the level of Zr 3d (185.1 and 182.7 eV). A broad signal appears in O 1s region, with peaks at 530 eV (531.5 eV on fresh catalyst) and 532.8 eV (shoulder on fresh catalyst). Taking into account that Ce has been taken as a reference to analyze eventual carbon formed, the peak obtained can be related to adventitious carbon as visible at 284.7 eV and can be detected before and after test in same form and position, by XPS along with Raman indicating that there is no change at the level of carbon formation. Quantification data allows to show that all the nickel species present after test are of Ni^{2+} nature similarly with the fresh catalyst, 60 % of the cerium species are Ce^{4+} and 40 % are Ce^{3+}, which is a relatively high value. Ce^{4+} decreases in percentage after test compared to the fresh catalysts (88 %). Moreover, the distribution of oxygen species changes after test to become 16 % O^{2-}, 80 % OH and 4 % O' (before test: 2 % O^{2-}, 70 % OH and 28 % O').

It is interesting to compare the present studied dried catalyst and the previously studied calcined catalyst (Figure 76); they present same binding energies for the different core levels studied. However, with the calcined catalyst 13 % metallic nickel is formed after test. The distribution between Ce^{3+} and Ce^{4+} species are similar after test for both catalysts with and without calcination. OH species (80 %) dominate greatly among oxygen species present in the dried catalyst after test. With the calcined catalyst after test, 53 % belongs OH species and 42 % belong to O^{2-} species.

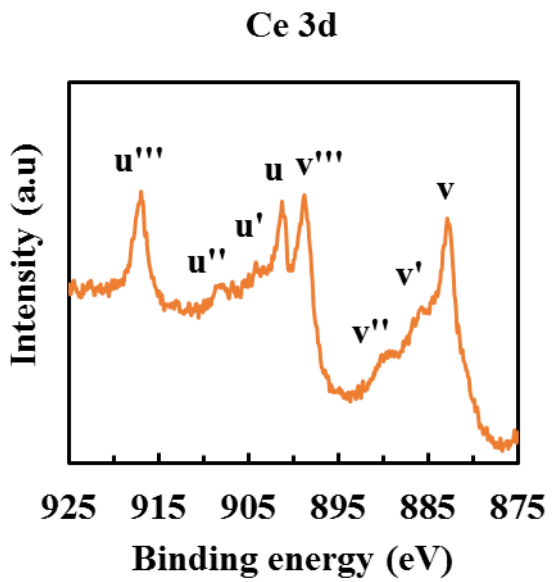
Ce 3d
Intensity (a.u)
u'''
u''
u'
u
v'''
v''
v'
v
925
915
905
895
885
875
Binding energy (eV)

(1)

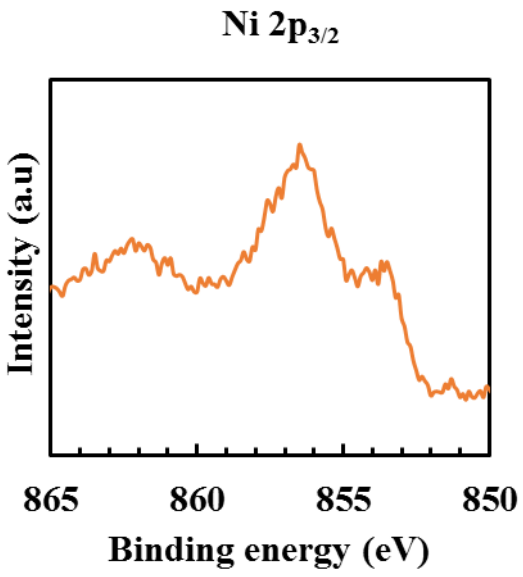
Ni 2p3/2
Intensity (a.u)
865
860
855
850
Binding energy (eV)

(2)

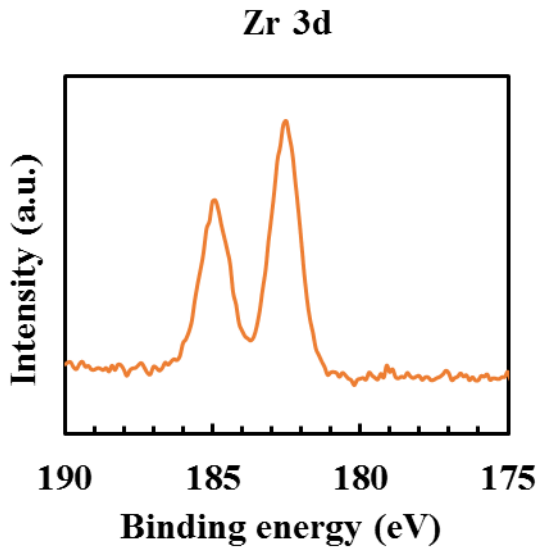
Zr 3d
Intensity (a.u.)
190
185
180
175
Binding energy (eV)

(3)

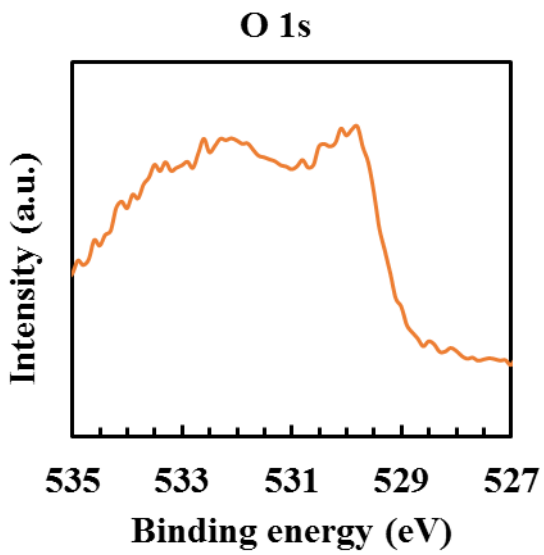
O 1s
Intensity (a.u.)
535
533
531
529
527
Binding energy (eV)

(4)

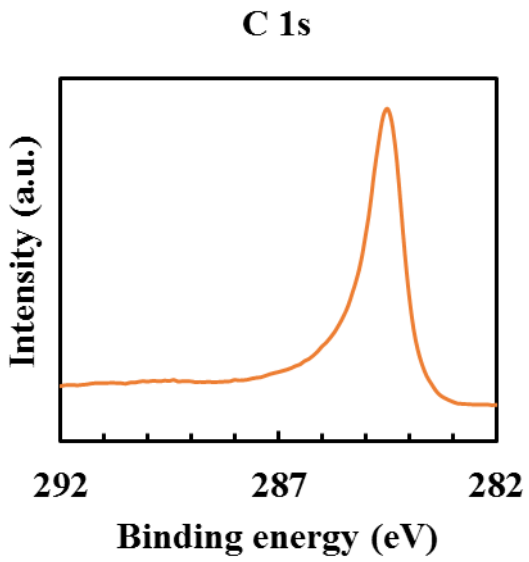

(5)

Figure 81 XPS spectra for $CeNi_5Zr_{0.5}O_y$ dried catalyst after test for 80 hours with a pretreatment in H_2 at 250 °C. 1) Ce 3d, 2) Ni $2p_{3/2}$, 3) Zr 3d, 4) O 1s and 5) C 1s.

Table 69 Binding energies for the different XPS signals obtained for $CeNi_5Zr_{0.5}O_y$ calcined and dried catalysts after test for 80 hours with a pretreatment in H_2 at 250 °C.

	Binding energy (eV)					
Catalyst	**Ni $2p_{3/2}$**	**Ni $2p_{3/2}$ satellite**	**Zr 3d**	**O 1s**	**Ce 3d**	**C 1s**
$CeNi_5Zr_{0.5}O_y$ (d)	856.1/853.4	861.4	185.1/182.7	532.8/530	917/901.5/899/883.1	284.7

Table 70 Quantification data obtained from XPS for atomic percentage in $CeNi_5Zr_{0.5}O_y$ calcined and dried catalysts after test for 80 hours with a pretreatment in H_2 at 250 °C.

	% at						
	Ni $2p_{3/2}$		Ce 3d		O 1s		
Catalyst	**Ni^0**	**Ni^{2+}**	**Ce^{4+}**	**Ce^{3+}**	**O^{2-}**	**OH**	**O'**
$CeNi_5Zr_{0.5}O_y$ (d)	0	100	60	40	16	80	4

III.7.2 $CeNi_xZr_{0.5}O_y$ dried catalysts after test with pretreatment of 200 °C after 31 hours

III.7.2.1 Raman analysis

The spent $CeNi_xZr_{0.5}O_y$ dried catalysts after the oxidative steam reforming process at 50 °C for 31 hours and after pretreatment in hydrogen at 200 °C are also analyzed by Raman (Figure 82 and Figure 83, Table 71. The F_{2g} ceria peak is very broad presenting a low signal, probably due to the intense S_1 signal. However, the F_{2g} ceria peak seems to shift to higher wavenumbers with

respect to the positions observed on fresh catalysts. The F_{2g} peaks originally present at 458, 454, 460 and 451 cm^{-1} on the fresh catalysts where x = 0.5, 1, 2 and 5, respectively are now present at 475.6, 464.8, 459.4 and 461.4 cm^{-1}, respectively. This shift is due to the formation of oxygen vacancies and Ce^{3+} cations [397, 398]. Similarly, more oxygen defects are created after test characterized by the increase of intensity of the S_1 and S_2 signals. These signals that previously lied in the range between 490 and 690 cm^{-1} appear now as a broad signal with an amplified S_1 peak positioned at 552.2, 559.2, 562.8 and 561 cm^{-1} for $CeNi_{0.5}Zr_{0.5}O_{y\ (d)}$, $CeNi_1Zr_{0.5}O_{y\ (d)}$, $CeNi_2Zr_{0.5}O_{y\ (d)}$ and $CeNi_5Zr_{0.5}O_{y\ (d)}$ respectively. Analyzing the spectrum obtained in the carbon region, it can be assured that using these catalysts carbon formation is eliminated totally (Figure 83).

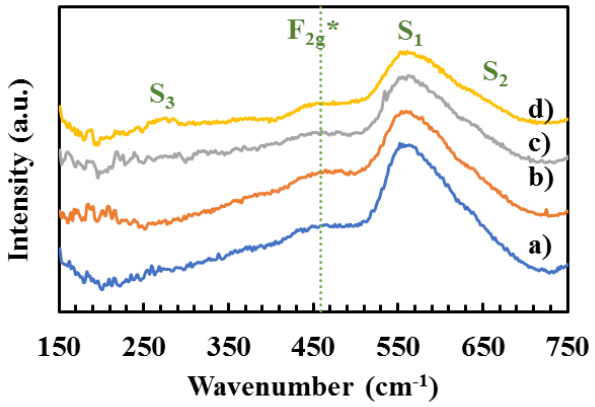

Figure 82 Raman spectra for $CeNi_xZr_{0.5}O_y$ dried catalysts after 31 hours test with a pretreatment in H_2 at 200 °C: a) x = 0.5, b) x = 1, c) x = 2 and d) x = 5.

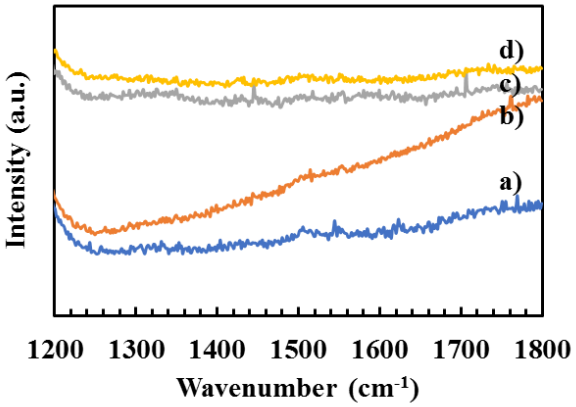

Figure 83 Raman spectra in the carbon region for $CeNi_xZr_{0.5}O_y$ dried catalysts after 31 hours test with a pretreatment in H_2 at 200 °C: a) x = 0.5, b) x = 1, c) x = 2 and d) x = 5.

Table 71 Raman signal positions for $CeNi_xZr_{0.5}O_y$ dried catalysts after test with a pretreatment in H_2 at 200 °C: a) x = 0.5, b) x = 1, c) x = 2 and d) x = 5.

X	F_{2g} ceria peak position (cm^{-1})	S_1 (cm^{-1})	Carbon (cm^{-1})
0.5	475.6	552.2	-
1	464.8	559.2	-
2	459.4	562.8	-
5	461.2	561	-

III.7.2.1 XPS analysis

The $CeNi_xZr_{0.5}O_{y\ (d)}$ catalysts after test of 31 hours in OSRE are also analyzed by XPS (Figure 84, Table 72), a main emission peak is observed in the Ni $2p_{3/2}$ region at about 855.5 – 856.1 eV with the satellite at about 861 eV. This main emission signal was observed previously on the

fresh catalysts at around 855 eV. This is evidencing that the Ni^{2+} cations are well maintained in strong interaction with other cations at the surface of the catalyst after test. The binding energies related to Zr 3d remain the same after test. The positions of binding energies for the Ce 3d signals show the main presence of Ce^{4+} cations. O 1s core levels exhibits a change in positions and distribution of the peaks after test. Before test, these catalysts presented peaks at about 531eV, however, after test, appears a strong main peak at around 530 eV for $CeNi_{0.5}Zr_{0.5}O_{y\,(d)}$, $CeNi_1Zr_{0.5}O_{y\,(d)}$ and $CeNi_2Zr_{0.5}O_{y\,(d)}$ in addition to a small shoulder present at 532 eV. With $CeNi_5Zr_{0.5}O_{y\,(d)}$, 3 peaks appear at 533.5/532.5/530 eV due to the fact of deposition of O' species on the surface of the catalyst. Some changes in the distribution of cerium and oxygen on the surface of the catalyst are observed in the data collected in Table 73. The distribution between Ce^{3+} and Ce^{4+} varies when considering the spent catalyst and the fresh catalyst where x = 0.5 and 2. With $CeNi_{0.5}Zr_{0.5}O_{y\,(d)}$, the distribution of cerium species which was 65 % Ce^{4+} and 35 % Ce^{3+} becomes 79 % Ce^{4+} and 21 % Ce^{3+} and with $CeNi_2Zr_{0.5}O_{y\,(d)}$, the distribution of cerium species which was 82 % Ce^{4+} and 18 % Ce^{3+} becomes 71 % Ce^{4+} and 29 % Ce^{3+}. However, $CeNi_1Zr_{0.5}O_{y\,(d)}$ and $CeNi_5Zr_{0.5}O_{y\,(d)}$ persist nearly the same quantification percentages before and after test. There is little evidence for metallic Ni in the XPS spectra of $CeNi_5Zr_{0.5}O_{y\,(d)}$ estimated to be about 13 % (with uncertainty due to high noise). This Ni^0 doesn't affect the activity or stability of the catalyst. Moreover, after test, the percentages of O^{2-} increase from 20 % to 51 %, with $CeNi_{0.5}Zr_{0.5}O_{y\,(d)}$, from 17 % to 62 % with $CeNi_1Zr_{0.5}O_{y\,(d)}$, from 10 % to 40 % with $CeNi_2Zr_{0.5}O_{y\,(d)}$ and from 2 % to 20 % with $CeNi_5Zr_{0.5}O_{y\,(d)}$. O' species are less present on the surface of the dried catalyst after test and are only present in very low amounts (4 %) on $CeNi_{0.5}Zr_{0.5}O_y$ and at 21 % on $CeNi_5Zr_{0.5}O_{y\,(d)}$. Signals related to carbon become broader due to the formation of C–C bonding at around 284.8 eV and C–O bonding at 286 eV. An additional signal at 282.8 eV, only visible on $CeNi_2Zr_{0.5}O_{y\,(d)}$ after test, could be attributed to the formation of metal carbides [399].

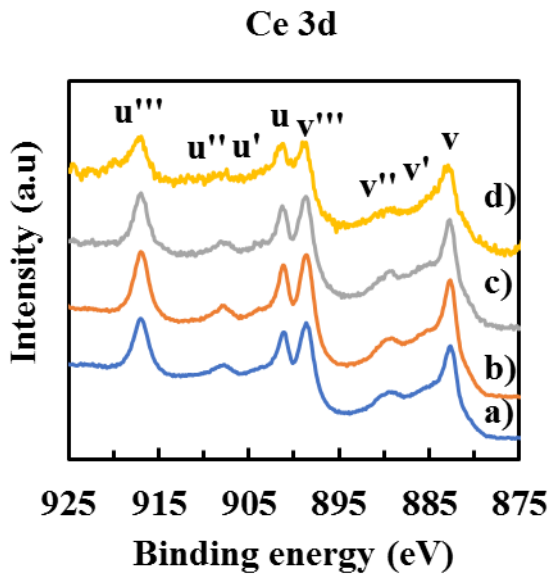
Ce 3d
u'''
u''
u'
u
v'''
v''
v'
v
d)
c)
b)
a)
Intensity (a.u)
925
915
905
895
885
875
Binding energy (eV)

(1)

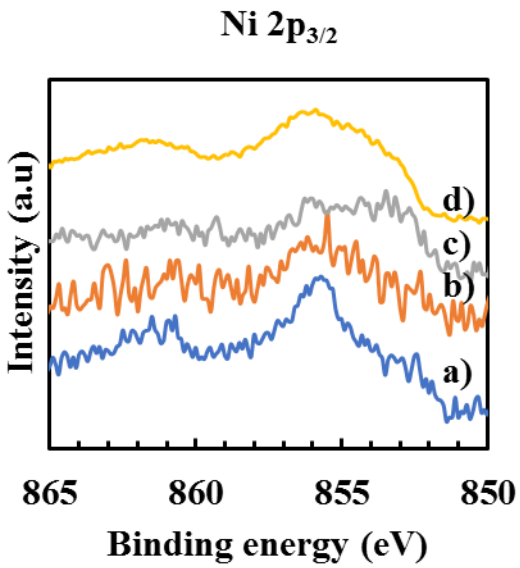
Ni 2p3/2
d)
c)
b)
a)
Intensity (a.u)
865
860
855
850
Binding energy (eV)

(2)

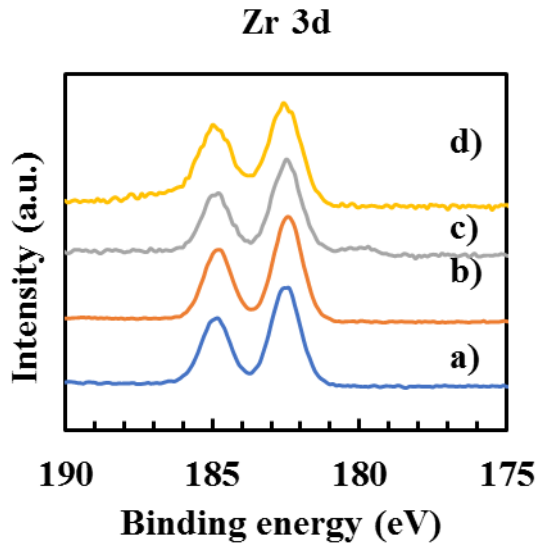
Zr 3d
d)
c)
b)
a)
Intensity (a.u.)
190
185
180
175
Binding energy (eV)

(3)

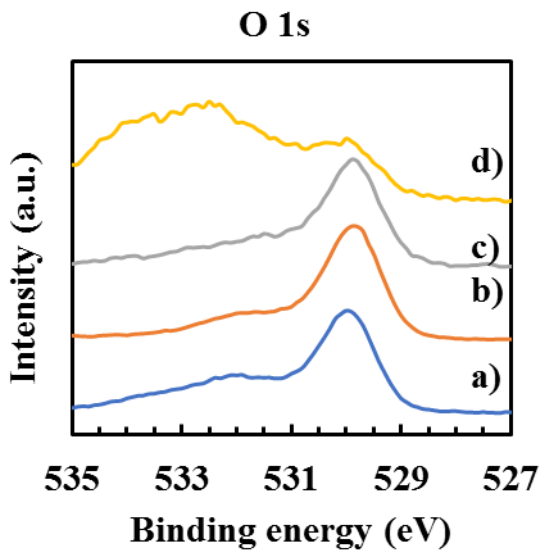
O 1s
d)
c)
b)
a)
Intensity (a.u.)
535
533
531
529
527
Binding energy (eV)

(4)

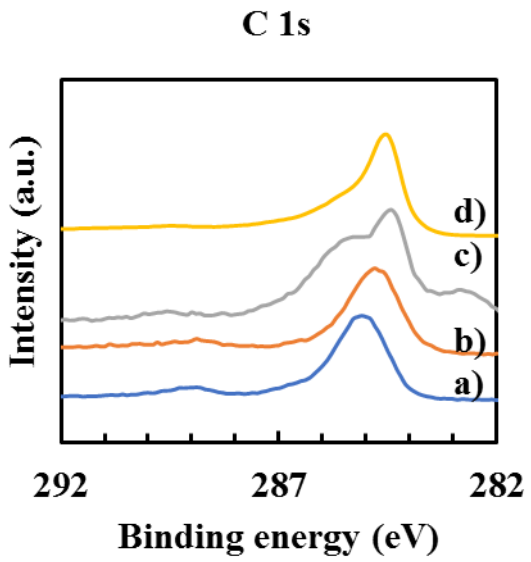

(5)

Figure 84 XPS spectra for $CeNi_xZr_{0.5}O_{y\ (d)}$ catalysts after test for 31 hours with a pretreatment in H_2 at 200 °C: a) x = 0.5, b) x = 1, c) x = 2 and d) x = 5. 1) Ce 3d, 2) Ni $2p_{3/2}$, 3) Zr 3d, 4) O 1s and 5) C 1s.

Table 72 Binding energies for the different XPS signals obtained for $CeNi_xZr_{0.5}O_y$ dried catalysts after test for 31 hours with a pretreatment in H_2 at 200 °C: a) x = 0.5, b) x = 1, c) x = 2 and d) x = 5.

	Binding energy (eV)					
Catalyst (d)	**Ni $2p_{3/2}$**	**Ni $2p_{3/2}$ satellite**	**Zr 3d**	**O 1s**	**Ce 3d**	**C 1s**
$CeNi_{0.5}Zr_{0.5}O_y$	855.7	861.5	184.8/182.4	532.1/530	917/901.1/898.6/882.6	285.1
$CeNi_1Zr_{0.5}O_y$	855.5	860.9	184.8/182.4	531.6/529.9	917/901.2/898.7/882.6	284.8
$CeNi_2Zr_{0.5}O_y$	856.1/853.5	861	184.8/182.5	529.9	917/901.3/898.7/882.7	284.5 /282.8
$CeNi_5Zr_{0.5}O_y$	855.9	861.3	185/182.6	533.5/532.5/530	917/901.3/899.1/883.3	284.5

Table 73 Quantification data obtained from XPS for atomic percentage in $CeNi_xZr_{0.5}O_y$ dried catalysts after test for 31 hours with a pretreatment in H_2 at 200 °C.

	% at						
	Ni $2p_{3/2}$		Ce 3d		O 1s		
Catalyst	**Ni^0**	**Ni^{2+}**	**Ce^{4+}**	**Ce^{3+}**	**O^{2-}**	**OH**	**O'**
$CeNi_{0.5}Zr_{0.5}O_{y\ (c)}$	0	100	79	21	51	45	4
$CeNi_1Zr_{0.5}O_{y\ (c)}$	0	100	82	18	62	38	0
$CeNi_2Zr_{0.5}O_{y\ (c)}$	0	100	71	29	40	60	0
$CeNi_5Zr_{0.5}O_{y\ (c)}$	13	97	86	14	20	59	21

III.7.3. $CeNi_5Zr_{0.5}O_y$ dried catalyst after test without *in-situ* pretreatment in H_2 after 80 hours

III.7.3.1 Raman analysis

On the spent $CeNi_5Zr_{0.5}O_{y\ (d)}$ catalyst after test of 80 hours without pretreatment in H_2 (Figure 85), the signal of the F_{2g} ceria peak is low and noisy and not possible to be positioned. Only a single broad signal at 534 cm^{-1} (along with the S_1 and S_2 signals) appears. On the fresh catalyst, the F_{2g} ceria peak was present at around 451 cm^{-1} and the different local vibrations due to oxygen vacancies related to the doping of the catalyst were between 490 and 690 cm^{-1}. In the zone of carbon peaks appear at 1308 cm^{-1} and 1589 cm^{-1} evidencing very low signal due to carbon. F_{2g} signal appears as a shoulder due to the hindering effect caused by the S_1 signal due to presence of oxygen vacancies and cerium complexes formed at the level of the catalyst and due to the extrinsic defect mode induced by oxygen vacancies that can be increased in case of the substitution of Ce^{4+} by lower valence cations in a solid solution. The oxygen vacancies could be more present in this case of catalyst where no pretreatment in hydrogen was applied, compared to the case where this catalyst was pretreated in hydrogen at a temperature of 250 °C (Figure 80), because the related local vibrations were lower in intensity in comparison to F_{2g} peak, which allowed to assign the F_{2g} peak at 470 cm^{-1} (Table 74).

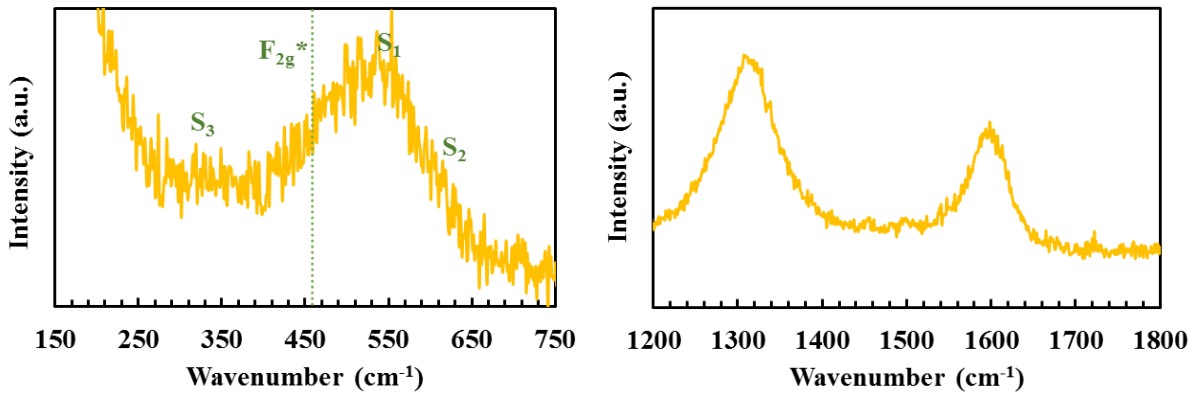

Figure 85 Raman spectra for $CeNi_5Zr_{0.5}O_{y\ (d)}$ catalysts after test of 80 hours without pretreatment in H_2 in a) ceria region and b) carbon region.

Table 74 Raman signal positions for $CeNi_5Zr_{0.5}O_y$ fresh dried and spent catalysts after test of 80 hours without pretreatment in H_2.

F_{2g} ceria peak position (cm^{-1})		**S_1 +S_2(cm^{-1})**		**Carbon (cm^{-1})**
fresh	**spent**	**fresh**	**spent**	**spent**
451	unresolved	490-690	534	1308-1589

III.7.3.2 XPS analysis

$CeNi_5Zr_{0.5}O_{y\ (d)}$ catalyst after test for 80 hours without pretreatment in H_2 is also analyzed by XPS and the corresponding results are presented in Figure 86 and Tables 75 and 76. The main emission signal of Ni $2p_{3/2}$ shows a doublet at 855.6/852.9 eV with the satellite peak being at about 861.6 eV. O 1s XPS signal shows a broad peak at 529.8 eV induced by the main presence of O^{2-} species, with a small shoulder at about 531.5 eV. In the Ce 3d XPS spectrum, the main peaks evidence the main presence of Ce^{4+} cations. Zr 3d spectra allows to see the presence of 2 signals at 184.8 and 182.5 eV, related to Zr^{4+}. A single carbon peak at 284.4 eV due to C–C bonding is only related to adventitious carbon in approval with Raman and mass variation analysis. Most samples that have been exposed to the atmosphere will have a detectable quantity of adventitious carbon contamination and can only be removed by removed by argon sputtering (unavailable in our Raman apparatus). In comparison to the fresh catalysts, changes at the level of the Ni $2p_{3/2}$ and O 1s levels can be reported. The main emission peak of Ni $2p_{3/2}$ presents the appearance of a shoulder at 852.9 eV, showing the presence of Ni^0. and 10 % of metallic nickel is estimated to be present at the surface of the catalyst after test without pretreatment in hydrogen. The majority of Ce cations is found to be Ce^{4+} (72 %) and the rest are in the state of Ce^{3+}. Oxygen species are can be attributed as 60 % O^{2-}, 35 % OH and 5 % corresponding to O' species. The percentages of Ce^{4+} decreases after test from 88 % (on fresh catalyst) to 72 % which was also noticed on the same catalyst pretreated in hydrogen at 250 °C (Table 70) where Ce^{4+} cations were estimated to be at 60 %. The percentage of O^{2-} which was of 7 % on fresh catalyst increases drastically after test without pretreatment. Interestingly, without pretreatment of the catalyst, metallic nickel is produced after test however with catalyst subjected to pretreatment in hydrogen low evidence for metallic nickel was collected after test.

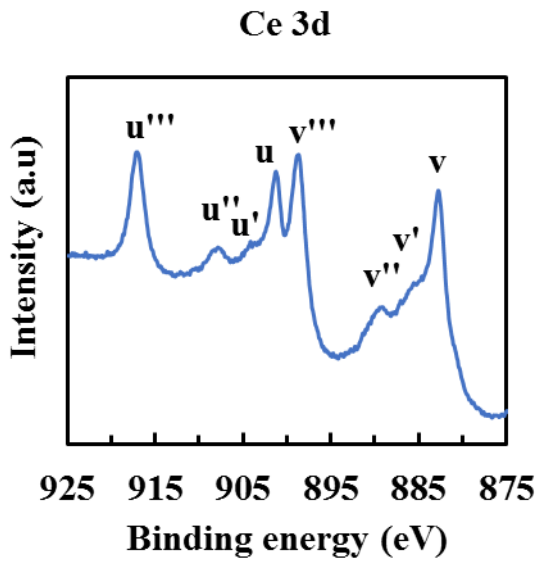
Ce 3d
u'''
u''
u'
u
v'''
v''
v'
v
Intensity (a.u)
925
915
905
895
885
875
Binding energy (eV)

(1)

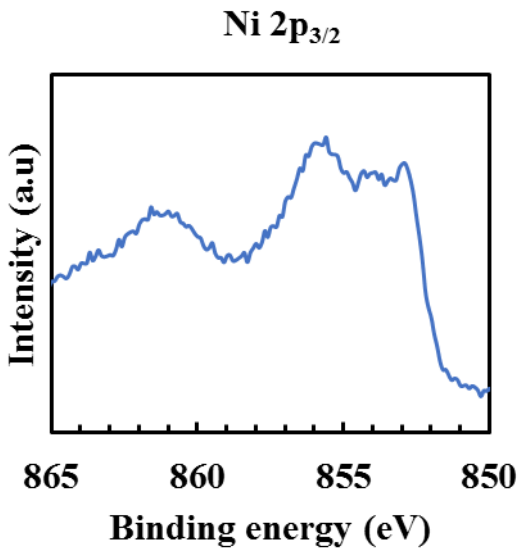
Ni 2p3/2
Intensity (a.u)
865
860
855
850
Binding energy (eV)

(2)

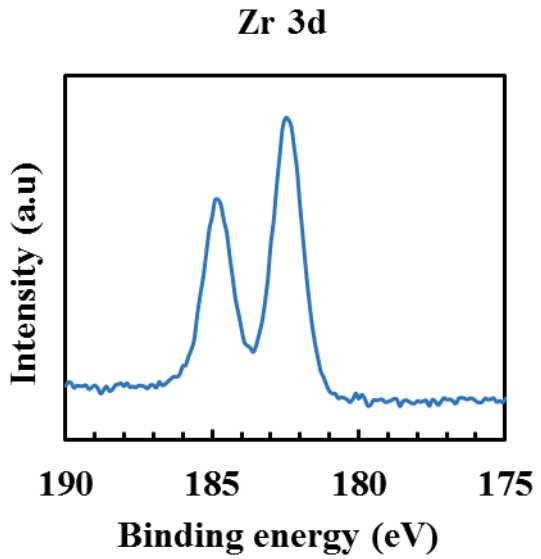
Zr 3d
Intensity (a.u)
190
185
180
175
Binding energy (eV)

(3)

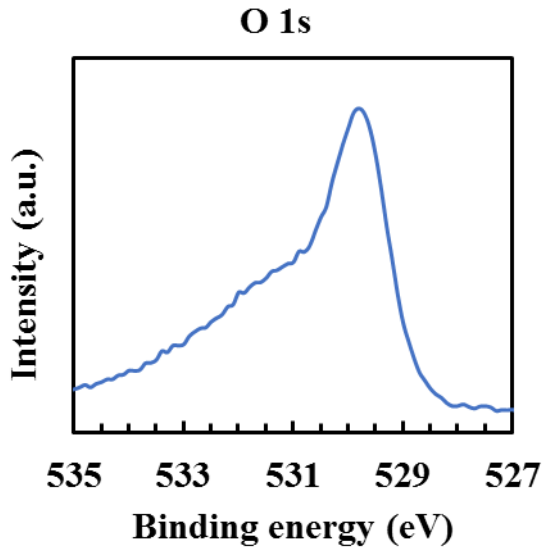
O 1s
Intensity (a.u.)
535
533
531
529
527
Binding energy (eV)

(4)

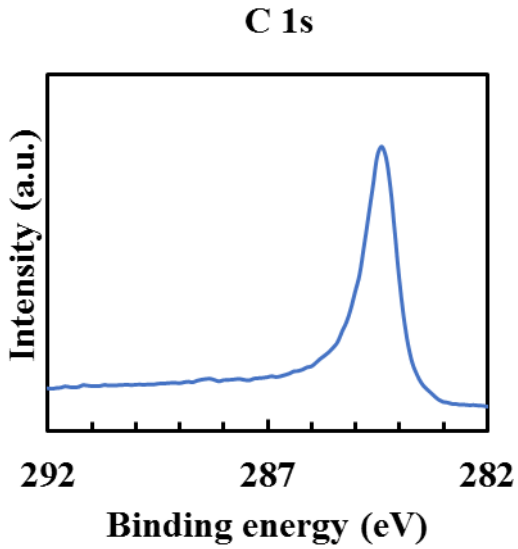

(5)

Figure 86 XPS spectra for $CeNi_5Zr_{0.5}O_{y\ (d)}$ catalysts after test for 80 hours without pretreatment in H_2. 1) Ce 3d, 2) Ni $2p_{3/2}$, 3) Zr 3d, 4) O 1s and 5) C 1s.

Table 75 Binding energies for the different XPS signals obtained for $CeNi_5Zr_{0.5}O_{y\ (d)}$ catalysts after test for 80 hours without pretreatment in H_2.

	Binding energy (eV)					
Catalyst	**Ni $2p_{3/2}$**	**Ni $2p_{3/2}$ satellite**	**Zr 3d**	**O 1s**	**Ce 3d**	**C 1s**
$CeNi_5Zr_{0.5}O_{y\ (d)}$	855.6/852.9	861.6	184.8/182.5	529.8	917/901.2/898.6/882.7	284.4

Table 76 Quantification data obtained from XPS for atomic percentage in $CeNi_5Zr_{0.5}O_{y\ (d)}$ catalysts after test for 80 hours without pretreatment in H_2.

	%at						
	Ni $2p_{3/2}$		Ce 3d		O 1s		
Catalyst $_{(d)}$	**Ni^0**	**Ni^{2+}**	**Ce^{4+}**	**Ce^{3+}**	**O^{2-}**	**OH**	**O'**
$CeNi_5Zr_{0.5}O_y$	10	90	72	28	60	35	5

III.8. Characterizations of $CeNi_xAl_{0.5}O_y$ calcined spent catalysts

III.8.1. $CeNi_xAl_{0.5}O_y$ calcined catalysts after 5 hours test with pretreatment of 250 °C

III.8.1.1. Raman analysis

The $CeNi_xAl_{0.5}O_y$ calcined catalysts after test of 5 hours in OSRE with a pretreatment in H_2 at 250 °C are reported in Figure 87. The F_{2g} ceria peak is low and broad, while the S_1 signal is

intense, so the position of F_{2g} ceria peak is an estimation (high uncertainty). F_{2g} ceria peak is localized at 455.9 cm^{-1} for the spent $CeNi_{0.5}Al_{0.5}O_y$ catalyst, at 454.1 cm^{-1} for $CeNi_1Al_{0.5}O_y$ spent catalyst and at 466.6 cm^{-1} for $CeNi_2Al_{0.5}O_y$ spent catalyst. S_1 signal which was initially located between 551 and 558 cm^{-1} on fresh catalysts shifts after test to higher positions at 562.8 - 561 cm^{-1}. Two bands at 1346 and 1599 cm^{-1} visible in the spectrum obtained on the compound with x = 1 are the characteristics of D and G band of carbon (Figure 88). As a matter of fact, carbon has been previously shown to be formed on $CeNi_1Al_{0.5}O_{y\ (c)}$ after test with an amount of 24 $mg/h.g_{catalyst}$. Ceria structure is modified due to the formation of complexes and creation of oxygen vacancies signaled by intense S_1 signal. As a consequence, the position of the F_{2g} ceria peak could shift to higher positions in all the cases (Table 77) compared to those obtained on fresh catalysts (at 452.9 cm^{-1} for $CeNi_{0.5}Al_{0.5}O_y$ and $CeNi_1Al_{0.5}O_y$ and at 456.5 cm^{-1} for $CeNi_2Al_{0.5}O_y$). As already reported before, the S_1 signal is caused by extrinsic defect mode induced by the increase of oxygen vacancies that can be increased in case of the substitution of Ce^{4+} by lower valence cations in a solid solution.

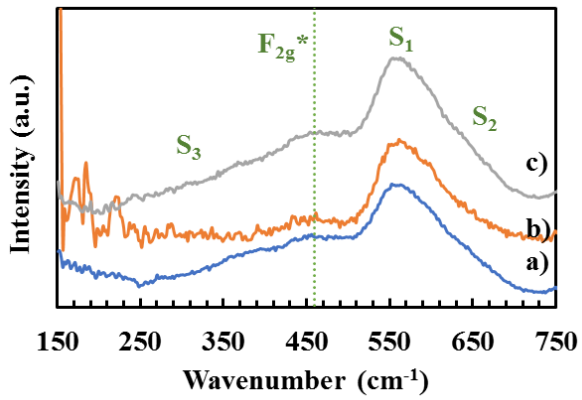

Figure 87 Raman spectra for $CeNi_xAl_{0.5}O_y$ calcined catalysts after 5 hours test with a pretreatment in H_2 at 250 °C: a) x = 0.5, b) x = 1, c) x = 2 and d) x = 5.

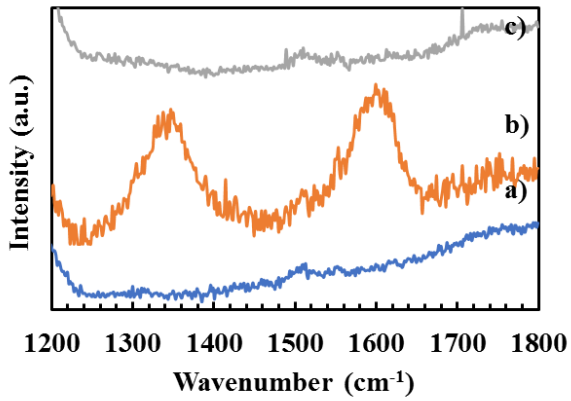

Figure 88 Raman spectra in the carbon region for $CeNi_xAl_{0.5}O_y$ calcined catalysts after 5 hours test with a pretreatment in H_2 at 250 °C: a) x = 0.5, b) x = 1, c) x = 2 and d) x = 5.

Table 77 Raman signal positions for $CeNi_xAl_{0.5}O_y$ calcined catalysts after 5 hours test with a pretreatment in H_2 at 250 °C: a) x = 0.5, b) x = 1, c) x = 2 and d) x = 5.

X	F_{2g} ceria peak position (cm^{-1})	S_1 (cm^{-1})	Carbon (cm^{-1})
0.5	455.9	562.8	-
1	454.1	561	1346, 1599
2	466.6	562.8	-

These results are in agreement with the presence of small nanoparticles and the solubility of Ni^{2+} (and Al^{3+}) into CeO_2 creating anionic vacancies that amount is increased after test.

III.8.1.2. XPS analysis

The XPS spectra obtained on the spent Al based catalysts after test for 5 hours with a pretreatment in H_2 at 250 °C are presented in Figure 89 and the corresponding binding energies are presented in Table 78. In general, some variations can be seen between the spectra of fresh and spent catalysts in the Ni $2p_{3/2}$ region. The main emission peak is observed at 855.3 eV, 856.6 eV and 856.1 eV in $CeNi_{0.5}Al_{0.5}O_y$, $CeNi_1Al_{0.5}O_y$ and $CeNi_2Al_{0.5}O_y$ respectively. In fact, this signal consists of 2 peaks appearing as a wide and broad single peak, that can be slightly differentiated when x = 1. Al 2p orbitals appear at around 74 eV in all the catalysts and almost at constant binding energy after test. The Ce 3d region shows the main presence of Ce^{4+} cations, with the presence of Ce^{3+} (Table 79). At the level of O 1s, all spent catalysts present a peak at 530 eV. Another additional peak is observed at 532.6 eV in $CeNi_1Al_{0.5}O_y$. There is a variation in the binding energies of the O 1s signals compared to fresh catalysts (530 and 531 eV). The oxygen species present in $CeNi_{0.5}Al_{0.5}O_y$ after test are 38 % O^{2-}, 57 % OH and 5 % O' (Table 79). With $CeNi_1Al_{0.5}O_y$ after test, an increase in OH species is observed after test to reach 81 % and that of O^{2-} becomes 13 % (before test 51 % O^{2-} and 42 % OH). Moreover, the distribution of cerium cations becomes 89 % Ce^{4+} and 11 % Ce^{3+} for $CeNi_{0.5}Al_{0.5}O_y$ (compared to 83 % Ce^{4+} and 17 % Ce^{3+}), 48 % Ce^{4+} and 52 % Ce^{3+} for $CeNi_1Al_{0.5}O_y$ (compared to 87 % Ce^{4+} and 13 % Ce^{3+}) and 39 % Ce^{4+} and 61 % Ce^{3+} for $CeNi_2Al_{0.5}O_y$ (compared to 94 % Ce^{4+} and 6 % Ce^{3+}). Thus, a decrease in Ce^{4+} species (reduction of the cerium cations) is observed after test when x = 1 and 2 and a slight increase in Ce^{4+} percentages is observed when x = 0.5 (oxidation of cerium species). Small evidence of metallic nickel is observed on $CeNi_2Al_{0.5}O_{y\ (c)}$ estimated to be around 4 % with high uncertainty due to difficulty in analyzing samples after test by XPS. On the $CeNi_1Al_{0.5}O_y$ catalyst, 24 mg/h.$g_{catalyst}$ were collected after test observed by XPS analysis and presented by a small shoulder in C 1s at around 286 eV related to graphitic carbon as reported in Raman analysis.

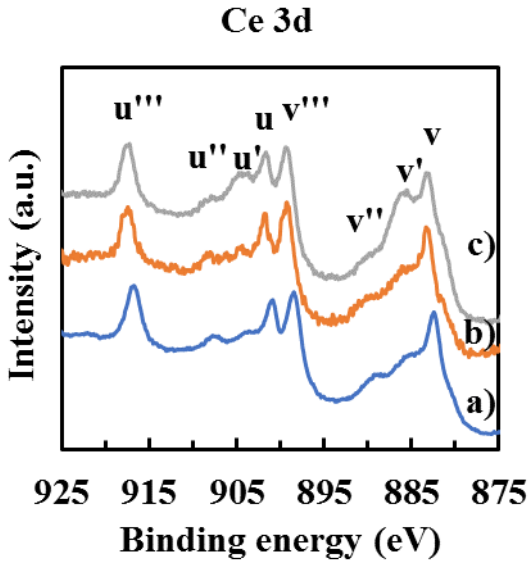
Ce 3d
u'''
u''
u'
u
v'''
v''
v'
v
c)
b)
a)
Intensity (a.u.)
925
915
905
895
885
875
Binding energy (eV)

(1)

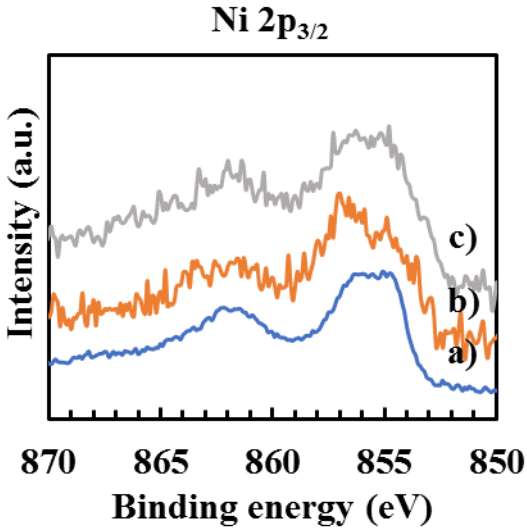
Ni 2p3/2
c)
b)
a)
Intensity (a.u.)
870
865
860
855
850
Binding energy (eV)

(2)

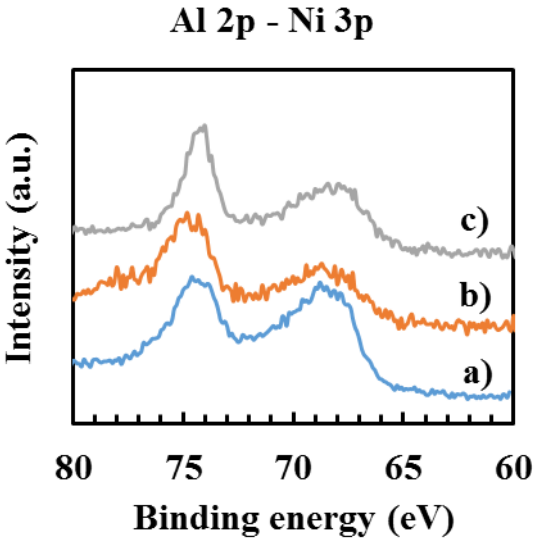
Al 2p - Ni 3p
c)
b)
a)
Intensity (a.u.)
80
75
70
65
60
Binding energy (eV)

(3)

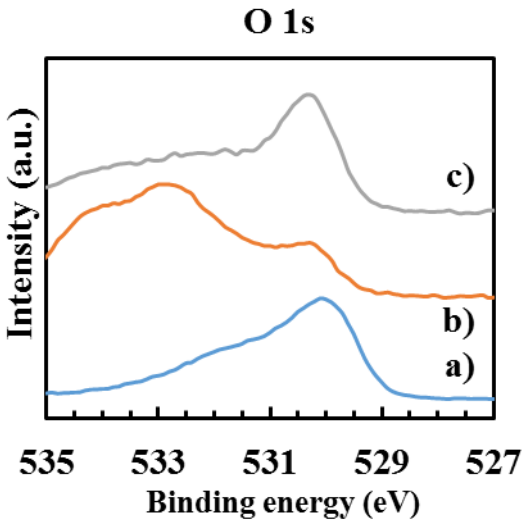
O 1s
c)
b)
a)
Intensity (a.u.)
535
533
531
529
527
Binding energy (eV)

(4)

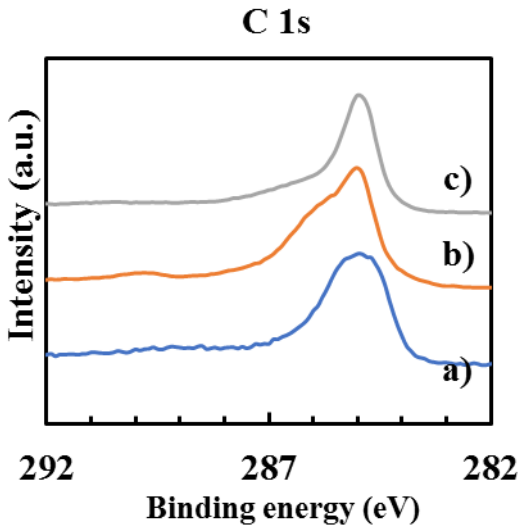

(5)

Figure 89 XPS spectra for $CeNi_xAl_{0.5}O_y$ calcined catalysts after test for 5 hours with a pretreatment in H_2 at 250 °C: a) x = 0.5, b) x = 1 and c) x = 2. 1) Ce 3d, 2) Ni $2p_{3/2}$, 3) Al 2p - Ni 3p, 4) O 1s and 5) C 1s.

Table 78 Binding energies for the different XPS signals obtained for $CeNi_xAl_{0.5}O_{y\ (c)}$ catalysts after test for 5 hours with a pretreatment in H_2 at 250 °C.

	Binding energy (eV)						
Catalyst (c)	**Ni $2p_{3/2}$**	**Ni $2p_{3/2}$ satellite**	**Al 2p**	**O 1s**	**Ce 3d**	**Ni3p**	**C1s**
$CeNi_{0.5}Al_{0.5}O_y$	855.3	861.7	74.8	530.3	917/900.2/898.7/882.7	69	285.2
$CeNi_1Al_{0.5}O_y$	856.6	860.9	74.4	529.9/532.6	917/901.2/898.8/882.9	68.3	284.6
$CeNi_2Al_{0.5}O_y$	856.1	861.2	73.8	530.1	917/901.4/899.1/883.1	68.5	284.8

Table 79 Quantification data obtained from XPS for atomic percentage in $CeNi_xAl_{0.5}O_{y\ (c)}$ catalysts after test for 5 hours with a pretreatment in H_2 at 250 °C.

	% at						
	Ni $2p_{3/2}$		Ce 3d		O 1s		
Catalyst	**Ni^0**	**Ni^{2+}**	**Ce^{4+}**	**Ce^{3+}**	**O^{2-}**	**OH**	**O'**
$CeNi_{0.5}Al_{0.5}O_{y\ (c)}$	0	100	89	11	38	57	5
$CeNi_1Al_{0.5}O_{y\ (c)}$	0	100	48	52	13	81	6
$CeNi_2Al_{0.5}O_{y\ (c)}$	4	100	39	61	32	62	6

III.8.2. $CeNi_xAl_{0.5}O_y$ calcined catalysts after 80 hours test with pretreatment at 300 °C

III.8.2.1. Raman analysis

Raman spectrum for spent aluminum-based compound is analyzed after 80 hours. test with a pretreatment in H_2 at 300 °C as shown in Figure 90. The numerical values of these signals are

presented in Table 80. A single sharp peak can be observed which could be attributed to the F_{2g} ceria peak. It appears at a wavenumber of 460.4 cm^{-1}close to the value obtained on simple calcined ceria. The signals observed previously in S_1 + S_2 zone are hardy observable after test which could be attributed to the fact of pretreatment in hydrogen at 300 °C. Although, carbon formation is not revealed by the mass variation method, however, the Raman spectrum obtained in the carbon region gives rise to 2 peaks at 1319 and 1593 cm^{-1} (the intensity reported in arbitrary units is zoomed). Nevertheless, this amount is low enough not to be detected by the previously mentioned method and not to cause deactivation of the catalyst.

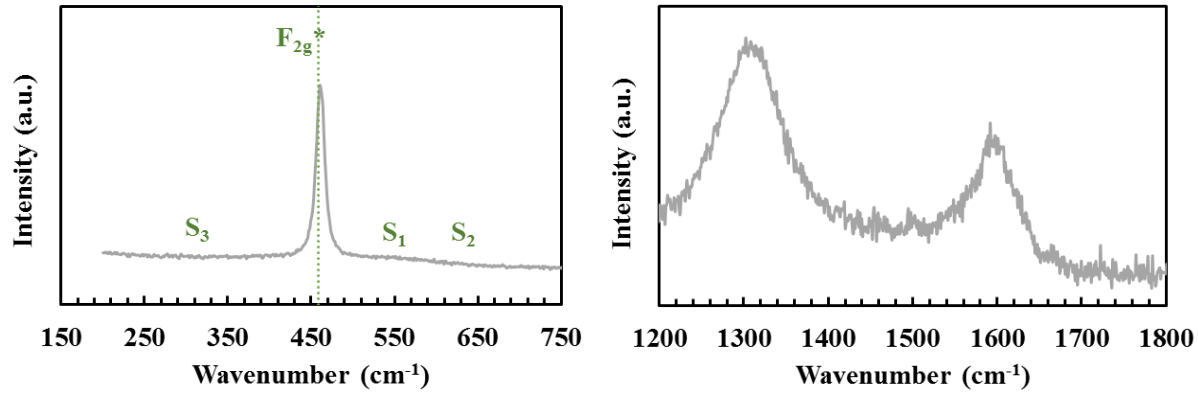

(a) **(b)**

Figure 90 Raman spectra for $CeNi_2Al_{0.5}O_y$ calcined catalysts after test of 80 hours with a pretreatment in H_2 at 300 °C in a) ceria region and b) carbon region.

Table 80 Raman signal positions for $CeNi_2Al_{0.5}O_y$ fresh calcined and spent catalysts after test of 80 hours with a pretreatment in H_2 at 300 °C.

F_{2g} ceria peak position (cm^{-1})		**S_1 +S_2(cm^{-1})**		**Carbon (cm^{-1})**
fresh	**spent**	**fresh**	**spent**	**spent**
456.5	460.4	558.1	-	1319, 1593

III.8.2.2. XPS analysis

Figure 91 shows the XPS spectra obtained on $CeNi_2Al_{0.5}O_y$ calcined catalyst after test for 80 hours with a pretreatment in H_2 at 300 °C. Ni $2p_{3/2}$ main emission peak is present at 855.7 eV (Table 81) evidencing the presence of Ni^{2+} cations which didn't change after test and its characteristic satellite peak being at 861 eV. The Ce 3d spectrum show clearly still the main presence of Ce^{4+} cations in all cases. It must be noted that Ce at 917 eV is used as a reference

to analyze carbon eventual formed. The B.E. for C 1s is at 284 eV in agreement with adventitious carbon which is in confirmation with the mass variation method that showed no carbon production after test. 2 unresolved peaks appear for O 1s at 533.2 eV and 529.9 eV corresponding to O^{2-}, OH and other O' species on the surface that could be due to adsorbed water or organic compounds, as, these positions were at lower values before test (529.8 and 532 eV). Al 2p core level remains the same binding energies after test (74.2 eV). XPS on this spent catalyst shows 100 % Ni^{2+} species (Table 82). Moreover, Ce 3d are distributed between 70 % Ce^{4+} and 30 % Ce^{3+}. So, the quantity of Ce^{4+} ion decreases after test (from 94 %). After 80 hours in OSRE, lots of organic substances or adsorbed water become deposited on the surface and as a result it can be seen that 68 % of oxygen species on the surface is a contribution of these molecules. Finally, it can be seen that the interactions between all these cations are still present even after test supported by the fact that binding energies remain the same even after 80 hours in OSRE. This probably explains why these catalysts have a high stability over time in OSRE.

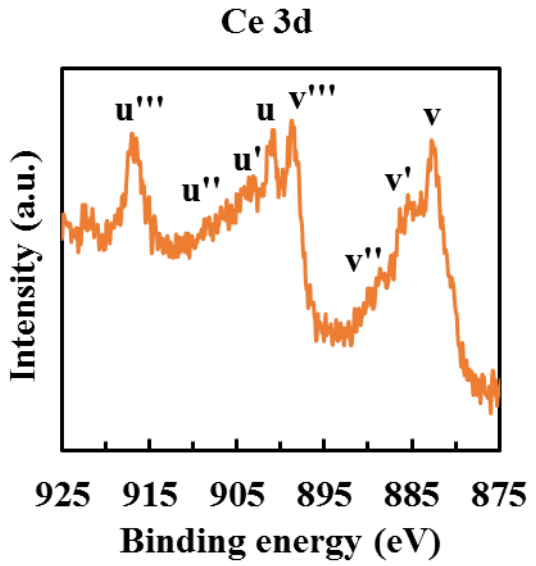

(1)

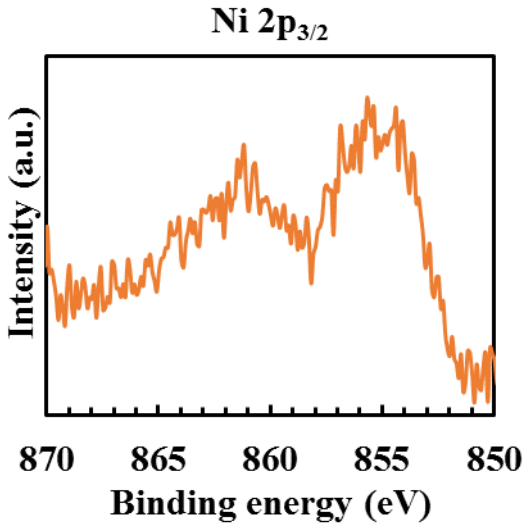

(2)

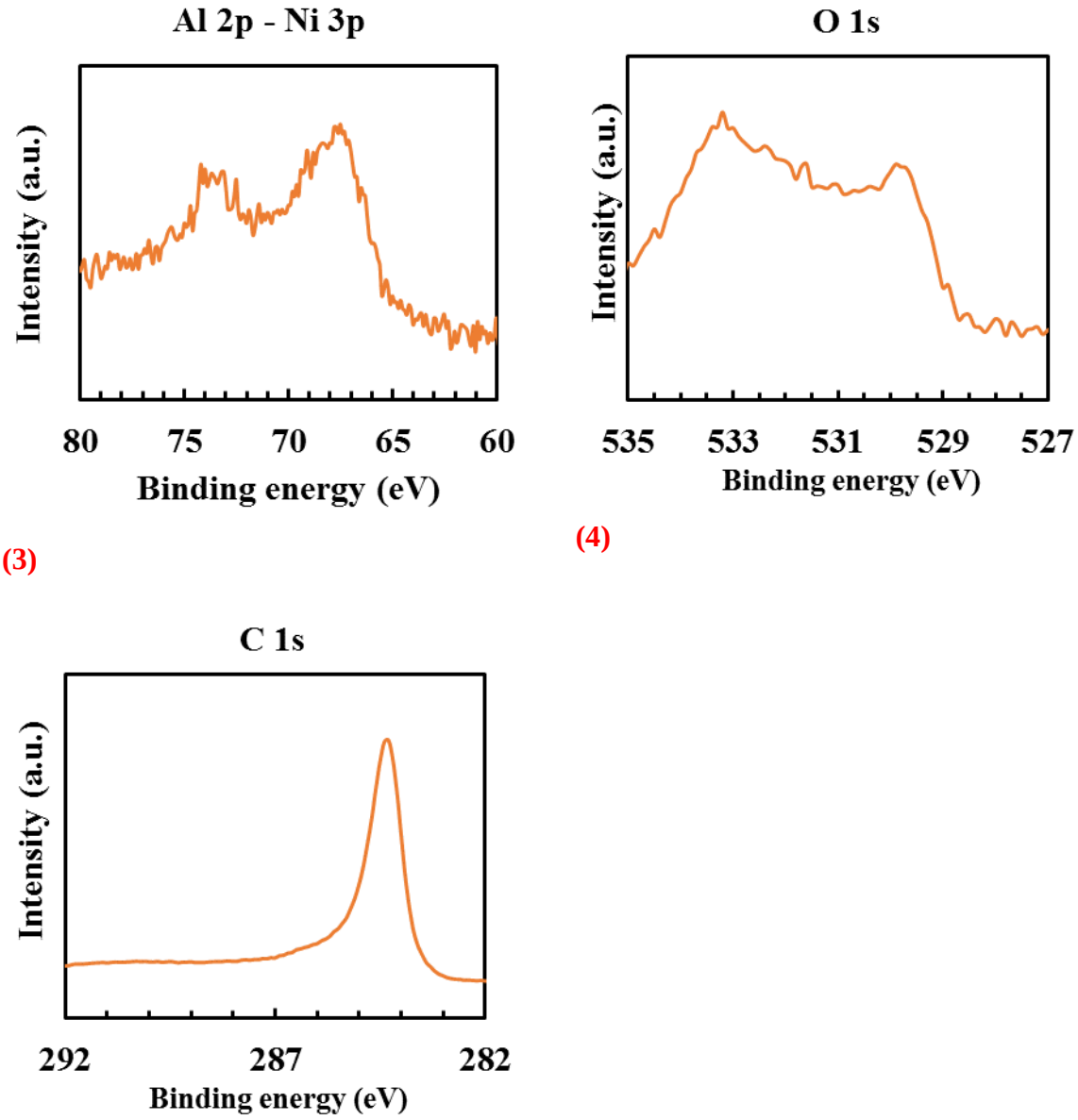

Figure 91 XPS spectra for $CeNi_2Al_{0.5}O_y$ calcined catalyst after test for 80 hours with a pretreatment in H_2 at 300 °C. 1) Ce 3d, 2) Ni $2p_{3/2}$, 3) Al 2p – Ni 3p, 4) O 1s and 5) C 1s.

Table 81 Binding energies for the different XPS signals obtained for $CeNi_2Al_{0.5}O_y$ calcined catalyst after test for 80 hours with a pretreatment in H_2 at 300 °C.

	Binding energy (eV)					
Catalyst	**Ni $2p_{3/2}$**	**Ni $2p_{3/2}$ satellite**	**Al 2p**	**O 1s**	**Ce 3d**	**C 1s**
$CeNi_2Al_{0.5}O_{y\ (c)}$	855.7	861.2	74.2	533.2/529.9	917/901/898.8/882.7	284.3

Table 82 Quantification data obtained from XPS for atomic percentage in $CeNi_2Al_{0.5}O_y$ calcined catalyst after test for 80 hours with a pretreatment in H_2 at 300 °C.

	% at						
	Ni $2p_{3/2}$		Ce 3d		O 1s		
Catalyst	Ni^0	Ni^{2+}	Ce^{4+}	Ce^{3+}	O^{2-}	OH	O'
$CeNi_2Al_{0.5}O_{y\ (c)}$	0	100	70	30	18	14	68

Conclusion

Different catalysts are prepared by the coprecipitation method: binary catalysts $CeNi_xO_y$ ($0.1 \leq x \leq 5$), ternary catalysts with aluminum $CeNi_xAl_{0.5}O_y$ ($0.5 \leq x \leq 2$) and ternary catalysts with zirconium $CeNi_xZr_{0.5}O_y$ ($0.5 \leq x \leq 5$). The catalysts are dried at 100 °C and a part of these catalysts are calcined under air at 500 °C. These catalysts are characterized by various techniques such as BET, XRD, Raman, TPR, XRF and XPS in order to obtain information on the texture, structure and properties of the samples. Some chosen samples are also analyzed by Raman and XPS after test by oxidative steam reforming under specific conditions.

The specific surface area of the calcined binary catalysts lies between 60 and 134 m^2/g and that of dried binary catalysts lies between 81 and 198 m^2/g. The specific area of dried Zr based catalysts is estimated to be between 186 and 112 m^2/g, larger than those of calcined Zr based catalysts that have a specific surface area between 71 and 130 m^2/g. Concerning Al based compounds, the specific surface area is estimated to be between 125 and 154 m^2/g and it has been shown that this specific surface area increases with the increase in Ni content in the catalyst.

XRF analysis shows that theoretical mass percentages of elements present in the catalyst are in agreement with the experimental mass percentages obtained after preparation of the catalysts. Only a slight deviation from theory is obtained for the percentage of Zr.

Whatever the catalyst is, with or without the presence of aluminum or zirconium dopants, XRD shows that the ceria phase is always present. According to Scherrer formula, the average crystallites size of ceria in these catalysts is between 3-5 nm in both binary and ternary catalysts, dried or calcined which is relatively lower than those of pure CeO_2 (8 nm) and relatively stable with the Ni content of the solid However, the ceria phase in $CeNi_{0.1}O_{y\ (c)}$ has the greatest average crystallites size among all (7 nm). CeO_2 peaks become broader which agrees with the decrease of CeO_2 average crystallites size in the mixed oxides. Moreover, there is a shift of the main XRD pattern of CeO_2 which is due to the substitution of Ce^{4+} cations by Ni^{2+} and Zr^{4+} cations

inside the CeO_2 lattice and to the formation of cerium-nickel solid solution. On calcined samples NiO exists with an average crystallites size of 12-14 nm, while, $Ni(OH)_2$ phase is found on dried samples and estimated to have a crystallites size of a 8-13 nm for $CeNi_xZr_{0.5}O_{y(d)}$ catalysts and 9 nm for $CeNi_xO_{y\,(d)}$. $Ni(OH)_2$ phase is only visible when $x \geq 0.5$.

Raman analysis of binary and ternary compounds shows a shift in F2g ceria peak originally present at around 460 cm^{-1} affected by disorders in the oxygen sublattice and/or grain size induced non-stoichiometry thus leads to line shifts and broadens with decreasing grain size and increasing lattice defects. It is shifted more to lower values on the dried binary catalysts than those of calcined binary catalysts. Vibrations between 500 and 700 cm^{-1} are visible on all the catalysts caused by extrinsic defect mode induced by oxygen vacancies that can be increased in case of the substitution of Ce^{4+} by lower valence cations Ce^{3+} and also other cations (Ni^{2+}, Al^{3+}, Zr^{4+}) assuming the formation of complexes in the ceria structure in the form of a solid solution due to the doping of the catalyst. Moreover, ceria nano structures exist at around 220 cm^{-1} and only visible on the calcined catalysts.

Different Ni^{2+} species are reducible according to the TPR analysis: those with strong interaction in solid solution of cerium and nickel (and Al, or Zr), those of small NiO nanoparticles possibly present (not visible by XRD), and larger NiO nanoparticles observed in XRD (not observed when $x = 0.1$. The good linearship between H_2 consumption and Ni amount of the catalysts proves the good incorporation of Ni inside the compounds and thus a successful coprecipitation when preparing the catalyst. Different analysis (Raman, TPR and XPS) agree on the presence of a Ni-Ce-(M)-O solid solution. XPS analysis show the presence of two environments for Ni^{2+} cations: in NiO and in strong interaction with cations of different nature. An extensive study gives for the binary catalysts a correlation between the nickel content and the percentage of each of these two environments: the higher the nickel content, the greater the percentage of Ni^{2+} in NiO environment. All the obtained results agree with the presence of small nanoparticles and the solubility of Ni^{2+} into CeO_2 creating anionic vacancies.

XPS insures the existence of O^{2-} lattice oxygen like in oxides of NiO and CeO_2 and oxygen species related to hydroxyl groups (OH^-) Before test only Ni^{2+} species are present in all samples. Cerium species are mostly (> 68%) found as Ce^{4+} cations, with the presence of Ce^{3+} cations. Some samples were then analyzed by XPS and Raman to highlight on the structural changes at the surface of the catalyst and to analyze carbon formation after oxidative steam reforming.

Globally, on a high majority of compounds, Raman analysis after test show that F_{2g} ceria peak becomes less intense in comparison to the local vibrations of the various oxygen deficiency complexes induced by oxygen vacancies increase. This ensures the continuous redox processes occurring in OSRE reaction leading to the good performance and stability over time. It appears that the substitution of Ce^{4+} by lower valence cations or other cations (Ce^{3+}, Ni^{2+}, Al^{3+}, Zr^{4+}) in a solid solution is still present after test, with anionic vacancies, and even increased.

The binding energies of the different XPS signals did not change even after 80 hours in OSRE indicating the persistence of the strong interactions between the different species present however variations in these ionic distributions has taken place. Most of the cerium species measured after test with *in-situ* pretreatment in H_2 at 250 °C are in the high oxidation state (Ce^{4+}). The percentage of Ce^{3+} cations in $CeNi_xO_y$ calcined catalysts after test increases with respect to Ce^{4+} insuring the reduction of some cerium species during test. However, under same conditions, $CeNi_xZr_{0.5}O_{y\ (c)}$ catalysts shows oxidation of these species except for $CeNi_5Zr_{0.5}O_{y\ (c)}$ catalyst that presents best catalytic performance among all. This $CeNi_5Zr_{0.5}O_{y\ (c)}$ catalyst shows even more reduction of Ce^{4+} species after 80 hours in OSRE, estimated at around 64 % Ce^{4+} (compared to 77 % after 31 hours). At this high Ni/Ce ratio, this slight reduction degree is even maintained on the dried catalyst (without calcination, $CeNi_5Zr_{0.5}O_{y\ (d)}$) after 80 hours in OSRE being previously pretreated in H_2 at 250 °C leading to the following balance: 60 % Ce^{4+} and 40 % Ce^{3+}. In Zr based solids (x = 0.5, 1, 2) *in-situ* pretreated in H_2 at 250 °C the presence of Ce^{4+} is well maintained under reaction stream and even better compared to those pretreated in H_2 at 200 °C where reduction of these species occur even if Ce^{4+} are the main dominating species. $CeNi_5Zr_{0.5}O_y$, dried or calcined, pretreated in hydrogen at 200 °C or 250 °C, insures the reduction of Ce^{4+} into Ce^{3+} unlike other Zr catalysts(x = 0.5, 1, 2). On Al based compounds, reduction of the cerium cations is observed after test when x = 1 and 2 and only a slight oxidation of Ce^{3+} is observed when x = 0.5. Big variations in oxygen composition between OH and O^{2-} groups are observed after test, probably related to the fact that the oxygen storage capacity and redox property of CeO_2 and modified ceria greatly influences the reaction pathway.

In most cases after test, nickel species present at the surface of the catalyst are Ni^{2+} cations. Small evidence of metallic nickel (Ni^0) is observed on $CeNi_2Al_{0.5}O_{y\ (c)}$ estimated to be around 4 % as well as on $CeNi_5Zr_{0.5}O_{y\ (d)}$ after test of 80 hours with around 10 %. Some evidences of Ni^0 (around 13 %) is collected too on $CeNi_5Zr_{0.5}O_{y\ (c)}$ with pretreatment in H_2 at 250 °C (after

80 hours) and pretreatment in H_2 at 200 °C (after 31 hours) that could be correlated to formation of carbon evidenced by Raman and XPS. The carbon reported in XPS and Raman is contributed by adventitious carbon in most cases, in agreement with the absence of carbon measured after test and Raman analysis.

This study makes proof that the previously prepared catalysts are enough stable to keep the oxidative steam reaction of ethanol under process and to avoid carbon formation.

Chapter IV: General discussion

Calcined and some dried, $CeNi_xO_y$ binary catalysts, ternary catalysts with aluminum $CeNi_xAl_{0.5}O_y$ or with zirconium $CeNi_XZr_{0.5}Oy$ are synthesized and characterized by different methods and then tested in oxidative steam reforming of ethanol (OSRE), with different reaction parameters such as O_2/EtOH ratio, pretreatment in hydrogen and pretreatment temperature, mass of catalyst, in order to see their impact on the conversions of ethanol and O_2, the gaseous products distributions (H_2, CO_2, CO, CH_4, acetaldehyde, acetone) as well as carbon formation.

The binary, dried and calcined catalysts, $CeNi_xO_y$ ($0.1 \leq x \leq 5$) are analyzed by different techniques such as XRF, BET, XRD, Raman, TPR and XPS. The dried catalysts have a specific surface area varying from 81 to 198 m^2/g. The same calcined catalysts have a lower specific surface, ranging from 60 to 134 m^2/g. Whatever the nickel content of the catalysts, the ceria phase is always present. For calcined catalysts, a phase corresponding to NiO appears when x is greater than or equal to 0.5. For the dried catalysts, a phase corresponding to $Ni(OH)_2$ is present when x is greater than or equal to 0.5. The Scherrer equation gives an average size of the NiO crystallites of 11 to 14 nm and the ceria phase of around 7 nm in calcined binary catalysts. The average crystallite size of $Ni(OH)_2$ and CeO_2 in binary dried catalysts are of about 9 nm and between 3 and 5 nm, respectively. The same analysis is carried out on the ternary catalysts, with either aluminum or zirconium. The specific surface area of dried Zr based catalysts is estimated to be between 186 and 112 m^2/g, larger than those of calcined Zr based catalysts that have a specific surface area between 71 and 130 m^2/g. Concerning Al based calcined compounds, this area is estimated to be between 125 and 154 m^2/g and it increases with the increase in Ni content in the catalyst. Whether the catalysts are with aluminum or zirconium, and regardless of their nickel content, all have a ceria phase. The NiO phase is present in all catalysts, except for $CeNi_{0.5}Al_{0.5}O_y$. It is therefore likely that when NiO phase is not detected, the Ce^{4+} cations inside the ceria phase are replaced by Ni^{2+} or Al^{3+} or Zr^{4+} cations with formation of a solid solution of cerium nickel (and aluminum or zirconium). The average sizes of NiO crystallites are between 5 and 9 nm for catalysts with aluminum (which shows that aluminum provides good dispersion), and 12 to 13 nm for catalysts with zirconium. Absence of separate ZrO_2 and Al_2O_3 XRD diffraction patterns indicates that Al and Zr ions are well dispersed. Similar results were reported in the literature for the CeO_2–ZrO_2 mixed oxide materials [400, 401]. Similar to the binary catalysts, these ternary catalysts exhibit different Ni^{2+} species that are reducible (TPR) in different environments [402]. When increasing the temperature

in H_2, different Ni^{2+} species are reducible according to this order: those in strong interaction in solid solution of cerium and nickel, those of small NiO nanoparticles possibly present (not visible by XRD), and those of NiO observed in XRD [190, 403]. This same analytical technique as well as Raman and XPS analysis all agree on the presence of a solid solution. All these analysis with the fact that the ionic radii of Ce^{4+} (0.9 Å) [339, 404] is greater than those of Ni^{2+} (0.7Å), Al^{3+} (0.53 Å) and Zr^{4+} (0.8Å) [405] are in agreement of formation of solid solution of Ce-Ni-(M)-O.

In the present study, several conclusions emerge, in particular that of saying that nickel plays a key role in the performance of the catalyst. The increase in nickel content in the catalysts can help promote the OSRE for hydrogen production. The study of $CeNi_xZr_{0.5}O_y$ dried catalysts after *in-situ* pretreatment in hydrogen at 250 °C under $EtOH/H_2O/O_2/N_2 = 1:3:1.7:N_2$ has shown different efficiencies for hydrogen production starting with 30 % of H_2 in products distribution with x = 0.5 till 47 % of H_2 when x = 5. Main products percentages increase with the increase in nickel content while CO and CH_4 decrease, in studied conditions. Same effect is observed on binary and ternary Al based catalysts, where the highest ethanol conversion and main products percentages are owed to catalysts with higher nickel content. Moreover, at a low O_2/EtOH ratio of 1.42, only catalysts with nickel over cerium ratios larger or equal to 1 are able to function well in OSRE without deactivation otherwise the catalysts deactivate during the first two hours under stream. This is consistent with the findings of Yan et al. [406] and Mondal et al. [174] over $Ni/CeO_2–ZrO_2$ catalysts. Increasing Ni content is known to increase the possibility of formation of carbon. It has been shown before on $Mg_2AlNi_XO_Y$ catalysts that with the lowest Ni content ($Mg_2AlNi_1O_Y$), the OSRE reaction requires higher starting temperature of about 390 °C then the oven temperature could be decreased and the required minimal oven temperature to maintain the reaction was at 215 °C to obtain minimal carbon formation [238]. At higher Ni/Ce ratios this starting temperature could be decreased to 200 °C while leading to carbon formation. However, in the used conditions here, the studied catalysts are stable enough not to lead to any carbon formation, with low and high nickel formulations, in most of the preparations and in the optimized conditions used.

Indeed, depending on Ni content and its environment in the catalyst, the results obtained vary considerably. In the literature, the transformation of ethanol has given rise to numerous reviews [33, 37, 407, 408], and nickel-based catalysts have been the subject of review because of the recognized strong activity of nickel [28-30]. Indeed, it has been reported since many years by

Yates et al. that nickel cleaves the O-H, -CH_2-, C-C and -CH_3 bonds of ethanol, in that order [409, 410]. Thus, Ni, allowing the difficult breaking of the C-C bond of ethanol, has been widely involved in the formulation of catalysts, in particular, as an active element for supported catalysts. It was reported very early that in the presence of Ni the activity of the catalysts increases very strongly, and makes it possible to move the conversion to a lower temperature. And, the key to low temperature performance (down to 300 °C) has been proposed to be the dehydrogenation of ethanol to adsorbed CH_3CHO species (CH_3CHO_{ads}) [137]. The very high activity of nickel has made it a good alternative to the use of noble metals, such as rhodium, a metal very active in ESR and OSRE but also very expensive. Thus, it has been reported in numerous publications that metallic nickel Ni^0 is the most active of the transition metals in ESR and OSRE [37, 408-414]. However, in parallel with its very high activity, Ni leads to the significant formation of carbon, which presents a major drawback. Consequently, much research has focused on optimizing the preparation and formulation of Ni-based catalysts in order to maintain high activity while limiting carbon formation. Although it is generally recognized that the determining (limiting) step is the breaking of the C-H bond, the exact nature of the active and selective nickel species is still the subject of debate in the literature.

Addition of zirconium improves the performance of the catalyst in OSRE. At a low value of 1.4 and low nickel content (x = 0.5), $CeNi_xO_y$ catalysts deactivate sooner after around two hours under stream and only by doping these catalysts with zirconium increases the stability of these compounds to prevent deactivation and improve ethanol conversion. At this ratio, high amounts of carbon are formed within time (around 274 mg/h.$g_{catalyst}$ using $CeNi_xO_{y\,(c)}$) in both series of binary and ternary Zr based catalysts however the amount of carbon formed in presence of Zr based catalysts is still inferior to those of binary catalysts. It was reported that ZrO_2 improves the oxygen storage capacity of CeO_2 which improves catalytic activity [303]. Fornasiero et al. reported too that catalysts based on $Ce_xZr_yO_z$ have a high OSC and redox property [415].

Doping the catalyst with Zr is better than doping with Al, since this can decrease the amount of byproducts obtained and eliminate the possible carbon formation that could be produced on Al based catalysts. Al compounds can be considered better when using low Ni/Ce ratio (0.5) since it can be started at lower temperatures unlike the Zr based compound with low Ni/Ce ratio. Doping $CeNi_xO_y$ catalysts with Zr leads to higher conversions of ethanol (97-100 %) compared to that doped with Al (86 – 96 %) and higher H_2 percentage with lower acetaldehyde percentage when considering x values higher than 0.5. Al_2O_3 being acidic was more prone to deactivation

on account of coke formation [416.] Oxides like CeO_2, ZrO_2, MgO, ZnO, and La_2O_3 or mixed oxides, could inhibit carbon deposition to some extent [137, 417, 418.]

O_2/EtOH ratio is an important factor in OSRE process. On $CeNi_1O_y$ binary catalyst an increase in O_2/EtOH ratio from 1.42 to 1.56 decreases carbon formation from 274 mg/h.$g_{catalyst}$ to 185 mg/h.$g_{catalyst}$. In order to eliminate carbon formation totally, it is necessary to increase this ratio to 1.7. Tarek found out that with O_2/EtOH ratios ranging from 0.1 to 1 mol of oxygen/mol of ethanol for a constant S/E ratio in the feed on 30 % Ni/CeO_2–ZrO_2 catalyst at 600 °C and at a fixed W/F_{AO} value of 9.17 Kgcat h/Kg mol[EtOH], conversion increased from 90 % to 95 % when O_2/EtOH ratio was changed from 0.1 to 0.2 and complete conversion of ethanol was achieved with O_2/EtOH ratio of 0.35 (600 °C) [174]. In our case, lower oven temperature of 50°C is used with higher O_2/EtOH ratio of 1.7. At this O_2/EtOH ratio, the studies on $CeNi_xO_y$ and $CeNi_xZr_{0.5}O_y$ (dried and calcined) catalysts where x = 0.5, 1, 2 and 5 under EtOH/H_2O/O_2/N_2 = 1:3:1.7:N_2 reaction mixture, finally leads to get the best catalytic results with $CeNi_5O_{y\,(d)}$ among the binary catalysts, where a conversion of 94 % ethanol is achieved with a products distribution of 49 % H_2, 34 % CO_2 and 16 % CO (where the pretreatment temperature is 250 °C). Yet $CeNi_5Zr_{0.5}O_{y\,(c)}$ is considered the best among binary and ternary catalysts under these conditions giving 100 % conversion of ethanol and the highest hydrogen percentage in products distribution (52 %), with 38 % of CO_2 and only CO (10 %) as a by-product. In literature, a minimum value of O/C-ratios of 1 was needed to reach an almost carbon free operation at 600 °C over Ni/$Ce_{0.6}Zr_{0.4}O_2$ and Ni/$MgAl_2O_4$ catalysts [419]. In that study, when oxygen was added to the system, the overall reaction changed from being endothermic at an O/C-ratio below 0.36 to exothermic at O/C-ratios above this value. This is similar to our observations leading to increase of the temperature of catalytic bed to values higher than 300 °C knowing that the oven temperature is fixed at 50 °C.

The calcination step subjected to the catalyst prior to OSRE has a drastic effect on carbon formation when considering low O_2/EtOH ratio of 1.42. The amount of carbon produced in OSRE with $CeNi_1O_y$ catalyst after calcination is around 13 times greater (274 mg/h.$g_{catalyst}$) than those on the dried catalyst (21 mg/h.$g_{catalyst}$). However, one can remark that the results obtained on the dried and calcined $CeNi_5Zr_{0.5}O_y$ and $CeNi_5O_y$ compounds are relatively small, while the dried compound requires much less energy to be prepared. Other studies showed that calcination was pivotal in deciding the activity and stability of Ni catalysts and that at a high calcination temperature of 900 °C, the textural and crystalline structure of the catalysts were

destroyed and that a low calcination temperature of 300 °C allowed the formation of carbon deposits on spent catalysts which easily led to catalyst deactivation [420]. In contrast, carbon deposition on spent catalysts calcined at 900 °C exhibited higher crystallization or graphitization, which was not affecting catalytic reaction stability.

The mass of the catalyst has to be considered during OSRE depending on the rate of feed gases and the diameter of the reactor. The study of increasing mass of catalyst of $CeNi_2Zr_{0.5}O_y$ and $CeNi_5Zr_{0.5}O_y$ calcined compounds proves that an increase of mass from 30 mg to 60 mg only leads to the formation of more carbon. The amount of carbon formed increases from 16 to 68 mg/h.$g_{catalyst}$ with $CeNi_2Zr_{0.5}O_{y\ (c)}$ and from 0 to 9.2 mg/h.$g_{catalyst}$ with $CeNi_5Zr_{0.5}O_{y\ (c)}$. Therefore, this value has to be optimized to avoid carbon formation and later possible deactivation of the system. The mass of catalyst used with respect to the feed amount affects the contact time during oxidative steam reforming. It has been reported that the amount of carbon should continuously increase as the space time increased leading to deactivation of the catalyst [421]. However, due to the redox properties of the support, this did not happen, and was attributed the stability of these Ce based catalysts to the high oxygen mobility of ceria, allowing the oxidation of carbon deposits and keeping the active surface of the catalyst clean from carbon [422].

Pretreatment of the catalyst in hydrogen plays a role in OSRE activity. Without pretreatment, the activation (starting) temperature under reaction stream of the catalyst must be raised till 250 °C (and in some cases to 280 °C) instead of 200 °C in addition to some carbon formation. The calcined binary compounds without pretreatment show better performance in OSRE when $x \leq 2$ in terms of higher concentrations of hydrogen and carbon dioxide formed compared to those with pretreatment in hydrogen. However, at high Ni content where x = 5, 14 mg/h.$g_{catalyst}$ of carbon are formed on binary catalysts without pretreatment in hydrogen gas. On the calcined catalysts doped with Zr, a pretreatment step can be more recommended when x = 1 and 2 to avoid carbon formation. However, on the dried catalysts doped with zirconium, when nickel content is low x = 0.5, lower ethanol conversion is obtained in addition to low H_2 % (around 27 %) in products distribution. The temperature of *in-situ* pretreatment in hydrogen chosen for the catalyst prior to the oxidative steam reforming reaction is important to consider depending on the first TPR peak obtained for the catalysts. Using $CeNi_2Zr_{0.5}O_{y\ (c)}$ as a catalyst, and with different pretreatment temperatures of 200 °C, 250 °C, 400 °C and 500 °C, only slight variations are obtained in products distribution and in none of them carbon is recorded. However, in

literature, it has been shown on some compounds that when treatment temperature was increased, mesoporous structure of ceria collapsed and the pore structure was significantly distorted at temperatures over 400 °C followed by a significant decrease in surface area and pore volume of these catalytic materials as a result of the increase in treatment temperature [423]. While the surface area of the catalyst pretreated (calcined/reduced) at 400 °C was of 82.8 m^2/g, it decreased to 12.8 m^2/g at the treatment temperature of 650 °C [423, 424]. The catalysts studied in this thesis creates lattice defects however enough stable not to cause drastic distortion of the lattice and later failure of catalytic performance even at 500 °C (the maximum pretreatment temperature studied).

As a matter of minimizing energy consumption, low pretreatment temperatures in hydrogen are used (200 °C and 250 °C) and the best results are obtained on the binary and ternary catalysts with high Ni/Ce ratio (x = 5). However, for aluminum-based compounds, a pretreatment temperature of 300 °C allows to eliminate carbon formation even if, it triggers higher percentages of CO and CH_3CHO (24.1 and 2.6 %, respectively) and lower H_2 percentage (38.2 %) than those obtained with pretreatment temperature of 250 °C (42.7 % H_2, 15.4 % CO and 2.1 % CH_3CHO) when x = 1. It has been previously proposed that the previous reduction of the catalyst in hydrogen generates the metallic phase directly in the catalytically active form [425] and that the presence of catalysts with Ni particles can triple the particle size after this process as a result of metal sintering, which can lead to rapid deactivation of the catalytic system [425, 426]. However, here, all the catalysts are structurally and chemically stable whether binary or ternary, dried or calcined wherein, H_2 percentage in products distribution remain almost not affected with and without the pretreatment process leading only to slight changes. Even in the absence of *in-situ* pretreatment in hydrogen for catalysts before OSRE, generally good ethanol conversions and products distribution percentages are obtained over time showing that the used material is able to produce readily partially reduced sites to initiate OSRE process., All of this point to the existence of a cooperative effect between cations, as was mentioned by other researches studying the promoting cooperative effect resulting by adding small amounts (1/15 molar ratio) of Ni, Fe, Cr, Re, Mn, W, Mo, V, and Ta oxides to a Co/Al_2O_3 catalyst on catalyst performance [425]. This effect helps to overcome the inherent problems or disadvantages of each active phase. And, thus the reduction of up to metallic state is avoided by the presence of strong interaction with other cations and thus leading to reactivation and regeneration of the sites

through increased oxygen mobility and storage capacity which is compatible with Raman and XPS results after test.

The studied catalysts present great stability over time (with O_2/EtOH ratio of 1.7) even after 31 hours under OSRE. The most interesting catalytic results are also conducted for 80 hours to prove the stability even for long term tests. Other groups of researchers reported a slight decrease in ethanol conversion for oxidative steam reforming of ethanol over a Ni-based ceria-zirconia catalyst [174, 427]. The stability of the catalyst persisted over time due to the strong metal-oxide interactions between metal and ceria that enhanced the transfer of oxygen-hydrogen species to the initially formed carbon residues and thus improved the oxidation of surface carbon and prevented the metal crystallites from encapsulation by carbon species [428]. The high stability and activity of the catalyst used here is supported by the high oxygen storage-release capacity of Ce-Ni-(Al, Zr)-O solid solution, which can help in carbon removal along with presence of ceria solids having large amount of labile oxygen together with the presence of oxygen gas in OSRE thus avoiding the pathway of deactivation by carbonaceous deposits, and/or can present active sites that are enough selective to avoid carbon formation. In addition, the incorporation of Zr, Al and Ni cations in CeO_2 enhances its lattice defects and the improved defect densities promote dissociation of water by forming bridging OH group as well as help to dissociate adsorbed ethanol molecules by forming Type II ethoxy species [285, 294]. This cooperative effect is validated by characterizing these catalysts by Raman and XPS techniques after test that ensures the persistence of these cations and their continuous transformation from one oxidative state to another by reduction and oxidation and the oxygen vacancies attributed to this process. More defects and oxygen vacancies are introduced into the lattice leading to shifts and broadness in the main F_{2g} ceria peak and appearance of typical Raman peaks. Variations in percentages of Ce^{3+} and Ce^{4+} are observed after test however the main species are found in the more oxidized state. Low evidence of metallic nickel is observed with $CeNi_5Zr_{0.5}O_{y\ (d)}$ after test of 80 hours, on $CeNi_5Zr_{0.5}O_{y\ (c)}$ with pretreatment in H_2 at 250 °C (after 80 hours) and pretreatment in H_2 at 200 °C (after 31 hours). All these experiments prove good tendency towards carbon elimination where no carbon is formed in almost all the conditions. In this context, in accordance to the present studies, the participation of nickel appears mainly in contribution to Ni^{2+} oxidation state as reported in all XPS results after test (with some exceptions evidencing formation of metallic nickel). The increase of Ni content allowing to

reach better OSRE results is related to the well maintaining of the Ni^{2+} cations during the OSRE process.

The objective of this study is to promote the products of the oxidative steam reforming reaction of ethanol (H_2 and CO_2) while minimizing the percentage of CO in the distribution of products as well as the formation of carbon. The main reactions that can occur during the reaction are shown in the following equations:

Steam reforming of ethanol: $C_2H_5OH + 3\ H_2O \rightarrow 6\ H_2 + 2\ CO_2$ equation (33)

Partial oxidation of ethanol: $C_2H_5OH + 1.5\ O_2 \rightarrow 3\ H_2 + 2\ CO_2$ equation (34)

And thus, the oxidative steam reforming of ethanol is:

$C_2H_5OH + a\ H_2O + b\ O_2 \rightarrow c\ H_2 + d\ CO_2$ equation (35)

However, as presented in the bibliographical section, many reactions can be carried out in parallel with the oxidative steam reforming of ethanol (Equations below).

1) Dehydrogenation of ethanol: $C_2H_5OH \rightarrow CH_3CHO + H_2$ equation (36)
2) Decomposition of ethanol into acetaldehyde: $C_2H_5OH \rightarrow C_2H_4O + H_2$ equation (37)
3) The decomposition of acetaldehyde: $C_2H_4O \rightarrow CH_4 + CO$ equation (38)
4) Boudouard's reaction: $2\ CO \rightarrow C + CO_2$ equation (39)
5) Hydrogenation of carbon monoxide: $CO + 3\ H_2 \rightarrow CH_4 + H_2O$ equation (40)
6) The water gas shift: $CO + H_2O \rightarrow CO_2 + H_2$ equation (41)
7) Dehydration of ethanol to ethylene: $C_2H_5OH \rightarrow C_2H_4 + H_2O$ equation (42)
8) The total decomposition of ethanol: $C_2H_5OH \rightarrow C + CO + 3\ H_2$ equation (43)
9) Hydrogenation of carbon dioxide: $CO_2 + 4\ H_2 \rightarrow CH_4 + 2\ H_2O$ equation (44)

These reactions generate product distributions that are very different from those obtained for an ideal oxidizing steam reforming. This explains why, depending on the reaction parameters and depending on the catalyst, totally different results can be obtained. The routes for carbon formation are mainly the following: (a) the ethanol dehydration to ethylene, followed by polymerization to coke; (b) the Boudouard reaction; and (c) the decomposition reaction and

CH_x species formation [137]. Ethanol dehydration to ethylene is usually associated to acidic sites [429]. The dehydration and cyclization of ethylene on strong acid sites results in the formation of polynuclear hydrocarbons, which remain strongly adsorbed on acid sites causing loss of activity or form multilayer coke layers fouling the catalyst [430]. However, in our work, the formation of carbon through this route cannot be considered as ceria is known as a basic compound. With Boudouard reaction, it has been reported that at low temperatures (lower than 400 °C), CO decomposed to C and CO_2, while at higher temperatures, between 500 and 800 °C, significant amounts of CO and CO_2 were present, while above 1000 °C, almost all the CO_2 reacted with C to form CO gas [431]. In our case, the catalytic bed temperature being less than 400 °C, Boudouard reaction tend to the direction of formation of carbon and carbon dioxide. However, since CO_2 and H_2 are the main products obtained by ideal oxidative steam reforming, CO_2 becomes in excess with respect to the equilibrium of Boudouard's reaction, that can lead to a reverse reaction allowing the elimination of carbon by this route and thus formation of carbon monoxide [432]. The route leading to carbon formation through decomposition of ethanol into acetaldehyde and its further decomposition to CO and CH_4 can only lead to carbon formation through Boudouard's reaction also. Finally, the more probable route for carbon formation is through total decomposition of ethanol. The carbon produced by this process could also react back through the inverse of Boudouard's reaction and lead to its elimination and thus allowing to reach a carbon free process for hydrogen production. Some scientists tried to minimize the carbon deposition problem by adding hydrogen to the feed instead of oxygen to hydrogenate unsaturated compounds like ethene and therefore decrease the deposition of carbon [419]. The additional H_2 ensured that the catalyst was reduced under the reaction conditions. It was investigated that [433] addition of H_2 at H/C-ratios between 0 and 5 at S/C-ratio of 1.5 led to a decrease in hydrocarbon yield and carbon deposition on Ni/CeO_2 and Ni/Al_2O_3 at 900 °C. In the present study, the stability of the materials and the auto regeneration of cations in the feed allows eventually to eliminate carbon formation (if this is the case) where at the same time, the hydrogen produced by the process can also lead to hydrogenation reaction leading to elimination of carbon. Oxygen introduced into the feed acts as a tool for carbon elimination in addition to the oxygen inside the lattice and in particular for ceria and Ce-Zr-O solid solution. It has been reported that the higher resistance to carbon formation observed for the embedded catalysts was a consequence of the higher oxygen mobility in these materials and that the capacity of the support to transfer oxygen from its structure to the coked metal promoted the

carbon removal mechanism [434, 393]. Under oxygen, the carbon produced can burn into carbon dioxide or carbon monoxide by the following reactions:

$C + O_2 \rightarrow CO_2$ (equation 45)

$C + 0.5\ O_2 \rightarrow CO$ (equation 46)

Moreover, the presence of oxygen can also slow down both the adsorption of H_2 on Ni sites hindering the reduction of Ni^{2+} into Ni^0, and the adsorption of CO or CH_4 products by formation of oxidative products (CO_2 and CO). And in case when carbon is formed, it prevents the dissolution of gasified carbon in Ni particles and further diffusion through the metal, hindering the nucleation and growth of filamentous coke [179].

Based on all the above results discussed, it is reasonable to conclude that $CeNi_xO_y$ and $CeNi_xM_nO_y$ catalysts have the same active species. That is the Ni cations strongly interacting with Ce cations in binary $CeNi_xO_y$ compounds and the Ni cations showing strong interactions with Ce and Zr or Al cations in ternary compounds. Such active Ni species either in the solid solution of Ce-Ni-O and Ni-Zr-(Al)-O and/or at the interface of small nanoparticles of NiO, CeO_2, or Ni-Zr-(Al)-O, can be easily reduced and reoxidized due to the strong interactions between Ni^{2+} cations and other cations (Ce^{4+}, Ce^{3+}, Zr^{4+} and Al^{3+}) in the oxide catalyst. Therefore, Ni-based mixed oxides with the same proportion of Ni among the metals (molar ratio) can demonstrate very similar catalytic performances for OSRE, but the selectivity and stability can be affected by the presence and nature of other elements. Therefore, it can proposed that the active and selective site belongs to a partially reduced catalyst (oxyhydride) involving an anionic vacancy, an O^{2-} species, and cations, which is formed during the *in-situ* H_2 treatment. The active site can be formed also under reaction mixture, as a slightly higher temperature is required to start the reaction (like 250 °C instead of 200 °C). The presence of ethanol in the reaction mixture, and in temperature can lead to similar site.

In our laboratory, a mechanism for the reduction of binary mixed oxides was proposed which takes into account the reduction of cerium [321] (Eq. 47 – 49):

1) $2\ Ce^{4+} + O^{2-} + H_2 \rightarrow 2\ Ce^{3+} + H_2O + \square$ equation (47)

2) $Ni^{2+} + O^{2-} + H_2 \rightarrow Ni^0 + H_2O + \square$ equation (48)

3) $2\ Ce^{4+} + Ni^0 \leftrightarrow 2\ Ce^{3+} + Ni^{2+}$ equation (49)

The partial reduction of the solid, during pretreatment in H_2 at low temperature (200 – 300 °C), with the increased formation of anionic vacancies allows the insertion of hydrogen atoms inside the solid. As a matter of fact, the heterolytic rupture of H_2 on a set formed by an anionic vacancy and an O^{2-} ion (equation 50) has been proposed, with the evidence of the formation of nano-oxyhydrides on these compounds [96, 97, 105, 157, 238, 323]. The elimination of hydroxyl groups can regenerate the site constituted of O^{2-} ions and anionic vacancy with the desorption of water (equation 51).

$$H_2 + O^{2-} + \square \rightarrow OH^- + H^- \qquad \text{equation (50)}$$

$$2\ OH^- \rightarrow O^{2-} + H_2O + \square \qquad \text{equation (51)}$$

The formation of the H^- (hydride) species and their insertion into mixed oxides are based on mechanisms proposed in previous works carried out in the laboratory in particular on cerium-nickel based compounds and doped with Al or Zr [321, 336, 435-441]. Highly reactive hydride species will react with O_2 to generate hydroxyl groups (equation 52). The ability of the solid to abstract hydrogen species from ethanol is the important step. Even when the catalyst is not pretreated and reduced in H_2, it exhibits a high redox system able to form oxygen vacancies and extracting hydrogen from ethanol once activated by temperature.

$$H^- + 0.5\ O_2 \rightarrow OH^- \qquad \text{(equation 52)}$$

The Ce and Zr based catalysts, known for their high oxygen mobility, allows it to give more promising catalytic performance [416] than that of Al as mentioned before. The diffraction peaks of ZrO_2 and Al_2O_3 were not found by XRD analysis of both fresh and spent catalysts where a solid solution with Zr or Al, Ni with ceria phase is formed. The presence of a solid solution of cerium and nickel and zirconium or aluminum makes it possible to increase strongly the oxygen mobility and thus the number of anionic vacancies created [393]. These mixed oxides based on ceria are known for their high oxygen storage capacity (OSC) and ability to store and release oxygen during reactions (redox properties). Moreover, the presence of Zr cations inside ceria phase further enhances the ceria OSC through the presence of the Ce-Zr-O solid solution, thermal and mechanical stability and promotes the water gas shift reaction [442, 443] and therefore in the OSRE, Ce and Zr based catalysts show better performance and greater stability and in

particular, more visible when the conditions of low nickel content and oxygen molar ratio together are set together.

Finally, these different observations make it possible to propose an active site consisting of 2 cations in close interaction in the solid solution of Ce, Ni, Zr/Al (Figure 92). This model presents the advantage to be in good agreement with the synergetic effect observed when several cations with strong interactions are in presence in a mixed oxide. Metallic Ni^0 can also participate in the reaction when it is present; however, all the results obtained cannot be explained by simply attributing the activity to this species since no or low evidence of Ni^0 species is found by XPS on all compounds presenting high performance. However, carbon formation could be related to its presence. Based on the proposed active sites for $CeNi_xO_y$ and $CeNi_xM_nO_y$ catalysts, the possible mechanism for ethanol transformation can be envisaged. Molecular adsorption of ethanol on the active site is the primary step in this process [444, 445] (equation 53), as can be observed from Figure 92. The hydroxyl group (OH) from the ethanol molecule dissociates to further obtain activated ethanol.

Then, at high O_2/EtOH ratio (1.7), the easy acetaldehyde transformation in the presence of water and oxygen (equation 55) can explain the results obtained.

$$O^{2-}\ M^{n+}\ \square + C_2H_5OH \rightarrow OH^-\ M^{n+}\ H^- + C_2H_4O \qquad \text{(equation 53)}$$

$$OH^-M^{n+}H^- + CH_3CH_2OH \rightarrow OH^-M^{n+}H^- + CH_3CHO + H_2 \qquad \text{(equation 54)}$$

$$C_2H_4O + H_2O + O_2 \rightarrow 2CO_2 + 3H_2 \qquad \text{(equation 55)}$$

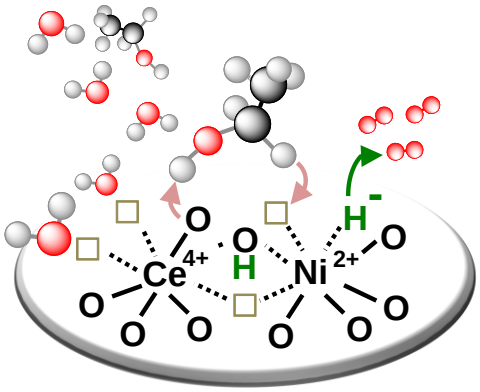

Figure 92 Proposition of active site on $CeNi_x(M_{0.5})H_zO_y$ nano-oxyhydride catalyst for EtOH activation. Ni^{2+}, Ce^{3+}, Zr^{4+} or Al^{3+} can replace a Ce^{4+} cation in the solid solution. □: anionic vacancy (position and number arbitrary).

The formed hydroxyl groups, can further be used for transformation of ethanol to CO_2 and H_2 as it has been shown that abundant OH^- groups favor CO transformation to CO_2 by water gas shift (equation 56) [99].

$$CO + H_2O \rightarrow CO_2 + H_2 \qquad \text{(equation 56)}$$

Besides, water can be also dissociated on an anionic vacancy and an O^{2-} species of the solid (equation 57). As a matter of fact, it has been shown that water dissociation can be realized when Ni^{2+} species can be stabilized in strong interaction [298] .The high reactivity of hydride species permits consumption of O_2 and then finally transformation of O_2 into the selective OH^- species (equation 52) and then into O^{2-} species which regenerate the active sites (equation 51).

$$H_2O + O^{2-} + \square \rightarrow 2\ OH^- \qquad \text{(equation 57)}$$

General conclusion

Hydrogen gas production by catalytic transformation of bio-ethanol is studied over Ni-based mixed oxide catalysts, $CeNi_xO_y$ and $CeNi_xM_{0.5}O_y$ where M = Al or Zr and x = 0.5, 1, 2 or 5. The catalysts are prepared by coprecipitation and analyzed by different methods. Elemental analysis proves the good preparation of these catalysts and their appropriate elemental composition. $CeNi_xO_y$ catalysts have a higher specific surface area for dried catalysts (81 to 198 m^2/g) than calcined ones (60 and 134 m^2/g). The specific surface area of dried Zr-based catalysts is estimated to be between 186 and 112 m^2/g, larger than those of calcined Zr-based catalysts that have a specific surface area between 71 and 130 m^2/g. Concerning Al-based compounds, this area is estimated to be between 125 and 154 m^2/g. Regardless of the catalyst, binary or ternary, dried or calcined, the ceria phase is present and has an average crystallites size between 3-5 nm. CeO_2 XRD diffraction patterns become broader following the decrease in CeO_2 average crystallites size. NiO phase is not always present at low Ni ratios. No phases associated to Zr or Al are visible by XRD. Different Ni^{2+} species are reducible according to the TPR analysis: those with strong interaction in solid solution of cerium and nickel (and Al, or Zr), those of small nanoparticles possibly present (not visible by XRD), and those observed in XRD. Finally, the Raman results are consistent with the formation of a solid solution of cerium and nickel. Moreover, previous analysis have shown that these mixed oxide catalysts are capable of storing large quantities of hydride-type hydrogen species, with formation of oxyhydride ($CeNi_xH_zO_y$ and $CeNi_xM_{0.5}H_zO_y$) compounds after pretreatment under H_2 at an adequate temperature.

The influence of several parameters on the products of the reaction is analyzed in oxidative steam reforming such as: the influence of the reaction mixture by varying O_2/EtOH ratio, pretreatment in hydrogen, mass of catalyst, calcination, Ni content, doping, as well as the stability of catalysts in OSRE over time.

With an O_2/EtOH ratio of 1.42, $CeNi_xO_y$ dried and calcined catalysts could only possess stability in OSRE over time when $x \geq 1$ however by adding zirconium, stability of catalytic results over time is achieved. The best results obtained under these conditions are with $CeNi_1O_y$ and $CeNi_2Zr_{0.5}O_y$ yet but with production of high amounts of carbon. Different O_2/EtOH ratios of 1.42, 1.56 and 1.7 are adjusted and used under same conditions mentioned before with the calcined catalyst $CeNi_1O_y$ showing that the main effect obtained is on carbon formation such that a little change in this ratio (from 1.4 to 1.56 to 1.7) allows the carbon amount droping from 274 $mg/h.g_{catalyst}$ to 185 $mg/h.g_{catalyst}$ and finally to 0 $mg/h.g_{catalyst}$ respectively after 5 hours in

OSRE. So, finally to limit carbon formation, the O_2/EtOH ratio of 1.7 is then used in the OSRE reaction studied. It is investigated that the main products distribution percentages increase with the increase in nickel content while CO and CH_4 decrease in both binary and ternary catalysts while maintaining total conversion of ethanol and stability of catalytic test over time (5 or 31 hours).

Without *in-situ* pretreatment in hydrogen, the activation temperature of the catalyst must be raised till 250 °C instead of 200 °C in addition to some carbon formation. With pretreatments of 200 °C, 250 °C, 400 °C and 500 °C, only slight variations are obtained in products distribution and in none of them carbon is recorded. As the objective of this study is to minimize the energetic consumption, some studies are conducted with a lower pretreatment temperature in hydrogen of 200 °C or 250 °C and others without pretreatment in hydrogen at all. In the case of catalysts without in-situ pretreatment in hydrogen, $CeNi_xO_{y\ (c)}$ and $CeNi_xZr_{0.5}O_{y\ (c)}$ catalysts require an activation temperature of 250 °C while $CeNi_xZr_{0.5}O_{y\ (d)}$ require an even higher temperature of 280 °C for activation. The calcined binary compounds without pretreatment show better performance in OSRE when $x \leq 2$ in terms of higher concentrations of hydrogen and carbon dioxide formed compared to those with pretreatment in hydrogen however, at high Ni content where x = 5, 14 mg/h.$g_{catalyst}$ of carbon are formed. Furthermore, on the dried catalysts doped with zirconium without in-situ pretreatment in H_2, when nickel content is low x = 0.5, lower ethanol conversion is obtained in addition to low H_2 % (around 27 %) in products distribution. *In-situ* pretreatment in hydrogen (at 200 °C or 250 °C) gas allows to eliminate carbon formation on calcined Zr based catalysts when x = 1 and 2.

The zirconium-based catalysts with $x \leq 2$ give better results with pretreatment temperature of 200 °C than that of 250 °C in terms of products distribution in the calcined series. However, at a higher Ni/Ce ratio of 5, this difference is no more noticeable and only slight variations are obtained with this little change in temperature. Similar results are obtained on the dried catalysts after pretreatment at 200 °C where it is shown that $CeNi_5Zr_{0.5}O_{y\ (d)}$ gives the best results among the dried series with higher performance in OSRE. 100 % of ethanol conversion is obtained using this catalyst with 50.9 % H_2, 40.8 % CO_2, 6.9 % CO and almost 0.9 % of CH_4 and 0.5 % CH_3CHO in products distribution. Calcination allows to get better catalytic results on catalysts with low Ni content however with higher nickel content, no evident variations are observed. All the studied compounds exhibit stability over 31 hours with no carbon formation except with $CeNi_2Zr_{0.5}O_y$ (dried and calcined) yet does not exceed 12 mg/h.$g_{catalyst}$. The study of higher mass

of catalyst is investigated on $CeNi_2Zr_{0.5}O_y$ and $CeNi_5Zr_{0.5}O_y$ calcined catalysts to reveal that an increase of mass from 30 mg to 60 mg only allows the formation of more carbon (from 16 to 68 mg/h.$g_{catalyst}$ with $CeNi_2Zr_{0.5}O_{y\ (c)}$ and from 0 to 9.2 mg/h.$g_{catalyst}$ with $CeNi_5Zr_{0.5}O_{y\ (c)}$).

Doping the catalyst with Zr shows much higher conversion of ethanol (97-100 %) compared to that doped with Al (83-96 %) and better distribution of products in terms of higher H_2 percentage and lower acetaldehyde percentage. However, at low Ni/Ce ratio (0.5), Al-based catalysts require lower starting temperature (200 °C) than those of Zr-based catalysts (250 °C) for OSRE after *in-situ* pretreatment in H_2 at 250 °C.

Catalysts under specific reaction conditions with the best results are conducted again for 80 hours in OSRE to check their stability for a long time ($EtOH/H_2O/O_2/N_2$ = 1:3:1.7: N_2 and D_L = 0.1 ml/min). $CeNi_5Zr_{0.5}O_{y\ (c)}$ pretreated in H_2 at 250 °C gives the best results: 100 % conversion of ethanol, and 51 % H_2, 36 % CO_2 and 12.6 % CO, 0.1 % CH_3CHO and 0.4 % CH_4 in products distribution. While $CeNi_5Zr_{0.5}O_{y\ (d)}$ pretreated in hydrogen at 250 °C leads to 100 % of ethanol conversion and 47.2 % H_2, 34.7 % CO_2, 15.6 % CO, 1.8 % CH_4 and 0.7 % CH_3CHO in products distribution. The same catalyst in same conditions, tested again without pretreatment in hydrogen, shows stable results as reported after 5 hours. Finally, $CeNi_2Al_{0.5}O_y$ pretreated in hydrogen at 300 °C allows 100 % conversion of ethanol distributed among the following products: 43.9 % H_2, 34.7 % CO_2, 18.8 % CO, 1.3 % CH_3CHO and 1.3 % CH_4 after 80 hours in OSRE. All the presented studies show high stability over 80 hours in OSRE as well carbon elimination during the process. The $CeNi_xH_zO_y$ and $CeNi_xM_nH_zO_y$ oxyhydrides (30 mg) obtained by H_2 treatment enable to completely convert ethanol (100 %) and produce H_2 at room temperature through the oxidative steam reforming of ethanol ($H_2O/EtOH/O_2$ = 3:1:1.7). The energy released from the strong exothermic reaction between the hydride species stored in the catalysts is used to drive the reaction, which allows lowering the oven temperature down to only 50 °C. A huge variation of temperature between the catalyst bed and the oven therefore can be observed. In the meantime the hydride species are continuously formed from ethanol to make the reaction sustainable. The Ni content strongly affects the products distribution while the performance is mainly related to the hydrogen storage capacity of the solid depending also on the Ni content. Both catalytic systems show very good stability after about 80 h on stream.

The percentages between $Ce^{3+}$and Ce^{4+} vary after test however the main contribution corresponds to Ce^{4+} cations. Raman analysis insures the increase of oxygen vacancies induced by the solids after test proving that the interactions between cations persist and even in higher

proportion after test. Some evidence for graphitic type carbon is obtained followed by low evidence of metallic nickel (around 10 %) with $CeNi_5Zr_{0.5}O_{y\ (d)}$ after test of 80 hours. Some evidences of Ni^0 (around 13 %) is collected too on $CeNi_5Zr_{0.5}O_{y\ (c)}$ with pretreatment in H_2 at 250 °C (after 80 hours) and pretreatment in H_2 at 200 °C (after 31 hours). Raman analysis shows that more defects and oxygen vacancies are introduced into the ceria lattice assuring the continuous redox processes occurring in OSRE reaction leading to the good performance and stability over time. The carbon reported in XPS and Raman is globally mainly due to adventitious carbon in agreement with the mass variation method of calculation.

The studied $CeNi_xO_y$ and $CeNi_xM_{0.5}O_y$ catalysts show very similar evolution of ethanol conversion and products distribution for OSRE with increased nickel content due to the homogenous distribution of the same active Ni species surrounded by different neighbor atoms. The catalysts show strong performance in OSRE in addition to being a convenient route for reducing the processing time prior to OSRE activation and reducing expenses by skipping the pretreatment step in hydrogen (due to ability of forming oxyhydrides under reaction at higher temperatures of 250 °C) and calcination of the catalyst. Such active Ni species either in the solid solution of Ce-Ni-O and Ni-Ce-(M)-O and/or at the interface of small nanoparticles of NiO, CeO_2, or Ni-Ce-(Al/Zr)-O, can be easily reduced and reoxidized (possibly existing as Ni^0, Ni^{2+}, $Ni^{\delta+}$ in the system) due to the strong interactions between Ni^{2+} cations and other cations (Ce^{4+}, Ce^{3+} Zr^{4+} and Al^{3+}) in the oxide catalyst.

The correlations between the physicochemical characterizations and the catalytic performances make it possible to conclude that the very important activity of the catalysts $CeNi_x(M_{0.5})O_y$, with M = Al or Zr, is due to the strong interactions existing between the nickel and the cerium cations (with aluminum or zirconium). Finally, taking into account all the results obtained, various discussions presented in the literature, as well as the structure of solids, an active site involving interacting Ni species strong with other cations, and a reaction mechanism involving hydride species are proposed. This active site belongs to a partially reduced catalyst (oxyhydride) involving an anionic vacancy, an O^{2-} species, and cations, which is formed during the *in-situ* H_2 treatment or upon high starting temperature of the reaction. Ethanol can be heterolytically dissociated on such a site and converted to different products depending probably on the nature of the other cation in presence and also the number of anionic vacancies.

Annex

Preparation of the catalysts:

The following catalysts $CeNi_xO_y$ (binary) or $CeNi_xM_{0.5}O_y$ (ternary), where M = Al or Zr were prepared using precursors based on nitrates: Ni $(NO_3)_2.6H_2O$ (purum > 97.0 % - Fluka), $Ce(NO_3)_3.6H_2O$ (purity ≥ 99.0 % - Fluka), $Al(NO_3)_3.9H_2O$ (ACS reagent ≥ 98 % - Sigma-Aldrich) and $Zr(NO_3)_4.5H_2O$. The method utilized is co-precipitation. The nitrates solution with a concentration of 0.5 mol/l is coprecipitated using a mixture of methanol and triethylamine (TEA). The resulting mixture is then mixed and filtrated. Finally, the catalyst obtained is dried overnight at a temperature of 100 °C and then calcined at a temperature of 500 °C. The masses of metallic nitrates are calculated based on the following formulas:

Mass $Ce(NO_3)_2 = C * V_{Ce} * M(Ce(NO_3)_2) / purity$

Mass $Ni(NO_3)_2 = C * V_{Ce} * M(Ni(NO_3)_2) / purity$

Mass $Zr(NO_3)_2 = C * V_{Ce} * M(Zr\ (NO_3)_2) / purity$

$V_{Ni} = V_{Ce} * x$

$V_{Zr} = V_{Ce} * y$

$C = 0.5$ mol/l

Characterizations of the catalysts:

X-Ray diffraction (XRD) analysis are conducted on a Brüker D8 Advance X-ray diffractometer. The diffractograms are recorded at $2\theta = 20\text{-}90°$, with a pitch of 0.02°. The average crystallites size was calculated based on the width of the main diffraction peak as assessed with the MDI Jade 6.5 software using the Scherrer equation from the most intense reflections observed for the NiO and CeO_2 crystallographic structures: (1 1 1), (2 0 0), and (2 2 0).:

$D_{hkl} = K \cdot \lambda / B \cdot \cos\theta$

Where;

K is a structure constant (0.9 for spherical crystals)

λ is the incident ray wavelength

B is the peak width at half height after correction for instrumental broadening

θ is the Bragg angle.

Surface area analysis (BET) analysis are carried out by physisorption of N_2 at 77 K on a TriStar II 3020 machine. Before being analyzed, the samples are evacuated at 150 °C for 3 hours.

Raman analysis are carried out on a LabRam Infinity machine equipped with a Nd-YAG light source at $\lambda = 532$ nm and at room temperature.

Temperature-programmed reduction (TPR) analysis are performed on the MicroMeritics Autochem II Chemisorption Analyzer. Hydrogen consumption is measured using a TCD detector. The sample is treated in a mixture composed of 5 % hydrogen and 95 % argon at a flow rate of 30 $ml.min^{-1}$. The temperature is increased to 1000 °C at a rate of 10 °C per minute.

Relative content of oxide is determined with the use of an energy dispersive micro-XRay Fluorescence spectrometer M4 TORNADO (Bruker). This instrument is equipped with 2 anodes a Rhodium X-ray tube 50 kV/600 mA (30 W) and a Tungsten X-Ray tube 50 kV/700 mA (35 W). For sample characterization, the X-rays Rhodium with a polycapillary lens enabling excitation of an area of 200 μm was used. The detector used is a Silicon-Drift-Detector Si(Li) with <145 eV resolution at 100000 cps (Mn Kα) and cooled with a Peltier cooling (253 °K). The measurement is done under vacuum (20 mbar). The elements, that can be measured by this instrument unit range from sodium (Na) to uranium (U). Quantitative analysis is done using fundamental parameter (FP) (standardless). As elements are present in stoichiometric compounds, its formula is used for quantification of the weight percent of each element. For each sample 36 points (of 200 μm) were analyzed.

The XPS analysis are carried out using the PRAS platform (Regional Surface Analysis Platform) using a KRATOS Axis Ultra machine under ultra-vacuum using a twin Al X-ray source (1486.6 eV) at a pass energy of 40 eV. The solid is placed on copper tape and then the charging effects are adjusted using the fact that the contaminating carbon should be at 285.0 eV. To calculate the percentages of the components, the peaks are decomposed and integrated using the Casa software.

Experimental Representation:

All the experiments discussed below are performed with an H_2O / EtOH equal to 3. The catalysts are previously pretreated in hydrogen with a flow rate of 33 ml/min at 250 °C overnight (unless mentioned that this step is skipped). After pretreatment, the line is purged with pure helium for 30 minutes (to avoid oxidation of the catalyst and remove H_2), and later, N_2, O_2 and ethanol-water mixture are introduced through a vaporizer (where the flow rate of O_2 and N_2 gas together is 60 ml/min and that ethanol/water liquid flow is of 0.1 ml/min). After that, oxygen is introduced to the line with a flow rate of 28.3 or 31 or 33.8 ml/min. The catalyst is deposit on a frit (having a thickness of 1 mm and porosity 3) in a tubular quartz reactor (diameter 4 mm and length around 46 cm). The frit is fixed in the middle of the tubular reactor at a height of 23 cm from the bottom of the reactor. Th reactor is surrounded by a tubular oven (around 35 cm tall) being regulated by thermocouples. The catalytic system is thermally isolated by quartz wool. A thermocouple is also fixed at the level of the catalyst to measure the temperature at the level of the catalyst. The test is started fixing the oven temperature at 200 °C. The temperature at the level of the catalyst increases after activation and is measured by the thermocouple. When this temperature stabilizes, the oven is fixed at 50 °C. The resulting gas mixture is analyzed using an Agilent gas chromatography AGILENT GC brand equipped with two thermal conductivity detectors (TCD) and a flame ionization detector (FID).

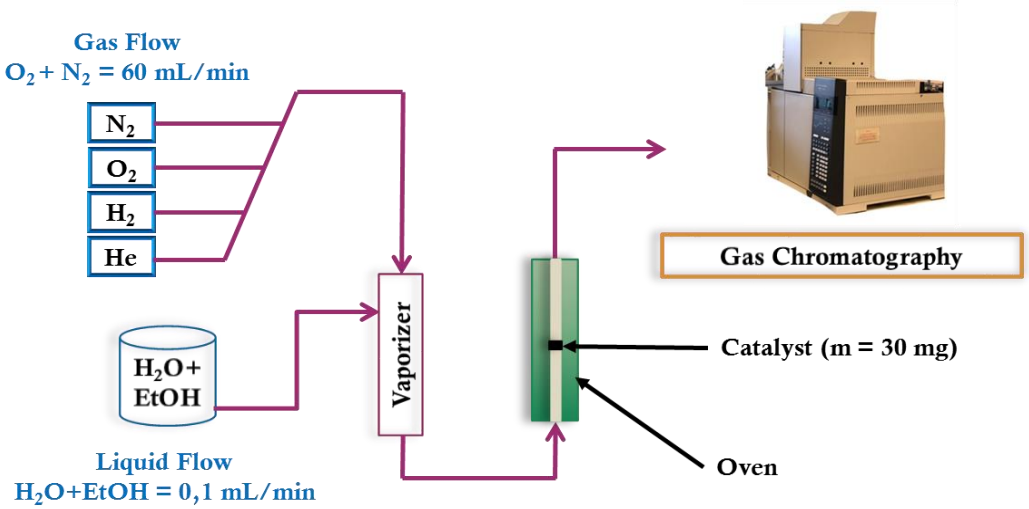

To calculate the conversion of ethanol and products distribution, the response factors of each compound are taken into account. The values are then multiplied by the areas of the peaks for each product to calculate the mole percentage and finally the percentage in products

distribution. The formulas used for the calculations of conversion of ethanol and products distribution are the following:

-Formula used for calculation of ethanol (EtOH) conversion

$\%\ Conversion_{EtOH} = (n_{EtOH(initial)} - n_{EtOH(final)}) * 100 / n_{EtOH(initial)}$

-Formula used to calculate the distribution of products (%)

$\%\ X = (nX * 100) / (\Sigma\ n_{Xproducts})$

Where, n is the number of moles,

$n_{EtOH(initial)}$ is the number of moles of ethanol entering the reactor,

$n_{EtOH(final)}$ is the number of moles of ethanol exiting the reactor,

X is the product formed which could be H_2, CO_2, CO, CH_4 or CH_3CHO.

-To calculate carbon formation after test, the mass variation method is used. The mass of the reactor (including the catalyst) after test is subtracted to the mass of the reactor (including the catalyst) before test. Before measuring, the reactors must be well dried at 100 °C.

$Mass_{carbon\ formed} = (mass_{reactor})_{after\ test} - (mass_{reactor})_{before\ test}$

Where, $mass_{reactor}$ is the mass of the system including the reactor and the catalyst.

References

[1] Website of NASA: https://climate.nasa.gov/resources/global-warming-vs-climate-change/ (last access: 10 September, 2021)

[2] BP Statistical Review of World Energy 2017. 52

[3] 20 January 2020, "Path to hydrogen competitiveness. A cost perspective", Hydrogen Council., www.hydrogencouncil.com

[4] Hydrogen Council. McKinsey study. www.hydrogencouncil.com (2017).

[5] F. Zhang, P. Zhao, M. Niu and J. Maddy, The survey of key technologies in hydrogen energy storage, Int. J. Hydrogen Energy 41, 14535-14552 (2016).

[6] B.C.R. Ewan and R.W.K. Allen, A figure of merit assessment of the routes to hydrogen, Int. J. Hydrogen Energy 30, 809–819(2005).

[7] T. da Silva Veras, T. S. Mozer, D. da Costa Rubim Messeder dos Santos and A. da Silva César, Hydrogen: Trends, production and characterization of the main process worldwide, 42, 2018-2033(2017).

[8] C. Acar, Y. Bicer, M. Emre Demir and I. Dincer, Transition to a new era with light-based hydrogen production for a carbon-free society: An overview, Int. J. Hydrogen Energy 44, 25347-25364 (2019).

[9] C. Acar and I. Dincer, Review and evaluation of hydrogen production options for better environment, J. Cleaner Production 218, 835-849 (2019).

[10] M. Frank, Alternative Fuels - The Future of Hydrogen (3rd Edition). Sustainable Energy & Development. (2013)

[11] G. Iaquaniello, F. Giacobbe, B. Morico, S. Cosenza, A. Farace, Membrane reforming in converting natural gas to hydrogen: Production costs, Part II, International Journal of Hydrogen Energy 33, 6595-6601 (2008).

[12] B. Lee, Hyunwoo Kim, H. Lee, M. Byun, Wangyun Won, Hankwon Lim, Technical and economic feasibility under uncertainty for methane dry reforming of coke oven gas as simultaneous H_2 production and CO_2 utilization, Renewable and Sustainable Energy Reviews 133, 110056 (2020).

[13] A. Waheed Bhutto, A. Ahmed Bazmi and G. Zahedi, Underground coal gasification: From fundamentals to applications, Progress in Energy and Combustion Science 39, 189-214 (2013).

[14] D. Mallick, P. Mahanta and V. Suryakant Moholkar, Co-gasification of coal and biomass blends: Chemistry and engineering, Fuel 204, 106-128 (2017).

[15] B. Pierre , G. Francois , P. Alessia, D. Jonathon, M. Gerard, D. Florence, M. Julien and G. Elisa, Low voltage water electrolysis: Decoupling hydrogen production using bioelectrochemical system. Int. J. Hydrogen Energy 43, 14867-14875 (2018).

[16] L. T. Mikka, E. Cséfalvay and Ar. Németh, Catalytic conversion to initial platform chemicals: chemistry and sustainability. Chem. Rev. 118, 506-613 (2018).

[17] A. Molino, V. larocca, S. Chaznese and D. Musmarra, Biofuels production by biomass gasification: a review. Energies 11 (2018).

[18] R. A. Sheldon, Metrics of green chemistry and sustainability: past, present, and future. ACS sustainable chemistry and engineering 6, 32-48 (2018).

[19] D. kumara and R. Singh, Pretreatment of lignocellulosic waster for biofuel production: a critical review. Renewable and sustainable energy reviews 90, 877-891 (2018)

[20] S. Naik, V. Goud, P. Rout, and A. K. Dalai, Production of first and second generation biofuels: A comprehensive review. Renew. Sustain. Energy Rev. 14, 578–597 (2010).

[21] J. Baeyens, Challenges and opportunities in improving the production of bio-ethanol. Prog. Energy Combust. Sci. 47, 60-88 (2015).

[22] H. Zabed, J.N. Sahu, A. Suely, A.N. Boyceand G. Faruq, Bioethanol production from renewable sources: Current perspectives and technological progress. Renew. Sustain. Energy Rev. 71, 475-501 (2017).

[23] C. Knocke and J. Vogt, Biofuels – challenges & chances: How biofuel development can benefit from advanced process technology. Eng. Life Sci. 9, 96-99 (2009).

[24] H. B. Aditiya, T. Mahlia, W. Chong, H. Nur, and A. Sebayang, Second generation bioethanol production: A critical review. Renew. Sustain. Energy Rev. 66, 631-653 (2016).

[25] F. Dumeignil, M. Capron, B. Katryniok, R. Wojcieszak, A. Löfberg, J. S. Girardon, S. Desset, M. Araque-Marin, L. Jalowiecki-Duhamel and S. Paul. Biomass-derived Platform Molecules Upgrading through Catalytic Processes: Yielding Chemicals and Fuels. J. Jpn Petrol. Institute 58, 257-273 (2015).

[26] V. Subramani, and C. Song, Advances in catalysis and processes for hydrogen production from ethanol reforming. Catalysis 20, 65-106 (2007).

[27] R.M. Navarro, M.A. Peña and J. Fierro, Hydrogen production reactions from carbon feedstocks: Fossil fuels and biomass, Chemical Reviews 107, 3952-3991 (2007).
[28] M. Ni, D. Leung and M. Leung, A review on reforming bio-ethanol for hydrogen production, Int. J. Hydrogen Energy 32, 3238-3247 (2007).
[29] P. R. de la Piscina and N. Homs, Use of biofuels to produce hydrogen (reformation processes). Chem. Soc. Rev., 37, 2459-2467 (2008).
[30] P. Piscina and A. Poullikkas, A comparative overview of hydrogen production processes. Renew. Sustain. Energy Rev. 67, 597-611 (2017).
[31] L.V. Mattos, G. Jacobs, B.H. Davis, F.B. Noronha, Production of hydrogen from ethanol: Review of reaction mechanism and catalyst deactivation, Chem. Rev. 112, 4094-4123 (2012).
[32] A. Haryanto, S. Fernando, N. Murali and S. Adhikari, Current status of hydrogen production techniques by steam reforming of ethanol: A review, Energy and Fuels 19, 2098-2106 (2005).
[33] N. Bion, D. Duprez and F. Epron, Design of nanocatalysts for green hydrogen production from bioethanol. ChemSusChem 5, 76-84 (2012).
[34] S. Li and J. Gong, Strategies for improving the performance and stability of Ni-based catalysts for reforming reactions, Chem Soc Rev 43, 7245-7256 (2014).
[35] A.Demirbas, Progress in Energy and Combustion Science 33, 1-18 (2007).
[36] J.L. Contreras, J. Salmones, J.A. Colín-Luna, L. Nuño, B. Quintana and I. Córdova, Catalysts for H_2 production using the ethanol steam reforming (a review), Int. J. Hydrogen Energy 39, 18835-18853 (2014).
[37] D. Li, X. Li and J. Gong, Catalytic reforming of oxygenates: state of the art and future prospects, Chem. Rev. 116, 11529-11653 (2016).
[38] N. Sanchez, R. Ruiz, V. Hacker, M. Cobo, Impact of bioethanol impurities on steam reforming for hydrogen production: A review, International Journal of Hydrogen Energy 45, 11923-11942 (2020).
[39] E. López, F. Dorado and A. de Lucas-Consuegra, Electrochemical promotion for hydrogen production via ethanol steam reforming reaction. Appl. Catal. B 243, 355-364 (2019).
[40] A.B. Calcerrada, A.R. de la Osa, E. Lopez-Fernandez, F. Dorado and A. de Lucas-Consuegra, Influence of the carbon support on the Pt–Sn anodic catalyst for the electrochemical reforming of ethanol. Int. J. Hydrogen Energy 44, 10616-10626 (2019).
[41] A. Dessì, Towards Sustainable H_2 Production: Rational Design of Hydrophobic Triphenylamine-based Dyes for Sensitized Ethanol Photoreforming. ChemSusChem 11, 793-805 (2018).
[42] B. Augusto, Nickel/gadolinium-doped ceria anode for direct ethanol solid oxide fuel cell. Int. J. Hydrogen Energy 39, 11196-11209 (2014).
[43] T. Lepage, M. Kammoun, Q. Schmetz, and A. Richel, Biomass-to-hydrogen: A review of main routes production, processes evaluation and techno-economical assessment. Biomass Bioenergy 144, 105920 (2021).
[44] S.Ogo, and Y.Sekine, Recent progress in ethanol steam reforming using non-noble transition metal catalysts: A review. Fuel Process. Technol. 199, 106238 (2020).
[45] L. Kaiwen, Y. Bin, and Z. Tao, Economic analysis of hydrogen production from steam reforming process: A literature review, Energy Sources Part B, 109-115 (2018).
[46] G. Birol, I. Önsan, B. ZKirdar and S.G Oliver, Ethanol production and fermentation characteristics of recombinant Saccharomyces cerevisiae strains grown on starch, Enzyme and Microbial Technology 22, 672-677 (1998).
[47] B, Bulawayo, J.M. Bvochora, M.I. Muzondo and R. Zvauya, Ethanol production by fermentation of sweet-stem sorghum juice using various yeast strains, World Journal of Microbiology and Biotechnology 12, 357-360 (1996).
[48] C.-F. Huang, T. Lin, G. Guo and W. Hwang, Enhanced ethanol production by fermentation of rice straw hydrolysate without detoxification using a newly adapted strain of Pichia stipites, Bioresource Technology 100, 3914-3920 (2009).
[49] L., Olsson, B. and H.-Hägerdal, Fermentation of lignocellulosic hydrolysates for ethanol production, Enzyme and Microbial Technology 18, 312-331 (1996).
[50] J. Llorca, P.R. de la Piscina, J. Sales and N. Homs, Direct production of hydrogen from ethanolic aqueous solutions over oxide catalysts. Chem. Commun. 641-642 (2001).
[51] E.Y. García and M.A. Laborde, Hydrogen production by the steam reforming of ethanol: Thermodynamic analysis. Int. J. Hydrogen Energy 16, 307-312 (1991).

[52] I. Fishtik, A. Alexander, R. Datta and D. Geana, A thermodynamic analysis of hydrogen production by steam reforming of ethanol via response reactions. Int. J. Hydrogen Energy 25, 31-45 (2000).
[53] A.T.F. Afolabi, C. Li and P.N. Kechagiopoulos, P. N. Microkinetic modelling and reaction pathway analysis of the steam reforming of ethanol over Ni/SiO_2. Int. J. Hydrogen Energy 44, 22816-22830 (2019).
[54] T.K. Phung, T.L.M. Pham, A. Nguyen, B. Vu, H.N. Giang, T. Nguyen, T. Huynh and H. Pham, Effect of Supports and Promoters on the Performance of Ni-Based Catalysts in Ethanol Steam Reforming Chemical Engineering and Technology 43, 672-688 (2020).
[55] M. Benito, Bio-ethanol steam reforming: Insights on the mechanism for hydrogen production. J. Power Sources 151, 11-17 (2005).
[56] J. Comas, M. Laborde and N. Amadeo, Thermodynamic analysis of hydrogen production from ethanol using CaO as a CO_2 sorbent. J. Power Sources 138, 61-67 (2004).
[57]A. N. Fatsikostas, I. Kondarides and X. Verykios, Production of hydrogen for fuel cells by reformation of biomass-derived ethanol. Catal. Today 75, 145-155 (2002).
[58] T. Nishiguchi, T. Matsumoto, H. Kanai, K. Utani, Y. Matsumura and W. Shen, Catalytic steam reforming of ethanol to produce hydrogen and acetone. Appl. Catal. A 279, 273-277 (2005).
[59] F. Aupretre, C. Descorme, D. Duprez, D. Casanave, D. Uzio, Ethanol steam reforming over $MgxNi_{1-x}Al_2O_3$ spinel oxide-supported Rh catalysts. J. Catal. 233, 464-477 (2005).
[60] B. Zhang Steam reforming of bio-ethanol for the production of hydrogen over ceria-supported Co, Ir and Ni catalysts. Catal. Commun. 7, 367-372 (2006).
[61] F. Frusteri, S. Freni, L. Spadaro, V. Chiodo, G. Bonura, S. Donato and S. Cavallaro, H_2 Production for MC Fuel Cell by Steam Reforming of Ethanol Over MgO Supported Pd, Rh, Ni and Co Catalysts. Catalysis Communications 5, 611-615 (2004).
[62] J.P. Breen, R. Burch and H.M. Coleman, Metal-catalysed steam reforming of ethanol in the production of hydrogen for fuel cell applications. Appl. Catal. B 39, 65–74 (2002).
[63] P. Ciambelli, V. Palma, V. and A. Ruggiero, Low temperature catalytic steam reforming of ethanol: The effect of the support on the activity and stability of Pt catalysts. Appl. Catal. B 96, 18-27 (2010).
[64] T. Hou, S. Zhang, Y. Chen, D. Wang and W. Cai, Promotional Effect of Ce-dopant on Al_2O_3-supported Co Catalysts for Syngas Production via CO_2 Reforming of Ethanol, Renew. Sustain. Energy Rev. 44, 132-148(2015).
[65] D. Zanchet, J.B.O. Santos, S. Damyanova, J.M.R. Gallo and J.M.C. Bueno, Toward Understanding Metal-Catalyzed Ethanol Reforming, ACS Catal. 5, 3841-3863 (2015).

[66] M. Goula, S. Kontou, S. and P. Tsiakaras, Hydrogen production by ethanol steam reforming over a commercial $Pd/\gamma\text{-}Al_2O_3$ catalyst. Appl. Catal. B 49, 135-144 (2003).
[67] M.N. Efimov, Ethanol steam reforming over CoRu nanoparticles supported on highly porous polymer-based carbon material. Catal. Commun. 128, 105717 (2019).
[68] A. Erdohelyi, J. Rasko, T; Kecskes, M. Toth, M. Domok and K. Baan, Hydrogen formation in ethanol reforming on supported noble metal catalysts. Catalysis Today 116, 367-376 (2006).
[69] L.P.R. Profeti, E.A. Ticianelli and E. Assaf, Ethanol steam reforming for production of hydrogen on magnesium aluminate-supported cobalt catalysts promoted by noble metals. Appl. Catal. A 360, 17-25 (2009).
[70] P. Osorio, C. Campos, R. Navarro, J. Fierro and P. Reyes, Improved ethanol steam reforming on Rh/Al_2O_3 catalysts doped with CeO_2 or/and La_2O_3: Influence in reaction pathways including coke formation. Appl. Catal. A 505, 159–172 (2015).
[71] P. Osorio-Vargasa, C. H. Campos, R. M. Navarro, J.L.G. Fierro and P. Reyes, $Rh/Al_2O_3\text{-}La_2O_3$ catalysts promoted with CeO_2 for ethanol steam reforming reaction. J. Mol. Catal. -Chem. 407, 169-181 (2015).
[72] T. Hou, Hydrogen production from ethanol steam reforming over Rh/CeO_2 catalyst. Catal. Commun. 58, 137–140 (2015).
[73] Kourtelesis, M., Moraes, T. S., Mattos, L. V., Niakolas, D. K., Noronha, F. B., & Verykios, X. The effects of support morphology on the performance of Pt/CeO_2 catalysts for the low temperature steam reforming of ethanol. Applied Catalysis B: Environmental 284, 119757 (2021).
[74] Martinelli, M., Castro, J. D., Alhraki, N., Matamoros, M. E., Kropf, A. J., Cronauer, D. C., & Jacobs, G. . Effect of sodium loading on Pt/ZrO_2 during ethanol steam reforming. Applied Catalysis A: General 610, 117947 (2021) https://doi.org/10.1016/j.apcata.2020.117947.

[75] M. Martinelli, C.D.Watson and G. Jacobs, Sodium doping of Pt/m-ZrO_2 promotes C–C scission and decarboxylation during ethanol steam reforming. International Journal of Hydrogen Energy 45, 18490-18501 (2020).

[76] R. Rangel, K. Rangel-Arreola, G. Díaz, P. Bartolo-Pérez and P. Quintana, Novel efficient {pt, ir}/$Ce_{1-x}Ru_xO_2$ catalysts for catalytic steam reforming of ethanol. Applied Physics A: Materials Science and Processing, 125, 8 (2019).

[77]J.L. Contreras, J. Salmones, J.A. ColinLuna, L. Nuño, B. Quintana, I. Górdova, B. Zeifert, C. Tapia and G.A. Fuentes Catalysts for H_2 production using the ethanol steam reforming (a review) Int. J. Hydrog. Energy 39, 18835-18853 (2014).

[78] P.D. Vaidya and J.A. Lopez-Sanchez Review of hydrogen production by catalytic aqueous-phase reforming Chemistry Select 2, 6563-6576 (2017).

[79] H. Song and U.S. Ozkan, Changing the oxygen mobility in Co/ceria catalysts by Ca incorporation: implications for ethanol steam reforming. J. Phys. Chem. A 114, 3796–3801 (2010).

[80] S.Q. Chen, H. Wang and Y. Liu, Perovskite La-St-Fe-O (St = Ca, Sr) supported nickel catalysts for steam reforming of ethanol: the effect of the A site substitution, Int. J. Hydrogen Energy 34, 7995-8005 (2009).

[81] A. Di Michele, Steam reforming of ethanol over Ni/$MgAl_2O_4$ catalysts. Int. J. Hydrogen Energy 44, 952–964 (2019).

[82] F. Wang, Embedded Ni catalysts in Ni-O-Ce solid solution for stable hydrogen production from ethanol steam reforming reaction. Fuel Process. Technol. 193, 94-101 (2019).

[83] A. Ishihara, A. Andou, T. Hashimoto and H. Nasu, Steam reforming of ethanol using novel carbon-oxide composite-supported Ni, Co and Fe catalysts. Fuel Process. Technol. 197, 106203 (2020).

[84] T.S. Rodrigues, Ni supported $Ce_{0.9}Sm_{0.1}O_{2-\delta}$ nanowires: An efficient catalyst for ethanol steam reforming for hydrogen production. Fuel 237, 1244–1253 (2019).

[85] J. L. Contreras, Production of hydrogen by ethanol steam reforming using Ni-Co-ex-hydrotalcite catalysts stabilized with tungsten oxides. Int. J. Hydrog. Energy 46, 6474-6493 (2020).

[86] G. Özkan and S. Gök, Active carbon-supported Ni, Ni/Cu and Ni/Cu/Pd catalysed steam reforming of ethanol for the production of hydrogen. Chem. Eng. J. 171, 1270-1275 (2011).

[87] Z. Xiao, C. Wu, L. Wang, J. Xu, Q. Zheng, L. Pan, J. Zou, X. Zhang and G. Li, Boosting hydrogen production from steam reforming of ethanol on nickel by lanthanum doped ceria. Appl. Catal. B Environ. 286, 119884 (2021).

[88] S. Chen, C. Pei and J. Gong, Insights into interface engineering in steam reforming reactions for hydrogen production, Energy & Environmental Science, 12, 3473 (2019).

[89] G. Zhou, L. Barrio, S. Agnoli, S.D. Senanayake, J. Evans, A. Kubacka, M. Estrella, J.C. Hanson, A. Martinez-Arias, M. Fernandez-Garcia and J.A. Rodriguez, High activity of $Ce_{1-x}Ni_xO_{2-y}$ for H_2 production through ethanol steam reforming: tuning catalytic performance through metal-oxide interactions, Angewandte Chemie 49, 9680-9684 (2010).

[90] R. Trane-Restrup, S. Dahl and A.D. Jensen, Steam reforming of ethanol: Effects of support and additives on Ni-based catalysts. Int. J. Hydrogen Energy 38, 15105-15118 (2013).

[91] R. Trane-Restrup, S. Dahl and A.D. Jensen, Steam reforming of ethanol over Ni-based catalysts: Effect of feed composition on catalyst stability. Int. J. Hydrogen Energy 39, 7735-7746 (2014).

[92] N. R. F. J. Sanchez-Sanchez, Ethanol steam reforming over Ni/$LaAl_2O_3$ catalysts: Influence of lanthanum loading, Catal Today 129, 336-365 (2007).

[93] J.W.C. Liberatoria, R.U. Ribeiro, D.Z. Anchet, F.B. Noronha and J.M.C. Bueno, Steam reforming of ethanol on supported nickel catalysts, Appl. Catal. A, 197-204 (2007).

[94] C. Cerdá-Moreno, J.F. Da Costa-Serra, J. F. and A. Chica, Co and La supported on Zn-Hydrotalcite-derived material as efficient catalyst for ethanol steam reforming. Int. J. Hydrogen Energy 44, 12685-12692 (2019).

[95] F. Díaz Alvarado and F. Gracia, Steam reforming of ethanol for hydrogen production: Thermodynamic analysis including different carbon deposits representation, Chem. Eng, J. 165, 649-657 (2010).

[96] C. Pirez, M. Capron, H. Jobic, F. Dumeignil and L. Jalowiecki-Duhamel, Highly Efficient and Stable $CeNiH_ZO_Y$ Nano-Oxyhydride Catalyst for H_2 Production from Ethanol at Room Temperature. Angew. Chem. Int. Ed 50, 10193 (2011).

[97] W. Fang, C. Pirez, S. Paul, M. Capron, H. Jobic, F. Dumeignil and L. Jalowiecki-Duhamel, Room temperature hydrogen production from ethanol over $CeNi_xH_zO_y$ nano-oxyhydride catalysts. ChemCatChem 5, 2207-2216 (2013).

[98] M. Sankirand and N. Sankir, Hydrogen Production Technologies. (John Wiley & Sons, 2017).

[99] Z. Liu, S.D. Senanayake and J.A. Rodriguez, Elucidating the interaction between Ni and CeO_x in ethanol steam reforming catalysts: A perspective of recent studies over model and powder systems. Appl. Catal. B 197, 184-197 (2016).

[100] H. Ma, Efficient hydrogen production from ethanol steam reforming over La-modified ordered mesoporous Ni-based catalysts. Appl. Catal. B 181, 321-331 (2016).

[101] T. Wang, Highly loaded Ni-based catalysts for low temperature ethanol steam reforming. Nanoscale 8, 10177-10187 (2016).

[102] L. Coleman, W. Epling, R. Hudgins and E. Croiset, Ni/Mg–Al mixed oxide catalyst for the steam reforming of ethanol. Appl. Catal. A 363, 52-63 (2009).

[103] M. Li, X. Wang, S. Li, S. Wang and X. Ma, Hydrogen production from ethanol steam reforming over nickel based catalyst derived from Ni/Mg/Al hydrotalcite-like compounds. Int. J. Hydrogen Energy 35, 6699-6708 (2010).

[104] A. F. Lucrédio, J. Bellido, and E. Assaf, Effects of adding La and Ce to hydrotalcite-type Ni/Mg/Al catalyst precursors on ethanol steam reforming reactions. Appl. Catal. A 388, 77-85 (2010).

[105] W. Fang, S. Paul, M. Capron, F. Dumeignil, and L. Jalowiecki-Duhamel, Hydrogen production from bioethanol catalyzed by $Ni_XMg_2AlO_Y$ ex-hydrotalcite catalysts. Appl. Catal. B 152-153, 370-382 (2014).

[106] F. Agüero, J.A. Alonso, M.T. Fernández-Díaz and L.E. Cadus, Ni-based catalysts obtained from perovskites oxides for ethanol steam reforming. J. Fuel Chem. Technol. 46, 1332-1341 (2018).

[107] M. Akiyama, Y. Oki, and M. Nagai, M. Steam reforming of ethanol over carburized alkali-doped nickel on zirconia and various supports for hydrogen production. Catal. Today 181, 4-13 (2012).

[108] N. Li, J. Pu, B. Chi and J. Li, Ethanol steam reforming with a Ni–$BaZr_{0.1}Ce_{0.7}$ $Y_{0.1}Yb_{0.1}O_{3-\delta}$ catalyst. Mater. Today Energy 12, 371-378 (2019).

[109] N. Wang, Y. Feng, Y. Chen and X. Guo, Lithium-based sorbent from rice husk materials for hydrogen production via sorption-enhanced steam reforming of ethanol. Fuel 245, 263-273 (2019).

[110] Possato, L. G. et al. Sol-gel synthesis of nanocrystalline MgO and its application as support in Ni/MgO catalysts for ethanol steam reforming. Appl. Surf. Sci. 542, 148744 (2021).

[111] S.D. Nobrega, Gradual Internal Reforming of Ethanol in Solid Oxide Fuel cells. Energy Procedia 28, 28-36 (2012).

[112] M. Kourtelesis, The effects of support morphology on the performance of Pt/CeO_2 catalysts for the low temperature steam reforming of ethanol. Appl. Catal. B Environ. 284, 119757 (2021).

[113] V.V. Galvita Ethanol decomposition over Pd-based catalyst in the presence of steam. React. Kinet. Catal. Lett. 76, 343-351 (2002).

[114] J.H. Lee, Hydrogen production on $Pd_{0.01}Zn_{0.29}Mg_{0.7}Al_2O_4$ spinel catalyst by low temperature ethanol steam reforming reaction. J. Energy Inst. 92, 1064-1076 (2019).

[115] Breen, J. P., Burch, R. & Coleman, H. M. Metal-catalysed steam reforming of ethanol in the production of hydrogen for fuel cell applications. Appl. Catal. B Environ. 39, 65–74 (2002).

[116] R. Dai, Dragon fruit-like Pt-Cu@mSiO_2 nanocomposite as an efficient catalyst for low-temperature ethanol steam reforming. Chem. Eng. J. 379, 122299 (2020).

[117] C. Diagne, H. Idriss, H. and A. Kiennemann, Hydrogen production by ethanol reforming over Rh/CeO_2-ZrO_2 catalysts. Catal. Commun. 3, 565-571 (2002).

[118] S. Jo, Reasonable harmony of Ni and Mn in core@shell-structured NiMn@SiO_2 catalysts prepared for hydrogen production from ethanol steam reforming. Chem. Eng. J. 288, 858-868 (2016).

[119] T. Moraesa, The study of the performance of $PtNi/CeO_2$–nanocube catalysts for low temperature steam reforming of ethanol. Catal. Today 242, 35-49 (2014).

[120] S. Cavallaro, V. Chiodo, S. Freni, N. Mondello and F. Frusteri, Performance of Rh/Al_2O_3 catalyst in the steam reforming of ethanol: H2 production for MCFC. Appl. Catal. A 249, 119-128 (2003).

[121] Y. Wang, Hydrogen production from steam reforming ethanol over Ni/attapulgite catalysts - Part I: Effect of nickel content. Fuel Process. Technol. 192, 227-238 (2019).

[122] M. Musso, M. Romero, R. Faccio and J. Bussi, Catalytic assessment of a Ni-La-Sn ternary metallic system in ethanol steam reforming and the influence of the Sn/La atomic ratio in the catalytic performance. Catal. Today 356, 408-418 (2019).

[123] S.M. de Lima, A.M. da Silva, L.O.O. da Costa, J.M. Assaf, L.V. Mattos, R. Sarkari, A. Venugopal and F.B. Noronha, Hydrogen production through oxidative steam reforming of ethanol over Ni-based catalysts derived from $La_{1-x}Ce_xNiO_3$ perovskite-type oxides, Applied Catalysis B: Environmental, 121-122, 1-9 (2012).

[124] D. Li, L. Zeng, X. Li, X. Wang, H. Ma, S. Assabumrungrat and J. Gong, Ceria-promoted Ni/SBA-15 catalysts for ethanol steam reforming with enhanced activity and resistance to deactivation, Applied Catalysis B: Environmental 176-177, 532-541 (2015).

[125] C.J. Liu, J. Ye, J. Jiang and Y. Pan, Progresses in the Preparation of Coke Resistant Ni-based Catalyst for Steam and CO_2 Reforming of Methane, Chemcatchem 42, 529-541 (2011).

[126] D. Li, M. Tamura, Y. Nakagawa and K. Tomishige, Metal catalysts for steam reforming of tar derived from the gasification of lignocellulosic biomass, Bioresource Technology 178, 53-64 (2015).

[127] D. Li, M. Koike, J. Chen, Y. Nakagawa and K. Tomishige, Preparation of Ni–Cu/Mg/Al catalysts from hydrotalcite-like compounds for hydrogen production by steam reforming of biomass tar, International Journal of Hydrogen Energy 39, 10959-10970 (2014).

[128] Y. Li, L. Zhang, Z. Zhang, Q. Liu, S. Zhang, Q. Liu, G. Hu, Y. Wang and X. Hu, Steam reforming of the alcohols with varied structures: Impacts of acidic sites of Ni catalysts on coking, Applied Catalysis A: General, 584, 117162 (2019).

[129] J.R. Jain and C.N. Pillai, Catalytic dehydration of alcohols over alumina: Mechanism of ether formation. J. Catal. 9, 322-330 (1967).

[130] F. Xue, C. Miao, Y. Yue, W. Hua and Z. Gao, Direct conversion of bio-ethanol to propylene in high yield over the composite of In_2O_3 and zeolite beta. Green Chem. 19, 5582-5590 (2017).

[131] H. Hattori, Heterogeneous Basic Catalysis. Chem. Rev. 95, 537-558 (1995).

[132] J.d.S. Lisboa, D.C.R.M. Santos, F.B. Passos and F.B. Noronha, Influence of the addition of promoters to steam reforming catalysts, Catal. Today 101,15-21 (2005).

[133] J.Y. Lin, L.W. Chen, C.K.S. Choong, Z.Y. Zhong and L. Huang, Molecular catalysis for the steam reforming of ethanol, Sci China Chem 58, 60-78 (2015).

[134] A. Denis, W. Grzegorczyk, W. Gac and A. Machocki, Steam reforming of ethanol over Ni/support catalysts for generation of hydrogen for fuel cell applications. Catal. Today 137, 453–459 (2008).

[135] P.D. Vaidya and A.E. Rodrigues, Insight into steam reforming of ethanol to produce hydrogen for fuel cells. Chem. Eng. J. 117, 39-49 (2006).

[136] L. Zhang, J. Liu, W. Li, C. Guo and J. Zhang, Ethanol steam reforming over Ni-Cu/Al_2O_3-M_yO_z (M = Si, La, Mg, and Zn) catalysts. J. Nat. Gas Chem. 18, 55-65 (2009).

[137] A. Fatsikostas and X. Verykios, Reaction Network of Steam Reforming of Ethanol Over Ni Based Catalysts. J. Catal. 225, 439-452 (2004).

[138] Yoo, S., Park, S., Song, J. H. and Kim, D. H. Hydrogen production by the steam reforming of ethanol over K-promoted Co/Al2O3-CaO xerogel catalysts. Mol. Catal. 491, 110980 (2020).

[139] J.F. Da Costa-Serra and A. Chica, Catalysts based on Co-Birnessite and Co-Todorokite for the efficient production of hydrogen by ethanol steam reforming. Int. J. Hydrogen Energy 43, 16859-16865 (2018).

[140] H. Huang, S. Yu, C.L. Chuang and C. Wang, Application of boron-modified nickel catalysts on the steam reforming of ethanol. Int. J. Hydrogen Energy 39, 20712-20721 (2014).

[141] R. Wu, Effect of boron doping and preparation method of Ni/$Ce_{0.5}Zr_{0.5}O_2$ catalysts on the performance for steam reforming of ethanol. Int. J. Hydrogen Energy 44, 14279-14289 (2019).

[142] W. Gac, M. Greluk, G. Słowik and S. Turczyniak-Surdacka, Structural and surface changes of cobalt modified manganese oxide during activation and ethanol steam reforming reaction. Appl. Surf. Sci. 440, 1047-1062 (2018).

[143] Z. Xiao, Engineering oxygen vacancies and nickel dispersion on CeO_2 by Pr doping for highly stable ethanol steam reforming. Appl. Catal. B. 258, 117940 (2019).

[144] H. Hsieh, Metal substituted pyrochlore phase $Li_xLa_{2-x}Ce_{1.8}Ru_{0.2}O_{7-\delta}$ (x = 0.0–0.6) as an effective catalyst for oxidative and auto-thermal steam reforming of ethanol. Catal. Sci. Technol. 9, 1406-1419 (2019).

[145] T. Stroud, Chemical CO_2 recycling via dry and bi reforming of methane using Ni-Sn/Al_2O_3 and Ni-Sn/CeO_2-Al_2O_3 catalysts. Appl. Catal. B 224, 125-135 (2018).

[146] L. Bobadilla, F. Romero-Sarria, M.A. Centeno, A. Odriozola, Promoting effect of Sn on supported Ni catalyst during steam reforming of glycerol. Int. J. Hydrogen Energy 41, 9234-9244 (2016).

[147] M. Greluk, M. Rotko, G. Słowik, G. and S.Turczyniak-Surdacka, Hydrogen production by steam reforming of ethanol over Co/CeO_2 catalysts: Effect of cobalt content. J. Energy Inst. 92, 222-238 (2019).

[148] M. Stoukides and C.G. Vayenas, The effect of electrochemical oxygen pumping on the rate and selectivity of ethylene oxidation on polycrystalline silver. J. Catal. 70, 137-146 (1981).
[149] I.V. Yentekakis, M Konsolakis, R. M Lambert, A Palermo and M Tikhov. Successful application of electrochemical promotion to the design of effective conventional catalyst formulations. Solid State Ionics 136–137, 783-790 (2000).
[150] D. Theleritis, S. Souentie, A. Siokou, A. Katsaounis and C.G. Vayenas, Hydrogenation of CO_2 over Ru/YSZ Electropromoted Catalysts. ACS Catal. 2, 770-780 (2012).
[151] J. González-Cobos, D. López-Pedrajas, E. Ruiz-López, J.L. Valverde and A. de Lucas-Consuegra, Applications of the Electrochemical Promotion of Catalysis in Methanol Conversion Processes. Top. Catal. 58, 1290-1302 (2015).
[152] A. de Lucas-Consuegra, Development of a new electrochemical catalyst with an electrochemically assisted regeneration ability for H_2 production at low temperatures. J. Catal. 274, 251-258 (2010).
[153] A. de Lucas-Consuegra, A. Caravaca, J. González-Cobos, J. Valverde and F.Dorado, Electrochemical activation of a non-noble metal catalyst for the water–gas shift reaction. Catal. Commun. 15, 6-9 (2011).
[154] A. Caravaca, A. de Lucas-Consuegra, C. Molina-Mora, J.L. Valverde and F. Dorado, Enhanced H_2 formation by electrochemical promotion in a single chamber steam electrolysis cell. Appl. Catal. B 106, 54-62 (2011).
[155] I.V. Yentekakis, Y. Jiang, S. Neophytides, S. Bebelis and C.J. Vayenas, Catalysis, electrocatalysis and electrochemical promotion of the steam reforming of methane over Ni film and Ni-YSZ cermet anodes. Ionics 1, 491-498 (1995).
[156] J. González-Cobos, J.L Valverde and A. de Lucas-Consuegra, Electrochemical vs. chemical promotion in the H_2 production catalytic reactions. Int. J. Hydrogen Energy 42, 13712-13723 (2017).
[157] L. Jalowiecki-Duhamel, C. Pirez, M. Capron, F. Dumeignil and E. Payen, Hydrogen production from ethanol steam reforming over cerium and nickel based oxyhydrides. Int. J. Hydrogen Energy 35, 12741-12750 (2010).
[158] W. Fang, S. Paul, M. Capron, A.V. Biradar, S.B. Umbarkar, M. Dongare, F. Dumeignil and L. Jalowiecki-Duhamel, Highly loaded well dispersed stable Ni species in $Ni_XMg_2AlO_Y$ nanocomposites: Application to hydrogen production from bioethanol. Appl. Catal. B 166-167, 485-496 (2015).
[159] Y. Sharma, A. Kumar, R. Prasad and S.N. Upadhyay, Ethanol steam reforming for hydrogen production: Latest and effective catalyst modification strategies to minimize carbonaceous deactivation. Renew. Sustain. Energy Rev. 74, 89-103 (2017).
[160] S.M. de Lima, Hydrogen production through oxidative steam reforming of ethanol over Ni-based catalysts derived from $La_{1-x}Ce_xNiO_3$ perovskite-type oxides. Appl. Catal. B 121-122, 1-9 (2012).
[161] A. Silva, The effect of support reducibility on the stability of Co/CeO_2 for the oxidative steam reforming of ethanol. Catal. Today 164, 234-239 (2011).
[162] A. Kumar, A. S. Mukasyan and E. E. Wolf, Combustion synthesis of Ni, Fe and Cu multi-component catalysts for hydrogen production from ethanol reforming, Applied Catalysis A 401, 20-28 (2011).
[163] W. Cai, Oxidative steam reforming of ethanol over Ir/CeO_2 catalysts: A structure sensitivity analysis. J. Catal. 286, 137-152 (2012).
[164] S. Liu, K. Zhang, L. Fang and Y. Li, Thermodynamic Analysis of Hydrogen Production from Oxidative Steam Reforming of Ethanol, Energy & Fuels 22, 1365-1370 (2008).
[165] H. Chen, Efficient and stable oxidative steam reforming of ethanol for hydrogen production: Effect of in situ dispersion of Ir over Ir/La2O3. J. Catal. 269, 281-290 (2010).
[166] O. Akdim, Oxidative Steam Reforming of Ethanol over $Ni-Cu/SiO_2$, Rh/Al_2O_3 and Ir/CeO_2: Effect of Metal and Support on Reaction Mechanism. Top. Catal. 51, 22 (2008).
[167] J.L. Bi, Y.Y. Hong, C. Lee, T. Yeh and B. Wang, Novel zirconia-supported catalysts for low-temperature oxidative steam reforming of ethanol. Catal. Today 129, 322-329 (2007).
[168] C. Du, Hydrogen production by steam-oxidative reforming of bio-ethanol assisted by Laval nozzle arc discharge. Int. J. Hydrogen Energy 37, 8318-8329 (2012).
[169] N. Peela and D.Kunzru, Oxidative steam reforming of ethanol over Rh based catalysts in a micro-channel reactor. Int. J. Hydrogen Energy 36, 3384-3396 (2011).
[170] S. Sengodan, R. Lan, J. Humphreys, D. Du and S. Tao, Advances in reforming and partial oxidation of hydrocarbons for hydrogen production and fuel cell applications, Renewable and Sustainable Energy Reviews 82, 761-780 (2018).

[171] C. Ruocco, V. Palma and A. Ricca, Experimental and kinetic study of oxidative steam reforming of ethanol over fresh and spent bimetallic catalysts. Chem. Eng. J. 377, 119778 (2019).
[172] R. M. Navarro, M. C. Álvarez-Galván, M. C. Sánchez-Sánchez, F. Rosa and J. L. G. Fierro, Production of hydrogen by oxidative reforming of ethanol over Pt catalysts supported on Al_2O_3 modified with Ce and La. Appl. Catal. B Environ. 55, 229-241 (2005).
[173] C.H. Campos, G. Pecchi, J.L.G. Fierro and P Osorio-Vargas, Enhanced bimetallic Rh-Ni supported catalysts on alumina doped with mixed lanthanum-cerium oxides for ethanol steam reforming. Mol. Catal. 469, 87-97 (2019).
[174] T. Mondal, K. Pant and A. Dalai, Oxidative and non-oxidative steam reforming of crude bio-ethanol for hydrogen production over Rh promoted Ni/CeO_2-ZrO_2 catalyst, Appl. Catal. A 499, (2015).
[175] G. Souza, N.M. Balzaretti, N. Marcílio and O. Perez-Lopez, Decomposition of Ethanol over Ni-Al catalysts: effect of copper addition. Procedia Eng. 42, 335-345 (2012).
[176] C. Montero, A. Ochoa, P. Castaño, J. Bilbao and A. Gayubo, Monitoring Ni^0 and coke evolution during the deactivation of a $Ni/La_2O_{3-\alpha}Al_2O_3$ catalyst in ethanol steam reforming in a fluidized bed. J. Catal. 331, 181-192 (2015).
[177] E. Kraleva, C.P. Rodrigues, M. Pohl, H. Ehrich and F.B. Noronha, Syngas production by partial oxidation of ethanol on $PtNi/SiO_2$–CeO_2 catalysts. Catal. Sci. Technol. 9, 634–645 (2019).
[178] S. Davidson, H. Zhang, J. Sun and Y. Wang, Supported metal catalysts for alcohol/sugar alcohol steam reforming. Dalton Trans. 43, 11782-11802 (2014).
[179] A. Passos, S.H. Pulcinelli, C.V. Santilli and V. Briois, Operando monitoring of metal sites and coke evolution during non-oxidative and oxidative ethanol steam reforming over Ni and NiCu ex-hydrotalcite catalysts. Catal. Today 336, 122-130 (2019).
[180] L. Zhang, Y. Wang and Q. Huang, Preparation and properties of K_2NiF_4-type perovskite oxides La_2NiO_4 catalysts for steam reforming of ethanol. Trans. Nonferrous Met. Soc. China 19, 1444-1449 (2009).
[181] A. Iriondo, Influence of La_2O_3 modified support and Ni and Pt active phases on glycerol steam reforming to produce hydrogen. Catal. Commun. 10, 1275-1278 (2009).
[182] S.M. de Lima, Study of catalyst deactivation and reaction mechanism of steam reforming, partial oxidation, and oxidative steam reforming of ethanol over Co/CeO_2 catalyst. J. Catal. 268, 268-281 (2009).
[183] A.J. Vizcaíno, A. Carrero and A. Calles, Hydrogen production by ethanol steam reforming over Cu–Ni supported catalysts. Int. J. Hydrogen Energy 32, 1450-1461 (2007).
[184] S.M. De Lima, Evaluation of the performance of Ni/La_2O_3 catalyst prepared from $LaNiO_3$ perovskite-type oxides for the production of hydrogen through steam reforming and oxidative steam reforming of ethanol. Appl. Catal. A 377, 181-190 (2010).
[185] J. Lu, Y. Lei, G. Wan, Z. Mei and Y. Luo, Weakening the metal-support strong interaction to enhance catalytic performances of alumina supported Ni-based catalysts for producing hydrogen. Applied Catalysis B: Environmental 263, 118177 (2019).
[186] C. Rodríguez, S. Moreno and R. Molina, Oxygen mobility and its relationship with the oxidative steam reforming of ethanol (OSRE). Appl. Surf. Sci. 485, 293-303 (2019).
[187] N. Srisiriwat, S. Therdthianwong and A. Therdthianwong, Oxidative steam reforming of ethanol over Ni/Al_2O_3 catalysts promoted by CeO_2, ZrO_2 and CeO_2–ZrO_2. Int. J. Hydrogen Energy 34, 2224-2234 (2009).
[188] F. Dalena, A. Basile and C. Rossi, Bioenergy Systems for the Future: Prospects for Biofuels and Biohydrogen. (Woodhead Publishing, 2017).
[189] M. Muñoz, S. Moreno and R. Molina, The effect of the absence of Ni, Co, and Ni–Co catalyst pretreatment on catalytic activity for hydrogen production via oxidative steam reforming of ethanol. Int. J. Hydrogen Energy 39, 10074-10089 (2014).
[190] M. Muñoz, S. Moreno and R. Molina, Synthesis of Ce and Pr-promoted Ni and Co catalysts from hydrotalcite type precursors by reconstruction method. Int. J. Hydrogen Energy 37, 18827-18842 (2012).
[191] A. Silva, M. Ribeiro, D. Cronauer, A. Jeremy, P. Gao, G. Jacobs, B. Davis, F. Noronha and L. Mattos, Ethanol reforming reactions over Co and Cu based catalysts obtained from $LaCoCuO_3$ perovskite-type oxides. Top. Catal. 57, 637-655 (2014).
[192] G.B. Sun, X.S. Wu and S.A. Kawi, Crucial role of surface oxygen mobility on nanocrystalline Y_2O_3 support for oxidative steam reforming of ethanol to hydrogen over Ni/Y_2O_3 catalysts. Appl. Catal. B 81, 303-312 (2008).

[193] W. Xu, Steam Reforming of Ethanol on Ni/CeO_2: Reaction Pathway and Interaction between Ni and the CeO_2 Support. ACS Catal. 3, 975-984 (2013).

[194] V. Palma, C. Ruocco and A. Ricca, Oxidative steam reforming of ethanol in a fluidized bed over CeO_2-SiO_2 supported catalysts: effect of catalytic formulation. Renew. Energy 125, 356-364 (2018).

[195] S. Weng, H. Hsieh, and C. Lee, "Hydrogen production from oxidative steam reforming of ethanol on nickel-substituted pyrochlore phase catalysts," Int. J. Hydrogen Energy, vol. 42, no. 5, pp. 2849-2860, 2017

[196] H. Chen, Hydrogen production via autothermal reforming of ethanol over noble metal catalysts supported on oxides. J. Nat. Gas Chem. 18, 191-198 (2009).

[197] V. Palma, C. Ruocco, E. Meloni and A. Ricca, Coke-resistant Pt-Ni/ CeO_2/SiO_2 catalysts for ethanol reforming. Chem. Eng. Trans. 57, 1675-1680 (2017).

[198] X. Han, Y. Yu, H. He, J. Zhao and Y. Wang, Oxidative steam reforming of ethanol over Rh catalyst supported on $Ce_{1-x}La_xO_y$ (x = 0.3) solid solution prepared by urea co-precipitation method. J. Power Sources 238, 57-64 (2013).

[199] D. Chatla, Effect of Zn addition on the performance of Ni/Al_2O_3 catalyst for steam reforming of ethanol. Appl. Catal. A 519, 85-98 (2016).

[200] X. Han, Y. Wang, Y. Zhang, Y. Yu and H. He, Hydrogen production from oxidative steam reforming of ethanol over Ir catalysts supported on Ce–La solid solution. Int. J. Hydrogen Energy 42, 11177-11186 (2017).

[201] S. Cavallaro, Ethanol steam reforming on Rh/Al_2O_3 Catalysts. Energy Fuels 14, 1195-1199 (2000).

[202] H. Hsieh, Y. S. Chen, S. F. Weng, Y. Hsieh and C. Lee, Ruthenium substituted pyrochlore metal oxide catalysts $Y_2Ce_{2-x}Ru_xO_{7-\delta}$ (x = 0–0.4) for oxidative steam reforming of ethanol. Int. J. Hydrog. Energy 45, 19291-19303 (2020).

[203] R. Baruah, M. Dixit, P. Basarkar, D. Parikh and A. Bhargav, Advances in ethanol autothermal reforming. Renewable and Sustainable Energy Reviews 51, 1345-1353 (2015).

[204] A. Casanovas Grau, J. Llorca, N. Homs, J. Fierro and P. Piscina, Ethanol reforming processes over ZnO-supported palladium catalysts: Effect of alloy formation. J. Mol. Catal. -Chem. 250, 44-49 (2006).

[205] S.M. de Lima, Steam reforming, partial oxidation, and oxidative steam reforming of ethanol over Pt/$CeZrO_2$ catalyst. J. Catal. 257, 356-368 (2008).

[206] M. Domok, M. Toth, J. Rasko, J. and A. Erdohelyi, Adsorption and reactions of ethanol and ethanol–water mixture on alumina-supported Pt catalysts. Appl. Catal. B 69, 262-272 (2007).

[207]S. Kugai, S. Velu, and C. Song, "Low-temperature reforming of ethanol over CeO_2-supported Ni-Rh bimetallic catalysts for hydrogen production," Catal. Letters 101, 255-264 (2005).

[208] S. Sharma, S. Aich and B. Roy, Low temperature steam reforming of ethanol over cobalt doped bismuth vanadate [$Bi_4(V_{0.90}Co_{0.10})_2O_{11-\delta}$ (BICOVOX)] catalysts for hydrogen production. J. Phys. Chem. Solids 148, 109754 (2021).

[209] A.C. Furtado, C. Alonso, M.P. Cantão and N.R.C. Fernandes-Machado, Support influence on Ni–Cu catalysts behavior under ethanol oxidative reforming reaction. Int. J. Hydrogen Energy 36, 9653-9662 (2011).

[210] C. Pirez, Steam reforming, partial oxidation and oxidative steam reforming for hydrogen production from ethanol over cerium nickel based oxyhydride catalyst. Appl. Catal. A 518, 78-86 (2016).

[211] C. Hung, S.L. Chen, Y.K. Liao, C.H. Chen and J.H. Wang, Oxidative steam reforming of ethanol for hydrogen production on M/Al_2O_3. Int. J. Hydrogen Energy 37, 4955-4966 (2012).

[212] R. Guil-Lopez, R. Navarro, M. Peña and J. Fierro, Hydrogen production by oxidative ethanol reforming on Co, Ni and Cu ex-hydrotalcite catalysts. Fuel Energy Abstr. 36, 1512-1523 (2011).

[213] G. Özkan and B. Şahbudak, Effect of molar ratio of water/ethanol on hydrogen selectivity in catalytic production of hydrogen using steam reforming of ethanol. Int. J. Hydrogen Energy 44, 9823-9829 (2019).

[214] F. Frusteri, Steam and auto-thermal reforming of bio-ethanol over MgO and CeO_2 Ni supported catalysts. Int. J. Hydrogen Energy 31, 2193-2199 (2006).

[215] H.S. Roh, Y. Wang and D.L. King, Selective production of H_2 from ethanol at low temperatures over Rh/ZrO_2–CeO_2 catalysts. Top. Catal. 49, 32-37 (2008).

[216] A. Trovarelli, Catalytic properties of ceria and CeO_2 -containing materials. Catal. Rev. 38, 439-520 (1996).

[217] P. Biswas and D. Kunzru, Oxidative steam reforming of ethanol over Ni/CeO_2-ZrO_2 catalyst. Chem. Eng. J. 136, 41-49 (2008).

[218] Y. Hsia, Effects of O_2 and H_2O in the oxidative steam-reforming reaction of ethanol on Rh catalysts. J. Phys. Chem. C 123, 11649-11661 (2019).

[219] V. Fierro, V. Klouz, O. Akdim and C. Mirodatos, Oxidative reforming of biomass derived ethanol for hydrogen production in fuel cell applications. Catal. Today 75, 141-144 (2002).
[220] S. Velu; N. Satoh; Chinnakonda S. Gopinath; K. Suzuki, Oxidative Reforming of Bio-Ethanol Over CuNiZnAl Mixed Oxide Catalysts for Hydrogen Production. 82(1-2), 145-152 (2002).
[221] H. Chen, Autothermal reforming of ethanol for hydrogen production over perovskite $LaNiO_3$. Chem. Eng. J. 160, 333-339 (2010).
[222] S. Velu, K. Suzuki, M. Vijayaraj, S. Barman and S Gopinath, In situ XPS investigations of $Cu_{1-x}Ni_xZnAl$-mixed metal oxide catalysts used in the oxidative steam reforming of bio-ethanol. Appl. Catal. B 55, 287-299 (2005).
[223] S. Tuti and F. Pepe, On the catalytic activity of cobalt oxide for the steam reforming of ethanol. Catal. Lett. 122, 196-203 (2008).
[224] A. Iulianelli, S. Liguori, A. Vita, C. Italiano, C. Fabiano and Y. Huang, The oncoming energy vector: hydrogen produced in Pd-composite membrane reactor via bioethanol reforming over Ni/CeO_2 catalyst, Catal. Today 259, 368-375 (2016).
[225] V.Palma, C. Ruocco, E. Meloni and A. Ricca, A. Renewable Hydrogen from Ethanol Reforming over CeO_2-SiO_2 Based Catalysts. Catalysts 7, 226 (2017).
[226] M. Muñoz, S. Moreno and R. Molina, Oxidative steam reforming of ethanol (OSRE) over stable NiCo–MgAl catalysts by microwave or sonication assisted coprecipitation. Int. J. Hydrogen Energy 42, 12284-12294 (2017).
[227] Z. Wang, C. Wang, S. Chen and Y. Liu, Co–Ni bimetal catalyst supported on perovskite-type oxide for steam reforming of ethanol to produce hydrogen. Int. J. Hydrogen Energy 39, 5644-5652 (2014).
[228] M. Greluk, G. Słowik, M. Rotko and A. Machocki, Steam reforming and oxidative steam reforming of ethanol over $PtKCo/CeO_2$ catalyst. Fuel 183, 518-530 (2016).
[229] S. Andonova, C.N. de Ávila, K. Arishtirova, J.M.C. Bueno and C. Damyanova, Structure and redox properties of Co promoted Ni/Al_2O_3 catalysts for oxidative steam reforming of ethanol. Appl. Catal. B 105, 346-360 (2011).
[230] Z.H. Li, X. Tian, T. Wang and B. Tian, Plasma treatment of Ni catalyst via a corona discharge. J. Mol. Catal. Chem. 211, 149-153 (2004).
[231] B. Roy, K. Loganathan, H.N. Pham, A.K. Datye and C.A. Leclerc, Surface modification of solution combustion synthesized Ni/Al_2O_3 catalyst for aqueous-phase reforming of ethanol. Int. J. Hydrogen Energy 35, 11700-11708 (2010).
[232] C. Liu, G.P. Vissokov and X. Jang, Catalyst preparation using plasma technologies. Catal. Today 72, 173-184 (2002).
[233] K. Sato, K. Kawano, A. Ito, Y. Takita and K. Nagaoka, Hydrogen production from bioethanol: oxidative steam reforming of aqueous ethanol triggered by oxidation of $Ni/Ce_{0.5}Zr_{0.5}O_{2-x}$ at low temperature. ChemSusChem 3, 1364-1366 (2010).
[234] X. Han, Y. Yu, H. He and J. Zhao, Low CO content hydrogen production from oxidative steam reforming of ethanol over CuO-CeO_2 catalysts at low-temperature. J. Energy Chem. 22, 861-868 (2013).
[235]Z. Wang, H. Wang and Y. Liu, $La_{1-x}Ca_xFe_{1-x}Co_xO_3$, a stable catalyst for oxidative steam reforming of ethanol to produce hydrogen. RSC Advances 3, 10027-10036 (2013).
[236] P. Biswas and A. Kunzru, Steam reforming of ethanol on $Ni–CeO_2–ZrO_2$ catalysts: Effect of doping with copper, cobalt and calcium. Catal. Lett. 118, 36-49 (2007).
[237] B. Banach and A. Machocki, "Effect of potassium addition on a long term performance of $Co–ZnO–Al_2O_3$ catalysts in the low-temperature steam reforming of ethanol: Co-precipitation vs citrate method of catalysts synthesis," Appl. Catal. A Gen. 505, 173-182 (2015).
[238] W. Fang, Y. Romani, Y. Wei, M. Jiménez-Ruiz , H. Jobic, S. Paul, and L. Jalowiecki-Duhamel, Steam reforming and oxidative steam reforming for hydrogen production from bioethanol over $Mg_2AlNi_xH_zO_y$ nano-oxyhydride catalysts, International Journal of Hydrogen Energy 43, 17643-17655 (2018).
[239] L. Coronel, J.F. Múnera, A.M. Tarditi, M. Moreno and L.M. Cornaglia, Hydrogen production by ethanol steam reforming over Rh nanoparticles supported on lanthana/silica systems. Appl. Catal. B 160-161, 254-266 (2014).
[240] K. Mudiyanselage, I. Al-Shankiti, A. Foulis, J. Llorca and H. Idriss, Reactions of ethanol over CeO_2 and Ru/CeO_2 catalysts. Appl. Catal. B 197, 198-205 (2016).
[241] S.F. Weng, Y.H. Wang and C.S. Lee, Autothermal steam reforming of ethanol over $La_2Ce_{2-x}Ru_xO_7$ (x=0–0.35) catalyst for hydrogen production. Appl. Catal. B 134-135, 359-366 (2013).

[242] T. Yamazaki, Behavior of steam reforming reaction for bio-ethanol over Pt/ZrO_2 catalysts. Appl. Catal. B 99, 81-88 (2010).

[243] C.-H. Wang, K.-F. Ho, J.Y.Z. Chiou, C.-L. Lee, S.-Y. Yang, C.-T. Yeh and C.-B. Wang, Oxidative steam reforming of ethanol over $PtRu/ZrO_2$ catalysts modified with sodium and magnesium, Catal Commun. 12, 854-858 (2011).

[244] A. Gutierrez, R. Karinen, S. Airaksinen, R. Kaila, and O.I. Krause, Autothermal reforming of ethanol on noble metal catalysts, Int. J. Hydrogen Energy 36, 8967-8977 (2011).

[245] G.A. Deluga, J.R. Salge, L.D. Schmidt and X. Verykios, Renewable hydrogen from ethanol by autothermal reforming. Science 303, 993-997 (2004).

[246] S. De, J. Zhang, R. Luque and N. Yan, Ni-based bimetallic heterogeneous catalysts for energy and environmental applications. Energy Environ. Sci. 9, 3314-3347 (2016).

[247] M. Youn, J. Seo, J. Jung, D. Park and I. Song, Hydrogen production by auto-thermal reforming of ethanol over Ni catalysts supported on ZrO_2: Effect of preparation method of ZrO_2 support. Int. J. Hydrogen Energy 33, 7457-7463 (2008).

[248] M.H. Youn, Hydrogen production by auto-thermal reforming of ethanol over Ni catalyst supported on ZrO_2 prepared by a sol–gel method: Effect of H_2O/P123 mass ratio in the preparation of ZrO_2. Catal. Today 146, 57-62 (2009).

[249] T. Nimmas, S. Wongsakulphasatch, C. Kui Cheng and S. Assabumrungrat, Bi-metallic CuO-NiO based multifunctional material for hydrogen production from sorption-enhanced chemical looping autothermal reforming of ethanol. Chem. Eng. J. 398, 125543 (2020).

[250] Q. Zhou, Auto-thermal reforming of acetic acid for hydrogen production by ordered mesoporous Ni-xSm-Al-O catalysts: Effect of samarium promotion. Renew. Energy 145, 2316-2326 (2020).

[251] M.D. Argyle and C.H. Bartholomew, Heterogeneous catalyst deactivation and regeneration: a review. catalysts 5, 145-269 (2015).

[252] M.A. Ocsachoque, J.I. Eugenio Russman, B. Irigoyen, D. Gazzoli and M.G. González,Experimental and theoretical study about sulfur deactivation of Ni/ CeO_2 and Rh/CeO_2 catalysts. Mater. Chem. Phys. 172, 69-76 (2016).

[253] F. Frusteri, S. Freni, V. Chiodo, L. Spadaro, O. Di Blasi and G. Bonura, Steam reforming of bio-ethanol on alkali-doped Ni/MgO catalysts: hydrogen production for MC fuel cell. Appl Catal A 270, 1-7 (2004)

[254] F. Liu, Y.H. Qu, Y.Z. Yue, G.L. Liu and Y. Liu, Nano bimetallic alloy of Ni-Co obtained from $LaCo_xNi_{1-x}O_3$ and its catalytic performance for steam reforming of ethanol, RSC Adv 5, 16837-16846 (2015).

[255] S. Iijima, Helical microtubules of graphitic carbon, Nature 354, 56-58 (1991).

[256] R. Espinal, E. Taboada, E. Molins, R.J. Chimentao, F. Medina and J. Llorca, Cobalt hydrotalcite for the steam reforming of ethanol with scarce carbon production, RSC Adv 2, 2946 (2012).

[257] P.K. de Bokx, A. Kock, E. Boellaard, W. Klop and J.W. Geus, The formation of filamentous carbon on iron and nickel catalysts: I. Thermodynamics, J Catal 96, 454-467 (1985).

[258] J. Rostrup-Nielsen, J. Anderson and M. Boudart, Catalytic steam reforming, Catalysis, Springer, Berlin Heidelberg, 1-117, (1984).

[259] D.L. Trimm, Coke formation and minimisation during steam reforming reactions, Catal. Today 37, 233-238, (1997).

[260] P.D. Vaidya and A.E. Rodrigues, Kinetics of steam reforming of ethanol over a Ru/Al_2O_3 catalyst (Article), Industrial and Engineering Chemistry Research 45, 6614-6618 (2006).

[261] A.L.A. Marinho, R.C. Rabelo-Neto, F.B. Noronha and L.V. Mattos, Steam reforming of ethanol over Ni-based catalysts obtained from $LaNiO_3$ and $LaNiO_3/CeSiO_2$ perovskite-type oxides for the production of hydrogen, Appl Catal A 520, 53-64 (2016).

[262] L.-C. Chen and S.D. Lin, The ethanol steam reforming over $Cu-Ni/SiO_2$ catalysts: effect of Cu/Ni ratio, Appl Catal B 106, 639-649 (2011).

[263] L.C. Chen, H.K. Cheng, C.W. Chiang and S.D. Lin, Sustainable hydrogen production by ethanol steam reforming using a partially reduced copper-nickel oxide catalyst, ChemSusChem, 8, 1787-1793 (2015).

[264] A. Birot, F. Epron, C. Descorme and D. Duprez, Ethanol steam reforming over $Rh/Ce_xZr_{1-x}O_2$ catalysts: impact of the $CO–CO_2–CH_4$ interconversion reactions on the H_2 production, Appl Catal B 17-25 79 (2008).

[265] M. Virginie, M. Araque, A.C. Roger, J.C. Vargas and A. Kiennemann, Comparative study of H_2 production by ethanol steam reforming on $Ce_2Zr_{1.5}Co_{0.5}O_{8-\delta}$ and $Ce_2Zr_{1.5}Co_{0.47}Rh_{0.07}O_{8-\delta}$: evidence of the Rh role on the deactivation process, Catal. Today 138, 21-27 (2008).

[266] A.G.M. Silva, P.A. Robles-Dutenhefner, A. Dias, H.V. Fajardo, A.S.P. Lovón and J.J. Lovón-Quintana, Gold, palladium and gold–palladium supported on silica catalysts prepared by sol–gel method: synthesis, characterization and catalytic behavior in the ethanol steam reforming, J. Sol-Gel Sci. Technol. 67, 273-281 (2013).

[267] F. Wang, W. Cai, H. Provendier, Y. Schuurman, C. Descorme and C. Mirodatos, Hydrogen production from ethanol steam reforming over Ir/CeO_2 catalysts: enhanced stability by PrO_x promotion, Int J Hydrogen Energy 36, 13566-13574 (2011).

[268] J.Y. Siang, C.C. Lee, C.H. Wang, W.T. Wang, C.Y. Deng and C.T. Yeh, Hydrogen production from steam reforming of ethanol using a ceria-supported iridium catalyst: effect of different ceria supports, Int J Hydrogen Energy 35, 3456-3462 (2010).

[269] V. Nichele, M. Signoretto, F. Pinna, E. Ghedini, M. Compagnoni and I. Rossetti, Bimetallic Ni-Cu catalysts for the low-temperature ethanol steam reforming: importance oF Metal-support Interactions, Catal Lett 145, 549-558 (2015).

[270] I. Rossetti, C. Biffi, C.L. Bianchi, V. Nichele, M. Signoretto and F. Menegazzo, Ni/SiO_2 and Ni/ZrO_2 catalysts for the steam reforming of ethanol, Appl. Catal. B 117–118, 384-396 (2012).

[271] X. Fan, Z. Liu, Y.A. Zhu, J. Tong, C. Zhang, J. Engelbrekt, J. Ulstrup, K. Zhu and X. Shou, Tuning the composition of metastable $Co_xNi_yMg_{100-x-y}(OH)(OCH_3)$ nanoplates for optimizing robust methane dry reforming catalyst, J. Catal. 330, 106-119 (2015)

[272] K. Yang, Y. Wang, Y. Yang, H. Hao and X. Han, The interfacial effect on H_2 production from oxidative steam reforming of ethanol over $Rh/Ce_{1-x}La_xO_{2-\delta}$ nanocatalysts. Current Nanoscience 16(5), 837-845 (2020).

[273] L.F. Bobadilla, Glycerol steam reforming on bimetallic $NiSn/CeO_2–MgO–Al_2O_3$ catalysts: Influence of the support, reaction parameters and deactivation/regeneration processes. Appl. Catal. A 492, 38-47 (2015).

[274] I. Barbarias, Catalyst performance in the HDPE pyrolysis-reforming under reaction-regeneration cycles. Catalysts 9, 414 (2019).

[275] US Ozkan, L Zhang and H. Song, Investigation of the reaction network in ethanol steam reforming over supported cobalt catalysts, Ind Eng Chem Res 49 (19), 8984-8989 (2010).

[276] G. de Souza, V.C. Avila, N.R. Marcílio and O.W. Perez-Lopez, Synthesis gas production by steam reforming of ethanol over M-Ni-Al hydrotalcite-type catalysts; M = Mg, Zn, Mo, Co, Procedia Eng 42, 1805-1815 (2012).

[277] L.V. Mattos and F.B. Noronha, Hydrogen production for fuel cell applications by ethanol partial oxidation on Pt/CeO2 catalysts: the effect of the reaction conditions and reaction mechanism, J Catal 233, 453-463 (2005).

[278] B. Banach, Selective production of hydrogen by steam reforming of bio-ethanol. Catal. Today 176, 28-35 (2011).

[279] T. Mondal, K.K. Pant, and A.K. Dalai, Mechanistic kinetic modeling of oxidative steam reforming of bioethanol for hydrogen production over $Rh–Ni/CeO_2–ZrO_2$ Catalyst. Ind. Eng. Chem. Res. 55, 86-98 (2016).

[280] K. de Oliveira Rocha, C.M.P. Marques and J. Bueno, Effect of Au doping of Ni/Al_2O_3 catalysts used in steam reforming of methane: Mechanism, apparent activation energy, and compensation effect. Chem. Eng. Sci. 207, 844-852 (2019).

[281] M. Li and G. Wang, The mechanism of ethanol steam reforming on the Co^0 and Co^{2+} sites: A DFT study. J. Catal. 365, 391-404 (2018).

[282] G. Jacobs, R.A. Keogh and B.H. Davis, Steam reforming of ethanol over Pt/ceria with co-fed hydrogen. J. Catal. 245, 326-337 (2007).

[283] P. Vaidya, W. Yi-jiang and A. Rodrigues, Kinetics of ethanol steam reforming for hydrogen production ethanol: science and engineering, 341-354 (2019)

[284]M. Ducousso. Gasification biochar reactivity toward methane cracking. Chemical and Process Engineering. Ecole des Mines d'Albi-Carmaux, (2015).

[285] P.Y. Sheng, A Yee, G.A. Bowmaker and H. Idriss, H_2 production from ethanol over $Rh–Pt/CeO_2$ catalysts: the role of Rh for the efficient dissociation of the carbon–carbon bond, J Catal 208, 393-403 (2002).

[286] H. Idriss, Ethanol reactions over the surfaces of noble metal/cerium oxide catalysts, Platinum Met Rev 48, 105-115 (2004).

[287] A. Yee, S.J. Morrison and H. Idriss, The reactions of ethanol over M/CeO_2 catalysts: evidence of carbon–carbon bond dissociation at low temperatures over Rh/CeO_2, Catal Today, 63, 327-335 (2000).

[288] J.L. Contreras, C. Tapia, G.A. Fuentes, L. Nuño, B. Quintana, J. Salmones, B. Zeifert and I. Córdova, Equilibrium composition of ethanol steam reforming reaction to produce H_2 applied to Ni, Co and Pt/hydrotalcite WOx catalysts, Int J of Hydrogen energy 39, 16608-16618 (2014).

[289] A.C. Basagiannis, P. Panagiotopoulou and X.E. Verykios, Low temperature steam reforming of ethanol over supported noble metal catalysts, Top Catal 51, 2-12 (2008).

[290] D.K. Liguras, D.I. Kondarides and X.E. Verykios, Production of hydrogen for fuel cells by steam reforming of ethanol over supported noble metal catalysts, Appl Catal, B, 43, 345-354 (2003).

[291] H. Idriss and E.G. Seebauer, Reactions of ethanol over metal oxides, J Mol Catal A, 152, 201-212 (2000).

[292] S.V. Chong, T.R. Griffiths and H. Idriss, Ethanol reactions over the UO2(1 1 1) single crystal: effect of the Madelung potential on the reaction selectivity, Surf Sci, 444, 187-198 (2000).

[293] H. Idriss and E.G. Seebauer, Effect of oxygen electronic polarisability on catalytic reactions over oxides, Catal Lett, 66, 139-145 (2000).

[294] J.H. Wang, C.S. Lee and M. Lin, Mechanism of ethanol reforming: theoretical foundations. J. Phys. Chem. C 113, (2009)

[295] A.M. Silva, Effect of the metal nature on the reaction mechanism of the partial oxidation of ethanol over CeO_2-supported Pt and Rh catalysts. Catal. Today 133-135, 755-761 (2008).

[296] B. Caglar, J.W. Niemantsverdriet and C.J. Weststrate, Modeling the surface chemistry of biomass model compounds on oxygen-covered Rh (100). Phys. Chem. Chem. Phys. 18, 23888-23903 (2016).

[297] B. Caglar, M.O. Ozbek, J.W. Niemantsverdriet and C.J. Weststrate, The effect of C–OH functionality on the surface chemistry of biomass-derived molecules: ethanol chemistry on Rh (100). Phys. Chem. Chem. Phys. 18, 30117-30127 (2016).

[298] J. Carrasco, D. López-Durán, Z. Liu, T. Duchoň, J. Evans and S.D. Senanayake, Situ and theoretical studies for the dissociation of water on an active Ni/CeO_2 catalyst: importance of strong metal–support interactions for the cleavage of O–H bonds, Angew Chem Int Ed 54, 3917-3921 (2015).

[299] (Patent) WO 2014/108636

[300] A. Iriondo, J.F. Cambra, M.B. Güemez, V.L. Barrio, J. Requies, M.C. Sánchez-Sánchez and R.M. Navarro, Effect of ZrO_2 addition on Ni/Al_2O_3 catalyst to produce H_2 from glycerol, Int. J. Hydrogen Energy 37 , 7084-7093 (2012).

[301] R. Guil-López, R.M. Navarro, M.A. Pen, and J. L. G. Fierro, Hydrogen production by oxidative ethanol reforming on Co, Ni and Cu ex -hydrotalcite catalysts, Int. J. Hydrogen Energy 36, 1512-1523 (2011).

[302] M. Muñoz, S. Moreno, and R. Molina, "Promoting effect of Ce and Pr in Co catalysts for hydrogen production via oxidative steam reforming of ethanol," Catal. Today 213, 33-41 (2013).

[303] T. Mondal, K.K. Pant, and A.K. Dalai, "Catalytic oxidative steam reforming of bio-ethanol for hydrogen production over Rh promoted Ni/CeO_2–ZrO_2 catalyst," Int. J. Hydrogen Energy 40, 2529-2544 (2015).

[304] A. L.M. Da Silva, L.V Mattos, J. P. Den Breejen, J. H. Bitter, K. P. De Jong, and F. B. Noronha, "Oxidative steam reforming of ethanol over carbon nanofiber supported Co catalysts," Catal. Today 164, 262-267 (2011).

[305] E.B. Pereira, N. Homs, S. Martí, J.L.G. Fierro, P. Ramírez, and D. Piscina, Oxidative steam-reforming of ethanol over Co/SiO_2, Co–Rh/SiO_2 and Co–Ru / SiO_2 catalysts: Catalytic behavior and deactivation / regeneration processes, J. Catal. 257, 206-214, (2008).

[306] J.Y.Z Chiou, C. Wang, S. Yang, S. Bi, C. Shen and C. Wang, reforming of ethanol to produce hydrogen over PtRuMg/ZrO_2 catalyst. Journal of Nanotechnology 2012, 573287 (2012).

[307] P.A. Dilara and J.M. Vohs, Structure sensitivity in the reaction of methanol on ZrO_2, Surf. Sci. 321, 8-18 (1994).

[308] P.G.J. Koopman, A.P.G. Kieboom and H.V. Bekkum, Characterization of ruthenium catalysts as studied by temperature programmed reduction, J. Catal. 69, 172-179 (1981).

[309] I. Iglesias, M. Forti, G. Baronetti and F. Mariño, Zr-enhanced stability of ceria based supports for methane steam reforming at severe reaction conditions. International Journal of Hydrogen Energy 44, 8121-8132 (2019).

[310] C. Ruocco, V. Palma and A. Ricca, hydrogen production by oxidative reforming of ethanol in a fluidized bed reactor using a PtNi/CeO_2SiO_2 catalyst. International Journal of Hydrogen Energy 44, 12661-12670 (2019)

[311] F. Wang, L. Zhang, J. Deng, J. Zhang, B. Han, Y. Wang, Z. Li, H. Yu, W. Cai and Z. Deng, Embedded Ni catalysts in Ni-O-Ce solid solution for stable hydrogen production from ethanol steam reforming reaction. Fuel Processing Technology 193, 94-101 (2019).

[312] Z. Gong, B. Laura, A. Stefano, D. SS, E. Jaime and K. Anna, Activity of $Ce_{1-x}Ni_xO_{2-y}$ for H_2 production through ethanol steam reforming: tuning catalytic performance through metal-oxide interactions, Angew. Chem. Int. Ed. 49, 9680-9684 (2010).

[313] W. Fang, Hydrogen production from transformation of bioethanol by Ni based catalysts. HAL 2013, University of Lille.

[314] B. Valle, B. Aramburu, A. Remiro, J. Bilbao and A.G. Gayubo, Effect of calcination/reduction conditions of Ni/La_2O_3–AAl_2O_3 catalyst on its activity and stability for hydrogen production by steam reforming of raw bio-oil/ethanol. Applied Catalysis B: Environmental 147, 402-410 (2014).

[315] M. Muñoz, S. Moreno and R. Molina, Promoter effect of Ce and Pr on the catalytic stability of the Ni-Co system for the oxidative steam reforming of ethanol, Appl. Catal. A Gen. 526, 84-94 (2016).

[316] G. Pio, C. Ruocco, V. Palma and E. Salzano, detailed kinetic mechanism for the hydrogen production via the oxidative reforming of ethanol. Chemical Engineering Science 237, 116591 (2021).

[317] C. Rodríguez, S. Moreno and R. Molina, Oxygen mobility and its relationship with the oxidative steam reforming of ethanol (OSRE). Applied Surface Science 485, 293-303 (2019).

[318] M. Muñoz, S. Moreno, and R. Molina, Oxidative steam reforming of ethanol (OSRE) over stable NiCo–MgAl catalysts by microwave or sonication assisted coprecipitation, Int. J. Hydrogen Energy 42, 12284-12294 (2017).

[319]S.M. deLima, A.M. da Silva, L.O. da Costa, U.M. Graham, G. Jacobs, B.H. Davis, L.V. Mattos, F.B. Noronha J. Catal. 268, 268-281 (2009).

[320] A. Iriondo, J.F. Cambra, M.B. Güemez, V.L. Barrio, J. Requies, M.C. Sánchez-Sánchez and R.M. Navarro, Effect of ZrO_2 addition on Ni/Al_2O_3 catalyst to produce H_2 from glycerol, Int. J. Hydrogen Energy 37, 7084-7093 (2012).

[321] C. Lamonier, A. Ponchel, A. D'Huysser and L. Jalowiecki-Duhamel, Studies of the cerium-metal–oxygen–hydrogen system (metal = Cu, Ni). Catal. Today 50, 247-259 (1999).

[322] A. Ponchel, A. Huysser, C. Lamonier and L. Jalowiecki-Duhamel, $CeNi_xO_y$ and $CeAl_zNi_xO_y$ solids studied by electron microscopy, XRD, XPS and depth sputtering techniques, Phys. Chem. Chem. Phys. 2, 303-312 (2000).

[323] W. Fang, C. Pirez, M. Capron, S. Paul, T. Raja, P. L. Dhepe, F. Dumeignil and L. Jalowiecki-Duhamel, Ce–Ni mixed oxide as efficient catalyst for H_2 production and nanofibrous carbon material from ethanol in the presence of water RSC Adv. 2, 9626-9634 (2012).

[324] Y. Wei, X. Liu, N. Haidar, H. Jobic, S. Paul and L. Jalowiecki-Duhamel, $CeNi_XAl_{0.5}H_ZO_Y$ nano-oxyhydrides for H_2 production by oxidative dry reforming of CH_4 without carbon formation. Applied Catalysis A: General 594, 117439 (2020).

[325] S.L. Zhong, L.F. Zhang, L. Wang, W.X. Huang, C.M. Fan and A.W. Xu, Uniform and Porous $Ce_{1x}Zn_xO_{2-\delta}$ solid solution nanodisks: Preparation and their CO oxidation activity, J. Phys. Chem. C 116, 13127-13132 (2012).

[326] G. Li, R. L. Smith and H. Inomata, Synthesis of nanoscale $Ce_{(1-x)}Fe_{(x)}O_{(2)}$ solid solutions via a low-temperature approach, J. Am. Chem. Soc. 123, 11091-11092 (2001).

[327] I. Kosacki, T. Suzuki, H.U. Anderson and P. Colomban, Raman scattering and lattice defects in nanocrystalline CeO_2 thin films, Solid State Ion. 149, 99-105 (2002).

[328] N. Paunović, Z. Dohčević-Mitrović, R. Scurtu, S. Aškrabić, M. Prekajski, B. Matović, and Z. V. Popović, "Suppression of inherent ferromagnetism in Pr-doped CeO_2 nanocrystals," Nanoscale 4, 5469 (2012).

[329] S. Loridant, Raman spectroscopy as a powerful tool to characterize ceria-based catalysts, Catal. Today 373 98-111 (2021).

[330] M. Palard, J. Balencie, A. Maguer, and J.-F. Hochepied, Effect of hydrothermal ripening on the photoluminescence properties of pure and doped cerium oxide nanoparticles, Mater. Chem. Phys. 120, 79-88 (2010).

[331] G. Zhang, Y.Sun, Y. Xu and R. Zhang, Catalytic performance of N-doped activated carbon supported cobalt catalyst for carbon dioxide reforming of methane to synthesis gas, Journal of the Taiwan, Institute of Chemical Engineers 93, 234-244 (2018).

[332] A. S. Al-Fatesh, Y. Arafat, S. O. Kasim, A. A. Ibrahim, A. E. Abasaeed and A. H. Fakeeha, In situ auto-gasification of coke deposits over a novel Ni-Ce/W-Zr catalyst by sequential generation of oxygen vacancies for remarkably stable syngas production via CO_2-reforming of methane, Applied Catalysis B: Environmental 280, 119445 (2021).

[333] N. Dharmaraj, P. Prabu, S. Nagarajan, C. H. Kim, J. H. Park, and H. Y. Kim, "Synthesis of nickel oxide nanoparticles using nickel acetate and poly (vinyl acetate) precursor," Mater. Sci. Eng. B Solid-State Mater. Adv. Technol. 128, 111-114 (2006).

[334] L. Barrio, A. Kubacka, G. Zhou, M. Estrella, A. Martínez-Arias, J. C. Hanson, M. Fernández-García, and J. Rodriguez, Unusual physical and chemical properties of Ni in $Ce_{1-x}Ni_xO_{2-y}$ oxides: structural characterization and catalytic activity for the water gas shift reaction, J. Phys. Chem. C 114, 12689-12697 (2010).

[335] I. Kosacki, T. Suzuki, H.U. Anderson and P. Colomban, Raman scattering and lattice defects in nanocrystalline CeO_2 thin films, Solid State Ion. 149, 99-105 (2002).

[336] L. Jalowiecki-Duhamel, H. Zarrou and A. D'Huysser, Hydrogen production at low temperature from methane on cerium and nickel based mixed oxides, Int. J. of Hydrogen Energy 33, 5527-5534 (2008).

[337] L. Pino, C. Italiano, A. Vita, M. Laganà and V. Recupero, $Ce_{0.70}La_{0.20}Ni_{0.10}O_{2-\delta}$ catalyst for methane dry reforming: Influence of reduction temperature on the catalytic activity and stability, Appl. Catal. B Environ. 218, 779-792 (2017).

[338] P. Mierczynski, A. Mierczynska-Vasilev, R. Ciesielski, M. Mosińska, M. Nowosielska, A. Czylkowska, W. Maniukiewicz, M. Szynkowska and K. Vasilev, High active and selective $Ni/CeO_2–Al_2O_3$ and $Pd–Ni/CeO_2–Al_2O_3$ catalysts for oxy-steam reforming of methanol, Catalysts 8, 380 (2018).

[339] L. Jalowiecki-Duhamel, S. Debeusscher, H. Zarrou, A. D'Huysser, H. Jobic and E. Payen, Hydrogen storage in $CeNi_XO_Y$ and $CeM_{0.5}Ni_XO_Y$ (M = Zr or Al) mixed oxides, Catalysis Today 138, 266–271 (2008).

[340] B. Janković, Isothermal reduction kinetics of nickel oxide using hydrogen: conventional and Weibull kinetic analysis, J Phys Chem Solids 68, 2233-2246 (2007).

[341] W. Ahmed, A.E. Awadallah and A. Aboul-Enein, $Ni/CeO_2–Al_2O_3$ catalysts for methane thermo-catalytic decomposition to Co_x free H_2 production. Int. J. Hydrog. Energy 41, 18484-18493 (2016).

[342] T. L. Barr, Quantitative Surface Analysis of materials, ASTM STP 643, N. S. Mcityre, Ed., American Society for testing and Materials, 83, (1978).

[343] E. Bêche, P. Charvin, D. Perarnau, S. Abanades and G. Flamant, Ce 3d XPS investigation of cerium oxides and mixed cerium oxide ($Ce_xTi_yO_z$). Surface and Interface Analysis 40, 264-267 (2008).

[344] A.P. Grosvenor, M.C. Biesinger, R. Smart and N.S. McIntyre, New interpretations of XPS spectra of nickel metal and oxides. Surf. Sci. 600, 1771-1779 (2006).

[345] AV Shchukarev and DV Korolkov, CEJC 2(2) 2004 347-362

[346] D. Hyun Moon, W. Jin Chung, S.W. Chang, S.M. Lee, S. Kim, J.H. Jeung, Y. Ro, J. Ahn, W. Guo, H.H. Ngo and D.D. Nguyen, Fabrication and characterization of Ni-Ce-Zr ternary disk-shaped catalyst and its application for low-temperature CO_2 methanation, Fuel 260, 116260 (2020).

[347] D. Srinivas, C.V.V. Satyanarayana, H.S. Potdar and P. Ratnasamy, Applied Catalysis A: General 246, 323-334 (2003).

[348] C. Bueno-Ferrer, S. Parres-Esclapez, D. Lozano-Castelló and A. Bueno-López, Relationship between surface area and crystal size of pure and doped cerium oxides. J. Rare Earths 28, 647-653 (2010).

[349] Y. Khani, F. Bahadoran, Z. Shariatinia, M. Varmazyari and N. Safari, Synthesis of highly efficient and stable $Ni/Ce_xZr_{1-x}Gd_xO_4$ and $Ni/_X\text{-}Al_2O_3$ (X = Ce, Zr, Gd, Ce-Zr-Gd) nanocatalysts applied in methane reforming reactions. Ceram. Int. 46, 25122-25135 (2020).

[350] G. Adachi and T. Masui, Synthesis and modification of ceria-based materials. In Catalysis by Ceria and Related Materials; Trovarelli, A., Ed.; Imperial College Press: London, UK, 51-83 (2002).

[351] L. Jalowiecki-Duhamel, H. Zarrou and D. Huysser, low temperature hydrogen production from methane on cerium nickel and zirconium based oxyhydrides, Catalysis Today 138, 124-129 (2008).

[352] A. Carley, S. Jackson, J. O'Shea and M. Roberts, The formation and characterisation of Ni^{3+} on X-ray photoelectron spectroscopic investigation of potassium-doped Ni(110)–O. Surf. Sci. 440, 868-874 (1999).

[353] N.V. Kosova, E. Devyatkina and V. Kaichev, Mixed layered Ni–Mn–Co hydroxides: Crystal structure, electronic state of ions, and thermal decomposition. J. Power Sources 174, 735-740 (2007).

[354] V. Kaichev, D. Teschner, A.A. Saraev, S. Kosolobov, A. Gladky, I.P. Prosvirin, N. Rudina and A. Ayupov, Blume, R. and M. Havecker,, Evolution of self-sustained kinetic oscillations in the catalytic oxidation of propane over a nickel foil. J. Catal., 334, 23-33 (2016).

[355] D.Alders, F.C. Voogt, T. Hibma and G.A. Sawatzky, Nonlocal screening effects in 2p X-ray photoemission spectroscopy of NiO (100). Phys. Rev. B 54, 7716-7719 (1996).

[356] C. Daza, O.A. Gamba, Y. Hernández, M.A. Centeno, F. Mondragón, S. Moreno and R. Molina, High-Stable Mesoporous Ni-Ce/Clay Catalysts for Syngas Production. Catal. Lett. 141, 1037-1046 (2011).

[357] Y. Wei, X. Liu, N. Haidar, H. Jobic, S. Paul and L. Jalowiecki-Duhamel, $CeNi_XAl_{0.5}H_ZO_Y$ nano-oxyhydrides for H_2 production by oxidative dry reforming of CH_4 without carbon formation. Applied Catalysis A: General 594, 117439 (2020).

[358] S. Loridant, raman spectroscopy as a powerful tool to characterize ceria-based catalysts, Catalysis Today, 2020 hal-02990852

[359] K. Sutthiumporn and S. Kawi, Promotional effect of alkaline earth over Ni–La_2O_3 catalyst for CO_2 reforming of CH_4: role of surface oxygen species on H_2 production and carbon suppression, Int. J. Hydrogen Energy 36, 14435-14446 (2011).

[360] Y. Wei, $CeNi_XAl_{0.5}H_ZO_Y$ nano-oxyhydrides for H_2 production by oxidative dry reforming of CH_4 without carbon formation. Appl. Catal. Gen. 594, 117439 (2020).

[361] M. Melchionna and P. Fornasiero, The role of ceria-based nanostructured materials in energy applications, Mater. Today 17, 349-357 (2014).

[362] E. Aneggi, M. Boaro, C. De Leitenburg, G. Dolcetti and A. Trovarelli, Insights into the redox properties of ceria-based oxides and their implications in catalysis, J. Alloys Compd. 412, 1096-1102 (2006).

[363] R. Di Monte and J. Kaspar, On the role of oxygen storage in three-way catalysis, Top. Catal. 28, 47-57 (2004).

[364] A. Trovarelli, Catalytic properties of ceria and CeO_2 -containing materials, Catal. Rev. 38, 439-520 (2006).

[365] A. Bueno-López, Diesel soot combustion ceria catalysts, Appl. Catal. B Environ. 146, 1-11 (2014).

[366] A. Trovarelli, C. De Leitenburg, M. Boaro and G. Dolcetti, The utilization of ceria in industrial catalysis, Catal. Today 50, 353-367 (1999).

[367] A. Bueno-López, K. Krishna, M. Makkee and J.A. Moulijn, Active oxygen from CeO_2 and its role in catalysed soot oxidation, Catal. Lett. 99, 203-205 (2005).

[368] A. Bueno-López, K. Krishna, M. Makkee and J.A. Moulijn, Enhanced soot oxidation by lattice oxygen via La3+ -doped CeO_2, J. Catal. 230, 237-248 (2005).

[369] E. Aneggi, C. de Leitenburg and A. Trovarelli, Ceria-based formulations for catalysis for diesel soot combustion, A. Trovarelli, P. Fornasiero (Eds.), Catal. By Ceria Relat. Mater. Imperial C, 565-621 (2013).

[370] Westermann, A.; Geantet, C.; Vernoux, P.; Loridant, S. Defects Band Enhanced by Resonance Raman Effect in Praseodymium Doped CeO_2, Journal of Raman Spectroscopy 47, 1276-1279 (2016).

[371] M. Yashima, H. Arashi, M. Kakihana and M. Yoshimura, Raman scattering study of cubic-tetragonal phase transition in $Zr_{1-x}Ce_xO_2$ solid solution. J. Am. Ceram. Soc. 77, 1067-1071 (1997).

[372] A. S. Al-Fatesh, Y. Arafat, S. O. Kasim, A. A. Ibrahim, A. E. Abasaeed, A. H. Fakeeha, In situ auto-gasification of coke deposits over a novel Ni-Ce/W-Zr catalyst by sequential generation of oxygen vacancies for remarkably stable syngas production via CO_2-reforming of methane, Applied Catalysis B: Environmental 280, 119445, (2021)

[373] R. Puskas, A. Kukovecz and Z. Kónya, Effects of carbon nanotube functionalization on the agglomeration and sintering of supported Pd nanoparticles. Adsorption 19, 501-508 (2018).

[374] Wenhao Fang, Sébastien Paul, Mickaël Capron, Ankush V. Biradar, Shubhangi B. Umbarkar, Mohan K. Dongare, Franck Dumeignil, Louise Jalowiecki-Duhamel, Highly loaded well dispersed stable Ni species in $Ni_XMg_2AlO_Y$ nanocomposites: Application to hydrogen production from bioethanol, Applied Catalysis B: Environmental 166–167, 485-496 (2015).

[375] R. Tuinstra, J. Koenig, Characterization of graphite fiber surfaces with Raman spectroscopy, Chem. Phys. 53, 1126 (1970).

[376] R.J. Nemanich and S.A. Solin, First- and second-order Raman scattering from finite-size crystals of graphite, Phys. ReV. B 20, 392 (1979).

[377] T. Livneh, T. Haslett and M. Moskovits, Distinguishing disorder-induced bands from allowed Raman bands in graphite, Phys. ReV. B 66, 195110 (2002).

[378] L.G. Cancado, M. Pimenta, B.A. Neves, M.S. Dantas, and A. Jorio, Influence of the atomic structure on the raman spectra of graphite edges, A. Phys. ReV. Lett. 93, 247401 (2004).

[379] H. Almkhelfe, J. Carpena-Núñez, T. Back and P. Amama, Gaseous product mixture from Fischer-Tropsch synthesis as an efficient carbon feedstock for low temperature CVD growth of carbon nanotube carpets. Nanoscale 8, 13476-13487 (2016).

[380] M. Biesinger, B. Payne, L. Lau, A. Gerson and R. Smart, X-ray photoelectron spectroscopic chemical state quantification of mixed nickel metal, oxide and hydroxide systems, Surf. Interface Anal. 41, 324–332 (2009).

[381] X. Haidi, S. Mengmeng, L. Shuang, L. Yuanshan, W. Jianli and C. Yaoqiang. Effect of the calcination temperature of cerium–zirconium mixed oxides on the structure and catalytic performance of WO_3 /$CeZrO_2$ monolithic catalyst for selective catalytic reduction of NO_x with NH_3. RSC Adv. 7, 24177-24187 (2017).

[382] G. Ferré, L. Burel, M. Aouine, F. Bosselet, S. Ntais, T. Epicier, F.J. Cadete Santos Aires, C. Geantet, A. Gaenzler, F. Maurer, M. Casapu, J.-D. Grunwaldt, S. Loridant and P. Vernoux, Exploiting the dynamic properties of Pt on ceria for low temperature CO oxidation, Appl. Catal. B, Catal. Sci. Technol. 10, 3904-3917 (2020).

[383] S. Wang, W. Wang, J. Zuo and Y. Qian, Study of the Raman spectrum of CeO_2 nanometer thin films, Mater. Chem. Phys. 68, 246-248 (2001).

[384] D. Hyun Moon, W.J. Chung, S.W. Chang, S.M. Lee, S.S. Kim, J.H. Jeung, Y.H. Ro, J.Y. Ahn, W. Guo, H.H. Ngo, D.D. Nguyen, Fabrication and characterization of Ni-Ce-Zr ternary disk-shaped catalyst and its application for low-temperature CO_2 methanation, Fuel 260, 116260 (2020).

[385] R. Di Monte, J. Kašpar, Nanostructured CeO_2–ZrO_2 mixed oxides, J Mater Chem, 15 (6) (2005), pp. 633-648

[386] S. Kacimi, J. Barbier, R. Taha and D. Duprez, Oxygen storage capacity of promoted Rh/CeC_2 catalysts. Exceptional behavior of RhCu/CeO_2, Catal Lett 22, 343-350 (1993).

[387] T. Montini, M. Melchionna, M. Monai and P.Fornasiero, Fundamentals and catalytic applications of CeO_2-based materials, Chem Rev 116, 5987-6041 (2016).

[388] Y. Madier, C. Descorme, A.M. Le Govic and D.Duprez, Oxygen mobility in CeO_2 and $Ce_xZr_{(1-x)}O_2$ compounds: study by CO transient oxidation and 18O/16O isotopic exchange, J Phys Chem B 103, 10999-11006 (1999).

[389] P. Puech, M. Kandara, G. Paredes, L. Moulin, E. Weiss-Hortala, A. Kundu, N. Ratel-Ramond, J. Plewa, R. Pellenq and M. Monthioux, Analyzing the raman spectra of graphenic carbon materials from kerogens to nanotubes: what type of information can be extracted from defect bands? C 5, 69 (2019).

[390] S.S. Kim, S.M. Lee, J.M. Won, H.J. Yang and S.C. Hong, Effect of Ce/Ti ratio on the catalytic activity and stability of Ni/CeO_2–TiO_2 catalyst for dry reforming of methane, Chem Eng J 280, 433-440 (2015).

[391] W.S. Dong, H.S. Roh, K.W. Jun, S.E. Park and Y.S. Oh, Methane reforming over Ni/Ce-ZrO_2 catalysts: effect of nickel content, Appl. Catal. Gen. 226, 63-72 (2002).

[392] H.S. Roh, K.Y. Koo, U.D. Joshi and W.L. Yoon, Combined H_2O and CO_2 reforming of methane over Ni-Ce-ZrO_2 catalysts for gas to liquids (GTL), Catal. Lett. 125, 283-288 (2008).

[393] André L.A. Marinho, Raimundo C. Rabelo-Neto, Florence Epron, Nicolas Bion, Fabio B. Noronha, Fabio Souza Toniolo, Pt nanoparticles embedded in CeO_2 and $CeZrO_2$ catalysts for biogas upgrading: Investigation on carbon removal mechanism by oxygen isotopic exchange and DRIFTS, Journal of CO_2 Utilization 49, 101572 (2021).

[394] A. Marinho, R. Rabelo-Neto, F. Epron, N. Bion, F. Toniolo and F. Noronha, Embedded Ni nanoparticles in CeZrO2 as stable catalyst for dry reforming of methane, Applied Catalysis B: Environmental 268, 118387 (2020).

[395] F. Ocampo, B. Louis, A. Kiennemann and A.Roger CO_2 methanation over Ni-Ceria-Zirconia catalysts: effect of preparation and operating conditions IOP Conf Ser: Mater Sci Eng, IOP Publishing 012007 (2017).

[396] I. Iglesias, A. Quindimil, F. Mariño, U. De-La-Torre and J.R. González-Velasco, Zr promotion effect in CO_2 methanation over ceria supported nickel catalysts, Int J Hydrogen Energy 44,1710-1719 (2019).

[397] D. Avisar and T. Livneh, The Raman-Scattering of A-Type Ce_2O_3, Vib. Spectrosc. 86, 14-16 (2016).

[398] C. Schilling, A. Hofmann, C. Hess and M.V. Ganduglia-Pirovano, Raman spectra of polycrystalline CeO_2: a density functional theory study, J. Phys. Chem. C 121, 20834-20849 (2017).

[399] AV Shchukarev and DV Korolkov, CEJC 2(2) 2004 347-362

[400] P. Kumar, Y. Sun, and R.O. Idem, Nickel-based ceria, zirconia, and ceria–zirconia catalytic systems for low-temperature carbon dioxide reforming of methane, Energy Fuel 21, 3113-3123 (2007).

[401] P. Biswas and D. Kunzru, Steam reforming of ethanol for production of hydrogen over Ni/CeO_2 – ZrO_2 catalyst: effect of support and metal loading, Int J Hydrogen Energy 32, 969-980 (2007).

[402] C.E. Daza, J. Gallego, J.A. Moreno, F.Mondragón, S. Moreno and R. Molina, CO_2 reforming of methane over Ni/Mg/Al/Ce mixed oxides, Catal Today 133-135, 357-366 (2008).

[403] C.E. Daza, C.R. Cabrera, S. Moreno and R.Molina, Syngas production from CO_2 reforming of methane using Ce-doped Ni-catalysts obtained from hydrotalcites by reconstruction method, Appl.Catal. A 378, 125-133 (2010).

[404] M.-F. Luo, Z.-L. Yan and L.-Y. Jin, Structure and redox properties of $Ce_xPr_{1-x}O_{2-\delta}$ mixed oxides and their catalytic activities for CO, CH_3OH and CH_4 combustion, J. Mol. Catal. A: Chem. 260, 157-162 (2006).

[405] V.R. Choudhary, A.S. Mamman and B.S. Uphade, CO_2 Reforming and Simultaneous CO_2 and Steam Reforming of Methane to Syngas over $Co_xNi_{1-x}O$ Supported on Macroporous Silica-Alumina Precoated with MgO, R.E. Babcock, Am. Chem. Soc., 224-240 (2002).

[406] C.F. Yan, F.F. Cheng and R.R. Hu, Hydrogen production from catalytic steam reforming of bio-oil aqueous fraction over Ni/CeO_2-ZrO_2catalysts, Int J Hydrogen Energy 35, 11693-11699 (2010).

[407] L.V. Mattos, G. Jacobs, B.H. Davis, and F.B. Noronha, Production of hydrogen from ethanol: Review of reaction mechanism and catalyst deactivation, Chem. Rev. 112, 4094-4123 (2012).

[408] J.L. Contreras, J. Salmones, J.A. Colín-Luna, L. Nuño, B. Quintana, I. Córdova, B. Zeifert, C. Tapia, and G.A. Fuentes, Catalysts for H_2 production using the ethanol steam reforming (a review), Int. J. Hydrogen Energy 39, 18835-18853 (2014).

[409] S. M. Gates, J. N. Russell, and J. T. Yates, Bond activation sequence observed in the chemisorption and surface reaction of ethanol on Ni(111), Surf. Sci. 171, 111-134 (1986).

[410] J. Xu, X. Zhang, R. Zenobi, J. Yoshinobu, Z. Xu, and J. T. Yates, Ethanol decomposition on Ni(111): observation of ethoxy formation by IRAS and other methods, Surf. Sci. 256, 288-300 (1991).

[411] F. Auprêtre, C. Descorme, and D. Duprez, "Bio-ethanol catalytic steam reforming over supported metal catalysts," Catal. Commun. 3, 263-267 (2002).

[412] J. L. Ye, Y. Q. Wang, Y. Liu, and H. Wang, Steam reforming of ethanol over Ni/$Ce_xTi_{1-x}O_2$ catalysts, Int. J. Hydrogen Energy 33, 6602-6611 (2008).

[413] F. Aupretre, C. Descorme, and D. Duprez, "Steam reforming catalysts for H_2 production from ethanol," Sci. Technol. 2, 303-306 (2003).

[414] F. Auprêtre, C. Descorme, and D. Duprez, Le vaporeformage catalytique: Application à la production embarquée d'hydrogène à partir d'hydrocarbures ou d'alcools, Ann. Chim. Sci. des Mater. 26, 93-106 (2001).

[415] P. Fornasiero, R.D. Monte, G.R. Rao, J. Kaspar, S. Meriani and A. Trovarelli, Rh-loaded CeO_2-ZrO_2 solid solutions as highly efficient oxygen exchangers: dependence of the reduction behavior and the oxygen storage capacity on the structural properties, J. Catal. 151, 168-177 (1995).

[416] D.R. Sahoo, S. Vajpai, S. Patel and K.K. Pant, Kinetic modeling of steam reforming of ethanol for the production of hydrogen over Co/Al_2O_3 catalyst, Chem. Eng. J. 125, 139-147 (2007).

[417] S. Freni, S. Cavallaro, N. Mondello, L.Spadaro and F. Frusteri, Production of hydrogen for MC fuel cell by steam reforming of ethanol over MgO supported Ni and Co catalysts, Catal Commun 4, 259-268 (2003).

[418] J. Comas, F. Mariño, M. Laborde and N. Amadeo, Bio-ethanol steam reforming on Ni/Al_2O_3catalyst, Chem. Eng. J. 98, 61-68 (2004).

[419] R. Trane-Restrup, S. Dahl and A.D. Jensen,, Steam reforming of ethanol over Ni-based catalysts: Effect of feed composition on catalyst stability, International Journal of Hydrogen Energy 39, 7735-7746 (2014).

[420] Y. Wang, D. Liang, C. Wang, M. Chen, Z. Tang, J. Hu, Z. Yang, H. Zhang, J. Wang and S. Liu, Influence of calcination temperature of Ni/Attapulgite on hydrogen production by steam reforming ethanol, Renewable Energy 160, 597-611 (2020).

[421] A.M. da Silva, L. O.O. da Costa, K.R. Souza, L.V. Mattos and F.B. Noronha, The effect of space time on Co/CeO_2 catalyst deactivation during oxidative steam reforming of ethanol, Catalysis Communications 11, 736-740 (2010).

[422] H. Song and U.S. Ozkan, J. Catal., Ethanol Steam Reforming over Co-based Catalysts: Role of Oxygen Mobility, Journal of Catalysis 261, 66-74 (2009).

[423] D. Terribile, A. Trovarelli, J. Llorca, C. De Leitenburg and G. Dolcetti, The synthesis and characterization of mesoporous high-surface area ceria prepared using a hybrid organic/inorganic route, J. Catal. 178, 299-308 (1998).

[424] A. Trovarelli, F. Zamar, J. Llorca, C. De Leitenburg, G. Dolcetti and J.T. Kiss, Nanophase fluorite-structured CeO_2–ZrO_2catalysts prepared by high-energy mechanical milling analysis of low-temperature redox activity and oxygen storage capacity, J. Catal. 169, 490-502 (1997).

[425] V. Dal Santo, A. Gallo, A. Naldoni, M. Guidotti and R. Psaro, Bimetallic heterogeneous catalysts for hydrogen production, Catal Today 197, 190-205 (2012).

[426] J.A. Moulijn, A.E. van Diepen and F. Kapteijn, Catalyst deactivation: is it predictable?: what to do?, Appl Catal A 212, 3-16 (2001).

[427] M. Patel, T.K. Jindal, K.K. Pant, Kinetic study of steam reforming of ethanol on Ni-based ceria-zirconia catalyst, Ind. Eng. Chem. Res. 52, 15763-15771 (2013).

[428] M. Greluk, W. Gac, M. Rotko, G. Słowik, S. Turczyniak-Surdacka, Co/CeO_2 and Ni/CeO_2 catalysts for ethanol steam reforming: Effect of the cobalt/nickel dispersion on catalysts properties, Journal of Catalysis 393, 159-178 (2021).

[429] J.I. Di Cosimo, V.K. Dıez, M. Xu, E. Iglesia and C.R. Apesteguıa, structure and surface and catalytic properties of Mg-Al basic oxides, J. Catal. 178, 499-510 (1998).

[430] C.H. Bartholomew and R.J. Farrauto, fundamentals of industrial catalytic process (second ed.), John Wiley & Sons, 654 (2006).

[431] M. Tangstad, J. Paul Beukes, J. Steenkamp and E. Ringdalen, 14 - Coal-based reducing agents in ferroalloys and silicon production, New Trends in Coal Conversion, Woodhead Publishing, 405-438 (2019).

[432]C.K.S. Choong, Z. Zhong, L. Huang, Z. Wang, T.P. Ang, A. Borgna, J. Lin, L. Hongand L. Chen, Effect of calcium addition on catalytic ethanol steam reforming of Ni/Al_2O_3: I. Catalytic stability, electronic properties and coking mechanism, Appl. Catal. Gen. 407 (1), 145-154 (2011).

[433] Laosiripojana N, Assabumrungrat S, Charojrochkul S. Steam reforming of ethanol with co-fed oxygen and hydrogen over Ni on high surface area ceria support. Appl Catal A Gen 327, 180-188 (2007).

[434] F.B. Noronha, E.C. Fendley, R. R. Soares, W.E. Alvarez and D.E. Resasco, Correlation between catalytic activity and support reducibility in the CO_2reforming of methane over $Pt/Ce_xZr_{1-x}O_2$ catalysts, Chem. Eng. J. 82, 21-31 (2001).

[435] L. Jalowiecki-Duhamel, Hydrogen storage and induced properties in non-metallic catalytic materials, Int., J. Hyd.,Energy 31, 191-195 (2006).

[436] A. Ponchel, A. D'Huysser, C. Lamonier and L. Duhamel $CeNi_xO_y$ and $CeAl_zNi_xO_y$ solids studied by electron microscopy, XRD, XPS and depth sputtering techniques, Phys. Chem. 2, 303-321, (2000).

[437] G. Wrobel, C. Lamonier, A. Bennani, A. D'Huysser and A. Aboukais, Effect of incorporation of copper or nickel on hydrogen storage in ceria, Journal of the Chemical Society, Faraday Transactions 92, 2001-2009 (1996).

[438] C.F. Aissi, M. Daage, G. Wrobel, M. Guelton, and J.P. Bonnelle, Reactive hydrogen species in the copper-chromium oxide system,, Applied Catalysis 3, 187-194 (1982).

[439] L. Jalowiecki-Duhamel, A. Monnier and Y. Barbaux, Hydrogen species and anionic vacancies on heteropolycompounds catalytic hydrogen reservoirs, Journal of Catalysis 176, 285-293 (1998).

[440] A. Sene, L. Jalowiecki-Duhamel, G. Wrobel and J. Bonnelle, Hydrogen species, vacancies, and alkadiene hydrogenation selectivity on copper-based hydrogen reservoirs, J. Catal. 144, 544 (1993).

[441] L. Jalowiecki-Duhamel, J. Carpentier and A. Ponchel, Catalytic hydrogen storage in cerium nickel and zirconium (or aluminium) mixed oxides, International Journal of Hydrogen Energy 32, 2439-2444 (2007).

[442] C. Diagne, H. Idriss, K. Pearson, M.A.G. Garcia and A. Kiennemann, Efficient hydrogen production by ethanol reforming over Rh catalysts. Effect of addition of Zr on CeO_2 for the oxidation of CO to CO_2, CR. Chim, 7, 617-622 (2004).

[443] C.D. Dave and K.K. Pant, Renewable hydrogen generation by steam reforming of glycerol over zirconia promoted ceria supported catalyst, Renew Energ. 36, 3195-3202 (2011).

[444] E. Akpan, A. Akande, A. Aboudheir, H. Ibrahim and R. Idem, Experimental, kinetic and 2-D reactor modeling for simulation of the production of hydrogen by the catalytic reforming of concentrated crude ethanol (CRCCE) over a Ni-based commercial catalyst in a packed-bed tubular reactor, Chem Eng Sci. 62, 3112-3126 (2007).

[445] Renika Baruah, Marm Dixit, Anand Parejiya, Pratik Basarkar, Atul Bhargav, Sudhanshu Sharma, Oxidative steam reforming of ethanol on rhodium catalyst – I: Spatially resolved steady-state experiments and microkinetic modeling, International Journal of Hydrogen Energy 42 (15), 10184-10198 (2017).

General Abstract

Title: Nano-oxyhydrides based on Ni and ceria, or doped with Zr or Al ceria, for the production of H_2 by low temperature oxidative steam reforming of ethanol

Hydrogen (H_2) is the future green energy and an important chemical, as the most used gas in industries. Today, 96% of H_2 production is from fossil fuels and the most competitive method for its production is the steam reforming of natural gas. It is urgently desirable to produce H_2 from renewable resources, such as biomass-derived products in order to increase energy self-sufficiency and preserve the environment. For this purpose, hydrogen production is studied by low temperature oxidative steam reforming of ethanol (OSRE) over $CeNi_x(M_{0.5})O_y$ (M = Al or Zr) mixed oxide catalysts. The influence of different parameters is studied such as nickel content, presence of Al or Zr, calcination, pretreatment in H_2, reduction temperature in H_2, mass of catalyst, and oxygen over ethanol ratio. With an oven temperature of 50 °C, nano-oxyhydride catalysts, containing hydride species inside the solids that are formed after adequate pretreatment in H_2 of the compounds, allow very interesting performances under $EtOH/H_2O/O_2$ = 1:3:1.7 reaction mixture reaching total EtOH and O_2 conversions with the formation of 50 % of H_2 in the products distribution (with mainly CO_2 and CO), without carbon formation. Doping the catalyst with Zr is beneficial at low O_2/EtOH ratio of 1.4 in particular, in ameliorating stability. Increasing O_2/EtOH ratio up to 1.7 helps in avoiding carbon formation. Highly performant and stable catalysts over 80 hours in OSRE are obtained. Moreover, conditions are proposed for the elimination of the pretreatment step in hydrogen and even calcination. Different physico-chemical characterizations (Raman, XRD, XPS, BET) are performed before test and some after test (Raman, XPS) insuring the presence of strong interactions between Ce and Ni species (and Zr or Al for ternary catalysts), in agreement with the presence of a Ce-Ni-(M)-O (M = Al or Zr) solid solution. Finally, an active site involving Ni^{2+} cations in strong interaction with other cations can be proposed.

Keywords : Heterogeneous catalysis, Oxidative steam reforming, Hydrogen, Ethanol, Cerium, Nickel, Aluminum, Zirconium, Solid solution, Oxyhydride, Low temperature, Hydrogen production, Hydride, Hydrogen storage

Résumé général

Titre : Nano-oxyhydrures à base de Ni et cérine, ou cérine dopée avec Zr ou Al, pour la production d'H_2 par vaporeformage oxydant à basse température de l'éthanol.

L'hydrogène (H_2) est la future énergie verte et un produit chimique important, en tant que gaz le plus utilisé dans les industries. Aujourd'hui, la production d'H_2 est à 96 % d'origine fossile et la méthode la plus compétitive pour sa production est le reformage à la vapeur du gaz naturel.. Il est urgent de produire de l'H_2 à partir de ressources renouvelables, telles que de produits dérivés de la biomasse afin d'augmenter l'autosuffisance énergétique et de préserver l'environnement. A cet effet, la production d'hydrogène est étudiée par vaporeformage oxydant de l'éthanol à basse température (OSRE) sur des catalyseurs oxydes mixtes du type $CeNi_X(M_{0.5})O_Y$ (M = Al ou Zr). L'influence de différents paramètres est étudiée, comme la teneur en nickel, la présence d'Al ou de Zr, la calcination, le prétraitement sous H_2, la température de réduction sous H_2, la masse de catalyseur et le rapport oxygène sur éthanol. Avec une température de four à 50 °C, les catalyseurs du type nano-oxyhydrures, contenant des espèces hydrure à l'intérieur du solide et formés après un prétraitement adéquat sous H_2, permettent des performances très intéressantes sous un mélange réactionnel $EtOH/H_2O/O_2$ = 1:3:1.7, avec des conversions totales de l'EtOH et de l'O_2 et la formation d'H_2 à 50 % parmi les produits formés (avec principalement du CO_2 et du CO), sans formation de carbone. Le dopage du catalyseur avec Zr est bénéfique pour un faible rapport O_2/EtOH de 1,4, améliorant la stabilité. L'augmentation du rapport O_2/EtOH jusqu'à 1,7 permet d'éviter la formation de carbone. Des catalyseurs très performants en OSRE et stables durant 80 heures sont obtenus. Par ailleurs, des conditions sont proposées pour la suppression de l'étape de prétraitement sous hydrogène et même de calcination. Différentes caractérisations physico-chimiques (Raman, XRD, XPS, BET) sont réalisées avant test et certaines après test (Raman, XPS) ; elles mettent en évidence des interactions fortes entre les espèces Ce et Ni (et Zr ou Al pour les catalyseurs ternaires), en accord avec la présence d'une solution solide Ce-Ni-(M)-O (M = Al ou Zr). Enfin, un site actif impliquant des cations Ni^{2+} en interaction forte avec d'autres cations peut être proposé.

Mots clés : Catalyse hétérogène, Reformage oxydant, Hydrogène, Ethanol, Cérium, Nickel, Aluminium, Zirconium, Solution solide, Oxyhydrure, Basse température, Production d'hydrogène, Hydrure, Stockage d'hydrogène.